SALINITY INTRUSION AND DISPERSION MODELLING IN A MALAYSIAN ESTUARY

By

ZULLKEFLE NORDIN
P.ENG, MIEM
B. Eng (Hons) in Civil Engineering
M. Sc in Civil Engineering – State University of New York at Buffalo

A Doctoral Thesis

Submitted in partial fulfilment of the requirements for the award of
Doctor of Philosophy of Loughborough University

JULY 2008

Abstract

The flow structures in rivers with floodplains vegetated with mangrove swamps were investigated in this thesis. Two natural estuaries namely Sedeli Estuary and Rompin Estuary were used in this study. Both estuaries are situated in the western coast of Malaysia and are about 100km apart. Field data were collected at both estuaries to compare their characteristics. Water levels, salinity reading and tide levels during high water were recorded for three days. They were used to calibrate the numerical modeling results.

Six different estuary layouts were used in this study. TELEMAC 2D was used to predict the velocity, water levels and salinity distribution at the apex and straight sections of compound meandering channels. The aim was to investigate how the shape factor, the presence of vegetated and non-vegetated floodplains and estuary configuration affected the velocity distributions, water levels and salinity distribution. Single and multiple Manning's were used to study the effects of Manning's on the results. Two mesh densities and three turbulence models were used in the simulation works for calibration and sensitivity analysis. Twenty simulation runs were done in this thesis to also study the effects of mesh independency and the choice of Manning's values on the results obtained. The results show that the vegetated floodplains are significant to the flow in the main channel. It was found that the flow at the apex and straight sections of the meandering channel showed some complexity due to the presence of vegetated floodplains, the tidal influence as well as the change of the inflow of freshwater into the system. The tidal flow within mangrove areas depend a large degree upon the submerged vegetation density with the tidal stage. In general, the results show that the choice of Manning's for floodplains, the main channel, and the estuary layouts will induce energy losses due to momentum the exchange between the main channel and floodplains.

Keywords: Shape factors, vegetated floodplain, non-vegetated floodplain, single and multiple Manning's coefficients, TELEMAC 2D, compound meandering channel, velocity and salinity distributions, straight and apex sections, meandering channel, bed formation, mesh densities.

ACKNOWLEDGEMENTS

First of all, I am grateful to my supervisors Dr. Cecil F. Scott and Professor Koji Shiono for all their guidance, encouragement and constructive criticism throughout the course of this work. They introduced me to the numerical modelling which enables me to reconcile my interests in physics and applied mathematics with the endeavours of engineering.

Special thanks also goes to Ms. Kate Day, Mr. John Baugh and Dr. Alan Cooper from HR Wallingford for their cooperation in providing me the TELEMAC software and license file which enable me to run the programme. I would also like to express my gratitude to Mr. Bruce Scott from the Loughborough University Computing Centre for his help and friendship during the early stage of this work.

I could not forget all the support and encouragement received from Dr. Ponnambalan Rameshwaran, Dr. Deepak Shukla, Dr. Keyur Vyas, Dr. Zulhelmi Ismail and others during my ups and downs while trying to get through my research.

I would like to say that I am indebted to my family and my parents, particularly to my wife Mrs. Rohana Jamaludin for her sacrifices, unconditional love, patience and enormous support. Without her I do not think that I can achieve what I have now. Special thanks also are dedicated to my three children, Farah Zuhana, Mohd. Farid and Farah Fatin for their support and understanding during the course of my research.

And finally, I would like to acknowledge the Public Services Department of Malaysia which is an agency of the Malaysian Government, for providing me with the financial support to develop this work. Last but not least, I would like to thank the Director General of the Public Works Department who motivated me to pursue my studies at the doctoral level.

Table of Contents

List of Figures

List of Tables

Page

List of Symbols

Roman Alphabet

$\bar{A}$ = Mean Water Surface Area

b = Breadth

d = Depth

C = Concentration , Chezy's Coefficient

C_e = Eddy Viscosity Coefficient

C_D = Drag Coefficient

D = Tidal Mean Depth

E = Eddy Viscosity

f = Coriolis Parameter

F_B = Internal Froude Number

Fr = Forude Number

F_T = Bulk Froude Number

g = Gravitational Acceleration

g' = Effective Acceleration

K_h = Horizontal Turbulent Diffusion Coefficient

K_v = Vertical Turbulent Diffusion Coefficient

M = Mass

Ri_E = Estuarine Richardson Number

Ri = Richardson Number

V_T = Tidal Prism Volume

H = Tidal Range

Q_R = River Flow Rate

T = Tidal Period

S = Salinity

S_o = Depth-Averaged Salinity

U = Root Mean Square

U10 = Wind Speed at Height 10 meters

$u.v.w$ = Velocity in x,y,z components in Cartesian Coordinates

$\bar{u},\bar{v},\bar{w}$ = Average Velocity in x,y,z components in Cartesian Coordinates

u_* = Surface Velocity, Bed Shear Velocity

u_f = Depth-Averaged Velocity

$\hat{u}$ = Vertically Average Velocity

x,y,z = Longitudinal, Transverse and Vertical Components in Cartesian Coordinates

Greek Alphabet

ξ = Mean Tidal Amplitude

$\Delta\rho$ = Density Difference

$\Delta\rho_x$ = Horizontal Density Difference

ρ = Density

δS = Salinity Difference Between Surface and Bottom

ε_v φ = Stratification Parameter

ω = Earth's Rotation Velocity

θ = Latitude

μ = Dynamic Viscosity

τ = Shear Stress

ε = Eddy Diffusivity

ε_t = Transverse Mixing Coefficient

ε_v = Vertical Mixing Coefficient

CHAPTER 1

INTRODUCTION

1.1 General

Rivers have been the major source of potable water for domestic and industrial use for ages. They are also become means of transportation, recreation and irrigation. The planning and effective management of the river system requires a thorough understanding of the flow mechanics and their characteristics. No doubt that this understanding is vital for administrating river management and rehabilitation projects such as shoreline protection, land reclamation, estuary deepening, river restoration and many others.

Rivers are commonly classified as straight, meandering and braiding (Leopold and Wolman, 1957) where meandering rivers are common in nature. Meandering rivers have attracted a great deal of attention of river engineers and scientists due to their complex flow mechanics. One of the environmentally attractive types is the two-stage channel which consists of a main channel and floodplains. The main channel is used to carry low river discharge at all times while the floodplains are used to carry excess river flows during floods and heavy storms. The assessment of flood discharge capacity associated with flood levels in compound river channels is uncertain. The flow patterns in such situations are complicated by the interaction of flows in the main channel and the floodplains. Furthermore, the complexity of flow patterns may increase due to variations of planform, such as bedform, bank slopes and meandering configurations and geometry which will affect the flow properties in compound channels.

The existence of vegetation is common in wetlands and along river reaches. It has a strong influence on physical and biological processes. With rapid development, which has taken place along rivers, the clearance of this vegetation has disturbed the ecology of the surrounding areas and the flow structures of the rivers. In the past, vegetation was treated as an additional resistance to the flow of a river since submerged and non-

submerged vegetation along riverbanks and floodplains usually contributes to the largest energy lost. Therefore, it is important to understand the behaviour of flow over vegetation to allow us to gain more knowledge on both flow velocity profiles and flow resistance with vegetated floodplains.

The hydrodynamic and hypsometry of a vegetated swamp estuary are extremely complex in nature. In the tidally estuary, the existence of vegetation on the floodplain further complicates the flow structures. During low tide, the flow is confined to the main channel but as the tide rises, the estuary overflows its banks and progressively flooding of the overbank vegetation occurs. In nature, most rivers are meandered and with vegetation along their banks. This vegetation along the river reach of a meandering channel affects the conveyances of both inbank and overbank flow conditions. It produces high resistance to flow and as a result, has a large impact on the water levels in rivers. Experiments show that channels and floodplains with different geometries give different flow resistance.

1.2 Research Background

Many research works have been carried out to study the flow through vegetation. These works used either physical modelling or numerical modelling. With the advancement of computer technology, numerical models are getting popular. The advantage of numerical modelling is that it is capable of capturing parameters, which are impossible to measure in physical modelling. Most of the past researches were to understand the effect on flow structures of rivers having straight configuration and vegetation either on the floodplains or inbanks. However, truly straight rivers are very rare in nature as they mostly meander in planform. However not many studies have been done on meandering rivers. Many of the researches done used physical modeling using straight channel. Most of the vegetation used in the studies are flexible and rigid. The vegetation used in the experiments was either submerged or non-submerged. The vegetation layout was arranged using different configurations and shapes to determine their effects on flow structures. Musleh and Cruise (2006), carried out an experiment using rigid unsubmerged vegetation on wide floodplain. They used rigidity with various vegetation layouts and density. They concluded that in the case of rigid vegetation, the flow resistance appeared

to be sensitive to the velocity with the effect becoming greater as the density of vegetation increased. For flexible vegetation, the velocity was more dominant than the flow depth. Maghadam and Kouwen (1997) carried experiments using flexible and non-submerged vegetation on the floodplain. They concluded that by using flexible vegetation, the drag force will be reduced as the mean velocity increases. Wilson *et al.* (2003) used submerged flexible vegetations (rods and rods with frond foliage) in their experiments. By varying the depth of flows, they measured velocities using Acoustic Doppler Velocimeter. They concluded that the additional drag that was exerted by the plants will reduce the mean flow velocity within the vegetated regions compared to the unvegetated ones. Similarly Carollo *et al.* (2005), carried out experiments using grasslike vegetation submerged fully in the channel. They concluded that the method by Maghadam and Kouwen (1997) gave an overestimate result of the flow resistance.

1.3 Research Approach

In this thesis, two-dimensional CFD code is applied to the real estuary. The estuary is 73.0 kilometres long meandering through the wetland throughout the entire length. The inflow data, the oscillation tide levels, salinity reading, and velocity information are determined by the field study. Shape factors are also carried out to study their significant effects on the simulated results. Six channel configurations and meshes are used in the simulation, some with or without floodplains. For model calibration and sensitivity analysis, ten other simulations are carried out using two values of Manning's coefficients *'n'* equal to 0.012 and 0.03, with two different meshes density.

Four additional simulations are carried out by taking the effects of vegetation into consideration. For these simulations, two mesh density is used. A single value Manning's coefficients *'n'* for the floodplain is used ($n = 0.1$) and two values of *'n'* ($n = 0.012$ *and* $n = 0.03$) for the channel are used for the simulations. In addition, two sections of the river reach (the straight and apex of the meandered sections) are considered to study the salinity distribution and flow structures caused by the vegetation on the floodplain.

1.4 Objectives

The primary aim of the research is to study the application of Computational Fluid Dynamics (CFD) in river and estuary modelling and to understand the flow mechanism in a tidally driven estuary. A finite element code is used to simulate the salinity intrusion and the effects of mangrove swamp on the flow structure in the Sedeli Estuary in Malaysia. In this study, the two-dimensional code is used for the numerical modelling works.

The objectives of this thesis are:

- To apply state-of-the-art Computational Fluid Dynamics, the TELEMAC code techniques, to the flow problems and salinity intrusion in estuaries and rivers.
- To enhance current knowledge on the effects of mangrove swamp and shape factors on the flow structures.
- To understand the effects of flow structures and velocity profile for meandering channels with vegetation on the floodplain.
- To study the characteristics of flow, velocity and salinity distribution on the vegetated floodplain during the ebbing and flooding conditions.
- To study the effectiveness of using CFD to model the salinity intrusion and flow structures on vegetated floodplains for real estuary.

1.5 Thesis Structure

This thesis is divided into seven chapters. A general description of the subject of this thesis, the research background, and objectives are outlined in the first chapter. The detailed review of previous researches associated with salinity intrusion, flow through vegetated floodplain and general characteristics of various types of estuaries and their classifications is included in **Chapter 2**. This chapter also included past researches using physical and numerical modelling. Also various types of numerical modelling are presented in this chapter.

Chapter 3 gives some theoretical background, which includes flow equations, turbulence and mixing flows in estuaries, longitudinal dispersion and shear effects,

salinity intrusion in estuaries and some common numerical models in river and estuary dynamics.

In **Chapter 4** includes the numerical parameters used in the TELEMAC software are included. Matters pertaining to mesh constructions, boundary conditions and solution algorithms are discussed. Modelling approaches, numerical issues and mesh approach are described in this chapter.

In **Chapter 5** the summary of the field data and the raw data analysis are outlined. In this chapter, the raw data are analysed based on their salinity, water levels and velocity profile. Two nearby estuaries are compared.

Chapter 6 describes the use of TELEMAC-2D to model the Sedeli estuary. A sensitivity and calibration analysis is carried out on the model. Comparisons are made between the simulation results and the observation data. In this chapter, shape factors and the use of different turbulent models are discussed. Different types of advection schemes, roughness coefficients and mesh densities are used in the simulations for the calibration and the sensitivity analysis. Analyses are also carried out to determine the flow structures at meandering and straight sections of the river with vegetation along the riverbanks. Detailed discussions on velocity distribution, water levels and salinity patterns for both sections are analysed to determine their similarities and differences during flooding and ebbing.

The important findings from **Chapter 5 and Chapter 6** are high- lighted in **Chapter 7** of this thesis. The major shortcomings and the summary finding of this research are mentioned in the final chapter followed by some recommendations for future research. References of the text quoted from published papers are included at the end portion of this thesis.

CHAPTER 2

LITERATURE REVIEW

2.0 Introduction

This Chapter is divided into four sub-topics. The first topic will briefly discuss the types of estuaries and how they are classified. This will then be followed by the discussion on flow for two-stage straight and meandering channels and their properties. This section will also discuss overbank and inbank flow characteristics for meandering channels. Thirdly, a more detailed discussion for flow through vegetated floodplain will be discussed. In this section, the effect of vegetation on the flow structures and the shear interaction between floodplain and river channel will also be discussed. Finally, a brief introduction to numerical modelling for one-dimensional (1-D), two-dimensional (2-D) and three-dimensional (3-D) will be discussed

2.1 Classification on Estuaries

Estuaries can be categorised into three main types based on the salinity distribution. Pritchard (1955), Cameron, and Pritchard (1963) have classified estuaries using stratification and salinity profile distribution as a criteria. They are highly stratified, partially mixed and well-mixed estuaries. **Figure 2.1** shows the relationship between depth and salinity for the three types of estuaries based on Cameron and Pritchard (1963). The degree of stratification maintained in an estuary is a result of a balance between two competing mechanisms (Simpson *et al.* 1990), that is the stratifying effects of velocity-induced straining, including both estuarine circulation and tidal motion and the homogenising effects of shear-induced mixing. The concept velocity-induced straining involves the tilting of isopycnals when acted upon by some sheared horizontal velocity profile. This action can result in a time rate of change of potential energy anomaly, φ, which represents the amount of energy input needed to homogenise a vertical density profile,

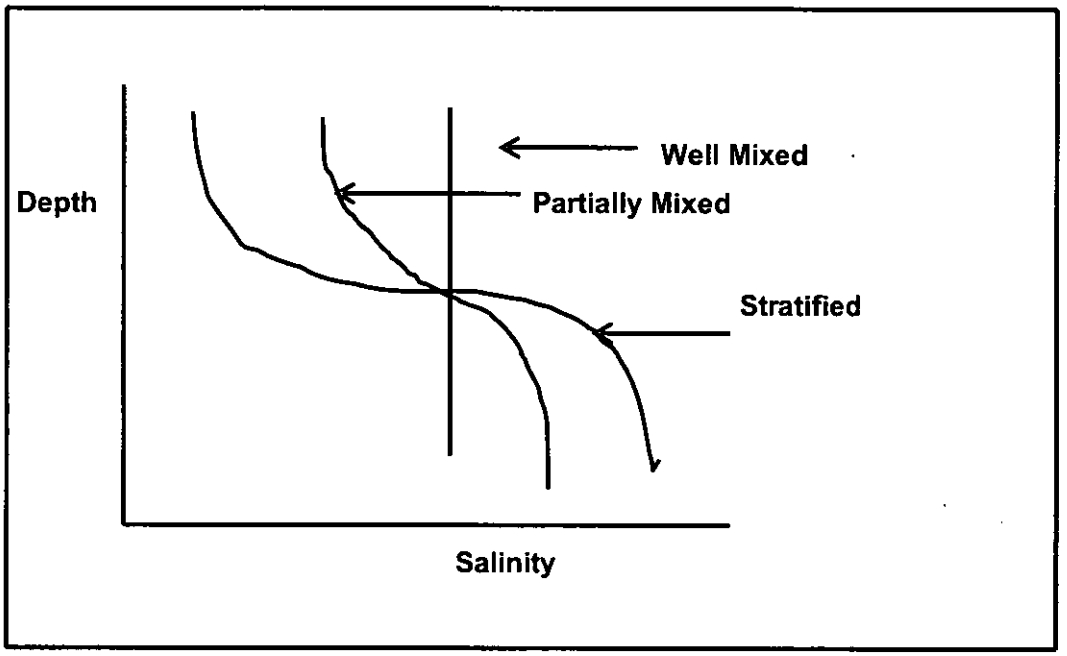

Figure 2.1 - Classification by Salinity (Cameron and Pritchard, 1963)

$$\frac{\partial \varphi}{\partial t} = \frac{g}{h}\frac{\partial \rho}{\partial x}\int_{-h}^{0}(u-\hat{u})z dz \qquad (2.1)$$

Where h is the depth of water and $\frac{\partial \rho}{\partial x}$ is the horizontal density gradient. The value of u is the velocity component along the estuary and $\hat{u}$ is the vertically average velocity along estuary. x and z are the longitudinal and vertical coordinates of an estuary respectively while φ is the gauged stratification in estuaries.

2.1.1 Highly Stratified Estuarine Flows

For a highly stratified salt-wedge estuary, the seaward freshwater will flow over a denser incoming saline water from the sea. The denser salt wedge will move upstream along the bottom until the freshwater flow forces balance the saline water. This causes the entrainment of saline water from bottom to the surface layer, smoothing out the halocline and transferring salt to the surface layer. Mixing occurs at the saline water/freshwater interface by entrainment, a process caused by viscous

shear forces between the two moving layers. Small amounts of denser saline water are mixed in the upper layers; more fluid enters the estuary near the bottom to compensate for the loss as more fluid left the estuary in the upper layers to achieve equilibrium of forces. **Figure 2.2** shows a typical cross-section of a highly stratified estuary. Examples of highly stratified estuaries are the Mississippi estuary in the United States and Vellar estuary in India.

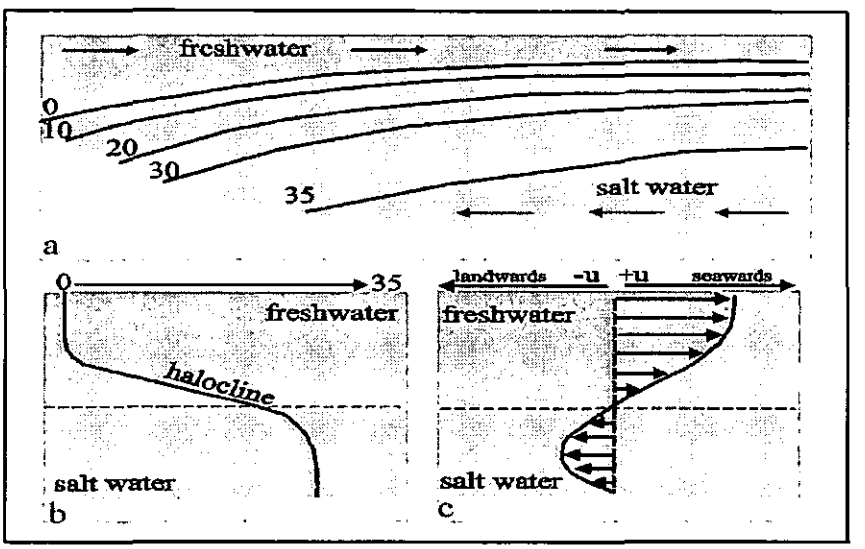

Figure 2.2 - Show a typical cross-section of a highly stratified estuary.

(a) The longitudinal section shows the water circulation. The upper arrows show the river flows seaward while the bottom arrows show the seawater flows landward. The salinity gradient is indicated by the water the lines.

(b) The cross-section shows the salinity profile with depth.

(c) The cross-section shows the net velocity with respect to the depth of a highly stratified estuary.

2.1.2 Partially Stratified Estuarine Flows

In a partially stratified estuary, the tidal energy dissipated by the bottom friction produces turbulence. Turbulent eddies will then mix the seawater upward with the freshwater, which then has net seawater flow in the upward direction. When the salinity of the upper surface water increases, the seaward surface flow will also increase to maintain river flow plus the additional upward mixing of the seawater. This

causes a compensating incoming flow along the bottom layer. It will then form a well-defined, two layer flow that is typical for a partially stratified estuary. The salinity structure in partially mixed estuary is different from a highly stratified estuary due to the efficient mixing of seawater and freshwater. Normally, in a partially mixed estuary, the river flow is low compared to the tidal prism. **Figure 2.3** shows a typical partially mixed estuary.

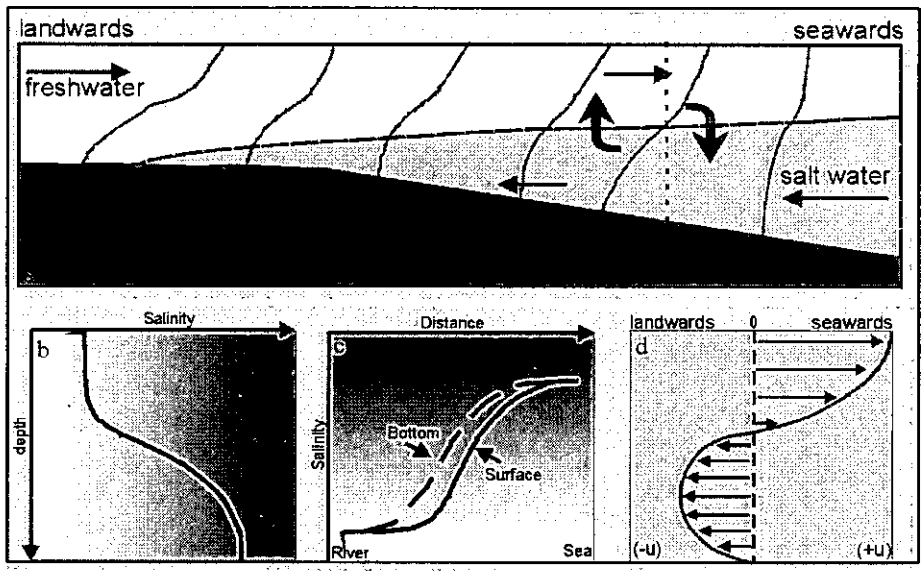

Figure 2.3 - Show a typical cross-section of a partially mixed estuary.
(a) The longitudinal section shows the circulation of seawater and freshwater at the interface and the salinity gradient.
(b) The cross-section shows salinity profile with depth taken at dotted line from (a).
(c) The cross-section shows the salinity gradient with distance at the bottom and surface of the partially mixed estuary.
(d) The cross-section shows the net velocity with respect to depth

2.1.3 Well Mixed Estuarine Flows

In this type of estuarine flow, the tidal flow is much larger than the river inflow. The turbulent generated by the bottom friction is enough to mix the entire column of water and this will result in a vertically homogeneous well- mixed estuary. If the estuary is wide, Coriolis force may lead to horizontal flow separation. In the

southern hemisphere, this flow will flow toward the sea on the left-hand-side and in the northern hemisphere on the right-hand-side. In a well-mixed estuary a salinity profile will show the same value from the surface down to the bed. However, as it moves upstream, the salinity concentration decreases with distance. **Figure 2.4** shows a typical well-mixed estuary.

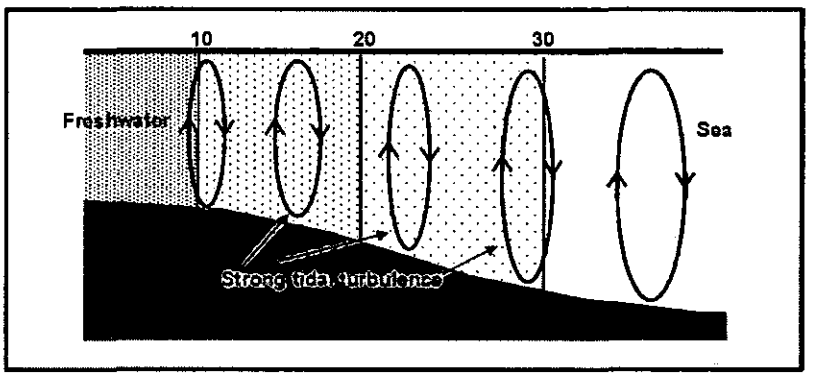

Figure 2.4 – Shows a typical cross-section of a well-mixed estuary. The ellipses shows the mixing of freshwater and seawater due to turbulence. The salinity is uniform throughout the cross-section of the estuary and decreases toward the landward.

2.2 Classification by Stratification-Circulation

The stratification of an estuary is controlled by the ratio of freshwater and seawater. In a large estuary, the freshwater may pass through several stages of estuary types. Seasonal changes to the freshwater flows have an influence on the formation of estuary types. Simmons (1955), Pritchard (1955), Hansen-Rattray (1966) and Fischer (1972) have tried to quantify the classification of estuaries based on their saline structure.

2.2.1 Simmons (1955)

The simplest classification was based on determining the quantity of fresh water flowing into an estuary over a tidal cycle in relation to the tidal prism (Simmons 1955 cited in Dyer, 1979). Simmons (1995) showed that the balance between estuarine mixing and flushing by the tides and fresh water inflows into the rivers strongly determines the saline structure of estuaries. The tidal prism is expressed simply as V_T,

Table 2.1 - Summary of Characteristics of Estuary Type based on Pritchard (1955)

Parameter	Highly Stratified Salt Wedge	Partially Mixed	Well Mixed
Flow Ratio	≥ 1.0	≈ 0.25	< 0.10
River Flow	High	Low-Intermediate	Low
Tidal Prism	Low	Intermediate-High	High
Width/Depth	Low	Intermediate	Intermediate
Depth	Shallow	Shallow-Intermediate	Shallow
Circulation Type	Seaward above Interface Landward below Interface	Seaward (Surface) Landward (Deep)	Seaward
Energy	Low	Intermediate	Intermediate-High

or volume of water contained in the estuary between high and low tides,

$$V_T = H\overline{A} \tag{2.5}$$

where H is the tidal range and $\overline{A}$ is the mean water surface area of the estuary. The relative effect of the river inflow to the tidal flows is expressed in terms of a coefficient R that is given by,

$$R = \frac{V_R}{V_T} \tag{2.6}$$

V_R is equal to Q_R multiplied by T where Q_R and T is the river flow rate and the tidal period respectively . Simmons (1955) relates the flow ratio R of freshwater flow to the estuary type. He shows that for a ratio of unity, the estuary is highly stratified. When the flow ratio ranges from 0.3 to 0.5, the estuary is partially mixed while a flow ratio of less than 0.1 is normally associated with well- mixed estuary.

Pritchard (1955) related the estuary depth and width to the flow ratio and found that as geometry of the estuary changes, the flow ratio will be affected, and thus the types will vary. Ippen and Harleman (1961) used the tidal properties of amplitude and phase to develop a relation between an energy and estuary mixing which was known as Ippen number. This number is a measurement of the amount of energy lost by the tidal wave relative to that used in the mixing of water column. They showed that if this number is high, it indicates that the estuary is well mixed and if it is low, the estuary is highly stratified. Changes in freshwater flow, and in the width and depth of the estuary have a significant influence on the tidal properties and therefore the accuracy of the tidal measurement will be needed if this method were to be used. **Table 2.1** shows the summary of all the estuaries type and their properties.

2.2.2 Hansen-Rattray (1966)

The Hansen and Rattray (1966) diagram was modified by Rattray and Uncles (1983). They developed a diagram that used salinity and velocity ratio parameter to classify estuaries. This is a two-parameter scheme and is commonly used in estuary classification. The first dimensionless parameter is stratification, which is the ratio of the surface to bottom salinity difference divided by the average cross-sectional salinity. The second parameter is circulation, which is defined as the ratio of the net surface velocity to the average cross-sectional velocity. The value of both parameters is used to determine the location of the studied estuary in the diagram. This location will then determine the types of estuaries. **Figure 2.5** shows the stratification and circulation parameters. A stratification parameter is given by,

$$\frac{\delta S}{S_o} = \frac{\text{difference in salinity from surface to seabed(tidally averaged)}}{\text{depth-averaged salinity (tidally averaged)}} \qquad (2.7)$$

and a circulation parameter is given by

$$\frac{u_s}{u_f} = \frac{\text{surface velocity(tidally averaged)}}{\text{depth-averaged velocity (tidally averaged)}} \qquad (2.8)$$

2.2.3 Fisher (1972)

The Hansen-Rattray (1966) circulation parameters can be calculated from a single survey taken over a couple of tidal cycles and do not require the knowledge of river inflow. They produced a diagram based on stratification and circulation as shown in **Figure 2.6**. Further, the Hansen-Rattray (1966) parameters can be related to more fundamental parameters in the form of a densimetric Froude number Fr and an estuarine Richardson number Ri_E (Fischer 1976)

$$Fr = \frac{Q_R}{bd\sqrt{g'd}} \tag{2.9}$$

$$Ri_E = \frac{g'Q_R}{bU_{rms}^{\ 3}} \tag{2.10}$$

Where b and d represent the breadth and depth of the estuary respectively, U_{rms} is the root means square of the tidal velocity and g' is the reduced to gravity given by,

$$g' = \frac{\rho S - \rho R}{\rho S} g \tag{2.11}$$

Fischer (1972) showed that the stratification was dependent on Ri_E while the circulation is mainly dependent on Fr as indicated in **Figure 2.7**

2.2.4 Comments on Simple Predictive Method

In simple predictive method, the assumption made is that the river flow is constant throughout. However, the estuarine water balance is dominated by fresh water inputs from storm water runoff, groundwater, direct rainfall onto the estuary surface, and evaporation that fluctuates over time. The Fischer (1972) approach is useful for estimating the estuary stratification if data of flow, bathymetric and tidal data are available. Estuary depth is a critical parameter in determining the saline structure of an estuary, as deeper estuaries are most likely to stratify. Although the use of Simmons

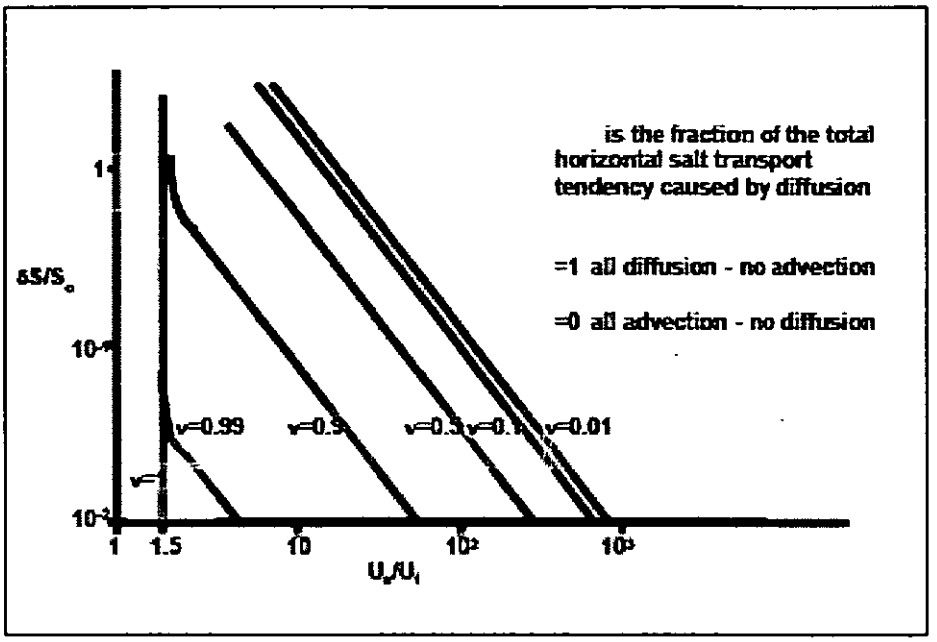

Figure 2.5 – The Stratification and Circulation Parameters

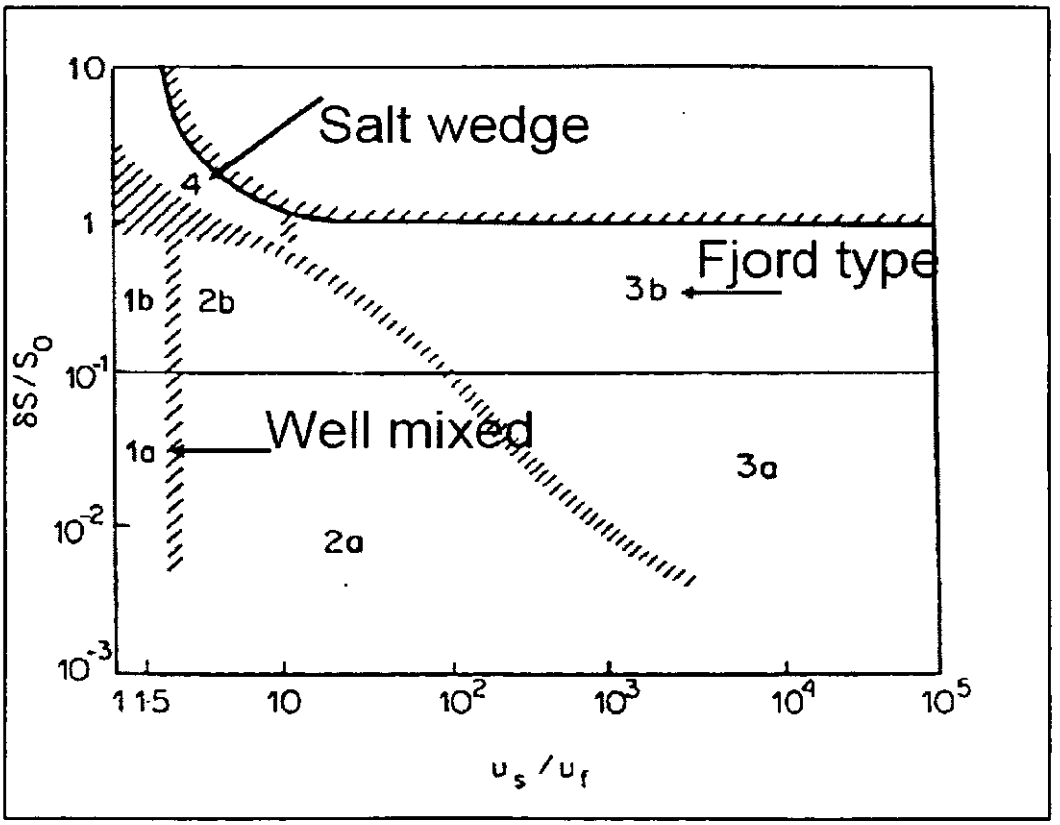

Figure 2.6 - Show the Hansen – Rattray diagram used to classify estuary based on stratification and circulation

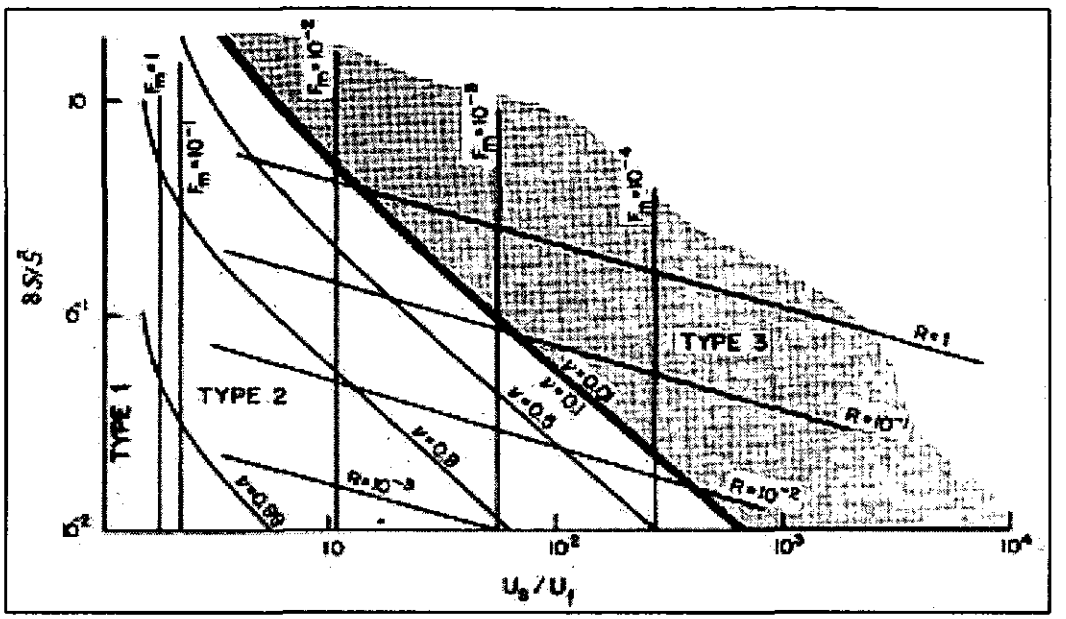

Figure 2.7 - Hansen-Rattray estuarine classification diagram Richardson number and densimetric Froude number as determined by Fisher (1972).

(1955) method was widespread, it makes no acknowledgement of the role of estuary depth in saline structure.

2.3 Estuarine Circulation

Tides are defined as periodic vertical or horizontal movements which have a coherent amplitude and phase relationship to some periodic geophysical force (Howarth and Pugh 1993). The tidal circulation can be influenced by a multitude of different factors including wind, density, size and shape of the estuarine basin. Some of the major factors of tidal circulation are the occurrences of spring and neap tides in the estuary. These tides coupled with the diurnal tides play a major role in velocity and circulation (Van der Kreek 1986). Festa and Hansen (1976) used various estuarine parameters and found that the river transport and Rayleigh number *(Ra)* had significant effects on estuarine circulation. They found that increasing the *Ra* through deepening the estuarine channel depth *H* resulted in an increase in circulation as well as strong salinity intrusion and an inward migration of the stagnation point. The horizontal

location of the stagnation point was found to be proportional to Ra and varies with H^3.

2.3.1 Effect of Wind on Circulation

Wind is usually the dominant force in large lake, open ocean and in some coastal areas but in estuaries it may or may not play a major role (Fischer *et al.* 1979). However if the estuary is wide, wind stresses can generate currents of considerable importance. Wind at a speed of 6m/s to 7m/s is most effective in moving surface waters. Wind-driven surface currents have speeds of about 2% of the wind speed. However, in water bodies with strong current such as in estuaries, wind stress often has a nominal effect compared to bottom shear stress.

The flow induced by wind stress acting parallel to the long axis of barotropic, non-rotating estuary was first noted by Csanady (1973). This circulation develops because of the imposed wind stress, bottom friction and the axial pressure gradient required to maintain no net flux across any section. In a shallow estuary where the effect of pressure gradient is weak, the flow is downward where the bottom stress balances the imposed wind stress. In deep part of the estuary, the flow is upward and the wind stress and bottom stress together balance the pressure gradient. De Castro *et al.* (2000) described in detail the effect of wind on circulation and applied the pressure gradient in their studies at the Laguna San Ignacio estuary on the Pacific coast of the Baja California peninsula in Mexico.

Uncles *et al.* (1990) carried out a study at Merbok estuary in Malaysia and concluded that winds are not a major factor in Malaysia. They found that wind speeds are generally weak where 60% of the time, they are less than $0.5ms^{-1}$ throughout the year.

2.3.2 Effect of Tides on Circulation

Tidal currents not only provide an alternating background to the density current flow but they also generate turbulence which promotes vertical mixing in estuary which will lead to the reduction of stability and influence the density circulation

(Bowden 1963). It will experience vertical shears from their interaction with the bed friction. If these shears are significantly large, then the vertical stratification will be eroded. Tidal currents are small in highly stratified and partially mixed estuaries compared to the well-mixed estuary. **Figure 2.8** shows a gravitational circulation in a partially mixed estuary.

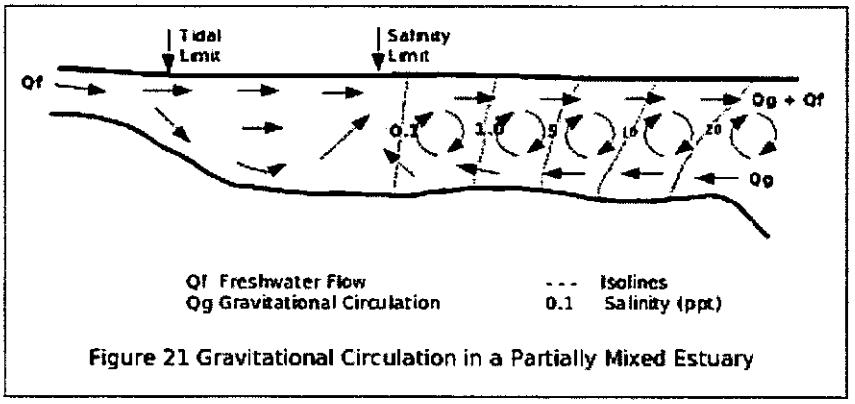

Figure 2.8 – Typical Gravitational Circulation in Partially Mixed Estuary (NSW Dept. of Land and Water Conservation)

2.3.3 Effect of Gravitational Circulation

Gravitational circulation is induced by horizontal differences in density. Two factors influencing density are temperature and salinity. Salinity is more important in coastal areas and inland, where strong changes in salinity occur. Temperature is important too, though its effects are more marked in the open ocean, where salinity is relatively constant and the temperature drives the stratification and circulation. Saline water is denser than freshwater due to the large number of salt dissolved in it. Consequently, fresh-water will flow above the saline water at the estuary.

The source of fresh water is usually situated higher than the sea. Due to gravity, it will flow downstream into the sea during the neap tide. In this case, the elevation difference drives the flow. Due to density differences, freshwater tends to flow over the sea water as freshwater come into contact with saline water. Thus formed a

stratified layer between the sea water and the fresh water. This creates a pressure gradient with the downward pressure of the freshwater pushing the saline water landward. This results in the "classical" estuarine circulation pattern in which there is a net outflow of water in the surface waters and a net inward flow near the bottom. The balance between river flow and tidal influence will determine how closely the actual pattern of flow in the estuary follows the expected "classical" estuarine flow. It is also interesting to note that in many temperate and tropical estuaries, much of the river discharge actually evaporates before reaching the ocean. For example, in Barnegat Bay, it takes approximately 100 days for the equivalent volume of water flowing in the upper river portion of the Bay to exit to the mouth.

2.4 Turbulence in Estuaries

Estuary flows are unsteady, non-uniform turbulent motions in which density differences normally play a major role. Therefore, turbulent processes are very important. They contribute significantly to the transport of momentum and mass, and greatly influence the velocity profile of the flow. These turbulent processes are highly variable in space and time. In estuary modelling, turbulent stresses and mass transports are normally expressed in terms of velocity and salinity.

Movement of water and solute in estuaries is governed by the turbulent mean flow and turbulent diffusion processes (Darbyshire and West 1992). Salinity, wind, bathymetry, the physical of the estuary and temperature are factors that influence the turbulence in estuaries.

2.5 Coriolis Force

Coriolis force is caused by the rotation of the earth. The parameter is defined as follows,

$$f = 2\omega \sin\theta \tag{2.12}$$

Where ω, the Earth's rotational velocity is equal to $7.25X10^{-5}$ radian where θ is the latitude of the estuary. Coriolis force also modifies circulation of river and ocean flow, causing water to veer toward the right in the Northern Hemisphere.

Consequently, the surface water tends to be fresher toward the right shore relative to the flow of the river, while salt wedge tends to flow toward its right (opposite sides). **Figure 2.9** shows the typical estuary flows in the Northern Hemisphere. Under normal conditions, the pycnocline tends to tilt to compensate for the Coriolis forces by tilting to the right.

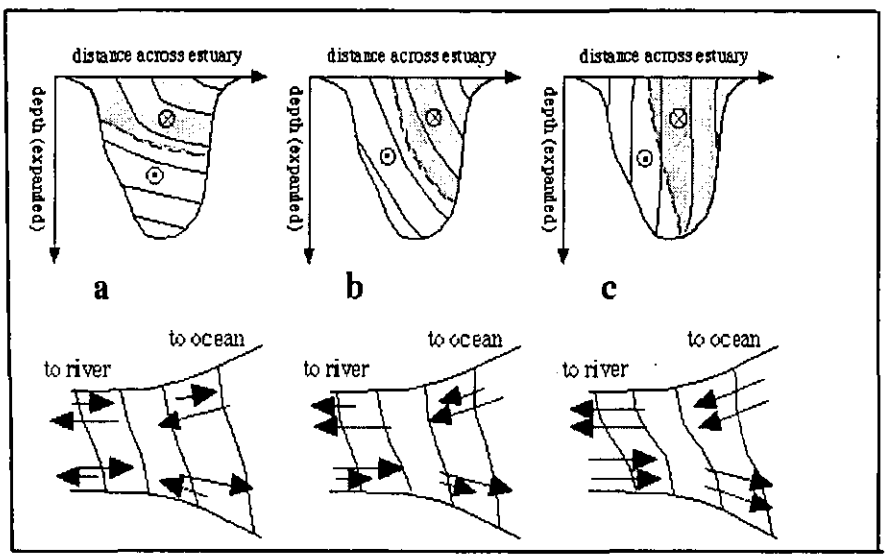

Figure 2.9 - Sketch of the circulation in three dimensions in estuaries (northern hemisphere).

(a) slightly stratified estuary with weak Coriolis effect;

(b) slightly stratified estuary with strong Coriolis effect;

(c) vertically mixed estuary with Coriolis effect.

Full lines indicate isohalines. The broken line indicates the boundary between the upper and lower layer; the upper layer is shaded. Purple arrows indicate upper layer currents, magenta arrows indicate lower layer currents. The cross-section for (a), (b) and (c) looking upstream direction. The situation in the southern hemisphere is the mirror image with respect to the estuary axis.

2.6 Compound Open Channel Flow

Many researchers have studied and published papers related to compound open channel flows. The compound open channels used in previous studies were either straight or they meandered with and without floodplain.

2.6.1 Main Channel and Floodplain

In nature, main channels and floodplains in general have different roughness coefficient due to the growth of vegetations on the latter. Because of the difference in velocity, higher roughness is induced than at the main channel. The velocity differences generate a shear layer between the main channel and floodplain and vertical vortices along the interfaces of the main channel and floodplain. Thus, the flows in the main channel and floodplain interact with each other and cause turbulent mixing due to the exchange of momentum between the fast flowing main channel and slow flowing floodplain. The vertical plain between the main channel and the floodplain in longitudinal direction experience considerable turbulent shear stress. The momentum transfer at the interface acts as an 'apparent shear stress' that will cause additional resistance to the flow (Myer 1978). Thus, it will reduce the flow velocity in the main channel and the conveyance capacity, where the parameters on floodplain increase (Rajaratnam and Ahmadi 1979). This makes compound channels less efficient compared to simple open channels without floodplains.

Sellin (1964) presented the photographic showing the existence of vortices at the main channel and floodplain interface. Experiments conducted by Zheleznyakov (1965; 1971) showed the mechanism of momentum transfer which is known as the 'kinematic effect'. He also showed that the main channel and floodplain interaction which is induced by shear is highest at the location above the bankfull depth and decreases as the depth of flow increases. Rajaratnam and Ahmadi (1979) made similar conclusions. Townsend (1968), demonstrated that vortices around the interface play a significant role in the transporting the finer sediment fraction from the deep main channel on to the floodplain. Tamai *et al.* (1986) illustrated that this phenomenon exists during the flows. Several researchers among whom are Fukuoka and Fujita (1989) used visualisation techniques to show that the momentum transfer by this vortices occurred around the main channel and floodplain interface. Similarly, Shiono and Knight (1989, 1990 and 1991) used Laser Doppler Anemometer to measure turbulence in compound channels with various side slopes. They found that the vertical profiles of the primary mean velocity in the middle of the main channel and at the

remote distances on floodplains agree with the two-dimensional logarithmic law. While in the complex shear layer region, the profiles of this logarithmic law do not exist, indicating that the flows are three-dimensional in nature.

2.6.2 Secondary Flow Structures

The presence of helical secondary flow circulation in the streamwise direction makes the flow structure further complex and three-dimensional in nature. In straight channel flows, this secondary flow circulations exist due to turbulence are normally known as 'turbulence driven' secondary flow circulation. Sometimes it is also known as Prandtl's second kind of circulation. The channel geometry, aspect ratio and cross-sectional shape have a significant impact on the secondary flows as described by Tominaga *et al.* (1989). The secondary flow circulations are extremely important because they influence the primary flow characteristics, bed shear stress, sediment transport and bed-forms as concluded by Nezu and Rodi (1985).

Muto and Shiono (1998) studied the three-dimensional flow structures in meandering channels with overbank flow based on velocity measurement using a two-component Laser Doppler Anemometer (LDA). They stated that the development of secondary flow for overbank flow structures is controlled by the flow interaction in the cross-over section as shown in **Figure 2.10**.

In addition, the flow interaction between the two layers also creates the shearing effect with the maximum shearing effect in overbank flow occurring at a relative depth of around 0.05. So, it can be noted that the secondary flow is a dominant factor influencing a compound meandering channel. By advecting flow, the secondary flow redistributes velocity and boundary shear stress as well as enhances the mixing and transport process and is highly responsible for the bank erosion process.

2.6.3 Compound Straight Channels

In compound straight channel flow, there exist two major secondary flow circulation cells as shown by Shiono and Knight (1989). A relatively strong upflow inclined towards the main channel from the top edge of the floodplain whilst

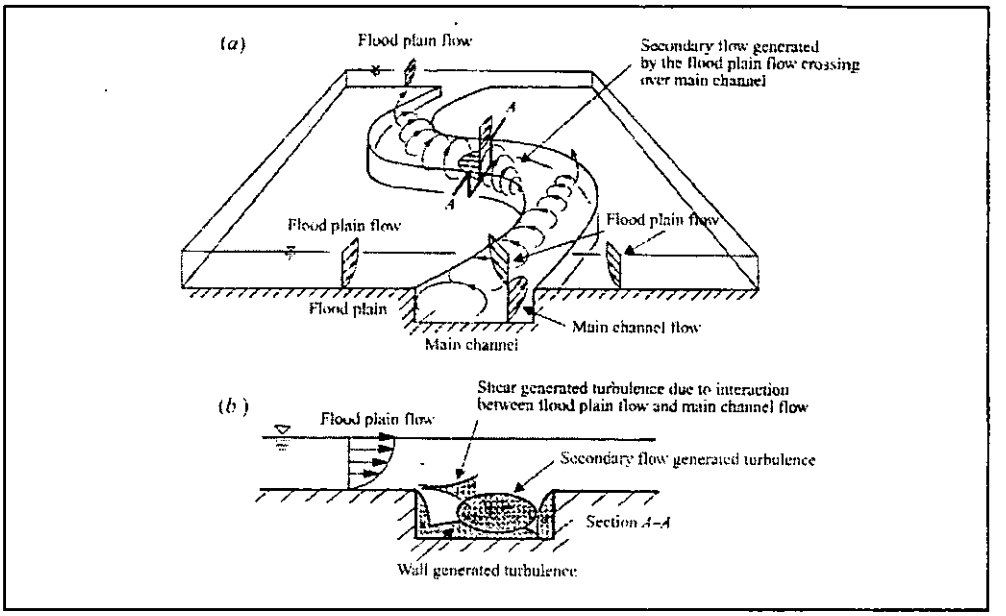

Figure 2.10 - Overall flow structure in meandering channel for overbank

(a) Secondary flow generation mechanism
(b) Contributions of flow mechanisms (turbulent shear, secondary flows and anisotropy of turbulence) towards the production of turbulence energy (after Shiono and Muto, 1998)

downflow occurred at the corner of the main channel can be seen in **Figure 2.11.** From the experiment, they show that these secondary flow circulation cells change strength with the change of main channel side slopes. On the floodplain area, there is only one single large secondary flow circulation that is observed, which extends laterally to quite a significant distance. Turbulence intensities are found to be anisotropic in the lateral shear locality. The complex flow mechanisms associated with the compound straight channel flows are conceptually presented by Shiono and Knight (1991) as shown in **Figure 2.12.** Several researchers used the fibre-optic LDA to measure the three velocity components and turbulence in straight compound channel with rectangular side slopes, found by Shiono and Knight (1989). They concluded that, for compound open channel flows, there exist unusual flow characteristics quite close to the main channel and floodplain interface region whereas in rectangular open channel, the main channel sidewall region is complex.

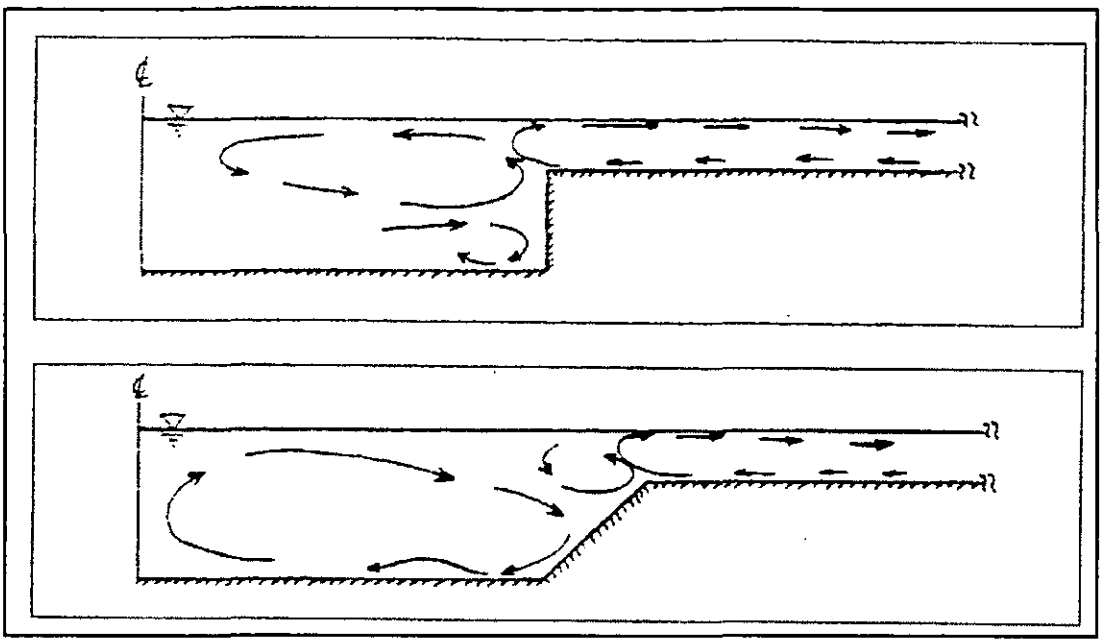

Figure 2.11 – Illustration of secondary flow circulation in compound straight channels with rectangular and trapezoidal across section (Shiono and Knight, 1989)

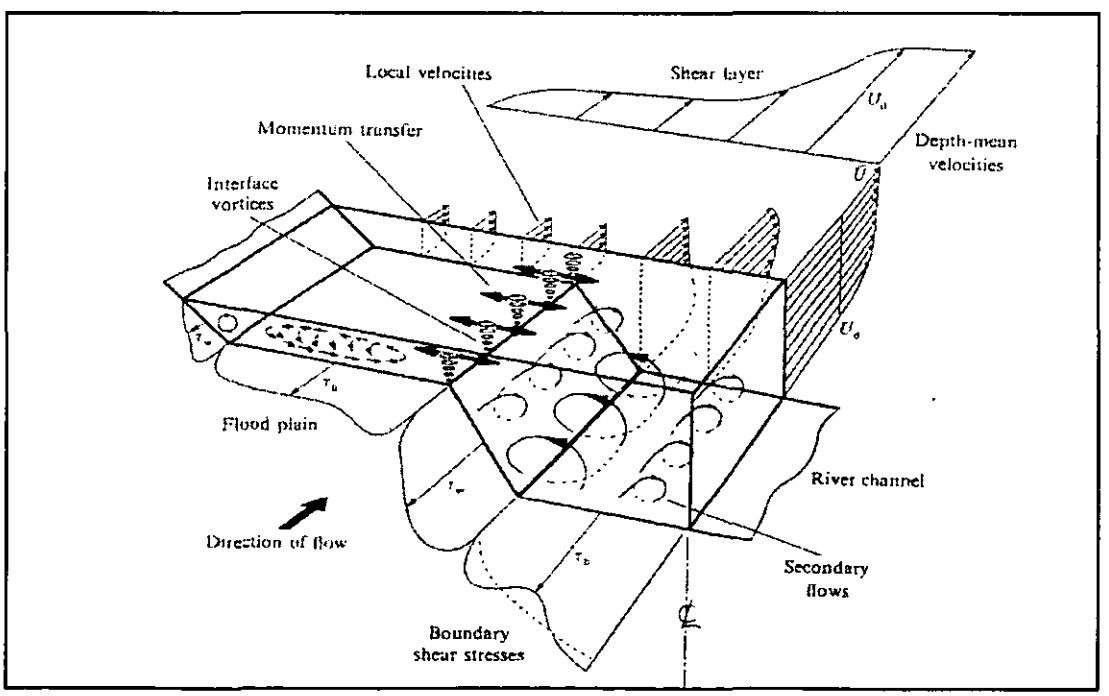

Figure 2.12 – Conceptual visualisation of the complicated flow mechanism found in compound straight channels with trapezoidal cross-section (Shiono and Knight, 1991)

They deduced that there exist a strongly inclined secondary current generated from the main channel and floodplain interface edge towards the free surface. A pair of secondary flow circulation is observed on the sides of the inclined upflow. The vortex that forms on the side of the floodplain is known as 'floodplain vortex' while the vortex on the side of the main channel is the 'main channel vortex'. Both of these vortices reach the free surface and cover the channel-floodplain junction region. At the sidewall region of the main channel, a horizontal flow from the sidewall towards the mid- section of the main channel appears at the free surface region.

Thus it formed a longitudinal vortex which Tominaga and Nezu (1990) called 'free surface vortex'. A similar pattern of secondary flow circulation was observed near the free surface as found in the case of rectangular open channel flows. The bottom vortex, which appeared at the corners of a rectangular open channel can also be seen during the flows. The magnitude of these secondary currents was found to be just slightly greater around the region of 4.0% higher than the maximum magnitude of secondary current found near the free surface in rectangular open channel flow

2.6.4 Compound Meandering Channels

The majority of laboratory scale experiments for compound meandering channels had been carried out as early as in the sixties. Flow in river channels with floodplains, the so-called compound channel, has been an area of significant research since Sellin (1964) discovered the momentum interaction effect. The investigation was intensified in the eighties and nineties among them are Yen and Yen (1983), Ervine and Ellis (1987), Keily (1990), James and Wark (1992), Willets and Hardwick (1993), Sellin *et al.* (1993), Greenhill and Sellin (1993), Ervine *et al.* (1993), Sellin and Willetts (1996), Knight and Shiono (1996), Willetts and Rameshwaran (1996) and Muto and Shiono (1998) , Patra and Kar (2001), Patra *et al.* (2004) and many others. Most of these experiments were done to investigate flow structures, mixing patterns, the behaviour and generation of secondary current energy losses and also the stage-discharge predictions.

Many of these experiments were done on the Flood Channel Facility (FCF) at

HR Wallingford, UK while others used flume at Aberdeen University, Bradford University, Loughborough University and a few other flumes available at other universities in the United Kingdom.

- ***Basic Flow Mechanism***

Shukry (1949) was among the earliest researchers to study the behaviour of flow around closed 'U' bend using a specially designed pitot sphere, which was capable of measuring the three velocity components. He observed a complex flow pattern being generated by the interference of a secondary flow circulation, which was quite similar to the straight flume approach. Due to the centrifugal force, the secondary circulations along the bend showed a continuous tendency to deviate from the original pattern of a straight flume approach to form a new one. He also defined the strength of secondary circulations as a ratio of the kinetic energy of the secondary flow to the total kinetic energy of a flow at a chosen section. The strength of these secondary circulations is inversely proportional to the Reynolds number and radius-breadth ratio. It also decreases with an increase in depth-breadth ratio. Its strength is also found to increase as the deviation angle of the bend increases.

The U.S Army Corps of Engineers in Vicksburg (1956) conducted a laboratory study on the compound meandering channel to investigate the effects of geometrical and flow parameters on the conveyance capacity of the channel. They tried to relate the effects of sinuosity of the main channel, radius of curvature of meander bend, ratio of floodplain area to the main channel, and the effects of roughness of the floodplain to the conveyance of the channel. They concluded that the compound meandering channels were less efficient hydraulically compared to the straight compound channel. Sellin and Willets (1996) concluded that an increase in sinuosity resulted in a decrease in discharge. They also showed that as the floodplain roughness increases, the discharge decreases significantly. Similarly, they found that by the reduction of floodplain area, the carrying capacity of the channel decreases.

- ***Main Channel and Floodplain Behaviour***

Ervine and Ellis (1987) investigated the behaviour of compound meandering

channel flows and the shear interaction between the main channel and floodplain. For this channel, they found that the flow in the main channel and floodplain was not parallel to each other as observed in compound straight channels. Ervine and Ellis (1987) further illustrated that the horizontal interface at the bankfull level was subjected to the co-flowing turbulent shear stress formed due to the velocity differences between the main channel and the floodplain flows. The component of the floodplain flow resolve ($U_f cos\theta$, where θ is bend angle at corresponding section) along the main channel direction is slow compared to main channel flow. They deduced that the apparent shear stress exerted on the horizontal interface at the bankfull is proportional to the differential velocity between the main channel and floodplain (U_{mc} - $U_f cos\theta$). The other component of floodplain flow ($U_f sin\theta$) enters the main channel and leaves the main channel at the adjoining floodplain region. Due to this action, the floodplain flow in the main channel is subjected to the expansion and contraction losses due to the floodplain flow entering and leaving the main channel respectively. Yen and Yen (1983) also observed the expansion and contraction, which took place when the flow from the floodplain crossed over the main channel and then re-entered the floodplain.

From the experiment conducted by James and Wark (1992) and Greenhill and Sellin *et al.* (1993), they concluded that the most influential factors in meandering channels with overbank flow are bed slope, channel shape, bed and floodplain roughness, relative flow depth of the floodplain, meander belt width, sinuosity and aspect ratio. In addition to this, James and Wark (1992) identified the four most important flow mechanisms in two-stage meandering channels as follows:

(a) The longitudinal velocities in the main channel tend to follow the meandering main channel side walls while the floodplain velocities are generally in the valley direction. Hence, the floodplain flows past over the main channel and induces a horizontal shear layer.

(b) Water passes from the main channel onto the floodplain and back into the main channel in the following meander bend. Hence, the proportion of the discharge

passed by the main channel and floodplain varies along a meander wavelength. These bulk exchanges of water between slow and fast moving regions of flow induce extra flow resistance.

(c) The energy loss due to the secondary flows in the main channel is greater than that of an equivalent simple channel and the secondary flows rotate in the opposite direction from that observed mostly in inbank flows.

(d) Flows on the floodplain outside the meander belt are usually faster than those within the meander belt. It would appear that the extra flow resistance induced by the meandering main channel has a relatively small effect on the outer floodplain.

In 1993, Willets and Hardwick investigated the overbank flow in a meandering channel in a small-scale laboratory flume. They described the overbank flow structure as highly three-dimensional, with strong secondary currents, momentum exchanges between the main channel and floodplain, and shear interaction on the horizontal interface region. These main features of the two-stage meandering with overbank flow are shown in **Figure 2.13**. The figure explains that the high velocity filament shifts from the outer bank to the inner bank as the flow approaches the downstream apex. A vigorous exchange of water from the floodplain drives a large secondary flow in the main channel. Large secondary cells grow along the outer bank upstream of each bend apex and decay rapidly downstream of the bend apex. Floodplain flow plunging into the main channel and leaving the main channel creates contraction and expansion exchange effects between the two regions of the channel.

- ***Energy Losses***

Envine and Ellis (1987) and Envine and Jasen (1989) have listed five main reasons for energy losses of the overbank flow in meandering channels. They are,

- Frictional head loss in the main channel
- Flow resistance on the floodplain due to additional roughness

- Secondary flow circulation which induces flow resistance
- Flow resistance due to the expansion and contraction of floodplain flows
- Flow resistance due to the vertical shear layer at the bankfull level

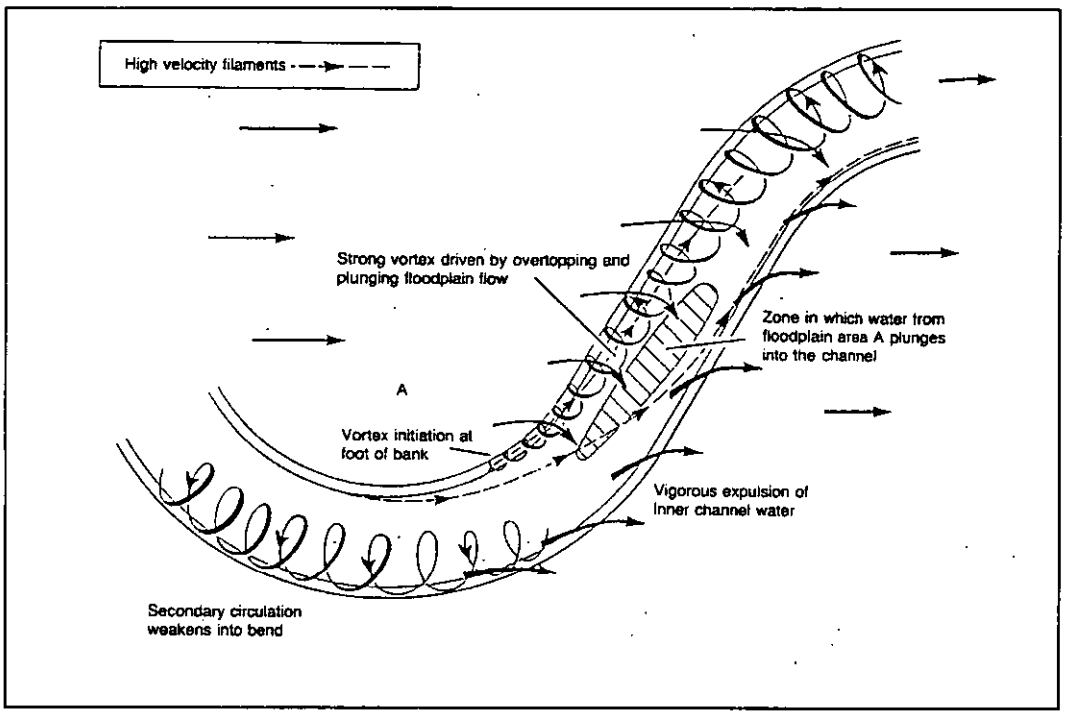

Figure 2.13 - Flow mechanism in compound meandering channel (after Willets and Hardwick, 1993)

As illustrated by James and Wark (1992), the flow resistance produced by the meandering channel has a minimal effect on the flow outside the meander belt width. Shiono *et al.* (1999) used the velocity and turbulence data, and quantified the energy losses for compound meandering channel. By taking into account the presence of shear layer at the bankfull level, they concluded that the dominant mechanism for energy loss varies according to sinuosity and relative depth. Sellin (1991) concluded that the influence of horizontal shear layer on the progressive development of secondary flow circulations is evident along the strong mixing region of the cross-over region of meandering channels. The shape of the secondary circulation cells along the cross-over region is found to be similar to that of trapezoidal and natural cross-section eventhough

their strength varies in both cases. James and Wark (1992) found the same flow mechanisms as previously reported by Tobes and Sooky (1967) and Ervine and Ellis (1987).

2.6.5 Velocity Distribution

Toebes and Sookey (1967), Mckeogh and Kiely (1989), James and Wark (1992), Shiono and Muto (1993), Shiono *et al.* (1993), Liu and James (1997), Muto and Shiono (1998), Lyness *et al.* (1998), and Liriono *et al.* (2001). Toebes and Sookey (1967) carried an investigation to measure the velocity for compound meandering channel and observed that the vectors of the horizontal resultant velocity had a divergence pattern, indicating strong interaction of vertical flow components. Mckeogh and Kiely (1989) found that the primary velocity vectors on the floodplain were essentially parallel to the valley slope direction, whereas the primary velocity flow in the main channel tends to follow along the course of the meandering channel wall direction during high overbank flow. Shiono *et al.* (1993) also reported a similar observation, hence the velocity differential between the floodplain flows and main channel flow created a lateral shear layer horizontally between these two regions. Furthermore, they suggested that, for the discharge assessment, it is best to use a horizontal division method at the shear layer interface between the main channel and floodplain.

James and Wark (1992) described the longitudinal velocities on the floodplain outside the meander belt as usually being faster than those found within the meander belt. This is due to an extra flow resistance induced by the meandering channel but this effect has less significance for the flow beyond the meander belt. Liu and James (1997) found that accounting only for frictional losses outside the meander belt would overestimate the conveyance of the section; nevertheless, the meander belt width to total floodplain width ratio affects the interaction between the main channel and the floodplain. With the smaller meander belt width in relation to the overall floodplain width, the effect of the meandering channel on the overall discharge is reduced. The flow will also be affected by obstructions on the floodplain, such as vegetation or buildings. Liriono *et al.* (2001) investigated the effect of obstructions on the floodplain

and found that the magnitude of the effect on water level due to such obstructions is strongly dependent upon the location of the obstructions.

Shiono and Muto (1993) measured the three-components of instantaneous velocity using a two-component Laser Doppler Anemometer in a trapezoidal cross-section meandering channel, with straight floodplain wall for inbank and shallow overbank flow cases at Dr = 0.15. In the case of overbank flows, a strong gradient of streamwise velocity in the vertical direction was observed at the start of the cross-over region. This was due to the plunging of the floodplain flows into and over the main channel, which ultimately triggers the generation of the secondary flow circulations. Since the experimental data was available only at seven different cross-sections along the meander, the exact point from which the secondary flow circulations started to be generated was not investigated. Based on the measured lateral and vertical shear stresses, they confirmed the large momentum exchange taking place in the region of strong interaction (the cross-over region) between the main channel and the floodplain flows. Later on, experimental work carried out by Muto and Shiono (1998) showed that in overbank flow the maximum velocity filament in the main channel occurred near the inner bank at the upstream apex section and moved progressively across the outer bank as it approached the downstream apex. Muto and Shiono (1998) also observed in overbank flow that the gradient of the streamwise velocity becomes larger in the cross-over region due to a strong interaction between the main channel and the floodplain flow.

Lyness *et al.* (1998) studied the hydraulic characteristics of overbank flows in a meandering mobile bed compound channel at the UK Flood Channel Facility (FCF). They carried out the experiment both for rough and smooth floodplains with a mobile bed channel using uniformly graded sediment. They found that for overbank flow with relative depth, and the Dr greater than 0.2, the average floodplain flow in the valley direction was greater than the main channel average flow velocity. Floodplain roughness progressively increased to single channel Manning's n and Darcy-Weisbach by up to 100 % and 300 % respectively in high overbank depth. The Manning's n value in the mobile-bed main channel is generally greater than the floodplain

Manning's *'n'* for both rough and smooth cases. At high relative depth, Dr greater than 0.4, the main channel and floodplain Manning's *'n'* values are identical, reflecting that the flow resistance is becoming more uniform in high overbank flows.

2.7 Effects of Vegetation on Flow Structures

Stream flows with vegetation on the floodplains are quite common in nature. This vegetation has a significant influence on flow structures of especially rivers with large floodplains. Thus, it is important to estimate accurately the impact of vegetation on the carrying capacity of rivers with floodplains (Choi and Kang, 2004). Wu, *et al.* (2001) used two-dimensional depth average mathematical models to investigate the influence of mangrove on flow structures. They found that the mangrove largely reduced the velocity on the floodplain and thus resulted in a significant increase in the velocity in the main channel. Mazda *et al.* (1995,1997) studied a drag force induced by the mangrove swamp in real life condition and found from the simulation results that it greatly reduced the flow in the longitudinal direction in the mangrove swamp and suggested that the vegetated floodplains effectively operates as a storage basin rather than a pass-way. Many researchers among them Struve *et al.* (2003), Elliot (2000), Antze *et al.*(2001), and Nicholas (2004) carried out laboratory experiments on flumes with vegetated floodplains and found that the drag forces created by the vegetation had influenced the flow structure in the main channel. Kouwen and Moghadam (1997, 2001) reported that the Manning's roughness coefficient increases proportionally to the square root of the flow depth, for a tree canopy with a linear relationship between momentum absorbing area and the depth of the submergence of the vegetation. The next section will discuss in detail works that had been carried out by other researchers pertaining to flows through vegetation.

2.7.1 Flow Resistance for Non-Rigid and Rigid Vegetation

Flow resistant problems in vegetated channel can be classified into submerged vegetation and unsubmerged vegetation flow. Most efforts to study vegetative resistance have concentrated on studying submerged and rigid roughness. There is only a small amount of available field data, other than overall roughness coefficients,

representing limited flow conditions. Most laboratory studies have been conducted using artificial roughness. Studies concerning flow resistance with vegetation had been conducted by Li and Shen (1973), Petryk and Bosmajian (1975), Fathi and Kouwen (1997), Nepf (1999), Wu *et al.* (1999), Kouwen and Fathi, (2000) and Jarvela (2002).

Recently, some researchers carried out experiments using actual plants (Kouwen and Fathi, 2000 and Jarvela, 2002). Li and Shen (1973) studied the effect of tall, unsubmerged vegetation on flow resistance by investigating the wake caused by various cylinder set-ups. Experimental results indicated that different patterns of cylinders significantly affected flow rates. For unsubmerged vegetations, they expanded their method to calculate the drag coefficient for a single plant in a group and further the friction factor for the vegetation. The governing equation for the friction factor is readily measurable physical properties in addition to the drag coefficients for longitudinal and lateral distances between the plants and the plant diameter. Drag coefficient is determined through an iterative process including empirical relationships, which are formulated from experiments on rigid cylinders.

Nepf (1999) carried out experiments using a cylinder-based model of vegetation resistance by including the dependence of the bulk drag coefficient, $\overline{C}_D$ on the vegetation density for $Re > 200$. This model confirms the drag, turbulence and diffusion in flow through emergent vegetation. The results show that the turbulence intensity is dependent on the vegetative drag and that for vegetative densities bigger than 1 %, the bed-drag and bed shear production are negligible compared to their vegetation counterparts. Further, the fraction of mean energy partitioned to turbulence depends on the morphology and flexibility of the stems and stem Reynolds number.

In any analytical method for estimating the contribution of vegetation to the total flow resistance, the drag force exerted by the vegetation on the flow must be considered. The flow velocity through vegetation is reduced due to the momentum from the fluid to the vegetation, which occurs due to the drag force. Wu *et al.* (1999) and Jarvela (2002) simulated an experiment for vegetation under uniform flow conditions in a straight channel and proposed a simplified model to estimate the

vegetation drag coefficient for submerged and non-submerged vegetation. They showed that the magnitude of the drag force exerted by a single vegetation element is a function of the frontal area of the element projected onto a plane perpendicular to the flow direction. In hydraulic calculations, it is convenient to use an expression for the drag force exerted in a controlled volume. The sum of the areas of the individual plant elements in the direction of flow for a control volume is the vegetation density.

Fathi and Kouwen (1997) and Kouwen and Fathi (2000) used coniferous tree saplings and branches in flume experiments and showed that the friction factor varied enormously with mean flow velocity due to the bending of the vegetation, and with flow depth as a result of an increase in the submerged momentum-absorbing area. The initial study showed a good correlation between the friction factor and the flow velocity normalized with a vegetation index, a parameter which took into account the effects of the shape, flexibility and biomass of the particular tree species.

2.7.2 Non-Rigid, Unsubmerged Vegetation on Floodplains

Fathi and Kouwen (1997) studied the case of non-rigid, unsubmerged, vegetation roughness on floodplains. They studied the effect of different values of velocity and depth of flow on the friction factor value. They also proposed a model to calculate the Manning's n or Darcy-Weisbach f friction factors for unsubmerged flexible vegetation in the vegetated zone of river cross-sections. They concluded that both the Darcy-Weisbach friction factor and Manning's n varied greatly with the mean channel flow velocity due to the bending of vegetation and with flow depth as a result of the increase of the submerged momentum-absorbing area. They also developed a dimensional analysis approach to obtain a relationship between rough conditions and flow conditions. The following section will review their work in this area.

- **The Effect of Velocity and Depth on the Friction Factor**

Fathi and Kouwen (1997) studied the effect that the depth of flow can have on the resistance to flow. Their main concern was that there might be an extreme variation of roughness with depth of flow due to the large increase in the momentum-absorbing area in the unsubmerged vegetation as the depth of flow is increased. This might lead

to a conclusion that all the available roughness equations, which are based on the relative roughness approach, would have a weak applicability in these circumstances. Their main concern was that the non-rigid vegetation on floodplains was usually assumed to behave as rigid roughness which could lead to large errors in the relationship between velocity and drag force. They developed a dimensional analysis approach that was supported by experimental results. The purpose of this approach was to obtain a relationship between roughness conditions in non-rigid vegetation flow, which includes the density and flexural rigidity of trees, and the flow condition, which includes velocity and depth of flow for floodplains and vegetation zones of natural waterways.

From the results, they found that a linear relationship appeared to exist between drag force and velocity. For a rigid roughness, the drag is expected to increase linearly with the square of the velocity. The difference can be explained by the deflection of the plant foliage area and the reduction of the drag coefficient C_D with the increase of the flow velocity. They concluded that if a linear increase of the momentum-absorbing area with the depth of flow can be assumed.

The Manning's roughness coefficient increases proportionally to the square root of the flow depth and is inversely proportional to the mean velocity. They also concluded that, regardless of tree species or foliage shape and distribution, the variation of the Manning's *'n'* with depth is due merely to the increase of the submerged momentum-absorbing area with the depth of flow, thus the density of vegetation is always a dominant parameter for the unsubmerged condition.

- **Friction Factor for Unsubmerged Flexible Vegetation**

Kouwen and Fathi (2000) proposed a model to calculate the Darcy-Weisbach friction factor *'f'* and Manning's *'n'* for unsubmerged, flexible vegetation in the vegetated zones of a river cross-section. The model accounts the effect of velocity, depth of flow and type of vegetation with readily defined and measurable parameters of flow and vegetation. The proposal was to help researchers to select the values of Manning's *'n'* for a particular condition of flow and vegetation and to give information

on how the resistance might change with velocity and flow depth.

The results of the experiments results showed large variations of Manning's *'n'* with velocity, flow depth, vegetative stiffness and density. The approach used depended on the approach by Fathi and Kouwen (1997). In this approach it was assumed that the dominant parameters for estimating the resistance parameter for flow through unsubmerged isolated plants in a canopy are C_D, which is the average drag coefficient based on the total frontal area of biomass, the flow properties and the vegetative properties. The flow properties considered are the average channel velocity, the density of the fluid, the fluid viscosity, the gravitational constant and the flow depth. The vegetative properties considered are the total upstream exposed area of submerged biomass, the flexural rigidity of the plant, the average canopy height and the characteristic length that represents the spacing or density of plant in a canopy. It was assumed that the bed shear stress is negligible compared to the total plant drag and that the plant stem and foliage are uniformly distributed. In the analysis, they developed a general mathematical model for estimating the friction factor *'f'* 'in flexible, unsubmerged vegetation. An important conclusion deduces by Kouwen and Fathi is that the variation of the Manning's *'n'* with the depth of flow is only due to the increase of submersion of the momentum-absorbing area with flow depth. The density of vegetation is always a dominant parameter for the unsubmerged condition.

2.7.3 In Rigid Unsubmerged Vegetation

Larger vegetation such as shrubs and trees are found in the floodplains adjacent to the main channel. This type of vegetation is a major influence on flow depth and resistance during overbank flooding. Li and Shen (1973) studied the effect of tall, unsubmerged vegetation on flow resistance by investigating the wake caused by various cylinder set-ups. Results indicated that different patterns or groupings of cylinders significantly affected flow rates. Since the larger types of vegetation constitute much of the resistance within floodplains, Petryk and Bosmajian (1975) proposed a method to calculate flow resistance based on the drag forces created by the larger plants. They derived an equation for Manning's *'n'* by summing the pressure

force, gravitational force, shear force and the drag force in the longitudinal direction.

There are some limitations on Petryk and Bosmajian's equation. The channel velocity must be small enough to prevent bending or distortion of the shape of the vegetation and large variations in velocity cannot occur across the channel. Vegetation must also be distributed relatively uniformly in the lateral direction. Finally, the flow depth must be less than or equal to the maximum vegetation height. During flooding, the velocities over the floodplains can be relatively high and large degrees of bending and distortion of vegetation will occur. Vegetation can also vary widely across a floodplain and flood depths often submerge vegetation. However, when tree trunks dominate sections of a floodplain, this method can be used for predicting the total roughness coefficient.

Kadlec (1990) studied the blockage and drag forces due to plants. The work focuses on determining the energy slope for wetland types of plants, especially grassy types of plants, and on wetland flows that are laminar to transitional in terms of Reynold's number. Since his study was limited to fairly low velocities, his analysis was based on the flow blockage of rigid plant stems and a small range of shallow flow depths. He acknowledged that the determination of Manning's '*n*' require flow data for different depths and would be quite difficult. Further, he proposed that flow resistance could be based on the summation of drag forces from individual plants, which is the basis for the theoretical development in his study.

- **Resistance Due to Drag Forces**

In order to be able to find the drag force on a body immersed in fluid, detailed information on the shear stress and pressure distribution on the body is needed. This is very difficult to accomplish, which is why the dimensionless drag coefficient, C_D, is used as an alternative. The values of C_D are found by means of a simplified analysis, numerical techniques, or an appropriate experiment. According to dimensional analysis arguments, the flow characteristics should depend on various dimensional parameters. The most important parameters of these are the Reynolds Number (*Re*) and Froude Number (*Fr*). The importance of the Froude Number increases for flow with a free

surface (Chow, 1959). At high Reynolds Number, form drag predominates and C_D becomes independent of *Re*. The drag becomes due almost entirely to the pressure distribution around the body (Bruce *et al.* 1994). This observation is also evident from bridge pier studies. According to Henderson (1966), the resistance to flow of normal bridge pier shapes is such that the drag coefficient is over unity. This implies that form drag is a substantial part of the total drag so that the Reynolds Number will be relatively unimportant.

Mazda *et al.* (2005) observed that the water flowing within mangrove swamps is resisted by the drag force due to mangrove tress and their roots, by the bottom friction on the uneven mud floor, and by the eddy viscosity due to turbulent motions of water through narrow openings between trees/roots. The mechanisms of the drag force in mangrove swamps include the effect of the bottom friction have been analysed quantitatively by Mazda *et al.* (1997b) and Magi (2000), while Mazda *et al.* (2004) and Okada (2004) have studied the eddy viscosity in mangrove swamps theoretically and in field observation. Further Mazda et al. (2005) concluded that using field data observation and basic fluid mechanics laws, the drag coefficient and the coefficient of eddy viscosity are found to be predictable as a function of the Reynolds Number based on the characteristic length scale of the vegetation. The characteristic length scale of the vegetation varies greatly with the vegetation species, vegetation density and tidal elevation. Both of these coefficients decrease with increasing value of Reynolds Number.

- **Factors Influencing the Friction Factor**

It is incorrect to assume that compound channels to have same the value Manning's *'n'* for channels and floodplain all the time, especially when discussing the case of vegetation roughness, which changes in height and density throughout the year. Manning's 'n' is the function of several factors.

The fluid property affecting flow resistance is the viscosity of the water. Cruise *et al.* (2003) explained this in determining the internal shear or deformation of the flow on the micro-scale level. Viscosity is introduced in fluid mechanics as a parameter in

the Reynolds number. It is known that for cases where the projection element of the bed roughness breaks through the laminar sub layer, the former will dominate the flow behaviour. The flow will then be fully rough and resistance will exist due to form drag on the projections. According to Henderson (1966), in this case the resistance coefficient is independent of the Reynolds Number. It is reasonable to assume that the same would be true for the case of rigid non-submerged flow where the effect of form drag is much more significant and the flow is fully rough. The concept that at high Reynolds numbers, the drag force is dependent upon inertia effects only, was also advanced by Gerhart and Gross (1985).

The flow conditions that are expected to have major effect on the friction factor are the velocity and depth. Fathi and Kouwen (1997) have studied the non-submerged non-rigid vegetation and concluded that the Darcy-Weisbach friction factor '*f*' and the Manning's '*n*' vary tremendously with the increase of flow depth due to an increase of the submerged momentum-absorbing area. For the case of the flow past rigid objects in an open channel, the friction factor will decrease with the increase of velocity as a result of changing conditions around the object.

2.8 Salinity Transport

The most direct way of finding salinity transports is to measure the current at various depths. The current in an estuary is usually dominated by the tide. The salinity field is moved back and forth with the tide, but the vertical salinity profile (the variation of salinity with depth) is not affected by the tidal movement. The basis for salt balance techniques is the diffusion equation for salt. For a two-dimensional estuary it can be written as,

$$\frac{\partial(uS)}{\partial x}+\frac{\partial(wS)}{\partial z}-\frac{\partial}{\partial x}\left(K_h\frac{\partial S}{\partial x}\right)-\frac{\partial}{\partial z}\left(K_v\frac{\partial S}{\partial z}\right)=0 \qquad (2.13)$$

u and w are the horizontal and vertical component of velocity, S is salinity, K_h and K_v are the horizontal and vertical turbulent diffusion coefficients for salt, x is the horizontal coordinate measured positive from the inner end of the estuary towards the

sea and z is the vertical coordinate measured positive downward. The first term in the equation expresses transport of salt by horizontal current (horizontal advection). The second term expresses transport of salt by vertical water movement (vertical advection). The third term represents the net transport of salt from horizontal turbulent mixing, and the last term gives the contribution to the salt transport from vertical turbulent mixing. Note that all turbulent mixing is the result of tidal action; the importance of turbulent mixing in the balance of salt transport processes therefore depends on the strength of the tide.

The equation can be simplified for the different classes of positive estuaries. In the salt wedge and highly stratified estuary all salt transport is achieved by advection only, and the diffusion equation for salt represents a balance between horizontal and vertical advection,

$$\frac{\partial(uS)}{\partial x}+\frac{\partial(wS)}{\partial z}=0 \tag{2.14}$$

The vertical velocity w here represents the effect of entrainment from the lower layer into the upper layer.

In the slightly stratified estuary movement of salt between the upper and lower layer is achieved by turbulent mixing. Horizontal mixing is still small and unimportant, and the diffusion equation gives a balance between three processes,

$$\frac{\partial(uS)}{\partial x}+\frac{\partial(wS)}{\partial z}-\frac{\partial}{\partial z}\left(K_v\frac{\partial S}{\partial z}\right)=0 \tag{2.15}$$

The vertically mixed estuary is characterised by vertically uniform property distributions, which means that all terms in the diffusion equation which express vertical changes vanish. This leaves again a balance between only two processes, horizontal advection and horizontal tidal turbulent mixing, which becomes essential to the balance,

$$\frac{\partial(uS)}{\partial x} - \frac{\partial}{\partial x}\left(K_h \frac{\partial S}{\partial x}\right) = 0 \qquad (2.16)$$

A variation on the last situation occurs in vertically mixed wide estuaries which display a significant lateral salinity variation (variation of salinity across the estuary). In such situations mixing in the lateral direction (horizontal mixing across the estuary) and lateral advection (water movement across the estuary) are usually more important than up-estuary diffusion (horizontal mixing along the axis of the estuary). The diffusion equation then represents a balance of three processes, one in the direction x of the estuary axis and two in the direction y across the estuary (v here refers to the velocity component in the y direction).

2.9 Numerical Modelling in Hydraulic Engineering

The application of numerical modelling in hydraulic engineering was recent compared to other engineering disciplines. This is due to, among others, the complexity of the problem and the uncertainty in defining the boundary conditions. Firstly, the domain to be considered is large with variables in all dimensions and dependent on the flow and boundary conditions. With the evolution of computers, complex problems in hydrodynamic can be solved with the introduction of numerical models. Abbott (1997) classified the use of models into several components base on their application. **Table 2.2** shows the schematisation of range of application of tidal modelling, Modelling can be divided into one dimensional, two dimensional and three dimensional modellings. Cerco (2003) discusses in detail both scientific and engineering modellings.

Various numerical models have been development over the years in trying to solve engineering problems to predict salinity intrusion, flows, water quality, sediment and pollutant transport. These numerical models are either available commercially or in public domain. Hydrodynamic software such as TELEMAC, CFX, MIKE 21, DIVAST, POM, SSIM and RMA-2 are some of the commercial and public domain numerical models that are available for solving engineering problems. In many engineering practices, a one-dimensional model is commonly used to simulate the

effects on the changes of bed topography of river estuaries, whereas a two-dimensional model is used to simulate flows in river estuaries, coastal zones, and wide rivers and to study salinity intrusion, sediment transport, pollutant dispersion, dam failure and other modelling works. At present, two-dimensional models are commonly used for engineering practices, because it gives better understanding of the problems compared to one-dimensional models.

As for a three-dimensional model, it is normally used for situations involving stratification, secondary currents, horizontal density effects and buoyant plumes. Due to its complexity and time consumption, three-dimensional modellings are normally concentrated on scientific research rather than in engineering practices. Several researchers have made an attempt to apply 3-D numerical modelling for real applications with little success. The reason is due to the difficulties in obtaining field data for the model input. The data are important for verification and validation of a model.

2.9.1 One-Dimensional (1- D) Modelling

Among the earliest of a mathematical formulation for the flow is related to the works of St. Venant. He formulated the unsteady flow equations describing a flood wave along the river. His mathematical model based on two partial differential equations accounting for mass and momentum conservation in the physical system can be expressed as follows,

$$B\frac{\partial h}{\partial t}+\frac{\partial Q}{\partial x}=q_s \tag{2.17}$$

$$\frac{\partial Q}{\partial t}+\frac{\partial}{\partial x}\left[\frac{\beta Q^2}{A}\right]+gA\frac{\partial h}{\partial x}+gA\frac{Q|Q|}{K^2}=0 \tag{2.18}$$

where B is the channel width and Q is the channel discharge. 'A' is defined as the wetted cross-section area and β is the momentum correction factor for non-uniform velocity profile. Whereas K and q_s is the channel conveyance and the lateral inflow

respectively and h is the water surface elevation.

The underlying assumptions made for both the equations are,

(i) The flow in the channel is one directional (where velocity is uniform over any cross-section and the water level is horizontal in transverse direction)

(ii) The streamline curvature is small and the vertical acceleration vertical is negligible (hydrostatics pressure)

(iii) The effects of boundary condition and turbulence can be accounted through the resistance laws analogous to those used for steady state flows

(iv) The overall average channel slope ø is small which is $\sin\theta = \theta$ and $\cos\theta = 1$.

Due to their non-linear nature, St. Vernant equations cannot be solved analytically, therefore the equations need to be discretised before solving using a numerical method. The most common method used in river modelling is the finite element technique such as MIKE11. In such case, the channel is discretised in different reaches, all of which are accounted for by a single typical representative cross-section.

One-dimensional numerical models originated from Isaacson, Stoker, and Troesh (1954), who modelled parts of Ohio and Mississippi rivers and subsequently ran a mathematical model for both rivers. With the rapid development of computer technology and numerical treatment, large-scale numerical models can be implemented by consulting firms such as SOGREAH of France for Mekong Delta Study and Senegal river study in 1960s and 1970s (Cunge *et al.* 1980). In this country, firms such as Mott MacDonald, Babtie Shaw, Molten, Sir William Halcrow and Partners and most Hydraulics Research Stations have developed their own river modelling codes.

In the United States, the U.S. Army Corp of Civil Engineers developed the HAC-RAS which are widely used in research and practice. A one-dimensional model

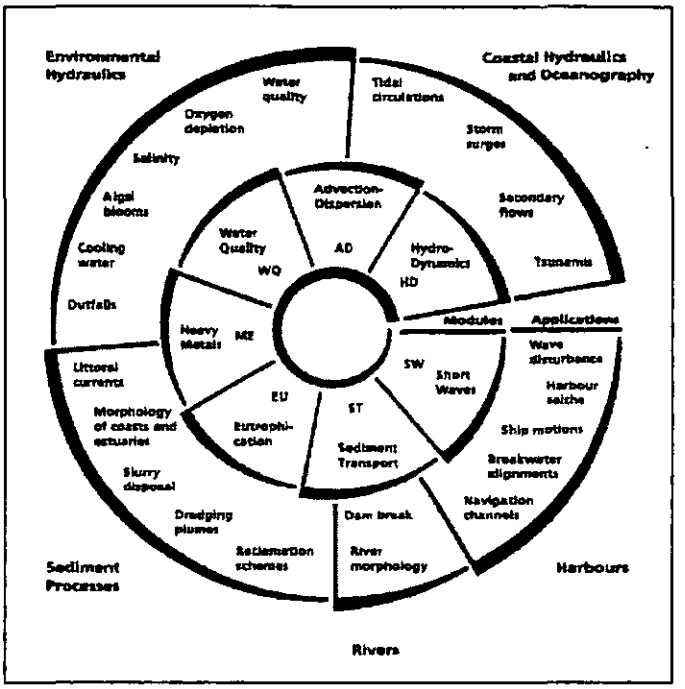

Table 2.2 –Schematisation of Range of Application of Tidal Modelling, Showing Relations to Other Areas of Modelling Activity (Abbott, M.B, 1997)

is commonly used for river modelling, in particular to determine the impact of serious flood events. Lin *et al.* (2002) developed FASTER which is used to predict water elevations, velocities and solute in a well mixed rivers or narrow estuaries.

2.9.2 Two Dimensional (2–D) Modelling

A two-dimensional model is based on the depth-average Navier-Stokes equations. The continuity and momentum equations can be written as follows,

$$\frac{\partial h}{\partial t}+\frac{\partial (hu)}{\partial x}+\frac{\partial (hv)}{\partial y}=0 \tag{2.19}$$

In x direction,

$$\frac{\partial u}{\partial t}+u\frac{\partial u}{\partial x}+v\frac{\partial u}{\partial y}=-g\frac{\partial Z}{\partial x}+F_X+\frac{1}{h}div\left[h(v_t+\mu)grad\bar{u}\right] \tag{2.20}$$

In y direction,

$$\frac{\partial v}{\partial t}+u\frac{\partial v}{\partial x}+v\frac{\partial v}{\partial y}=-g\frac{\partial Z}{\partial y}+F_Y+\frac{1}{h}div\left[h(v_t+\mu)grad\vec{v}\right] \qquad (2.21)$$

Where v_t, μ, h is the turbulent viscosity, dynamic viscosity and water depth. Whereas F_X, F_Y *and* Z is the source terms and the position of free surface elevation respectively.

The basic assumptions used in 2-D models are,

(i) The vertical velocity is neglected

(ii) The wavelength is relatively larger than the depth of flow

(iii) The velocity is uniform over the depth

(iv) The effects of boundary friction can be accounted for through resistance law similar to those used in 1-D model.

The first models used a finite difference technique (Leendertsee 1967,1978; Vreugdenhil and Wijbenga 1982) and the method of characteristics (Towmson 1974). Among the numerical codes available that use the finite difference techniques are DIVAST (Depth Integrated Velocity and Solute Transport), originally developed by Falconer (1980) , POM (Princeton Ocean Model) by Mellor and Blumberg (1983), TRIM 2D (Tidal, Residual, Inter-Tidal Mudflat) by Cheng (1982), MIKE 21 developed by the Danish Hydraulic Institute. With the development of the finite element method (Brebbia *et al.*1978; Wang *et al.*1985) and associated numerical techniques (Brookes and Hughes 1982; Hervouet 1992) enhanced hydraulic codes were produced. Among them are the RMA-2 by King and Norton (1978), and TELEMAC 2-D by Hervouet (1991). The finite element method has proven to be very useful in representing complex geometries; however, it is a demanding method to implement numerically and has been associated with mass-conservation difficulties.

The third method is the finite volume method used to solve the full Navier-Stokes equations (Patankar and Spalding 1972; Demirdzic *et al.* 1987; Karki and Patankar, 1988). The finite volume method is conservative, numerically accurate, and

simple. It has been applied to a few two and quasi three-dimensional flow problems (Wilson *et al.* 2003a, 2003b; Lai and Yen 1992). Early application of two-dimensional work has been focused on lake and coastal applications. Among them are Paltzmann (1958) in his investigation on surge storm in lakes. Kuiper and Vreugdenhil (1973) uses a shallow water approach in investigating a variety of steady state problem and river channel. McGuirk and Rodi (1978) and Lean and Wearne (1979) used two-dimensional analysis to reproduce recirculation effects in harbours and estuaries, and Falconer (1984) for simulation of water quality prediction in tidal embankments.

At present, the focus has extended to include flood and dam break analysis in particular after the considerable works related to wetting-and-drying and adaptive meshing were carried out (Lynch and Gray 1980; Akanbi and Katopodes 1988; Molinaro and Natale 1994; Tchamen and Kawahita 1994,1998). Bates *et al.* (1993,1996) demonstrated the capability of the finite element code TELEMAC 2D to reproduce the transit of a flood wave and the flood map dynamically. The present codes did support river model of up to 60 km (Bates, Anderson and *et al.* 1996*)*. Other researchers like Wijbenga (1985), Akanbi and Katopodes (1988), King and Roig (1991), Paquier and Farissier (1997), Sleigh *et al.* (1998) and Rameshwaran and Shiono (2003) have documented the use of the two-dimensional approach for flood modelling. Hervouet and Rouge (1996) and Zoppou and Robert (1999) used the shallow water equations to replicate the catastrophic collapse of the Malpasset dams and water supply reservoir.

2.9.3 Three-Dimensional (3-D) Modelling

The applications of three-dimensional modelling in the civil engineering fields are quite recent. TRISULA (Delft Hydraulics, The Netherlands), MIKE 21 (Danish Hydraulics Institute) and TELEMAC 3D (EDF-DER, France) are among the first such commercial packages available in the market. These packages are not fully three-dimensional as they rely on the hydrostatic assumption to obtain a solution on a layer-average format (the results from two-dimensional solution stacked vertically). Vertical velocities are determined from the conservation of mass. As such, these codes are unsuitable for complex three-dimensional flow features and can be referred to as quasi

three-dimensional codes. They are not designed for detailed three-dimensional flows with fast vertical velocities. Their main applications are in the field of coastal and ocean engineering where a layered approach is adequate to account for the relative low vertical velocities. Their objective is to represent horizontal currents, salinity, and temperature gradient in water column (Peltier *et al.* 1996; Gross *et al.* 1999) Leendertsee *et al.* (1973), Blumberg and Mellor (1983), Hall *et al.* (1992), Peltier *et al.* (1996) have applied this model to compute flow, water quality and sediment transport in seas and estuaries. Liggett (1969), Koutitas and O'Connor (1980), Falconer *et al.* (1980) used the above type model to determine the recirculation of currents in bays and lakes.

Whereas others such as Benqué *et al.*(1982), Blumberg *et al.* (1993), have an attempt to reproduce velocity fields in rivers even for flood flow (by Ammer and Valentin, 1993). Lavedrine (1996,1997), Wilson *et al.* (2003) and Olsen (2003) reproduced a Flood Channel Facility test. In cases where sediment transportation is investigated in channels, the hydrostatic pressure assumption shows its limitations. This is due to the failure to reproduce the pressure-driven recirculation (Shimizu *et al.* 1990), and the flow concentration at the inflection point of a bend in a large depth ratio flooded channel (Fukuoka and Watanabe, 2000).

2.10 Summary

Estuary can be classified by its topography, salinity profile, and stratification-circulation process as discussed in this chapter. For topography, the estuary can further sub-divide according to their physical properties. Whilst for the salinity profile, the estuary can be sub-divided into three categories namely stratified, partially mixed, and well mixed. Among the main factors that affect the category are inflow of freshwater upstream, tidal effect, wind effect, temperature and density difference between the inflow of freshwater and the seawater at the estuary. For the stratification-circulation classification, the stratification is controlled by the ratio of freshwater and seawater. Simmons (1955) relates the freshwater flow per tidal cycle to the estuary type and concluded that if the ratio is unity the estuary is highly stratified. If it is between 0.5 to

0.3 it is partially mixed whereas 0.1 and below is well-mixed. Hansen-Rattray (1966) developed a diagram based on the stratification and circulation. They used the stratification and circulation parameters to classify an estuary. Fishers (1972) used a relationship of Froude Number and Richardson Number to classify an estuary.

Most of the previous studies for flow through vegetation were carried using physical model. The vegetation used was either rigid or flexible made from rod and artificial foliage. The velocity readings are measured as the depth of flow varies. The majority of the researchers used straight channels with large floodplain and with fully submerged vegetation.

Numerical modelling for one-dimensional, two-dimensional, and three-dimensional together with their applications in the civil engineering practices were discussed. Their advantages and disadvantages were also mentioned in this chapter.

CHAPTER 3

GOVERNING EQUATIONS AND THEORETICAL BACKGROUND

3.0 Introduction

The fluid flow is assumed to be Newtonian, incompressible and having constant physical properties. The flow is based on the principles of continuity of mass and conservation of momentum within the body of fluid concerned. It is governed by a time-averaged formulation of Reynolds Average Navier-Stokes equations. These equations are derived from Newton's Second Law of motion, which relates the forces exerting on the system and the rate of change of momentum of that system. This chapter presents the governing equations of flows in estuarine waters.

3.1 Two Dimensional (2-D) Flows

The two-dimensional Shallow Water or St. Venant equations are obtained by depth averaging the Navier Stokes equations. The new variables obtained are means values over the depth. The two components of the horizontal depth averaged velocities, u and v is given by,

$$u = \frac{1}{h}\int_{Zf}^{Z} U_1 dz \quad \text{and} \quad v = \frac{1}{h}\int_{Zf}^{Z} U_2 dz \tag{3.1}$$

where Zf is the bottom elevation and Z = free surface elevation as shown in **Figure 3.1** The height of water is denoted by 'h'.

Solving the above equations will determine the values of u, v and h in the entire domain with respect to the functions of time, initial and boundary conditions.In applying the above equations, the assumption made is that the vertical acceleration is considered negligible, thus the hydrostatic pressure is given by the following expression,

$$-\frac{1}{\rho}\frac{\partial p}{\partial z} - g = 0 \tag{3.2}$$

where p(x,y,z) is given by the following expression; $-\rho gz$ + constant

The constant is chosen so that the p(x,y,Z)= 0 where Z is the level of free surface. The atmospheric pressure is assumed to be zero. Thus the pressure function will lead to,

$$p(x,y,z) = \rho g(Z-z) \tag{3.3}$$

$$p(x,y,zf) = \rho g(Z-Zf) = \rho gh \tag{3.4}$$

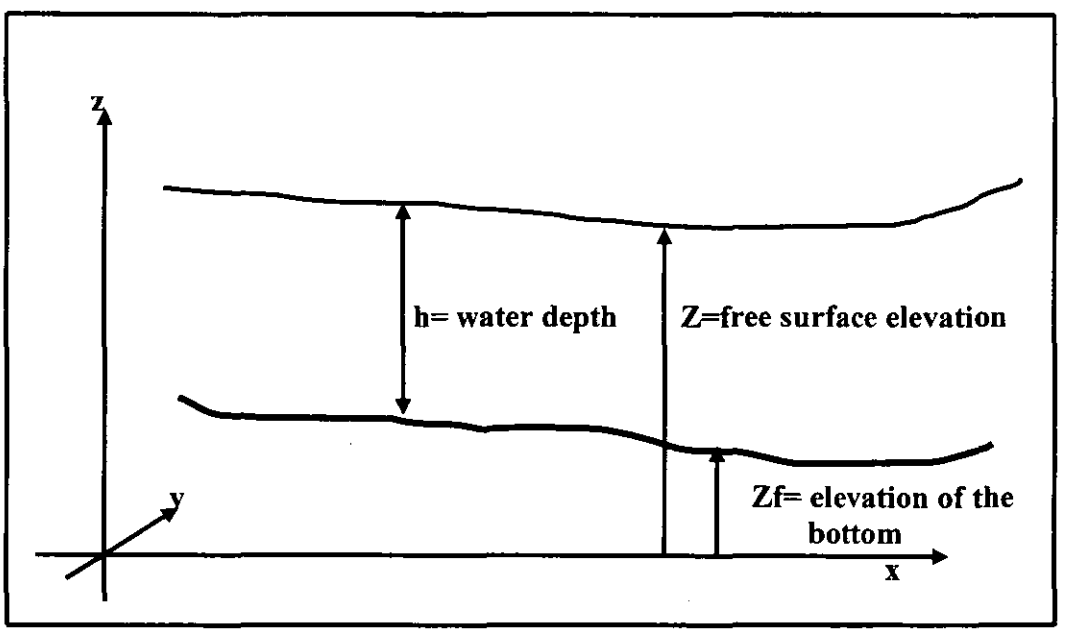

Figure 3.1 – Definition of Bottom Topography and Free Surface

Equations (33) and (34) is the pressure at the surface and bottom respectively. The water depth is denoted by h.

Figure 3.1 shows the definition of free surface and bottom topography. For the St. Venant equations, the vertical velocity is assumed small and will not be considered in the

equation. This approximation is linked to the hypothesis of hydrostaticity that requires the vertical accelerations to be negligible. The step slope should be avoided against the flow direction. The impermeability of the bottom and free surface can be written as,

$$\frac{\partial Z}{\partial t}+U^{s}.n=0 \text{ and } \frac{\partial Zf}{\partial t}+U^{f}.n=0 \tag{3.5}$$

where U^s is the free surface velocity and U^f is the bottom velocity. 'n' is defined as the vector normal to the surfaces with the components. $(\partial Z/\partial t, \partial Z/\partial y, -1)$ and n is not equal to 1. The derivation of Shallow Water Equations is based on Leibnitz's Rules according to the following formula,

$$\frac{\partial}{\partial x}\int_{zf}^{Z} F dz = \underbrace{\int_{zf}^{Z}\frac{\partial F}{\partial x}dz}_{1} + \underbrace{F(x,y,Z)\frac{\partial Z}{\partial x}}_{2} - \underbrace{F(x,y,Zf)\frac{\partial Zf}{\partial x}}_{3} \tag{3.6}$$

where F is defined as flux in x, y and Z direction. Where Z and Zf is defined as free surface elevation and elevation of the bottom (bed)

For the permeability condition, the second and third terms will disappear.
The averaging procedure of the non-linear terms will give rise to a new expression contained in the three-dimensional variables. This expression is given by,

$$\frac{\partial}{\partial y}\int_{zf}^{Z} U_1 U_2 dz = \frac{\partial}{\partial y}(huv) + \underbrace{\frac{\partial}{\partial y}\int_{zf}^{Z}(U_1-u)(U_2-u)dz}_{dispersion} \tag{3.7}$$

The second term on the right hand side of the above expression cannot be reduced to a simpler form unless U_1 and U_2 are constant in vertical. This term is generally called the dispersion term. The existence of this dispersion term will limit the Shallow Water Equations, if the horizontal velocity varies excessively along the vertical.

For two-dimensional flows, the continuity and the momentum equations are given by the following formula,

Continuity equation,

$$\frac{\partial h}{\partial t} + u.\vec{\nabla}(h) + h\,\mathrm{div}(\vec{u}) = 0 \tag{3.8}$$

Momentum equations,

$$\frac{\partial u}{\partial t} + \vec{u}.\vec{\nabla}(u) = -g\frac{\partial Z}{\partial x} + S_x + \frac{1}{h}\mathrm{div}(hv_t\vec{\nabla}u) \tag{3.9}$$

$$\frac{\partial v}{\partial t} + \vec{u}.\vec{\nabla}(v) = -g\frac{\partial Z}{\partial y} + S_y + \frac{1}{h}\mathrm{div}(hv_t\vec{\nabla}v) \tag{3.10}$$

Tracer conservation,

$$\frac{\partial T}{\partial t} + \vec{u}.\vec{\nabla}(T) = S_T + \frac{1}{h}\mathrm{div}(hv_T\vec{\nabla}T) \tag{3.11}$$

The St. Venant equations are derived from Navier-Stokes equations by averaging the vertical depth of flows. Where S_x and S_y is a vector source terms (friction, Coriolos force and wind stress) in x and y direction respectively. v_t is the kinematic turbulent viscosity and S_T is the source term. Z is the free surface elevation as shown in **Figure 3.1**

3.2 Three Dimensional (3-D) Flows

Three dimensional flows solve the Navier-Stokes equations with free surface elevation. The governing equations are given as follow,

Continuity Equations,

$$\mathrm{div}(\vec{u}) = 0 \tag{3.12}$$

Momentum equations,

$$\frac{\partial u}{\partial t} + \vec{u}.\vec{\nabla}(u) = -\frac{1}{\rho_0}\frac{\partial p}{\partial x} + \mathrm{div}\left(v_t\vec{\nabla}u\right) + S_x \tag{3.13}$$

$$\frac{\partial v}{\partial t}+\vec{u}.\vec{\nabla}(v)=-\frac{1}{\rho_0}\frac{\partial p}{\partial y}+\mathrm{div}\left(\nu_t\vec{\nabla}v\right)+S_y \tag{3.14}$$

The hydrostatic pressure is given by,

$$p=\underbrace{\rho_0 g(Z-z)}_{p_0}+\underbrace{\rho_0 g\int_z^S\frac{\Delta\rho}{\rho_0}\partial z}_{\Delta p} \tag{3.15}$$

For 3-D Tracer Conservation the equation is given by,

$$\frac{\partial T}{\partial t}+\vec{u}.\vec{\nabla}(T)=\mathrm{div}\left(\nu_T\vec{\nabla}T\right)+S_T \tag{3.16}$$

where h is the depth of water in meters and u,v,w is the velocity component in the x,y,z directions. T is the tracer in g/l or °C and g is the gravitational acceleration (m/s^2). The term S_x,S_y is the source or sink terms measured in m/s^2 and S_T is the source or sink of tracer measured in g/l/s. ν_t, ν_T is the turbulent viscosity and tracer diffusion coefficient having the unit of m^2/s, whereas Z, t and x and y are the free surface elevation meters, time in second and horizontal space components respectively. P_0 is the reference density while p is the pressure and $\Delta\rho$ is the variation in density.

3.3 Bottom Friction

Bottom friction is important in the computation of flow in rivers and estuaries. It has a significant impact on the results of water depth and velocity. In two-dimensional expression, bottom friction is given by,

$$\vec{\tau}=\frac{1}{2}\rho Cf\,|u|\,u$$

where ρ is the density, u is the flow velocity and Cf is the friction coefficient. In hydraulic, Cf is generally replaced with the Chezy coefficient and is given by $\sqrt{2g/Cf}$

3.3.1 Chezy's Law

According to Chezy law, the friction force will appear in a non-conservative momentum equation having the following form,

In longitudinal direction,

$$F_x = -\frac{1}{\cos\theta}\frac{g}{hC^2}u\sqrt{u^2+v^2} \tag{3.17}$$

In transverse direction,

$$F_y = -\frac{1}{\cos\theta}\frac{g}{hC^2}v\sqrt{u^2+v^2} \tag{3.18}$$

where θ is the bottom slope and h is the water depth. u and v are the velocity in longitudinal and transverse directions of flow. Whereas the Strickler coefficient is $C = K R_H^{1/6}$ where R is the hydraulic radius.

3.3.2 Manning's Law

Manning's formula is commonly used for bottom frictions in rivers and estuaries. It is given by the following equations,

$$F_x = -\frac{1}{\cos(\theta)}\frac{gn^2}{h^{4/3}}u\sqrt{u^2+v^2} \tag{3.19}$$

$$F_y = -\frac{1}{\cos(\theta)}\frac{gn^2}{h^{4/3}}v\sqrt{u^2+v^2} \tag{3.20}$$

where n denotes the Manning's coefficient and θ is the bed slope. g denotes the gravitational acceleration.

3.3.3 Nikuradse's Law

According to Nikuradse's Law, the Chezy coefficient is obtained from the following formula,

$$C=7.83 \text{ Log } (12\frac{h}{k_s}) \tag{3.21}$$

where h is the depth of water and k_s, is the size of sand grain.

3.4 Turbulent Flow

One of the major problems in the analysis of turbulent flow is in the choice of turbulence models (Viollet, 1977). From constant eddy to a full Reynolds-stress modelling, the complexity of the model increases so as in the prediction of accuracy of the model.

Turbulence modelling is generally based on Reynolds-Average Navier-Stoke Equations (RANS) decomposition of velocity, pressure and body force. The equations can be written as follows,

$$\left.\begin{array}{ll} \textit{For velocity,} & U_i = \overline{U}_i + U_i' \\ \textit{pressure,} & p = \overline{p} + p' \\ \textit{body force,} & f_i = \overline{f}_i + f_i' \end{array}\right\} \tag{3.22}$$

where U_i, p, f_i is the local velocity, pressure and body force respectively. The values $\overline{U}_i, \overline{p}, \overline{f}_i$ denote the mean velocity, pressure and body force. Whereas U_i', p', f_i' is the fluctuating velocity, pressure and body force .

Reynolds equations can be written as follows,

$$\frac{\partial(\rho\overline{U_i})}{\partial t}+\frac{\partial(\overline{U_iU_j})}{\partial x_j}=\frac{\partial}{\partial x_j}\left(-\overline{p}\delta_{ij}+\mu\left(\frac{\partial\overline{U}_i}{\partial x_j}+\frac{\partial\overline{U}_j}{\partial x_i}\right)-\underbrace{\overline{\rho u_i' u_j'}}_{R_{ij}}\right)+\rho\overline{f}_i+\rho g_i \tag{3.23}$$

where R_{ij} is known as the Reynolds tensor stress.

By applying the Boussinesq eddy viscosity concept, the Reynolds tensor stress can be expressed in terms of the local velocity gradient and yields the following expression,

$$\underbrace{-\rho\overline{u_i'u_j'} = \rho\nu_t\left(\frac{\partial\bar{U}_i}{\partial x_j}+\frac{\partial\bar{U}_j}{\partial x_i}\right)}_{\text{Bousineseq Hypothesis}} \underbrace{-\frac{2}{3}\rho k\delta_{ij}}_{2} \tag{3.24}$$

where δ_{ij} is the Kronecker delta which is 1 if i=j and 0 if $i \neq j$ and the value of k is given by $k = 0.5|u_i u_j|$. ν_t is defined as the turbulent viscosity.

The second term (2) in the above expression is small and often neglected. Substituting equation (3.24) into Reynolds equation will lead to the following expression,

$$\frac{\partial\bar{U}_i}{\partial t}+\frac{\partial\overline{U_iU_j}}{\partial x_j} = -\frac{1}{\rho}\frac{\partial\bar{p}}{\partial x_i}+\frac{\partial}{\partial x_j}\left(\underbrace{\nu+\nu_t}_{\nu_e}\left(\frac{\partial\bar{U}_i}{\partial x_j}+\frac{\partial\bar{U}_j}{\partial x_i}\right)\right)+\bar{f}_i+g_i \tag{3.25}$$

The effective viscosity is given by $\nu_e = \nu + \nu_t$, where ν and ν_t is defined as the kinematics viscosity and turbulent viscosity respectively. The above equation is also known as the three-dimensional Shallow Water Equations.

By taking the depth-average over the depth of water, the Reynolds equations will reduce to,

$$\frac{\partial(hu_i)}{\partial t}+\frac{\partial(hu_iu_j)}{\partial x_j} = -hg\frac{\partial Z}{\partial x_i}+\frac{\partial}{\partial x_j}\left(\underbrace{(\nu+\nu_t)}_{\nu_e}\left(\frac{\partial u_i}{\partial x_j}+\frac{\partial u_j}{\partial x_i}\right)\right)+\underbrace{h\bar{f}_i+(R_{i3}^{surf}-R_{i3}^{bot})}_{hF_i} \tag{3.26}$$

R_{i3}^{surf} and R_{i3}^{bot} is the vertical average Reynolds stress, surface and bottom respectively. Where i , j is referred to 1 , 2 and similarly with u_i, u_j referred to $\bar{U}_i$; $\bar{U}_j$. Then body and friction forces is denotes by hF_i.

3.5 Turbulence Modelling

In both engineering and academia, the most frequently employed turbulence models are the Eddy Viscosity Models (EVM). Although the rapidly increasing computer

advancement in the last decades, the simplistic models of EVMs still dominate the Computational Fluid Dynamics (CFD) community (Bredberg 2001).

Of all the turbulence models approach available, Reynolds Average Navier-Stokes (RANS) is used extensively in CFD. The time-average formulation approximates flow turbulence through the introduction of a suitable turbulence model and constitutes the best practical approach to the simulation of three dimensional flow problems in engineering. Turbulence closure models are required to formulate the unknown Reynolds stress terms or measurable quantities.

3.5.1 Constant Eddy Viscosity Models

This model is the most rudimentary turbulence model, though often used in hydraulic engineering. It consists of specifying a constant turbulent viscosity for the whole domain. For depth-average calculations, the turbulent viscosity is given by,

$$\nu_t = \mathrm{ku.h} \tag{3.27}$$

u. is the bottom frictional velocity, h is the water depth and k is a constant equal to 0.0765 (Rastogi and Rodi 1978).

This model is normally used in simple flow situation and it is valid in quasi-2D large water bodies, where it is always in an equilibrium state between the main driving force of the flow and the bottom friction, in which turbulence only plays a minor role.

3.5.2 Elder's Turbulence Model

Elder model is an extension of Taylor (1953) analysis on turbulent flow in pipe (Elder,1959). In this model, the different values of viscosity can be specified along and across the current. The longitudinal and lateral dispersion coefficient is given by,

$$k_l = a_l u.h \quad \text{and} \quad k_t = a_t u.h$$

where k_l and k_t are the longitudinal and transverse dispersion coefficients respectively. a_l and a_t are the dimensionless dispersion coefficient in longitudinal dispersion normally equals to 6.0 and transverse equals to 0.6. Whereas u_* is the frictional velocity and h is the water depth.

3.5.3 Prandtl's Mixing-Length Model

One of the first turbulence models to appear is the mixing-length model by Prandtl. It uses the turbulent mixing-length scale l_m, as the length scale. The velocity scale is computed using the length and velocity gradient. It is given by,

$$u \sim l_m \frac{\partial \bar{U}}{\partial y}$$

The mixing-length model thus becomes,

$$\nu_t \sim l_m^2 \left| \frac{\partial \bar{U}}{\partial y} \right|$$

with the Reynolds stress given by the Boussinesq hypothesis as shown in equation (3.24). The mixing-length is closely connected to the idea of a turbulent eddy or vortex. Such eddy would be restricted by the presence of a wall, and hence the length scale should be very close to a wall. The idea by Prandtl's is that the turbulent scale varies linearly with the distance to the wall and may be used as an initial condition for the turbulent mixing scale which equals to,

$$l_m = ky$$

where k is von Karman constant equals to 0.41 and y is a distance normal to the wall.The mixing-length models make the eddy viscosity local, in the meaning that the turbulence is only directly affected by surrounding flow, through the

local value of $\frac{\partial \bar{U}}{\partial y}$.

3.5.4 One Equation Model

In order to avoid the local behaviour of the mixing-length models, a transport equations is needed for some turbulent quantity. A model that could conserve turbulence should improve the predictions of flows that depend on both the streamwise and the wall-normal (cross stream) positions.

A most interesting turbulent quantity is the trace of Reynolds stresses. It is reasonable to believe that for an increasing normal stress, the shear stresses would also increase, and hence k (kinetic energy) can be used to determine the relationship with Boussinesq hypothesis. The eddy viscosity is generally described as a product of a velocity scale and a length scale. Using the turbulent kinetic energy as a transport quantity, the eddy viscosity is modelled as

$$\nu_t = c_\mu \sqrt{k} l \tag{3.28}$$

where k is a kinetic energy given by,

$$\frac{\partial k}{\partial t} + \bar{U}_j \frac{\partial k}{\partial x_j} = \frac{\partial}{\partial x_i}\left(\frac{\nu_t}{\sigma_k}\frac{\partial k}{\partial x_i}\right) + \nu_t\left(\frac{\partial \bar{U}_i}{\partial x_j} + \frac{\partial \bar{U}_j}{\partial x_i}\right)\frac{\partial \bar{U}_i}{\partial x_j} - C_D \frac{k^{3/2}}{l} \tag{3.29}$$

The level of kinetic energy in the flow primarily depends on the constant C_D, and the turbulent viscosity is determined by the value of C_D (a value of 0.08 is recommended).

3.5.5 Two-Equations Models

Two equation models use all the turbulent kinetic energy as one of the solved turbulent quantities. Apart from the transport equation k, the model will add another transport equation for second turbulent quantity. The main difference between these models is the choice of this quantity.

- ***k – ε model***

In the $k-\varepsilon$ model, the viscosity is expressed as a function of the turbulent kinetic energy and its dissipation rate given by,

$$\nu_t = c_\mu \frac{k^2}{\varepsilon} \tag{3.30}$$

The full set of $k-\varepsilon$ model equation is as follows,

$$\frac{\partial k}{\partial t} + \bar{U}_i \frac{\partial k}{\partial x_i} = \frac{\partial}{\partial x_i}\left(\frac{\nu_t}{\sigma_k}\frac{\partial k}{\partial x_i}\right) + P - \varepsilon \tag{3.31}$$

$$\frac{\partial \varepsilon}{\partial t} + U_i \frac{\partial \varepsilon}{\partial x_i} = \frac{\partial \varepsilon}{\partial x_i}\left(\frac{\nu_t}{\sigma_\varepsilon}\frac{\partial \varepsilon}{\partial x_i}\right) + \frac{\varepsilon}{k}(c_{1\varepsilon}P - c_{2\varepsilon}\varepsilon) \tag{3.32}$$

where P is the product of kinetic turbulent energy by shear and is given by,

$$P = \nu_t\left(\frac{\partial \bar{U}_i}{\partial x_j} + \frac{\partial \bar{U}_j}{\partial x_i}\right)\frac{\partial \bar{U}_i}{\partial x_j} \tag{3.33}$$

The constant of the k–ε model is calibrated on two classical experiments, the free decay of the grid turbulence and the flow that develops between two parallel walls. For the first experiment, it permits to find a value for constant $c_{2\varepsilon}$, while the second, will yield the constant values of c_μ and $c_{1\varepsilon}$. Finally the constant c_k and c_ε are optimised, by considering the performance of the k-ε model for both test cases with different values for these constants. The constants that are commonly used is shown in Table 3.1.

Table 3.1 - The Constant of k–ε model (Hervouet and Bates, 1996)

c_μ	$c_{1\varepsilon}$	$c_{2\varepsilon}$	σ_k	σ_ε
0.09	1.44	1.92	1.0	1.3

The depth-average form of this standard k-ε model is used based on Rodi (1993). The vertical-averaged gives rise to supplementary production terms in both equations due to bed shear,

$$P_{kv} = c_k \frac{u_*^3}{h} \varepsilon = (C_D k^{2/3})/\Delta \quad \text{where}, \quad c_k = \frac{1}{\sqrt{Cf}}$$

$$P_{\varepsilon v} = c_\varepsilon \frac{u_*^4}{h^2} \qquad \text{where } c_\varepsilon = 3.6 \frac{c_{\varepsilon 2}\sqrt{c_\mu}}{Cf^{3/4}}$$

P_{kv} is the kinetic energy product term and $P_{\varepsilon v}$ is the dissipation rate product term. Whereas Cf is the frictional coefficient and u_* is the bottom fiction velocity

- **$k-\omega$ model**

The $k-\omega$ model was originally developed by Kolmogorov where he used the reciprocal approach to the time scale or vorticity. For Two Equation models which is the secondary quantity is commonly referred to as the specific dissipation rate of turbulent kinetic energy. The different secondary turbulent terms are,

One Equation model , k-l ; $\nu_t = c_\mu \sqrt{k} l$ *where l - dimension (m)*

Two-Equation model , k–ε ; $\nu_t = c_\mu \frac{k^2}{\varepsilon}$ *where ε – dimension (m^2/s^3)*

k–ω ; $\nu_t = \beta_\mu \frac{k}{\omega}$ *where ω - dimension (s^{-1})*

The success of the above models is based entirely on the wall dependency and type of boundary conditions used in the simulation.

3.4.6 Large-Eddy Simulation (LES) Technique

LES is conceptually situated between the direct numerical simulation of all turbulence scales and Reynolds Averaged Navier-Stokes (RNAS) models in which only the mean flow is calculated. The LES technique has two advantages over classical turbulence modelling. Firstly, the LES only concerns the sub-grid scales where the overall

flow pattern is much less sensitive to the turbulence model. Secondly, the sub-grid scale is less dependent and thus more isotropic than the large scales. It is therefore much easier to define the sound turbulence model.

The most well known sub-grid scale model for LES is the Smagorinsky model, which can be seen to be a generalised form of Prandtl mixing length model. The Smagorinsky model is given by,

$$\nu_t = l^2 S \qquad \text{where } l = C_s \Delta \qquad \text{where } \Delta \text{ is the grid spacing.}$$

and

$$S = \left[\frac{1}{2} \left(\frac{\partial \bar{U}_i}{\partial x_j} + \frac{\partial \bar{U}_j}{\partial x_i} \right) \left(\frac{\partial \bar{U}_i}{\partial x_j} + \frac{\partial \bar{U}_j}{\partial x_i} \right) \right]^{1/2} \tag{3.31}$$

The constant C_s ranges from 0.17 to 0.23. The principal difference with the mixing length model is the use of the grid space instead of a physically based length scale. The one-equation model is often employed as sub-grid scale model with the sub-grid turbulent viscosity given by

$$\nu_t = c_\mu' \sqrt{k} \Delta \qquad \text{where } k \text{ is the sub-grid kinetic energy.} \tag{3.32}$$

The expression for the dissipation rate that is built from the grid spacing and the sub-grid kinetic energy is given by,

$$\varepsilon = (C_D k^{2/3}) / \Delta \tag{3.33}$$

The LES is meant to take into account the full 3D structure of the flow and it is restricted to 3D applications.

3.5 Flow Through Vegetation

The drag force for flow through flexible vegetation is given as,

$$F_D = C_D \tfrac{1}{2} \rho V^2 A \tag{3.34}$$

F_D and C_D are the drag force and drag coefficient respectively. Whereas ρ is the density, V is the mean velocity and A characteristic area of the vegetation normal to the flow. By rearranging equation (3.34) in terms of boundary shear stress according to Petryk and Bosmajian (1975), the expression becomes,

$$\tau_o = F_D/a = ½ C_D (A/a) \rho V^2 \quad (3.35)$$

where a is the bed cross sectional area. From Darcy's equation, the friction factor is given by,

$$f = 8 V_*^2/V^2 \quad (3.36)$$

where V_*^2 is the shear velocity which is equal to (τ_o/ρ). Equation (3.36) will reduce to

$$f = 8\tau_o / \rho V^2 \quad (3.37)$$

By substituting equation (3.35) into (3.37),

$$f = 4C_D (A/a) \quad (3.38)$$

The shear stress for wide channel is given by,

$$\tau_o = \gamma y S_f \quad (3.39)$$

where S_f is the friction slope given by,

$$S_f = S_o - dy/dx - udv/gdx \quad (3.40)$$

where S_o is the bed slope.

3.6 Summary

The governing equations used for flow in two-dimensional and three-dimensional modelling have been given in this chapter. Firstly, the derivations for the continuity and momentum equations in Cartesian coordinates with tracers are discussed. Secondly, bottom frictions in two-dimensional modelling using Manning's, Chezy's and Nikuradse's

Laws are derived. They are used in the simulations. Finally, six different turbulence models that are available in the numerical modelling are discussed. Among them are Constant Eddy Viscosity, Prandtl's Mixing-Length, One and Two Equation models, Elder's and Large Eddy Simulations.

In many engineering practices, a one- dimensional model is commonly used to simulate the effects on the changes of bed topography of estuaries or rivers. Whereas a two-dimensional model is commonly used to simulate flows in estuaries, coastal zones, wide rivers salinity intrusion, sediment transport, pollutant dispersion, dam failure and other modelling works. At present, two dimensional models are commonly used for engineering practices, because it gives better understanding of the problems compared to one-dimensional models.

A three-dimensional model is commonly used for situations involving stratification, secondary currents, horizontal density effects and buoyant flumes. Due to its complexity and time consuming nature, three-dimensional modellings are normally concentrated to scientific research rather than in engineering practices. Several researchers have made attempts to apply the 3-D numerical modelling in real-life applications with little success among them Morvan (2001). The reason is due to the difficulties faced in obtaining field data for the model input. The data are important for verification and validation of a model.

CHAPTER 4

GRIDS, BOUNDARY CONDITIONS AND SOLUTION TECHNIQUES

4.0 Introduction

Through the improvements of hardware and algorithms, digital modelling implements can be used to solve problems related to fluid mechanics. The increase in environment-related problems and the concurrent water uses have raised more complex and multidisciplinary issues. Consequently, the scopes of application for digital implants are becoming wider and more challenging.

The computational hydrodynamic model has becomes a powerful tool for engineers and scientists in accessing the impact of salinity intrusion in the river systems. They also allowed the user to predict the impact of river input on coastal water, the reduction of or enhanced river flows and to assess the dilution/dispersion capacity of the receiving water body. Computational models offer the possibility to test the numerical scenarios that are impossible to do in the physical model (Falconer and Lin, 1999). This chapter presents the governing equations and algorithms used for TELEMAC in solving the flow in coastal and estuarine waters.

4.1 Mesh Generation, Boundary Conditions, Solution Techniques of TELEMAC

Many researches have been carried out to improve the representation of the computational domain with different types of grid generation techniques. Generating meshes is to discretise a geometric domain into many small and simple shapes such as triangles and quadrilaterals for two-dimensional problems. Numerical meshes can be divided into two categories namely structured and unstructured meshes. They can be generated for the two or three dimensions.

4.1.1 Structured Two Dimensional Meshes

Structured meshes give a simple and most efficient approach for solving the Shallow Water Equations using finite difference approach. The structured mesh uses a significantly less memory space than the unstructured mesh with the same numbers of elements.

Structured meshes have been used in many numerical models, among them is the SIMSYS2D. It is a two-dimensional model developed by Leendtertse, that solves vertically averaged long-wave and transport heat equations, and salt and other water quality problems using a rectangular grid by space staggered approach. Wang (1978) used a finite element method to develop Circulation Analysis with Finite Element Explicit method (CAFEX). It is a two-dimensional model with triangular meshes used to solve vertically averaged equations for the two-dimensional flow.

Numerical models which based on the structured meshes have some limitations. They are normally unable to resolve features of a complex geometric domain, which lead to inaccurate model predictions. Furthermore, they become inefficient in regions where high velocity or concentration gradients exist. This is due to lack of local adaptation as a small grid size has to be used through the flow domain. Some numerical problems may occur at flow boundaries because of poor resolution that produces excessive diffusion and vorticity.

Nested and patched grids are used to overcome the limitations of the structured grid models. The nested model with a refined mesh is embedded inside a course mesh. This refined mesh is normally imposed at regions of interest in the coarse domain. In patching modelling, a single rectangular region in the model domain is divided by grid squares to form a sub-grid, which is known as the patch. The difference between the patch modelling and the nested modelling is that the patch may be assumed as a single fine grid with all other grid squares forming a coarse grid. Alstead (1994) concluded that patched modelling technique has an advantage over the nested modelling because it gives better accurate flow and water level predictions.

Another type of structured grid is the boundary fitted curvilinear grid, which is used to overcome the resolution problems. It provides a better representation of complex geometry. In using the curvilinear models, resolution and computational problems are separated. The physical space with the resolution problems are represented on a grid of varying mesh sizes. This is done so that the refine grid spacing can be obtained where it is required. For regions that are less needed, the coarse grids can be used. The curvilinear grid is then mapped onto the computational space of a rectangular grid. Curvilinear co-ordinate system can either be orthogonal or non-orthogonal.

4.1.2 Unstructured Two-Dimensional Meshes

The unstructured meshes were developed to improve the resolution at boundaries and in regions where steep gradients exist. It provides geometric flexibility and simplicity so that the grid can be adapted to flow features. Grid generation algorithms are necessary with which a mesh adapted to local features can be generated and local refinement can be controlled. Much research focus on the development of mesh generators. Different types of unstructured grids exist which include the triangular, tetrahedral, quadrilateral, hexahedral grids, prismatic and mixed grids. Wang (2000) concluded that mixed grids or hybrid grids are more effective than any other grids.

Many unstructured grid generators have been developed over the years, among them are ANGUS, MATISSE, STABEL and many others. One of the widely used algorithms is the multilevel grid generation in which multiple levels of coarse grids are generated by coarsening in each co-ordinate direction and having finer grids embedded in coarse cells. Studies have shown that when applying a multilevel approach to the SIMPLE algorithm, it was found that there was an increase in convergence speed of the computation. Wood (1996), Chen *et al.* (1997) , Sheng *et. al.* (1999), Botasso and Shephard (2000) and Teigland and Eliassen (2001) are among the researchers who solved the fluid flow problems using the multilevel algorithm. They concluded that the multilevel algorithm produced faster convergence to the solution and it was economical in terms of memory requirement.

TELEMAC uses Finite Element Method with a non-structured grid. It is used to solve water flows, solute and sediment motions in the fluvial, coastal hydraulic, estuarine, lacustrine and groundwater domain problems. The software was developed by the Laboratoire National d'Hydraulique of France in collaboration with HR Wallingford, UK. TELEMAC modelling system software is available as TELEMAC-2D and TELEMAC-3D. The version 5 series runs on PC base using Digital Visual Fortran compiler. For this research the latest version of TELEMAC V5P4 is used in all the simulation works.

4.1.3 TELEMAC-2D

TELEMAC-2D solves the horizontal depth-averaged free surface flow of the Saint-Venant (Shallow Water Equations) equations in two dimensional modelling. It uses a finite element method and a computation mesh of triangular elements to solve the equations. Results at each node of the computation mesh are the depth-averaged velocity components and water depth. TELEMAC-2D is designed to tackle problems associated with transcritical flows, floods, dam-breaks analysis, tidal flats and storm surges (Hervouet and Janin 1994)

4.1.4 TELEMAC-3D

TELEMAC-3D solves three-dimensional Navier-Stokes equations with a free surface boundary conditions and advection-diffusion. For the three-dimensional, the pressure is assumed to be hydrostatic. Like TELEMAC-2D, it uses the same finite element method to compute the horizontal mesh and the vertical mesh.

In constructing the three-dimensional mesh, the first stage is to construct a two-dimensional mesh similar to TELEMAC-2D. It consists of triangles that cover the computational domain horizontally. Secondly, it will reproduce along the vertical layers to form the prisms as shown in **Figure 4.1**

4.2 Finite Element Method

Finite Element Method (FEM) is mathematically consistent in approach. Idelsohn and Onate (1994) have made a comparison between the finite element and the

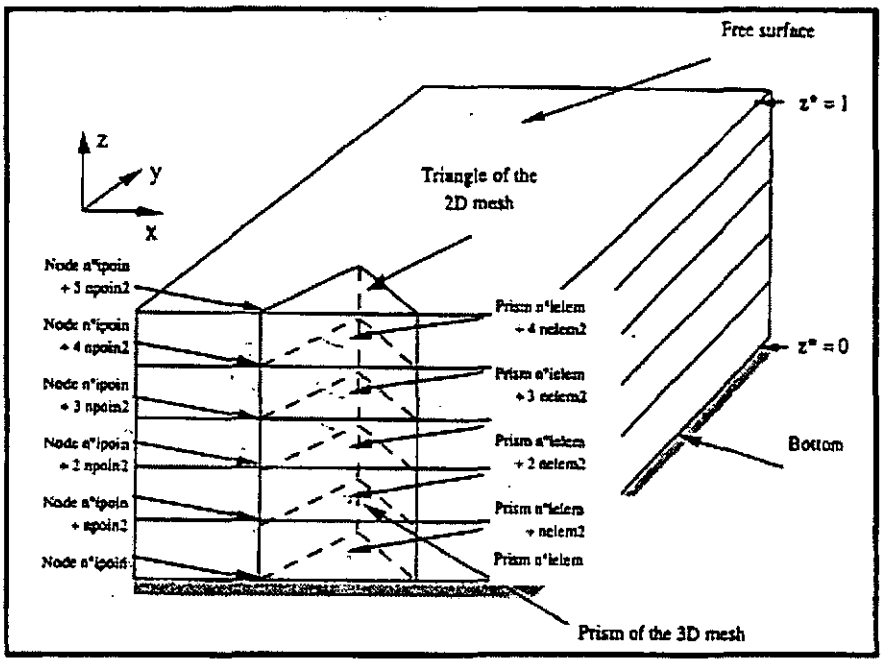

Figure 4.1 – Typical Three Dimensional Mesh

finite volume and concluded that both techniques are equivalent.

The geometry in space is discretised into series of elements within which the Navier-Stokes equation are valid. In FEM the discretisation of a partial differential equations normally processes a true spatial dimension where it can be continuously interpolated inside each element. This is because the polynomial functions will relate the continuous variables in space to nodal values. This means that if a polynomial is parabolic, it is assumed that the variables will vary accordingly inside an element. Inside each element, a variable φ can be written as follows,

$$\varphi = \sum_{l}^{M} N_l . \varphi_l \qquad (4.1)$$

Where M is the number of element nodes and N_l is a polynomial base (shape function). φ_l is defined as the values of variable sought at node .

Differentiating equation (4.1) will lead to the following expression,

$$\frac{\partial \varphi}{\partial x} = \sum_{I}^{M} \frac{\partial N_I}{\partial x} . \varphi_I \qquad (4.2)$$

This decomposition of the continuous functions implicates some conditions regarding the convergence of the model towards correct numerical solution (Morvan 2001). Convergence is defined as the property of a numerical method to produce a solution that approaches the exact solution as the grid spacing is reduced to zero (Versteeg and Malalasekera 1995).

In FEM, the domain is broken into sets of discrete finite elements that are generally unstructured mesh. This mesh is generally triangular or quadrilateral, while in three-dimensional modelling, the shape of the mesh is tetrahedral. The distinguishing feature of FEM is that the equations are multiplied by a weight function before being integrated over the entire domain (Ferziger and Peric 1993, Third Edition).

The FEM can be formulated in several methods such as direct, variational and weighted residual methods. Of the three methods, the latter is often used in most of the fluid mechanic problems. For the weighted-residual method, there are three formulations used which are as follows;

a. the collocation formulation
b. the least square
c. the Galerkin's formulation

Among the three formulations, Galerkin's formulation is widely used for formulation for free-surface fluid flow simulation where the diffusion term is of prime importance.

4.3 Grids Geometry and Mesh Construction For TELEMAC

Under this sub-topic, the importance of mesh generation and its resolutions are discussed.

4.3.1 The Geometry

The surface geometry is built from the data points of known values. This data can be digitised using some of the commercial softwares available. For this research work, ERDAS Imaging software is used to digitise the location of Sedeli river and its estuary from the topographic maps. This software is capable of digitising rivers and estuaries to their actual latitude and longitude coordinates.

In TELEMAC 2D, the surface generated is built automatically from the information of data points. It can be modified manually by the creation of structured lines that will enhance ground surface features such as bank lines. The two-dimensional modelling is based on the code that will reflect its surface nature. Only the bottom geometry is originally created from the entire domain. Whereas for the three-dimensional modelling is created at each step as the water height is calculated from the resolution of two-dimensional Navier-Stokes problems on the bottom grid. It is then elevated to the prisms from the information of the surface mesh. In TELEMAC code, there is no clear distinction between geometry and mesh. In fact both processes are inter-connected, for example the structure lines are used to shape the geometry; it also can act as constraint lines for the mesh. These lines should be used to stress the main topographical features of the geometry in order to structure the grid. It is particularly important that they are used when the grid is coarse to ensure that shape changes in the topography (riverbank and bottom lines) are well captured by the numerical grid.

4.3.2 Mesh Construction

Mesh which represents computational domain in discrete form is an important element for the numerical solution. It is used to solve partial differential equations for finite difference, finite element and finite volume methods. The accuracy of the numerical

solution in the physical domain depends on the error in the solution itself, as well as the mesh size and interpolation. Commonly, the errors of a numerical computation at the nodes arise from several distinct sources. Among them are errors caused by the size and shape of the grid cell. Hence, quantitative and qualitative properties of the mesh play a significant role in numerical analysis.

Generally, the following guidelines are commonly used in the generation of mesh,

1. Mesh must consist of small elements, which give accurate solutions and phenomenon associated with physical quantities, such as turbulence.
2. Mesh element must not be folded or degenerate at any point or line.
3. The mesh must be compatible with the physical geometry.

TELEMAC is based on the finite element method in which variables are calculated at each mesh node, and the variation of a variable on a cell surface is given as a sum of each node variable multiplied by an interpolation function and a weighing function. It uses flexible, unstructured, triangular finite element mesh, which is based on Delaunay triangulation. When the connection of neighbouring mesh nodes varies from point to point, the mesh is called unstructured mesh. Unstructured meshes are particularly advantageous for discretising complex geometries as they give more flexibility and robustness for handling the computational domain. Triangular elements are the simplest two-dimensional elements and can be produced from quadrilateral cells by constructing interior edges. These meshes are generated using an adaptive mesh generator called *MATISSE*. The spatial resolution is adjusted locally (that is, more resolutions at locations of interest) where necessary, that makes the software more economical in terms of computation time and hardware requirement.

4.3.3 Mesh Resolution

For many numerical modelling applications the problem of specifying an optimum mesh resolution remains unbounded and mesh construction objective becomes a priori rules which do not exist (Hardy *et al.* 1999). Mesh resolution plays an important role in

any numerical modelling. It is interrelated to the properties of the numerical scheme and grid size. Hankin *et. al.* (2001) used different mesh resolutions in predicting velocities. They found that the size of the meshes selected for any numerical modelling has a significant impact on the results obtained. Similarly Hardy *et al.* (1999) used different resolution meshes in applying to a complex geometry of river topographies to obtain a grid independence solution.

Based on the study of the River Stour, in Dorset and River Culm, in Devon, Bates *et al.* (1995) concluded that even a low resolution mesh discretisation for the TELEMAC-2D model can provide a reasonable approximation to the bulk flow through a reach-scale floodplain system. However, for simulations of complex heterogeneous flow, then the choice of mesh resolution becomes critically important. Mesh resolution affects the model solution in three ways;

a. Insufficient density point in the computational domains relative to gradients of computed variables will lead to coarse representation of the domain. This will give rise to an inaccurate numerical solution

b. The low resolution leads to the loss of topographic information resulting from the model discretisation construction.

c. There exist an interaction between process scale and mesh resolution

In this thesis, six different finite element meshes size were used in the simulations but only two were selected for the analysis purposes as shown in **Table 6.1** and **6.3** in Chapter 6.

4.4 Numerical Discretisation

TELEMAC code depends on an operator-splitting technique to solve the St. Venant and Navier-Stokes equations,

a. solution of a hyperbolic problem (convection)

b. solution of parabolic problem (diffusion)

A hyperbolic problem can be solved directly either by using the Method of Characteristics (MOC) or Finite Element Methods (FEM) (Janin *et al.*, 1979a). While for parabolic problems, they are formulated as a finite element variational process. Both problems are solved at each time step.

4.4.1 Discretisation of the Convection Terms

Method of Characteristics advection can solve the solution fastest compared to the Streamline Upwind Petrov Galerkin (SUPG) when advection is dominant. It has a good physical property in terms of upwind and monotonicity. One of the disadvantages of MOC is that, it can be quite diffusive and not suitable for achieving mass-conservation at the coarse mesh area. Alternatively, for advection of depth, it has to be treated in the first part of the equation using Petrov-Galerkin methods of the form,

$$W_i = N_i + \frac{\Delta t}{2}.(\nabla.N_i) \tag{4.3}$$

Where $W_i \neq N_i$. For α equal to unity, the scheme can be shown to be equivalent to a first order upwind scheme. In TELEMAC an unconditionally stable discretisation is available in the form of SUPG (Brooks and Hughes 1982). For the solution to be stable, the weight function is de-centred in the direction of the flow by Courant Number, $Cr = |U|.\frac{\Delta t}{\Delta x}$ instead of α so that $W_i = N_i + \frac{\Delta t}{2}.(\nabla.N_i)$. It is recommended that the value for Cr be less than 1 in order to obtain accurate results. Mass conservation for the MOC and SUPG can be improved by implementing sub-iteration, which will lead to the refinement of the quality of the convection velocities.

4.4.2 Discretisation of Diffusion Terms

For discretisation of diffusion term, the software uses a finite element variation to be applied to the diffusion step equation of the following form,

$$\frac{\vec{U}_D - \vec{U}_c}{\Delta t} - \nabla(\nu \nabla \vec{U}) = 0 \qquad (4.4)$$

It is then formulated in the fixed mesh as a finite element variational problem by the integration process.

4.4.3 Choice of Discretisation Schemes

The choice of finite element approach and the solution of algorithm will determine the scheme. The MOC is recommended for solving velocities whereas the SUPG is recommended for the calculation of the advection of water depth. In TELEMAC both schemes can be used simultaneously for the difference variables when solving the same problem (Horritt 2000). Hardy *et al.* (2000) proposed to solve the convection terms for velocity and turbulence by MOC and advection of flow depth by SUPG.

4.5 Boundary Conditions

The choices of boundary conditions play a crucial role in the simulation of complex problems by TELEMAC. The code provides several alternatives on types of boundary conditions that can be used.

TELEMAC is mainly developed for maritime and coastal applications where in the choice of the boundary conditions to be applied is made simpler. Physically, the boundaries are classified as liquid and solid boundaries, depending on the impermeability conditions. Across solid boundary, no flow can take place and the friction coefficient is to be provided or determined by the turbulence closure scheme used. The computation starts from quiescent initial elevation. In order to speed up the convergence, often an initial elevation of the water level is prescribed throughout the domain. The relative increment of time stepping termination tolerance can be set-up using key words provided by the code. The following boundary conditions can be used for the simulations.

- Prescribed constant flow rate Q in m^3/s at the inlet location
- Prescribed tidal water elevation at the open boundary (outlet)

- Prescribed tracer value (salinity and temperature) at the open boundary (outlet)
- Friction coefficient at the bed of the river in the form of Manning's coefficient n
- Zero transverse gradients of velocity u (m/s) (i.e du/dy = 0) and zero transverse velocity v (m/s) at the solid wall boundaries.

4.5.1 Open Boundary Conditions

Bates *et al.* (1998) recommended either an inflow or velocity at the inlet or a fixed water depth at the outlet prescribed for an open boundary conditions. Dirichlet boundary conditions are implemented at the inlet and outlet nodes for the two main variables that is $\bar{U}$ and h.

For the turbulence quantities (for k-ε model only), the inlet conditions are set internally in the software, making used of a local equilibrium assumption as follows;

$$k = \frac{u_*^2}{\sqrt{c_\mu}} \quad ; \quad \varepsilon = \frac{u_*^3}{K - k_s} \tag{4.5}$$

These conditions are calculated from the shear velocity.
The turbulent eddy viscosity is calculated using the following expression;

$$\nu_t = c_\mu \frac{k^2}{\varepsilon} \tag{4.6}$$

At the outlet, a von Neumann boundary condition is defined as follows;

$$\frac{\partial k}{\partial n} = 0 \text{ and } \frac{\partial \varepsilon}{\partial n} \tag{4.7}$$

4.5.2 Boundary Conditions at Walls and Bottom

Non-slip boundary conditions are imposed at walls and bottom, in order to model the friction and impermeability effects on walls. In the mixing length turbulent model,

a simple law of the wall is defined as follows;

$$C = \frac{1}{k} \cdot \ln\left(\frac{\Delta Z}{k_s / 4}\right) + 4.9 \tag{4.8}$$

Where ΔZ is the distance between the first node and the bottom and C is a constant (Janin *et al.*, 1997a) k_s is the grain particle size in millimetres and k is the von Karman constant which has a value of 0.41.

In this case, the fluid shear stress is assumed equal to a quadratic function of the following form,

$$\vec{\tau} = \frac{1}{2} \rho C_f |u| \vec{u} \tag{4.9}$$

Where $C_f = \sqrt{\frac{2g}{C}}$ and is the Chezy's Coefficient which is a two-dimensional approach

4.5.3 Boundary Condition At The Free Surface

A standard impermeable condition is applied to reduce the velocity normal to the wall to zero. In the absence of wind, a zero-shear of the horizontal wind is known. These wind effect will be applied as a boundary condition.

4.6 Solution Algorithm

TELEMAC relies on an operator-splitting technique as its algorithm solution. This approach enables the solution of the equations in stages, using an intermediate solution.In TELEMAC, the algorithm is incorporated to account for the influence of partially wet elements on the solution.

4.6.1 Convection

TELEMAC calculates the initial guess from a partial differential equation made of the unsteady and convection terms. This is known as a convection step and is given by the

following expression;

$$\frac{\vec{U}^{n+1} - \vec{U}_c}{\Delta t} - \frac{1}{\rho}\nabla p - \vec{S}ource = 0 \tag{4.10}$$

Where $\vec{U}$ is convection velocity and $\vec{U}^n$ is a velocity at the previous time step. Equation 4.14 is explicit in time. However, the problem is that $\vec{U}$ and $\vec{U}^n$ are not calculated on the mesh.

4.6.2 Diffusion

From the convection stage, the propagation-diffusion equation is given in the form of the following form;

$$\frac{\vec{U}_D - \vec{U}_c}{\Delta t} - \nabla(\nu \nabla \vec{U}) = 0 \tag{4.11}$$

It is formulated in the fixed mesh as a finite element variational problem by an integration process. Several sub-iterations can be requested in order to enhance the calculation of a non-linear problem.

4.6.2 Propagation-Convection

The propagation step is governed by the following expression,

$$\frac{\vec{U}^{n+1} - \vec{U}_c}{\Delta t} - \frac{1}{\rho}\nabla p - \vec{S}ource = 0 \tag{4.12}$$

In TELEMAC 2D, it is used to yield water depth values at each node.

4.7 Numerical Solver

Operator splitting technique offers the most efficient solver for each stage of computation. The solution of equation turbulent kinetics energy (for $k-\varepsilon$ model) due to the simplification of finite element is more efficient compared to the variational matrix. Equation 4.15 is a parabolic equation, which can be solved by Method of Characteristics. The solution to this equation can be determined by solving the value of U_i^{n+1} along the

characteristics curve of a known value U_i^n. For U_i^n to remain constant on the characteristics curve, it has to satisfy the following functions;

$$\frac{dx^*}{dt} = U_x = U$$

$$\frac{dy^*}{dt} = U_y = V$$

$$\frac{dz^*}{dt} = U_z^* = W^*$$

The determination of the characteristics curve is made by using a Runge-Kunta method with an explicit velocity field at time 'n', that is with $U=U^n$, $V=V^n$ and $W^*=W^{n*}$.

Using this two-step approach simplifies the iteration of the problem matrix 'A' by reducing it to a positively symmetrical diffusion matrix A' after the first step (elimination of convection-matrix component) (Hervouet and Van Haren, 1995). It is used for Conjugate Gradient (CG) methods, and particularly suit the Generalized Minimal Residual (GMRES) method.

4.8 Summary

The governing equations used in TELEMAC for the fluid flow in estuarine have been provided in this chapter. Firstly, the governing equations for TELEMAC -2D were discussed, considering the incompressible fluid in the form of depth-averaged velocity. For TELEMAC-3D, the depth is considered to be non-hydrostatic. This is followed by the discussion on Finite Element formulation. Secondly, mesh generations and their theoretical background used in TELEMAC 2D and 3D were described. Finally, the algorithms used in the TELEMAC system were elaborated in detail in this chapter. This is followed by some general discussion on the boundary conditions normally used for hydrodynamic simulations for fluid flow.

TELEMAC code was chosen because it has incorporated a Streamline Upwind

Petrov-Galerkin (TELEMAC Manual 2002) and an oscillation- free solution (Brooks and Hughes 1982) and also its algorithm takes care of the partially wet elements in the mesh. The model comes with several turbulence models in its computation. A single value of turbulent viscosity (ν_t) parameter is specified to each turbulence model. The model sensitivity to this parameter is dependent on the scale of the element. It becomes less sensitive as the element size increases. For reach scale models the friction term dominates the parameterisation problem and the impact of ν_t is of a relatively reduced consequence. This approach will minimise the computational cost.

For this study, the grid generator used is Matisse, which produces the unstructured triangular meshes in two-dimensional form. Matisse is able to refine the mesh size at places of interest. TELEMAC uses a post processor called RUBEN to view the output results.

CHAPTER 5

ANALYSIS OF SEDELI AND ROMPIN ESTUARIES

5.0 Introduction

This section describes the data analysis on the field data collected for Sedeli and Rompin estuaries. The primary data readings were taken for a period of three days. They were taken on different dates which coincided with the highest spring tides. This is to get the maximum salinity intrusion for both the estuaries. The data for this study was obtained from the field works done by the Public Works Department of Malaysia. Due to the limited data available for this study, two estuaries were chosen to determine their similarities and characteristics. Both of these estuaries are situated about 100 km apart as shown in **Figure 5.1**. Both rivers flow through the mangrove's swampy floodplain and discharge the freshwater into the South China Sea. The main objective of this comparison is to determine the salinity profile and flow structures for these two estuaries. Comparison of these estuaries were made based on their bed profiles, water levels, flow velocities, tidal characteristics and salinity readings taken along the estuaries during the spring tides. The results from this analysis would then be compared with the numerical modelling. It would also be used for model calibration. The data collected were tabulated as in **Table 5.1**

5.1 Sedeli Estuary

Sedeli Estuary lies in the eastern coast of Malaysia. The estuary has a total catchment area of 1,820 square km and is 120 km long as shown in **Figure 5.2**. The estimated yield for Sedeli River is about 170 million litres per day (MLD). Freshwater flows through a low lying swampy floodplain vegetated with mangrove. The swamp occupied most of the floodplains along the estuary. These swamps have depths ranging from 1.0 m to 2.0 m. They were normally inundated during high water and high river flows especially during the monsoon season.

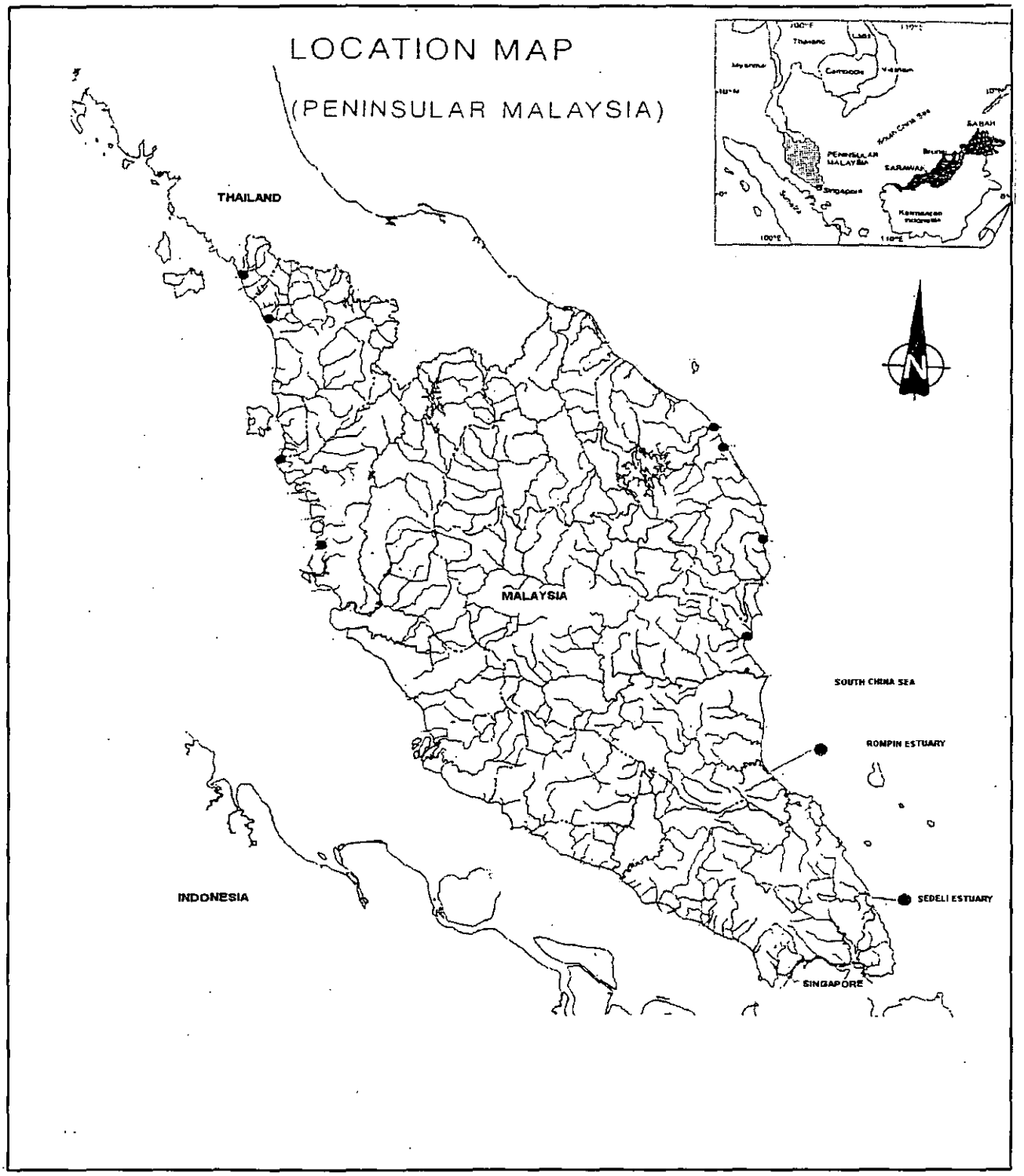

Figure 5.1 – Location map showing the locations of Sedeli and Rompin Estuaries on the eastern coast of Malaysia Peninsula

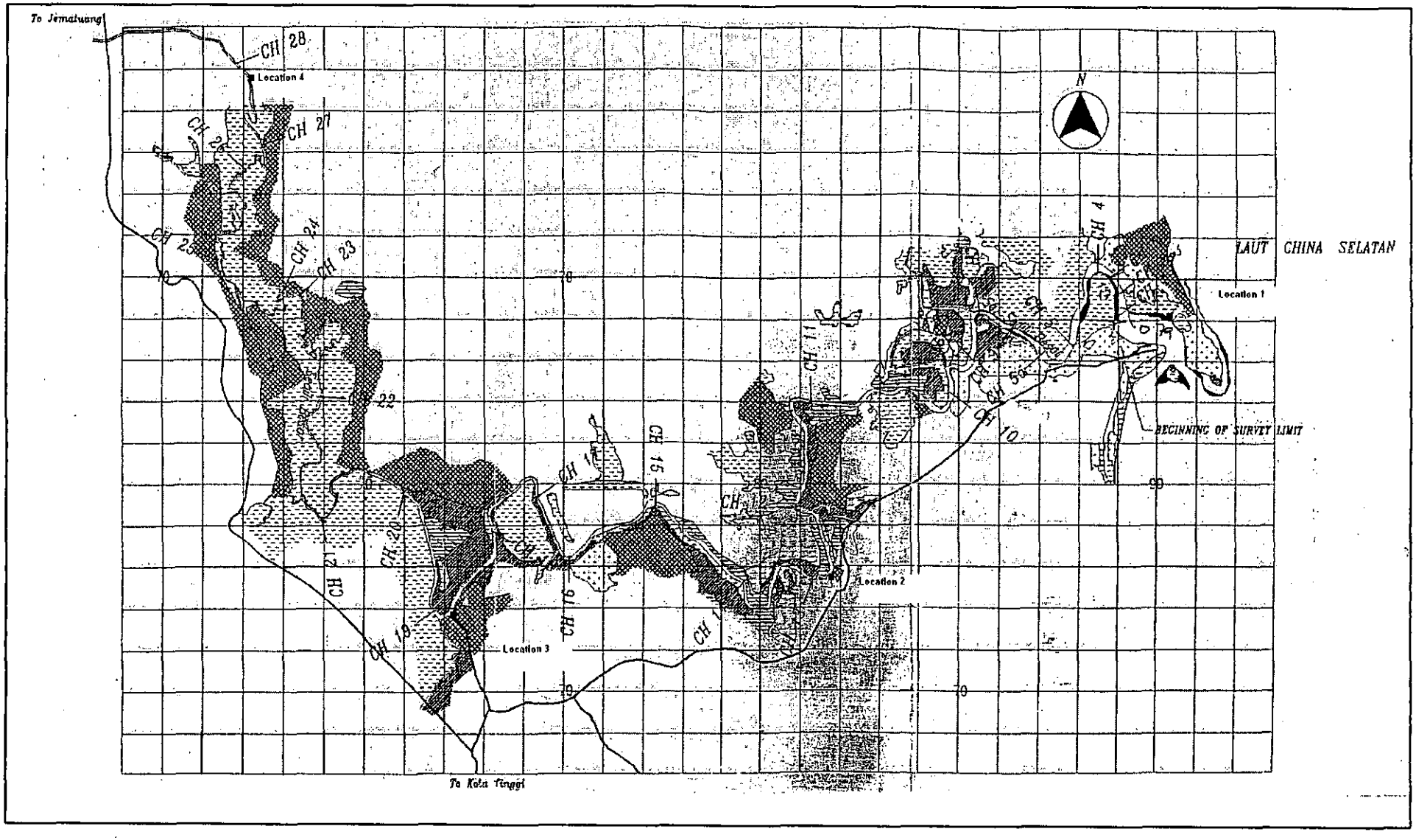

Figure 5.2 –Location of the 28 cross-sections of Sedeli Estuary which is approximately 120 km long. The floodplains were covered with Mangrove swamp.

Table 5.1 – List of Raw Data for the Sedeli and Rompin Estuaries

No	Parameters	Sedeli River	Rompin River
1.	Date	24.6.98 – 26.6.98	10.7.98 – 12.7.98
2.	Salinity Data (at location 2)	Available (1 location)	Available (1 location)
3.	Discharge Data (at location 4)	Available (1 location)	Available (1 location)
4.	Current meter Location (location 4)	Available (1 location)	Available (1 location)
5.	Water Level Location (at location 1, 2, 3 and 4)	Available (4 locations)	Available (4 locations)
6.	Gauging Location (location 4)	Available (1 location)	Available (1 location)
7.	Hourly Salinity (along the river)	Available 3 days	Available 3 days
8.	Salinity Profile (at location 2)	Available 3 days	Available 3 days
9.	Tidal Data (at estuary mouth)	Available (1 location)	Available (1 location)
10	River Cross-section	Available (28 sections)	Available (18 sections)
11	Longitudinal Cross-sections	Available (1 location)	Available (1 location)

5.1.1 Sedeli Estuary Cross-Sections

Twenty-eight (28) cross-sections were measured along the river reach by a surveyor. This cross-section would be used for numerical modelling. They were taken at an interval of 1 to 5 km apart. The distance and the cross-sections are shown in **Table 5.2** and in **Appendix A** at the end of this chapter. For the purpose of this research, only sections 12, 13 and 14 which was about 17.62km, 20.12km and 23.30km measured from the estuary mouth would be discussed in detailed. The study would base on characteristics of the bed profiles at the sections as shown in **Figure 5.3**. The analysis would base on bed profile peculiarities. The salinity as shown in **Figure 5.4,** shows that there was a steep decrease in salinity reading between the13th km to the 24th km. Similarly the deepest section of the river profile was also formed at this location

Table 5.2 – Sedeli Estuary Cross-Sections Distance Measured from Estuary

Cross-Sections Distance	
Section 1 -	0.0 km
Section 2 -	0.5km
Section 3 -	1.42km
Section 4 -	2.54 km
Section 5 -	4.64km
Section 6 -	5.60km
Section 7 -	6.560km
Section 8 -	7.68km
Section 9 -	8.98km
Section 10 -	10.26km
Section 11 -	14.22km
Section 12 -	17.62km
Section 13 -	20.12km
Section 14 -	23.30km
Section 15-	26.26km
Section 16 -	29.02km
Section 17 -	30.63km
Section 18 -	33.13km
Section 19 -	35.83km
Section 20 -	38.75km
Section 21 –	42.11km
Section 22–	46.15km
Section 23 –	48.74km
Section 24 –	51.11km
Section 25 –	54.31km
Section 26 –	57.55km
Section 27 –	60.55km
Section 28 –	62.90km
Section 29 –	73.00km

as shown in **Figure 5.5**. Three longitudinal riverbed sections were plotted along the centre and also on both sides of the river bank.

Figure 5.3 shows the cross-sections at sections 12, 13 and 14 (17.62 km , 20.12 km and 23.30 km from the estuary mouth) looking upstream towards the estuary. Section 12 was at one of the apexes of the river which also happened to be at the meandering section. The left side of the cross-section shows an inner section of the apex. **Figure 5.3**, shows the left bank of the apex which has a gentler gradient compared to the right bank. This type of formation is normally found in areas where river flows are dominating.

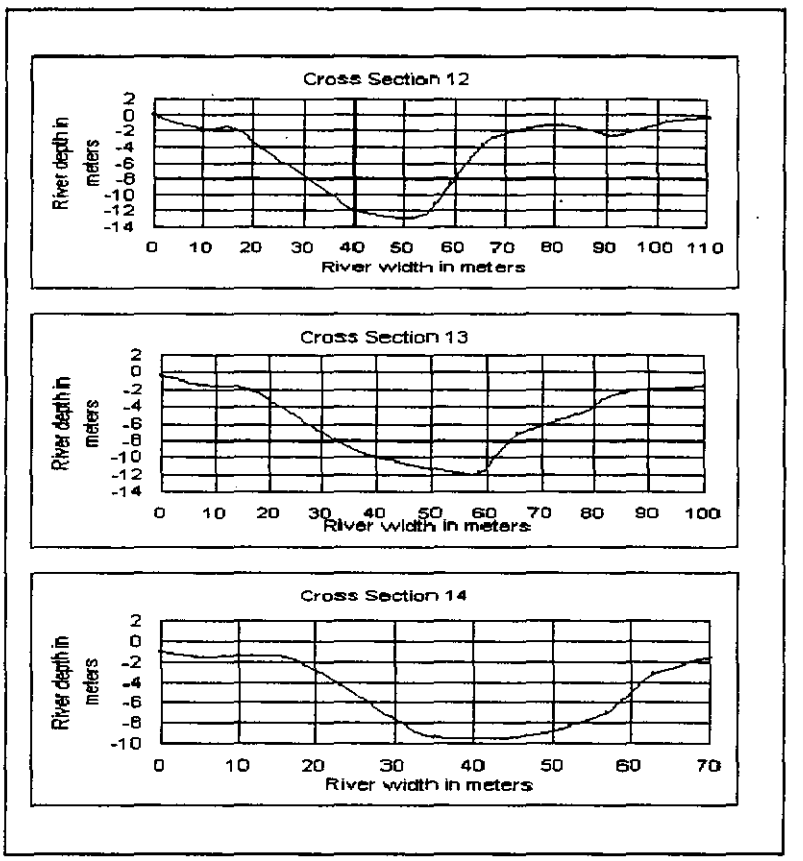

Figure 5.3 - Sedeli River Cross Sections at 12, 13 and 14

The deepest section was found to be closer to the right bank of the river. This was due to the stronger influence of the river flow. The right bank was situated at the outer section of an apex of the meandering section. Being at the outer section, it experienced a greater secondary current effect where most of the scouring processes took place (Sponner 2003). The salinity reading at section 12 ranged from 9ppt to 16ppt during high water as shown in **Figure 5.4**. At this section, the floodplain was covered with mangrove swamp. Section 13 (location 2) was chosen because most of the data measured were taken at this section. This section was situated at the straight section of the river profile. From the cross-section, there was a different pattern of bed formation. The deepest section was also closer to the right bank. This was due to the combination of river and swamp flows which influenced the bed formation at this section. At this section, the water from the swamp

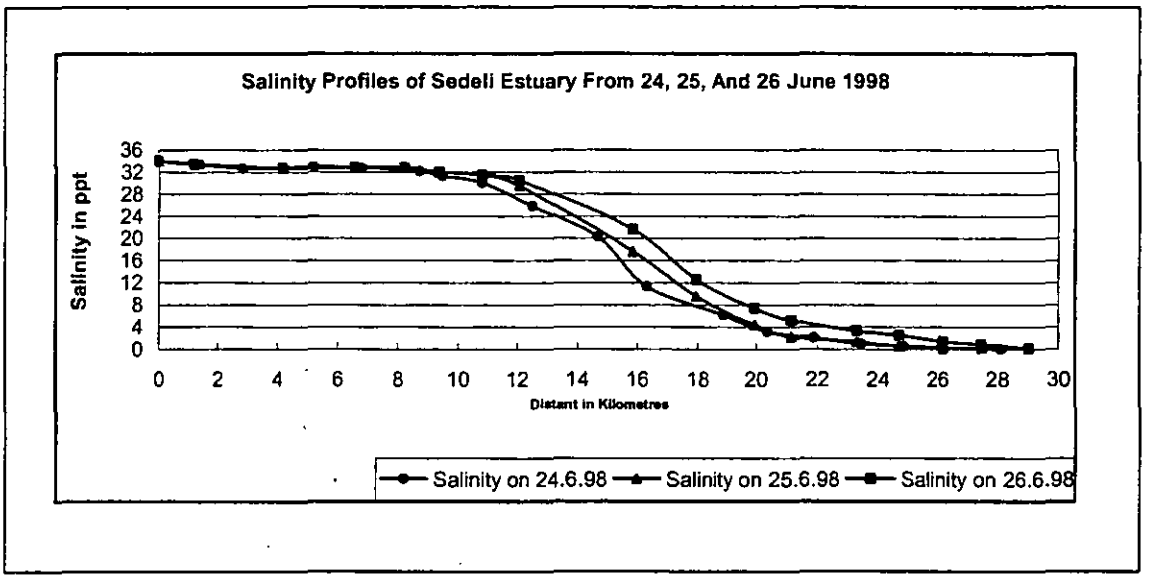

Figure 5.4 – Salinity against Distance on 24.6.98 – 26.6.98 (the left hand of the figure is the ocean and the distances are measured from the estuary mouth)

plunged into the river creating a variation of velocities which would induce higher turbulence zone in the area where the velocity was maximum. This would lead to greater scouring effects at the right bank of the river (Liu 1991; Morisawa 1985; Ligent & Schiara 1998). This can be seen from Figure 5.3, where the right bank has a larger floodplain compared to the left plain. The velocity during ebbing is higher on the right bank as shown in **Figure 6.27** in Chapter 6 of this thesis (Ismail 2007). From **Figure 5.4**, the salinity reading at this location was 3ppt and it can be concluded that tidal influence at this location was minimum. The possibility was that water from the swamp flowed into the river and thus influenced the formation of bed profiles. Section 14 was located at the straight section of the river. It was observed that the bed formation was symmetrical. The deepest location was at the centre of the river. **Figure 5.4** shows that the salinity reading at this section was quite low, thus tidal influence on the bed formation was negligible. The formation of this bed profile was due to the combination of the river flow and the swamp flow. This phenomenon on bed formation was similar to that at section 13.

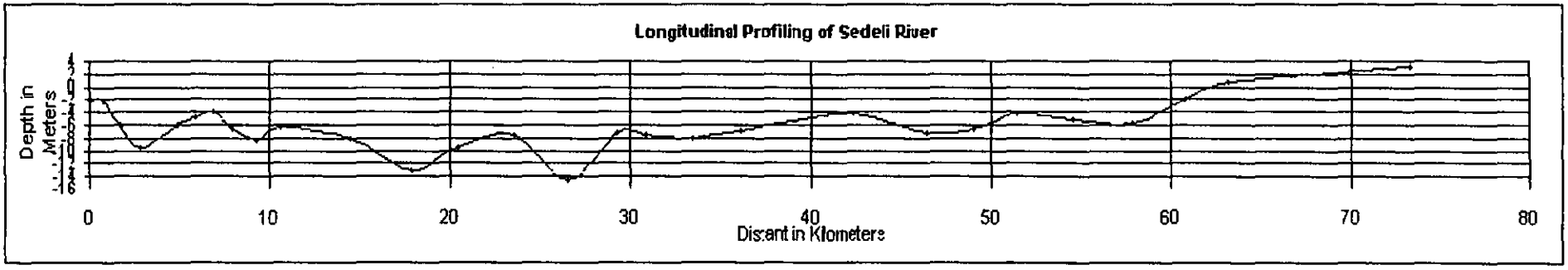

(A) - Longitudinal Profiling of Sedeli River at Right Section of the River

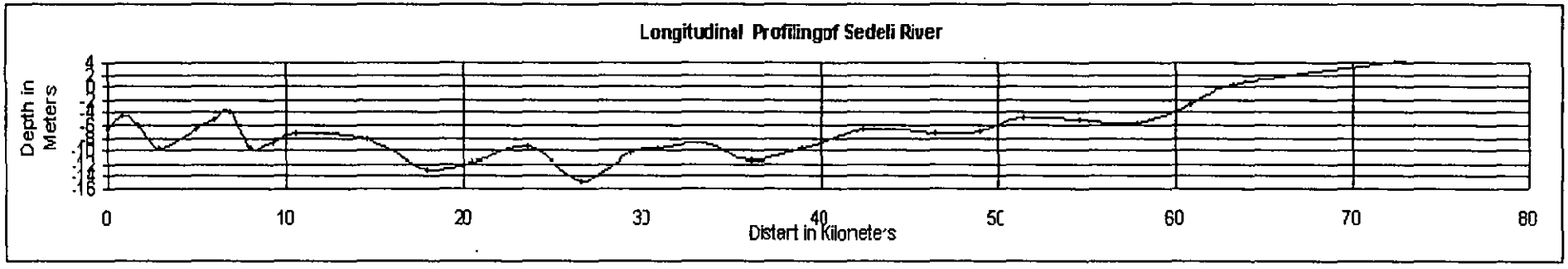

(B) - Longitudinal Profiling of Sedeli River at the Middle Section of the River

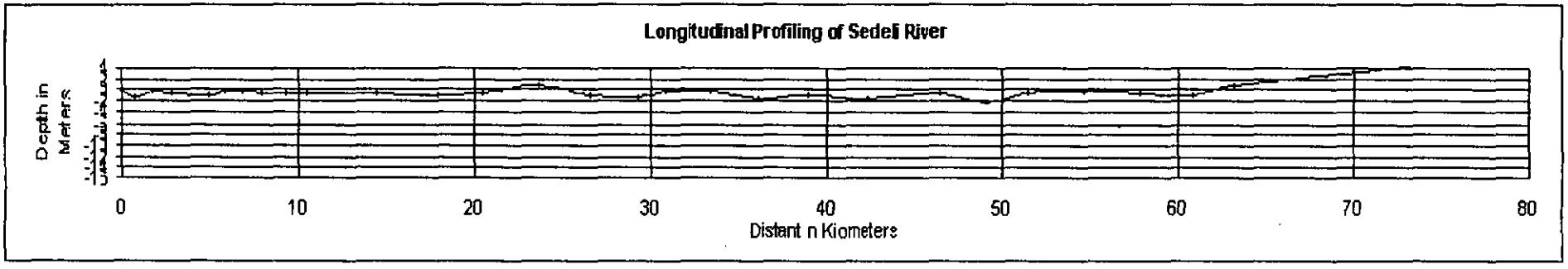

(C) – Longitudinal Profiling of Sedeli River at the Left Section of the River

Figure 5.5 – Longitudinal Profiling of Sedeli River

Figure 5.5 shows the longitudinal sections of the river. The deepest point was found to be at the 28th kilometres away from the river mouth. Also at this region there was a change of bed gradient from positive to negative. In **Figure 5.4**, the salinity reading shown at this location was almost zero. The river flow here dominated over the tidal effect. This was also the region where fresh water and saline water mixed vigorously. Saline water has a very weak stratification, whereby it destabilises itself and mixes with fresh water. This mixing would lead to the circulation process where fresh water and saline water vigorously mix vertically. The effect of this circulation process would cause the scouring at the bed of the river to take place.

5.1.2 Sedeli Estuary Field Measurements

The field measurements were carried out for a period of three days starting from 24/6/98 to 26/6/98. The measurements were done during the highest spring tides in order to obtain the maximum salinity intrusion. The results obtained would be used for numerical model calibration. The field measurements consist of the following parameter,

- Water levels with time series
- Current/flow speed time series
- Salinity with time series
- Salinity profiles time series
- Tidal data.

Tide data were obtained from self-recorded equipment which was installed at the tide station situated about 4.0 km from the station 1.

5.1.3 Water Level Measurements

All the water level instruments were self-recorded. The recorded levels were then converted to the Land Survey Datum. Global Positioning Systems (GPS) were used to determine the exact position of these stations. Water levels were taken at stations 1, 2, 3 and 4 along the estuary. The first reading was taken at the estuary mouth and the next three readings were at 20.12 km, 54.31 km and 73.00 km from the estuary mouth. **Figure**

5.6 shows the summary of the water levels at the four locations. Water levels were taken for a period of 69 hours from 23.6.98 to 26.6.98. The readings were taken simultaneously during high water at all the four stations. The first location was at the jetty, which was just after the estuary mouth followed by Kg. Sayang, Kg. Mawai and Batu 18.

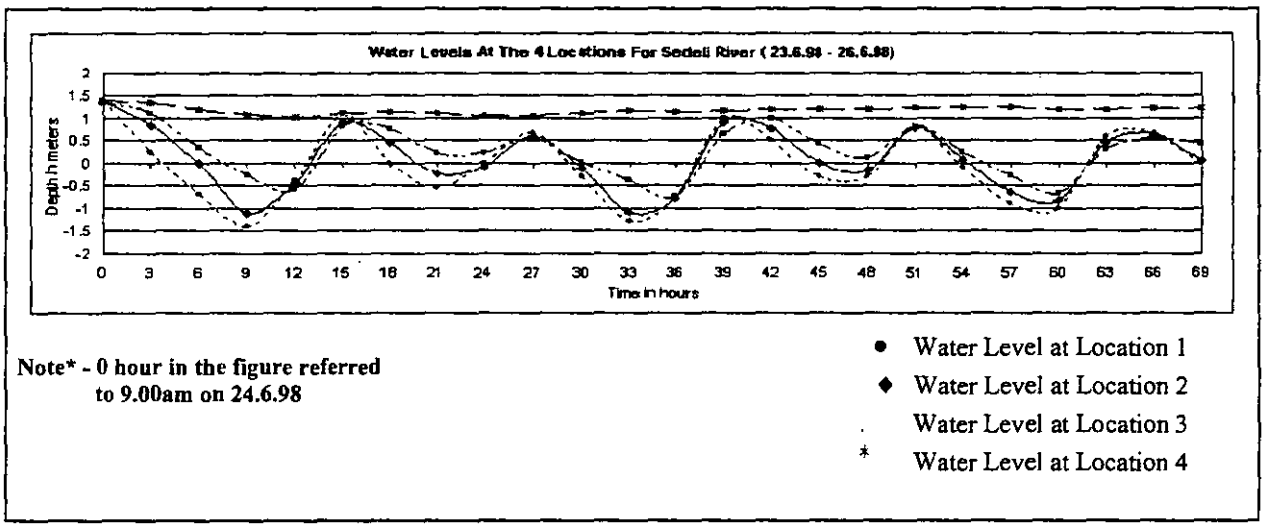

Figure 5.6 – Water Levels for Sedeli River at Locations 1 – 4

From **Figure 5.6**, it can be seen that the effect of tide was predominant at three locations. The highest water level occurred at 1500 hour which was 1.1metre above the mean sea level while the second high water occurred at 2700 hours which was at 0.7 metre. Similarly, ebbing occurred twice daily. The low water level was –0.55m at 2100 hour and -1.4 metres below mean sea level at 3330 hour. These values were compared with other three locations to determine the flow characteristics.

Location 1 had a strong tidal effect since it was closer to the sea. The fluctuations of this water level were strongly influenced by the tidal fluctuation of the sea. **Figure 5.6** shows there was a slight phase lag of water levels between *location 1* and *location 2*. At *location 3*, the difference of water levels from *location 1* was 1.0 metre (66.7%). Similar to *location 1* and *location 2,* the water levels at this location fluctuate. This is interesting

since the salinity intrudes up to 29.0km upstream, whereas the tide propagates at least to 34.5 km from the estuary mouth. This was due to the movement of water from the swamp during flooding and ebbing where during flooding the water from the river would flow on to the floodplain which was covered with mangrove swamp. The presence of this vegetation would retard the flow of water to the swamp thus creating turbulence and affecting the flow of water in the river. At *location 4*, there was no significant fluctuation of water level. This was to be expected since this location was situated at 73.0 km away from the river mouth. The water level at this location was the same as the levels of inflows.

It can be seen that there are phase differences at the three locations during flooding and ebbing. A very interesting phenomenon occurred at this estuary. Firstly, there was a slight phase difference just after the high water. This was due to the inflow of water from the swamp into the estuary. As mentioned previously the presence of vegetation on the floodplain had some significant effects on the flow of water in the river. During flooding, the vegetation would retard the flow on the floodplain while during ebbing, the flood water entered the river at a slower rate compared to the tide. Secondly, the water levels at the three locations intersected immediately after the second high water as shown in **Figure 5.6**. At this condition, the water level gradient was level throughout the estuary from *location 1* to *location 3*. This again was due to the inflow of water from the swamp into the river channel which made the water level in the river and on the floodplain to be levelled at all the three locations. In this situation, the water was in a state of equilibrium and was relatively stagnant where there was a transition period from flooding to ebbing. The only difference from the first phenomenon was that the swamp velocity was much slower because the first high water was higher than the second high water. The conclusion that can be drawn from this phenomenon is that the presence of the swamp had a significant effect on the flow structures in the estuary. **Figure 5.7** shows the tide levels against time with respect to the mean sea levels taken at the estuary mouth. **Figure 5.8** shows the characteristic of tides from 1.6.98 to 30.6.98 measured at the estuary mouth. Both figures show the tide levels at the estuary mouth and the tide monitoring station

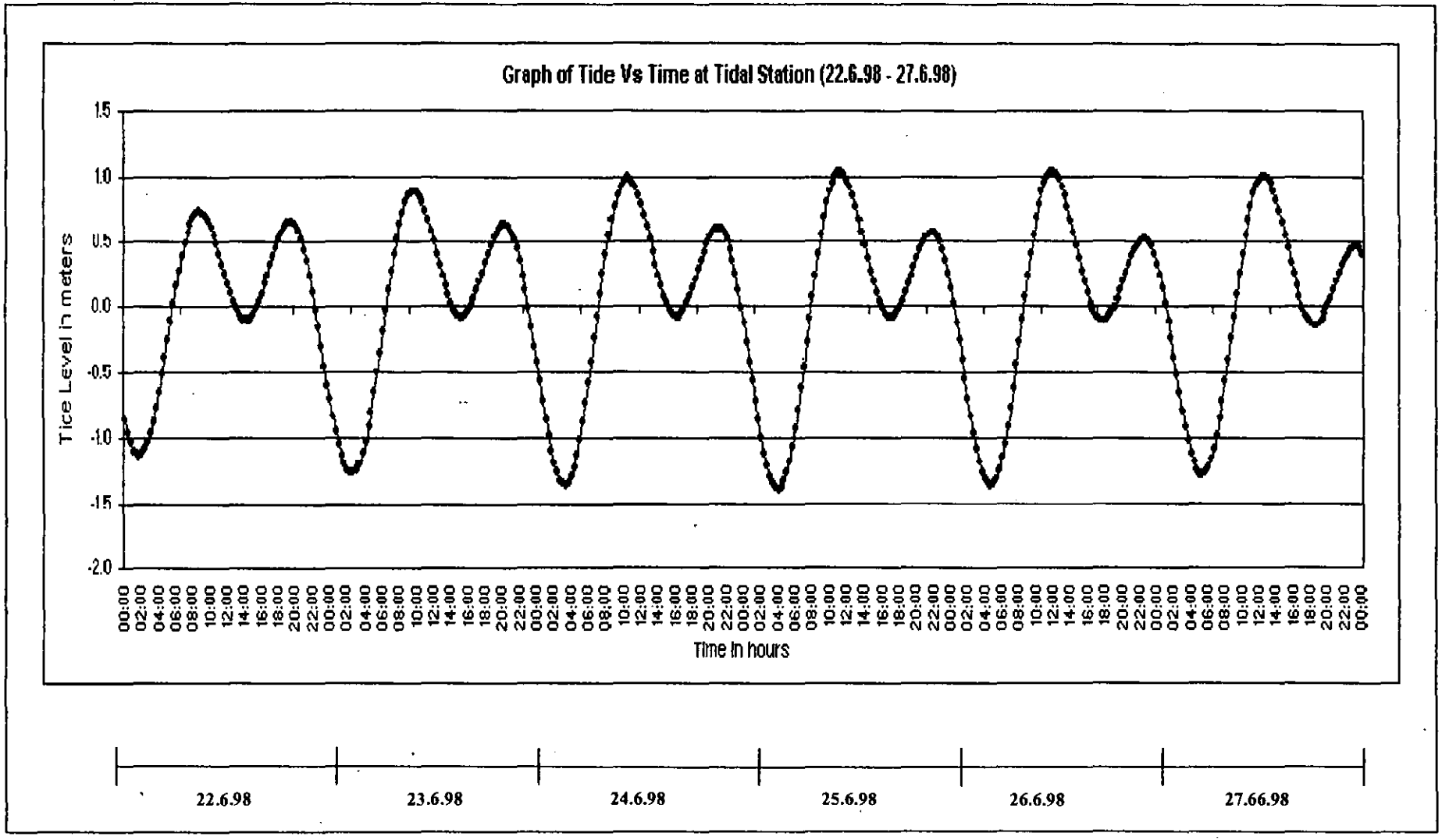

Figure 5.7– Tide Level against Time with respect to Mean Sea Level

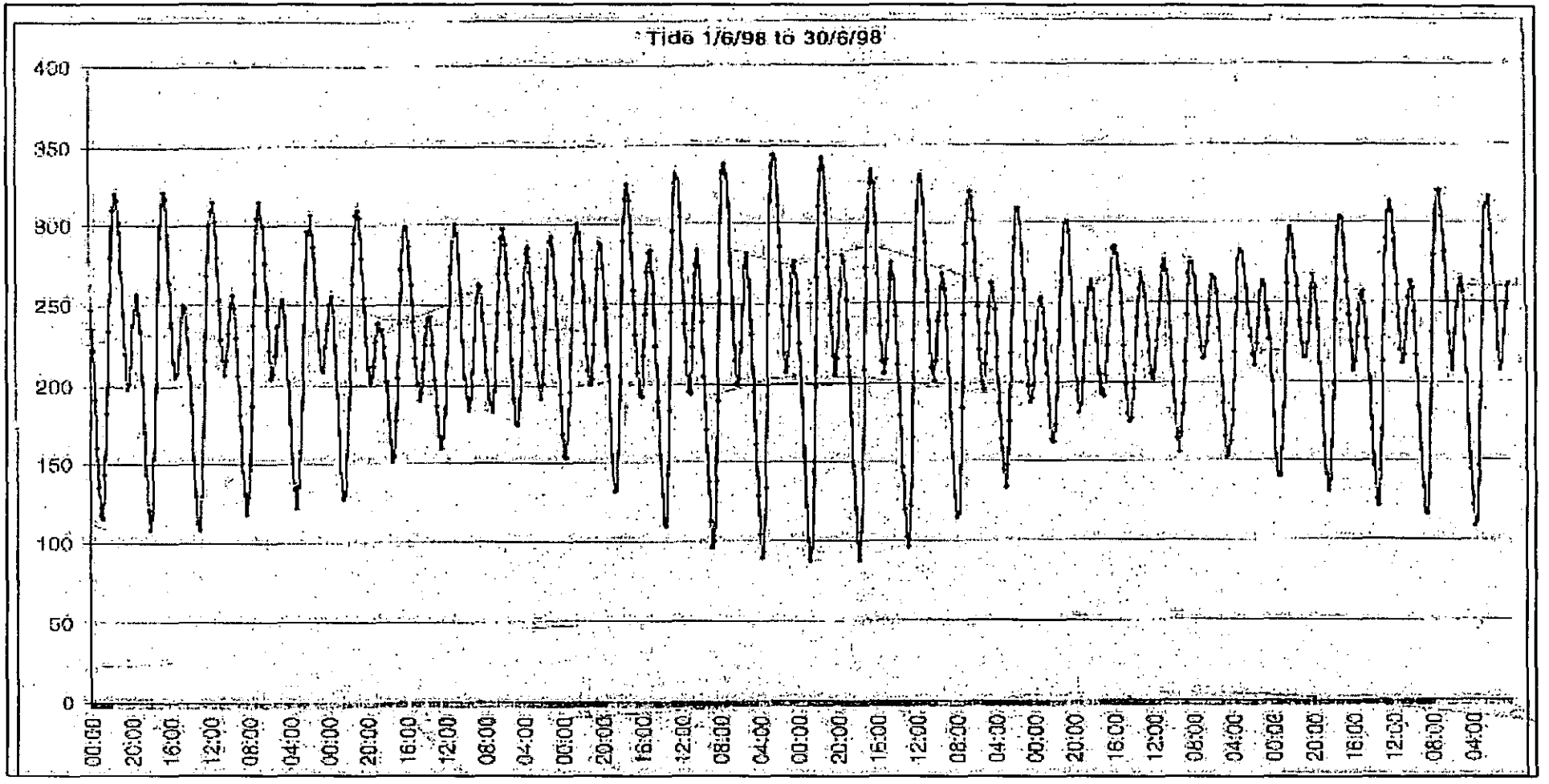

Figure 5.8 – Tidal Reading at Sedeli Estuary from 1.6.98 – 30.6.98 Measured at the Estuary Mouth

which was 25km away from the estuary mouth. The tides at these locations were diurnal with two high water in a day. The measured tides at the estuary mouth happened to be the maximum high water for the month as shown in **Figure 5.8**.

5.1.4 Current/Flow Measurements

Three current meters were installed to measure the velocities at the centre of the river at Batu 18 (*fourth location*). This location was situated at the uppermost end of the estuary. The flow reading from the current meters are shown in **Figure 5.9**. The current meters which contained data loggers were self recorded. They were capable of recording water temperatures, flow velocities and directions of current in the river. The time series discharges were determined from the product of the velocity with the cross-sectional area of the river at the measured point. These flows varied from 53 m^3/s to $1m^3/s$. The high inflow in the river was normally caused by rainfall in the catchment's area since there was no dam to regulate the flow.

5.1.5 Salinity Measurements

Vertical salinities were measured at the centre of the river at Kg. Sayang *(location 2)* by using a calibrated salinity probes. Samplings were done at every hour. Salinity readings were taken at every 1 metre depth in order to detect the difference of salinity concentration in the river at various depths. This procedure is carried out for a period of 12 hours from 0800 hours to 2000 hours. **Figure 5.10** shows the results of salinity readings for the three days.

Figure 5.10, shows the salinity reading of 0.01 ppt at -1.0 metre below the surface of the water. Zero reading was detected at the depth of -2 metres downward at 0800 hours. During this time the river discharge was $5.0m^3/s$ and the tide level was at mean sea level (MSL). **Figure 5.9** shows the flow discharge of the river in m^3/sec of a period of 4 days (from 23.6.98 to 26.6.98) measured at *location 4*. Salinity increased as the river started to stratify at 1200 hours to 1400 hours which coincided with high water. **Figure 5.10**, shows the salinity difference between the top and bottom layers which was equal to 2.2ppt at 1300 hours on 24.6.98. During this time, the river discharge is $30m^3/s$. At 1400 hours, the

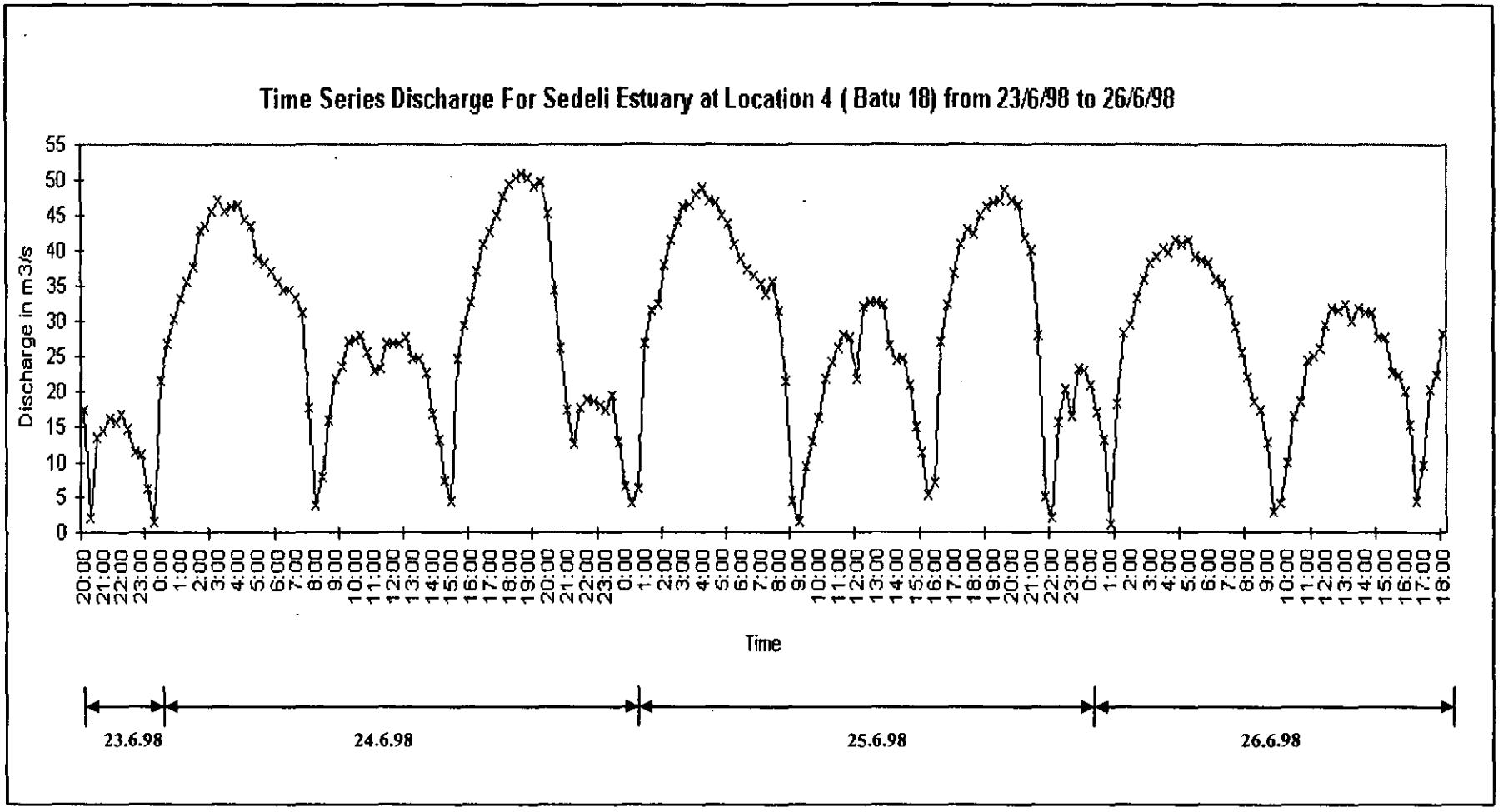

Figure 5.9 – Flow against Time at Location 4 (Batu 18)

salinity reading was zero and the discharge was $50m^3/s$. Similar phenomenon was observed during stratification on 25.6.98. On 26.6.98, the salinity at the top and bottom layers was 3.4ppt and 5.6ppt respectively. The salinity difference between the two layers was 2.2ppt which was similar to the reading on 24.6.98. This was due to the inflow of water from the swamp discharged into the river.

5.1.6 Salinity Profile

The salinity readings were taken using a salinity probe at the middle section of the river. The reading was taken at every 1.0m depth interval below the surface of the water during high water. The first reading was taken at the mouth of the estuary and moved inland. This reading was then averaged out at each point along the river reach. **Table 5.3** shows the time and water level during the salinity reading was measured at the second *location*. The measurement was stopped once the salinity recorded zero reading. The results of this salinity distribution were shown in **Figure 5.4. Table 5.4** shows the salinity readings for a period of three days. This reading represents the instantaneous salinity at the point of measurement.

From **Figure 5.4**, it was observed that the salinity reading was constant, ranging from 34.0ppt to 29.5ppt and from 0.0^{th} km to 12^{th} km. After this location there was a sharp decrease in salinity readings. The behaviour of shape is similar to other estuaries in this region, hence salinity dispersion or mixing occurs. However there were minor effects due to the presence of swamps on the floodplains. This was due to several factors that can be observed from the field data. Firstly, the water from the swamp flows into the river and diluted the saline water in the river during high tide. Secondly, the river has a negative gradient of – 0.029% from the estuary mouth towards the 28^{th} km. After this location, it has a positive gradient of 0.033%. From the longitudinal cross-sections, the bed had a valley shape formation. Freshwater would fill the lowest location and it would then dilute the saline water during flooding. This would reduce the salinity reading at the bottom of the river.

Table 5.3 – Water Level and Time at location 2 of Sedeli Estuary

Time in Hours	Water Level in Meter
0800	-1.0
0900	-1.2
1000	-1.0
1100	-0.5
1200	-0.3
1300	0.0
1400	0.5
1500	1.0
1600	0.8
1700	0.3

Water Level at location 2 on 24.6.98

Time in Hours	Water Level in Meter
0800	-1.0
0900	-1.1
1000	-1.0
1100	-0.8
1200	-0.5
1300	0.0
1400	0.5
1500	0.9
1600	1.2
1700	0.8
1800	0.5
1900	-0.2

Water Level at location 2 on 25.6.98

Time in Hours	Water Level in Meter
0800	-0.5
0900	-0.7
1000	-0.8
1100	-0.7
1200	-0.3
1300	0.0
1400	0.4
1500	0.6
1600	0.7
1700	0.8

Water Level at location 2 on 26.6.98

Table 5.4 – Salinity along Sedeli Estuary with Respect to Time and Distance

1. Salinity along Sedeli Estuary on 24.6.98

Time	Distance in Km	Salinity in ppt
10.25	0.00	34.00
10.30	1.42	33.40
10.34	2.84	32.63
10.39	5.23	32.93
10.44	6.80	32.75
10.49	8.74	32.12
10.53	9.49	31.23
10.58	10.79	30.07
11.00	12.50	25.84
11.05	14.65	20.30
11.10	16.33	11.36
11.15	18.89	6.19
11.20	20.39	3.15
11.25	21.89	2.11
11.28	23.46	1.02
11.33	24.85	0.59
11.37	28.13	0.00

2. Salinity along Sedeli Estuary on 25.6.98

Time	Distance in Km	Salinity in ppt
10.59	0.00	34.00
11.04	1.22	33.40
11.09	4.19	32.73
11.13	6.59	32.77
11.17	8.24	32.75
11.21	9.38	32.00
11.24	10.80	31.47
11.27	12.05	29.52
11.32	15.86	17.61
11.36	17.95	9.58
11.41	19.96	4.41
11.46	21.15	2.26
11.51	23.31	1.37
11.54	24.69	0.57
11.58	26.20	0.25
12.04	27.49	0.20
12.07	29.04	0.18

Table 5.4 – Salinity Along Sedeli Estuary With Respect To Time and Distance

3. Salinity along Sedeli Estuary on 26.6.98

Time	Distance in Km	Salinity in ppt
12.50	0	34.00
12.55	1.24	33.40
12.59	3.26	32.73
13.04	5.2	32.77
13.09	6.94	32.75
13.12	8.29	32.00
13.15	9.78	31.47
13.20	11.12	30.52
13.22	12.74	21.61
13.25	14.75	12.58
13.30	16.84	7.41
13.34	18.93	5.20
13.39	20.33	3.37
13.43	22.11	2.57
13.47	23.77	1.40
13.52	25.36	0.91
13.56	26.88	0.18
14.00	28.01	0.00

Figure 5.11 shows the water level and salinity measurement recorded at *location 2* for a period of 3 days from 24.6.98 to 26.6.98 which coincided with high waters. It can be seen that there was some correlations between the salinity distributions and the water level. The salinity reading has a maximum value during the high water level. The salinity reading was detected only during high water while during low high water no reading was detected at this location. Similar salinity readings pattern was observed for the next three days

5.1.7 Characteristics of Sedeli Estuary

Salinity distribution was used to determine the type of the Sedeli estuary. Based on **Figure 5.10,** it was observed that the stratification formation was very weak as shown at 13:00 hour on 24.6.98, 14:00 hour on 25.6.98 and 15:00 hours on 26.6.98. At times there

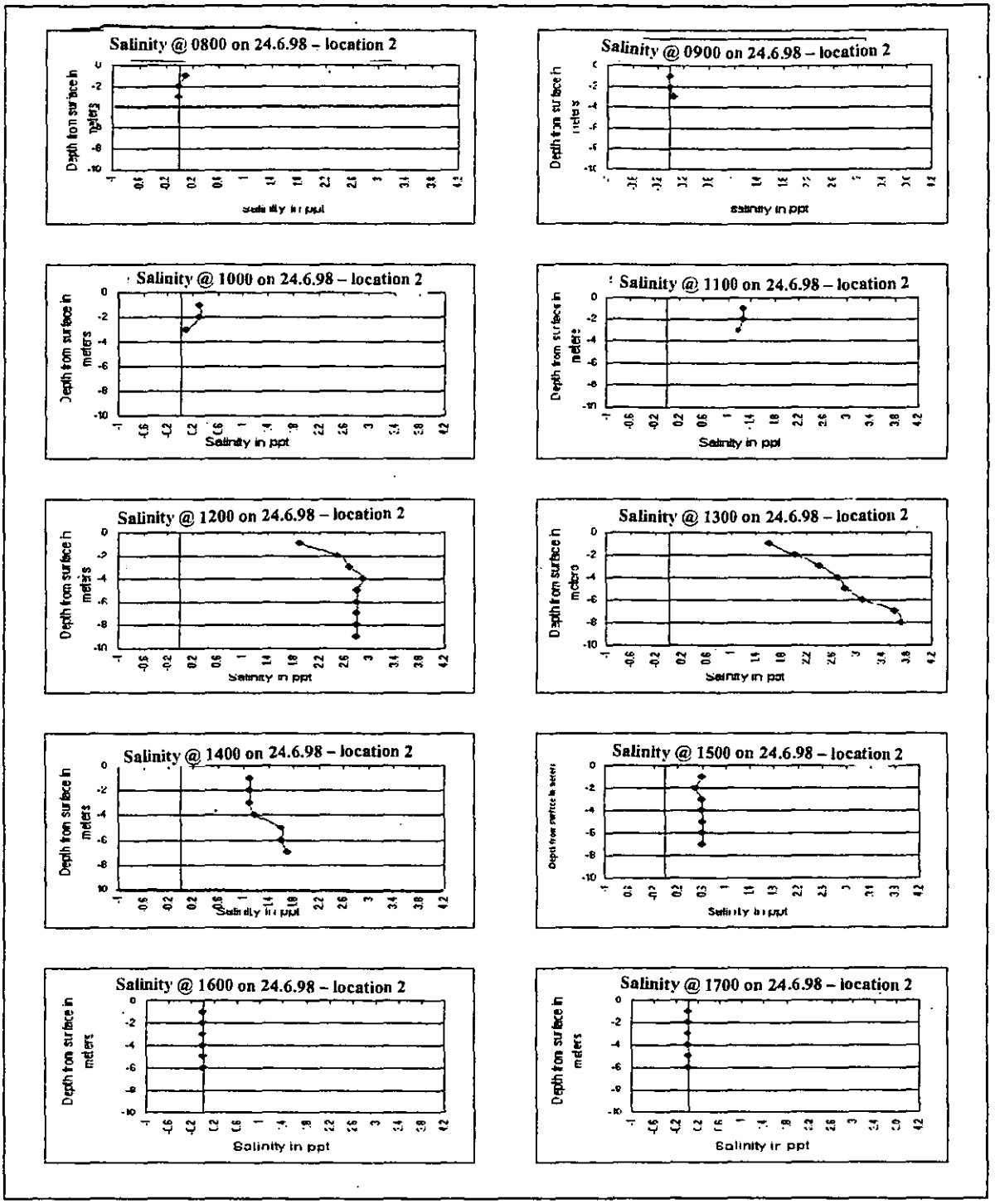

Figure 5.10 – Salinity Profile at Location 2 on 24/6/98 (cont)

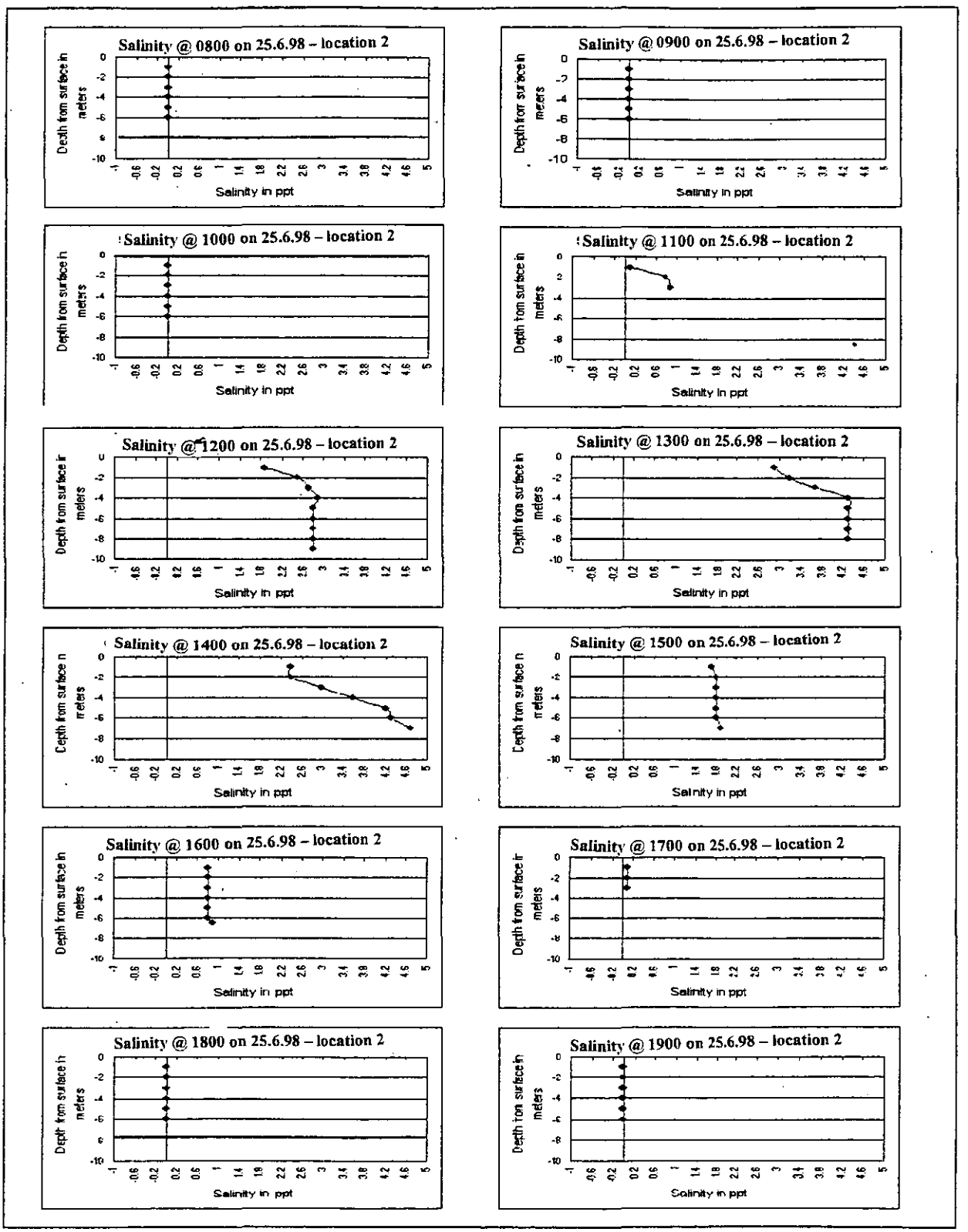

Figure 5.10 – Salinity Profile at Location 2 on 25/6/98 (cont)

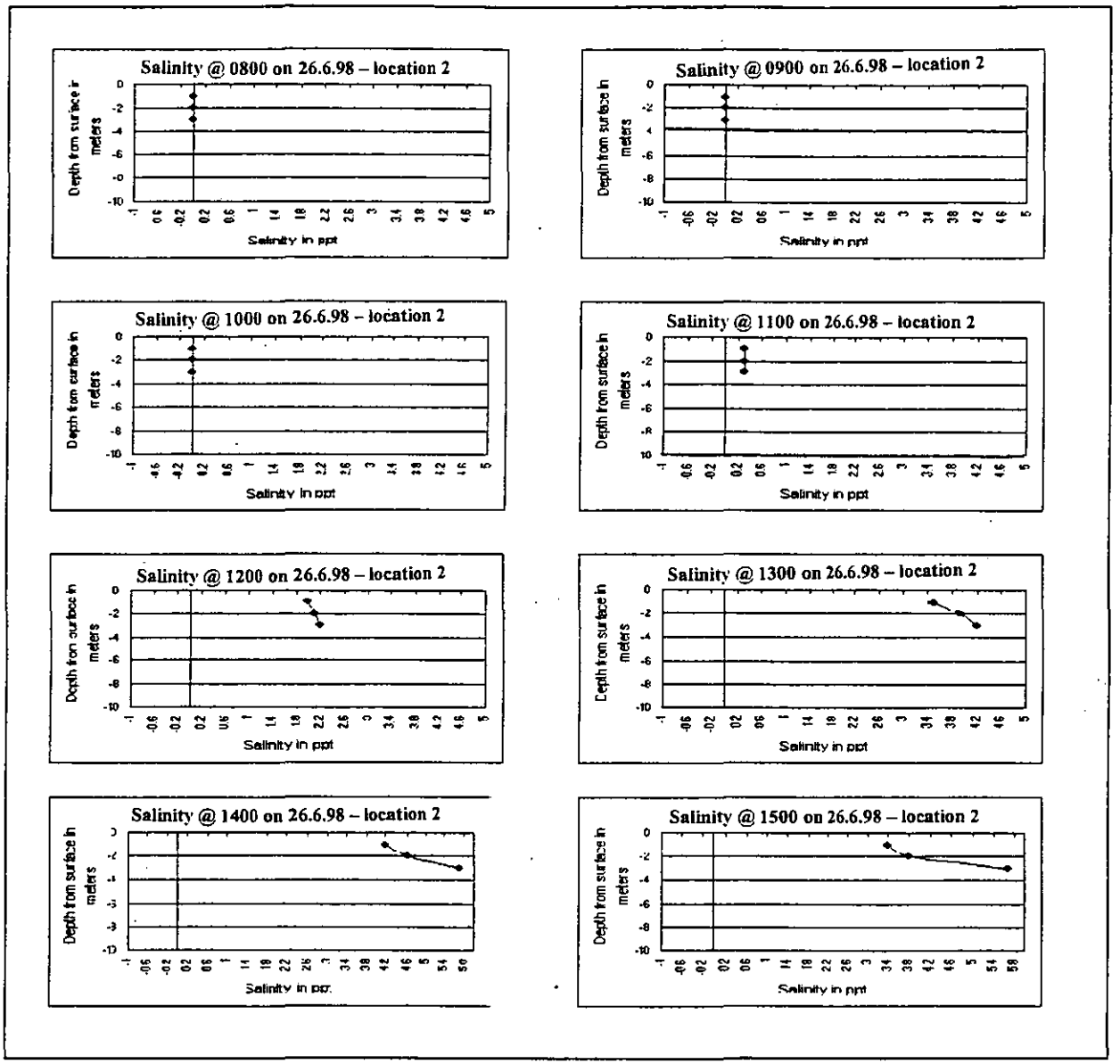

Figure 5.10 – Salinity Profile at Location 2 on 26/6/98

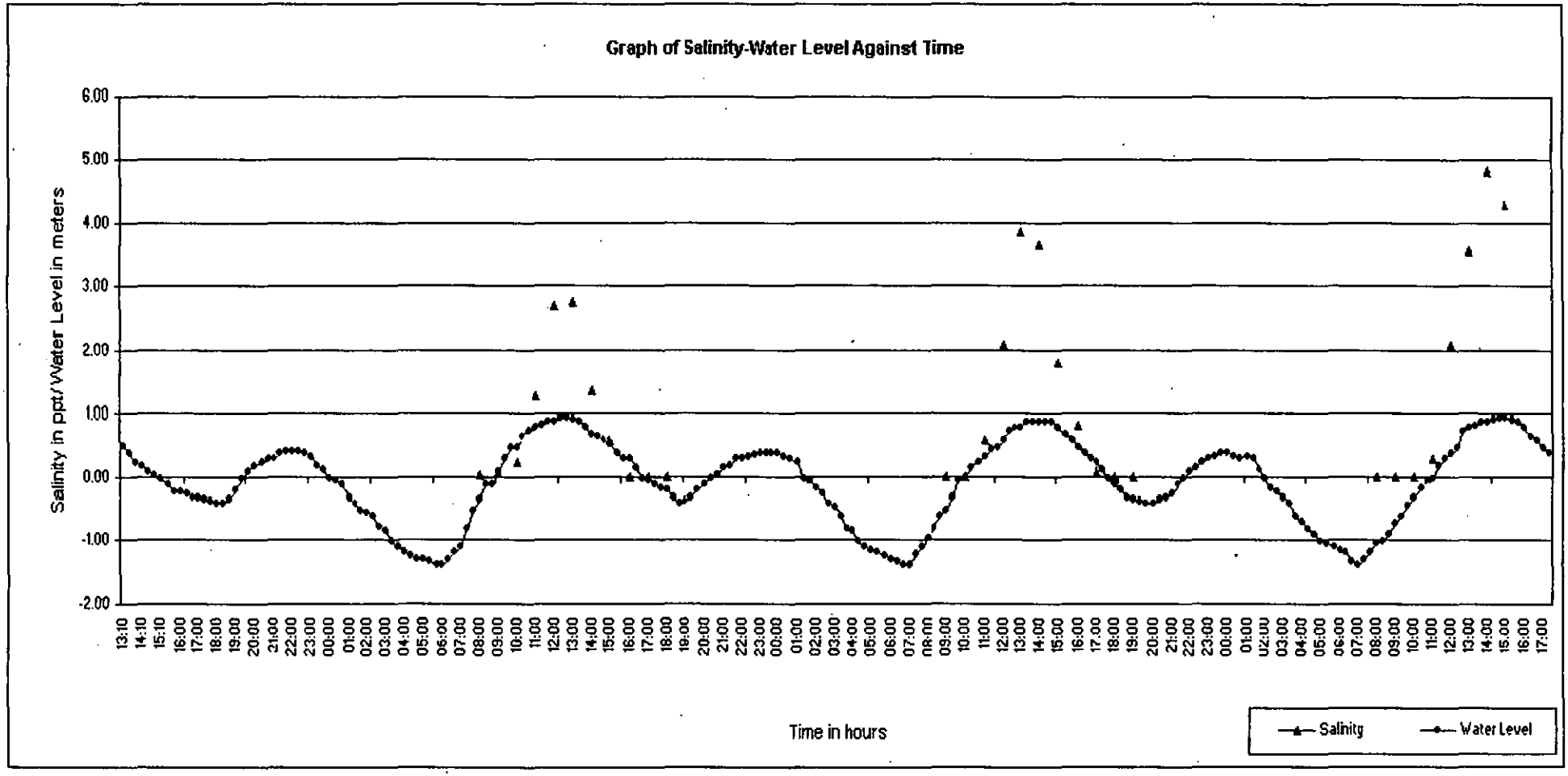

Figure 5.11 – Water Level and Salinity against Time at location 2 from 24.6.98 to 26.6.98

were slight stratifications formed across the river depth. On 24.6.98, the stratification only occurred from 12:00 hour to 14:00 hour with salinity reading ranging from 1.4ppt to 3.8ppt. The salinity then decreased to 0.2ppt across the depth of the river. Similarly on 25.6.98, the stratification occurred from 12:00 hour to 14:00 hour with a salinity reading ranging from 2.2ppt to 4.6ppt before it diluted to 0.2ppt. Similar observation was also observed on 26.6.98. For most of the time, the salinity reading was found to be 0.5% less than the salinity reading at the estuary mouth which was 34ppt. **Table 5.5** shown the analysis of the Sedeli Estuary using Simmons (1955) method to determine the classification of stratification. The results showed that for most of the time, the stratification was in well-mixed category. Therefore it could be concluded that the Sedeli estuary can be classified as a well-mixed estuary. The saline water at this estuary penetrated to a distance of 29.0 kilometres from the estuary mouth during spring tides as shown in **Figure 5.4.**

Tidal readings for the 365 days (1.1.1998 to 31.12.98) were recorded at the estuary mouth. The result was plotted as shown in **Figure 5.12.** The figure shows that there were two spring and two neap peaks for every six months. The tides had two tidal cycles with two levels of high and low waters for a period of 25 hours as shown in **Figure 5.10**. Due to this characteristic, the tide for this estuary can be classified as a diurnal tide which was quite common around the South China Sea.

Figure 5.6 shows the longitudinal sections of the river. The Sedeli river had a positive gradient from the estuary mouth to a distance of 29.0km upstream which happened to be the deepest location of the river. From this location onward the river had a negative gradient. Overall the longitudinal section appeared like a trough with the deepest location at the 29th km. The estuary mouth and the end of the river had a higher elevation compared to the middle section of the river. Due to this lower elevation, the deepest location acted like a reservoir which trapped the freshwater during low water (Uncles *et al.* 1990; Morisawa 1985). It would then dilute the incoming saline water during high water which was why the saline water does not flow beyond the 29th kilometres as shown in **Figure 5.4.** Several factors influenced the bed formation. These factors were river discharge,

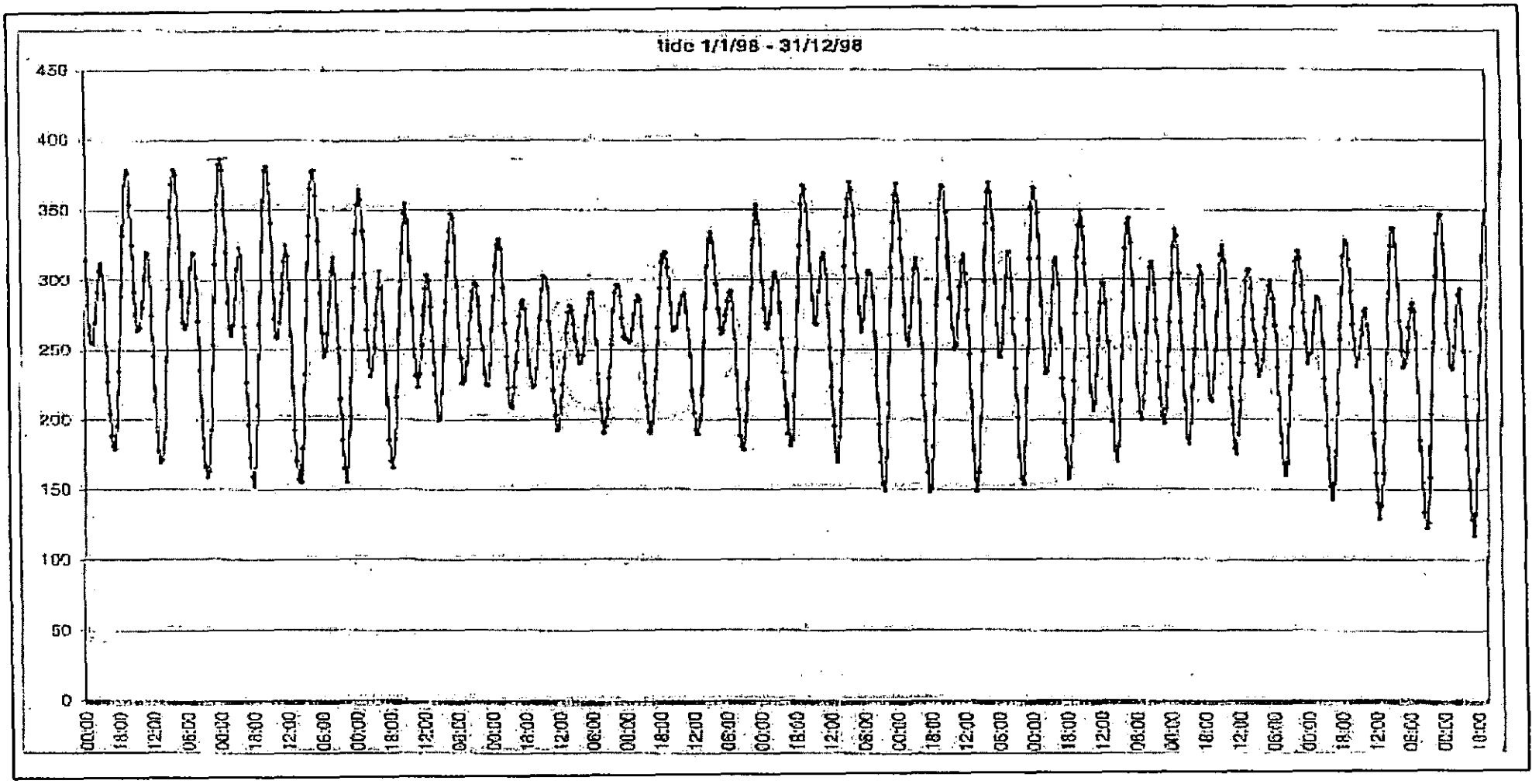

Figure 5.12 – Tide Reading at Sedeli Estuary from 1.1.09 – 31.12.98 Measured at the Estuary Mouth

Table 5.5 – Analysis of Salinity Stratification using Simmons (1955) for Sedeli Estuary

Time	0800	0900	1000	1100	1200	1300	1400	1500	1600	1700
Simmons (1955)	0.0	0.0	0.0	1.3	0.38	0.5	0.59	0.12	0.12	0.0
Type of Stratification	W	W	W	H	P	P	P	W	W	W

Analysis of Salinity Stratification using Simmons (1955) Method for Sedeli Estuary at location 2 on 24.6.98

Time	0800	0900	1000	1100	1200	1300	1400	1500	1600	1700
Simmons (1955)	0.0	0.0	0.86	0.16	0.38	0.8	0.39	0.0	0.0	0.0
Type of Stratification	W	W	I	P	P	H	P	W	W	W

Analysis of Salinity Stratification using Simmons (1955) Method for Sedeli Estuary at location 2 on 25.6.98

Time	0800	0900	1000	1100	1200	1300	1400	1500
Simmons (1955)	0.0	0.0	0.0	0.0	0.15	0.21	0.31	0.53
Type of Stratification	W	W	W	W	P	P	P	H

Analysis of Salinity Stratification using Simmons (1955) Method for Sedeli Estuary at location 2 on 26.6.98

I – Inflow of Water from Floodplain

H – Highly Stratified

P – Partially Stratified

W – Well-Mixed

Table 5.6 - Characteristic of Water Levels for Sedeli Estuary

		Date	Time	Q m^3/s	Tide Level
1	High Water	25.6.98	12:00 hours	35.0	0.75m
2	Low Water	25.6.98	08:00 hours	10.0	-0.5m

tidal effect and flow of water from the floodplains. This phenomenon was very complex in nature and coupled with other variables taken into consideration

Figure 5.7, Figure 5.9 and Figure 5.11 were used to determine the characteristics of the flow for Sedeli estuary. The first analysis was done during high water at 12:00 hour on 25.6.98 and the second during low water at 08:00 on 25.6.98. **Table 5.6** shows the summary of high and low water used in the analysis.

During high water, the water level at *location 1*(at the estuary mouth) was 1.0m above the Mean Sea Level (MSL) which equal to the tide level at 12:00 hours. While the water levels at *location 2, 3 and 4* were equal to 0.9m, 0.8 and 1.0m respectively. Tidal influenced similar to the water level at *locations 1* could be observed at *location 3*. The water level at *location 4* does not show any signed of tidal influenced since it was situated at the remote end of the river.

5.1.8 Conclusion

This section discusses the types and some of the properties of Sedeli Estuary. The main finding discussed in this section is the effect of vegetation flow structures in the river channel and on the formation of bed gradients. The effect of secondary currents on river bed formation could be observed at section 12, where the outer section of the apex had a deeper bed formation compared to the inner section. This observation complemented with other researchers' finding as mentioned in the literature review. Similarly at section 13 and section 14, the bed formations were influenced by the flow of water from the floodplains during ebbing and flooding. The bed gradient and the vegetation on the

floodplains also influenced the formation of the river bed. The salinity intrusion into the river system also played a significant role on the bed formation.

The second finding was the effect of vegetation on the water level in the river channel. As mentioned earlier, the flow from the floodplains influenced the water level during ebbing and flooding. For this estuary, the salinity intruded to a distance of 29km upstream but the effect of tidal influenced could be detected up to a distance of 34km upstream.

5.1 Rompin Estuary

Like the Sedeli Estuary, the Rompin Estuary lies in the eastern part of Malaysia. It was situated about 100km to the north of Sedeli Estuary as shown **Figure 5.1**. Rompin Estuary originated from a hilly area in the southern part of Chini Lake as shown in **Figure 5.13**. The lake is not regulated by any dam or gate. In fact, the lake is the source of freshwater supply to the estuary. The Rompin Estuary flows in a south east direction passing through a low lying swampy floodplain vegetated with mangrove swamps. It then discharges the freshwater into the South China Sea. The total catchment area is 4,285 square km and the length of the river is approximately 250 km long. The yield from this catchment was 245 million liters per day (MLD). The size of the Rompin Estuary is about three times larger and about twice the length of the Sedeli Estuary.

5.2.1 Rompin Estuary Cross-Sections

Seventeen cross-sections were done at this estuary. The sections were located at an interval of 1km to 5km apart as shown in **Appendix B**. For the purpose of bed analysis, only six cross–sections (sections 7, 8, 9, 10, 11 and 12) were studied. **Figure 5.14** shows the cross-sections at the six locations. The distance between these cross-sections from the estuary mouth was shown in **Table 5.7**. All cross-sections were plotted facing upstream. This chapter described the bed formation for all the six cross sections as mentioned above.

Section 7 was situated at the straight section of the river which was about 18.95 km upstream from the estuary mouth. Similar methodology was used to determine the factors that caused the bed formation at this estuary. This cross-section showed typical bed formation at a straight channel where river flow was dominant. The floodplains at this section were vegetated with swamps. Similar to section 7, section 8 was also at a straight section of the river and it was about 20.45 km away from the estuary mouth. Similarly the floodplain was vegetated with swamp on the right bank of the river. The bed formation was quite similar to section 7. Salinity reading at this section ranging from 7ppt to 8ppt for the three days. The average velocity at this section was 40cm/s and it was relatively very strong as shown in **Figure 5.20.** By comparing the salinity reading with the average

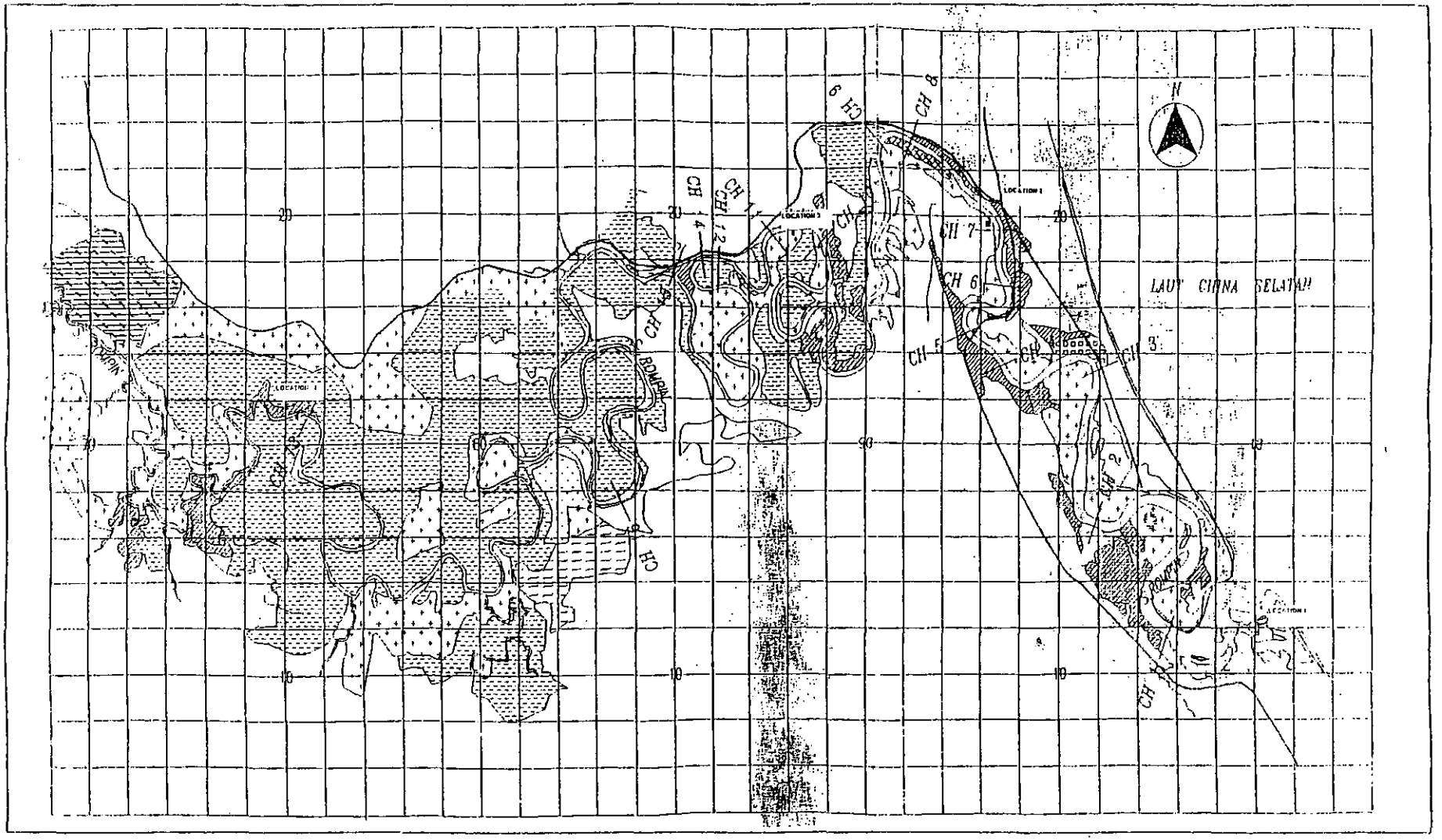

Figure 5.13 – Location of Cross Sections of Rompin Estuary

velocity taken at the same section, it could be concluded that the river flow was dominating over the tidal influence. (Morisawa 1998).

Table 5.7 – Cross-Sections of Rompin Estuary

Rompin Estuary Cross-sections	
Cross-Sections	Distance in Km
1	0.00
2	3.00
3	8.95
4	12.90
5	15.70
6	16.95
7	18.95
8	20.45
9	23.20
10	24.95
11	37.55
12	39.05
13	41.55
14	42.15
15	52.15
16	67.75
17	91.95

Section 9 was located at about 2.75 km upstream of section 8. This section was located at the apex of the meandering section of the river. The cross-section showed that the right bank had a greater erosion effect than the left bank. This was a typical phenomenon for bed formation at the apex of meandering section as discussed in the Sedeli Estuary. The cross-section showed that the tidal played a major factor on the bed formation. Section 10 was located at the straight section of the river and it was about 24.95 km away from the estuary mouth. The cross-section showed the right bank had a

steeper gradient than the left bank. The deepest location occurred at the right bank. At this section only the right floodplain was covered with swamp. During ebbing, the water from both the floodplains would flow into the river. The flow of water on the right floodplain was retarded due to the higher flow resistance compared to the flow on the left bank. With a steeper gradient, the water from the floodplain would plunge vigorously into the river with a high kinetic energy during ebbing. This would create a circulation effects on the right bank which would cause a scouring effect to take place at the right bank of the river. The presence of vegetation on the floodplain played a significant role on the bed formation at this section. The salinity reading from the cross section at this location was relatively low ranging between 4.0ppt to 6.0ppt as shown in **Figure 5.11**. A similar pattern of bed formation was observed or section 11 and section 12.

Figure 5.15 shows the longitudinal profile of salinity distribution. The figure showed there was a sharp decreased in salinity reading after the 8km. The deepest location was situated at 39km away from the estuary mouth. This estuary had a negative gradient of -0.05% from the estuary mouth to a distance of 39km upstream and after this location it had a positive gradient of 0.038%. As discussed in the Sedeli Estuary, the point of intersection of positive and negative gradients would cause a circulation effect which would lead to the scouring effect at the river bed.

Figure 5.16 shows the longitudinal bed level of the Rompin Estuary located at three different locations along the river reach. The deepest location was situated at a distance of 39km away from the estuary mouth. **Figure 5.15** shows the salinity reading at this location was zero. This phenomenon was similar to the Sedeli Estuary as discussed earlier. The deepest location acted as a trough which trapped the freshwater during ebbing. This freshwater would resist the saline water from propagating upstream. With a huge inflow of freshwater it would dilute the saline water during flooding. A significant conclusion that can be drawn from this behaviour was that during the process of mixing between the saline water and the freshwater, it would cause a difference in density level. This would cause a circulation which would lead to the scouring at the river bed. This sediment would precipitate at the location where the circulation and the flow were weak.

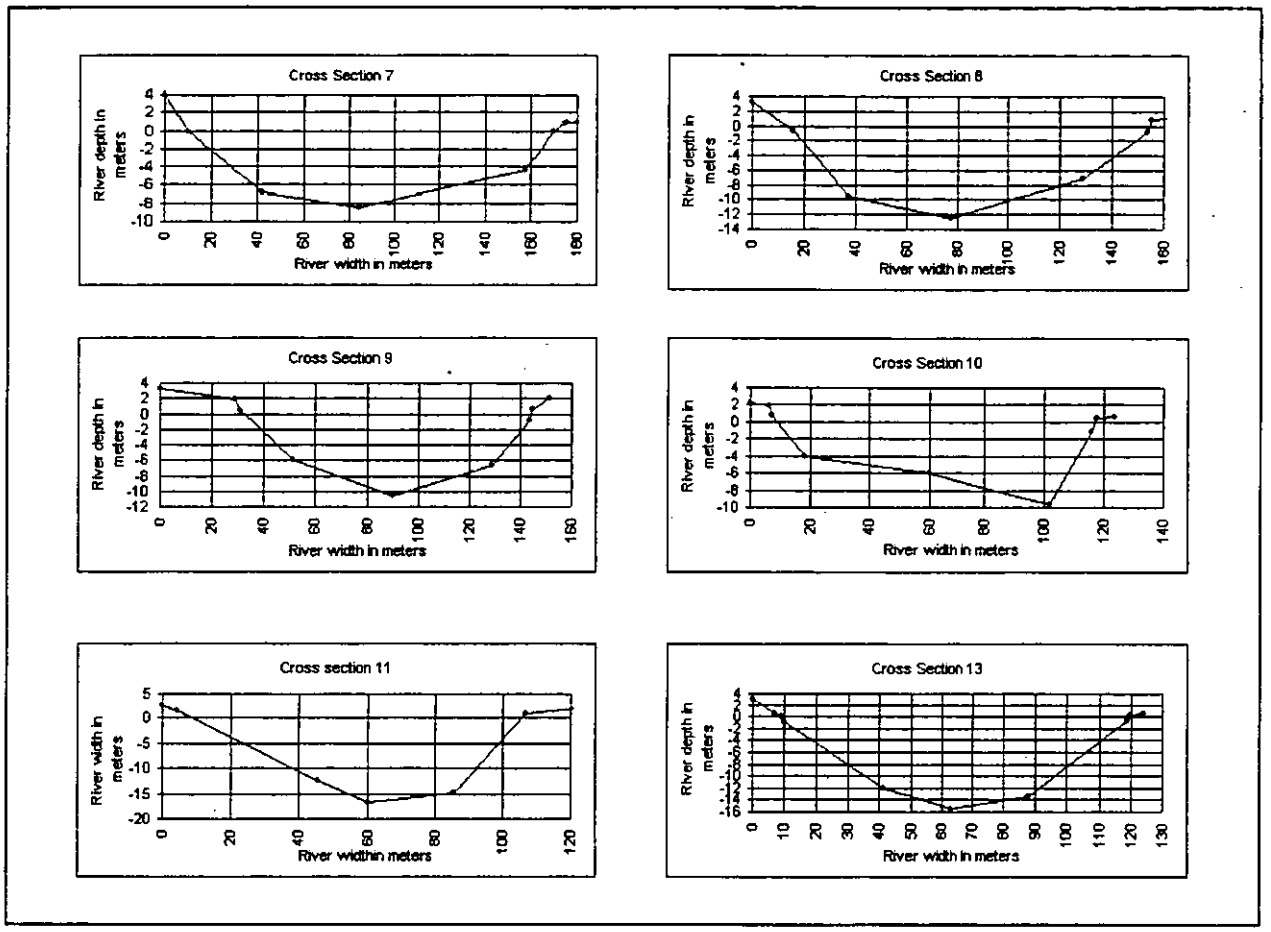

Figure 5.14 – Rompin Estuary Cross-Sections

5.2.2 Rompin Estuary Field Data

Like Sedeli Estuary, all field measurements were recorded for a period of three days from 10.7.98 to 12.7.98. This measurements were taken at *location 2* (section 7) during the spring tide. At the Rompin Estuary there was no tidal station installed around the vicinity. The high water was calculated based on the tide tables published by The Royal Malaysian Navy. The main objective in analysing this estuary was to determine whether there were similarities between the two estuaries. So that a comparison could be made between the two estuaries since the field data collected was limited. The field data collected for this estuary consisted of the following parameters,

- Water level with time series
- Salinity with time series
- Salinity profile with time series
- River flows.

5.2.3 Water Level Measurements

Like the Sedeli Estuary, all equipments used were self-recorded. GPS equipment was used to locate the exact position of these locations. **Figure 5.17** shows the water levels at the *4 locations* along the Rompin Estuary. The *first location* was located at the estuary mouth and the next *3 locations* were situated at a distance of 18.95km, 37.55km and 91.95km away from the estuary mouth respectively. At *location 1*, the water level had two levels of high water and low water for a period of 25 hours. At this location the water level was quite similar to the tidal levels as documented in the tides table published by the Malaysian Royal Navy.

From the above figure, the first high water was 1.5m and it occurred at time T= 10:00 hour on the 11.7.98, while the second high water was 0.25m at time T = 21:00 hour. The two low waters occurred at time T = 03:00 hours and T = 17:00 hour with the water level was about -1.3m and -0.3m respectively. At *location 2*, the water level fluctuated between 1.5m to -0.3m. Similarly, at this location the water level has two high and two

low waters. The water level fluctuated in a sinusoidal pattern ranged between 1.5m and -0.3m. The high and low water at this location lapsed about 5 hours compared with the water level at *location 1*. Unlike location 1, *Location 2* was situated at the low lying where the river runs almost paralleled with the beach. There was no swamp on both sides of the riverbank. Comparison was made on the water level characteristic for both estuaries. For the Sedeli estuary, most area was covered with mangrove swamp while for the Rompin estuary, only certain area was vegetated with mangrove swamp.

At *location 3*, there was some sign of tidal influenced eventhough this location was situated at a distance of 37.55 km away from the estuary mouth. The water level fluctuated which ranging from 0.5 meter to -1.0 which was far less than the *first location*. The time lapsed during the high water and the low water was about 4 hours compared with the water level at *location 1*. The area surrounded this location was vegetated with mangrove swamps on both side of the banks. Compared to *location 2*, the fluctuation at this location was higher. A distinct observation made at this location was that there was no time lapsed between the two locations. The water level fluctuated having a similar pattern as shown in **Figure 5.17**. Only during low water, the water level at this location was higher compared to the *first location*. While for high water, the reading was far less than the *first location*. The *fourth location* was situated at a distance of 91.95km from the estuary mouth. Similarly at this location, the area was surrounded with mangrove swamps on both side of the river banks. The water level at this location does show some fluctuation. These fluctuations were due to the inflow of freshwater from the upstream instead of the tidal effects. The water level fluctuated ranging from 1.5m and –1.0m. The overall comparison made for both estuaries would be discussed at the end of this chapter.

5.2.4 Salinity Measurements

Like the Sedeli Estuary, a similar methodology was used for the salinity measurement at Kg. Bangkong (*location 2*). **Figure 5.18** shows the summary of salinity readings for the two days. In **Figure 5.18**, the salinity reading was 2ppt throughout the depth at 08:00 hour. During this period the freshwater flow rate was 8.23m^3/s and the tide was at low water as shown in **Figure 5.19**. The salinity reading started to increase from

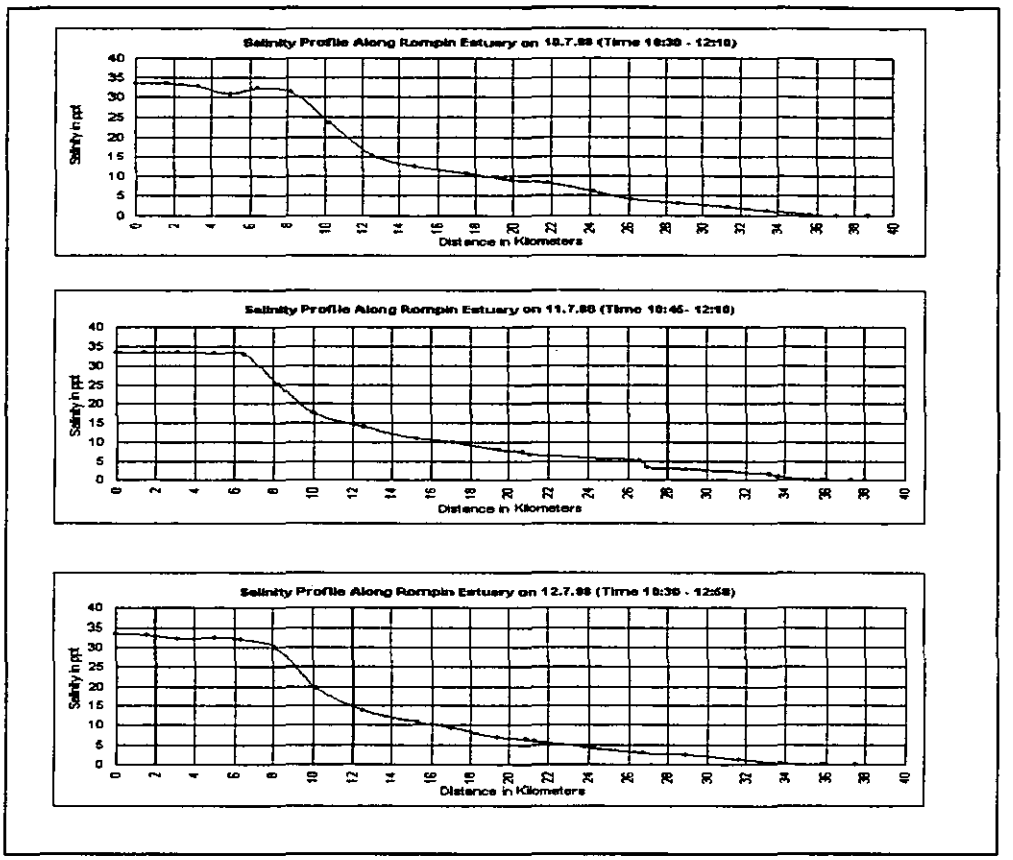

Figure 5.15– Salinity Reading at Rompin Estuary from 10.7.98 – 12.7.98

09:00 hour and reached a maximum reading of 11ppt at 14:00 hour. During this period the inflow of freshwater was 7.70m^3/s and the tide was at high water. The water at this location was thoroughly mixed since the salinity reading showed it had a constant value throughout the depth. The salinity reading then started to decrease to 5.0ppt from 15:00 hour to 19:00 hour. During this interval the tide was ebbing. Similar phenomenon was observed on the 11.7.98, where there were traces of salinity concentration found in freshwater eventhough the tide was ebbing. This was due to the inflow of saline water from the swamp into the river. This occurred was due to the presence of vegetation on the floodplain which delayed the flow of water into the river. The floodplain was filled with saline water during flooding. During ebbing, the saline water would flow into the river and

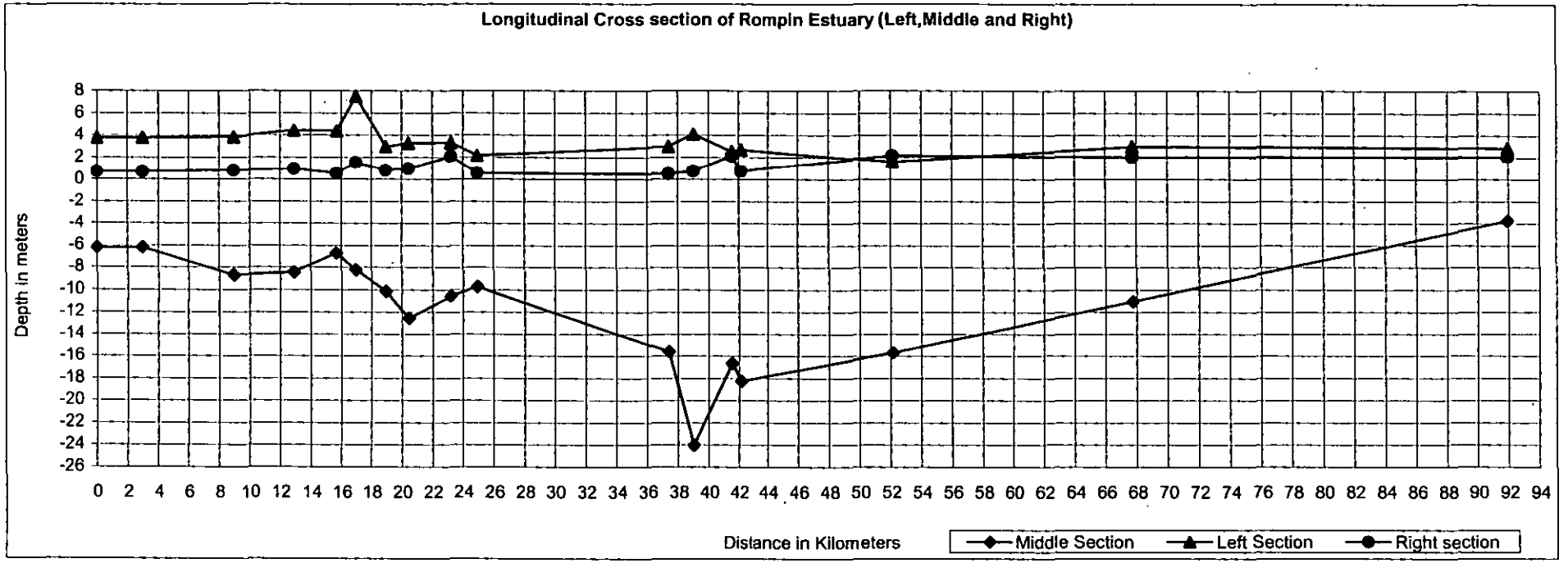

* Right section is on the right bank looking upstream
** Left section is on the left bank looking upstream
*** Zero is referred to mean sea level

Figure 5.16– Longitudinal Sections of Rompin Estuary

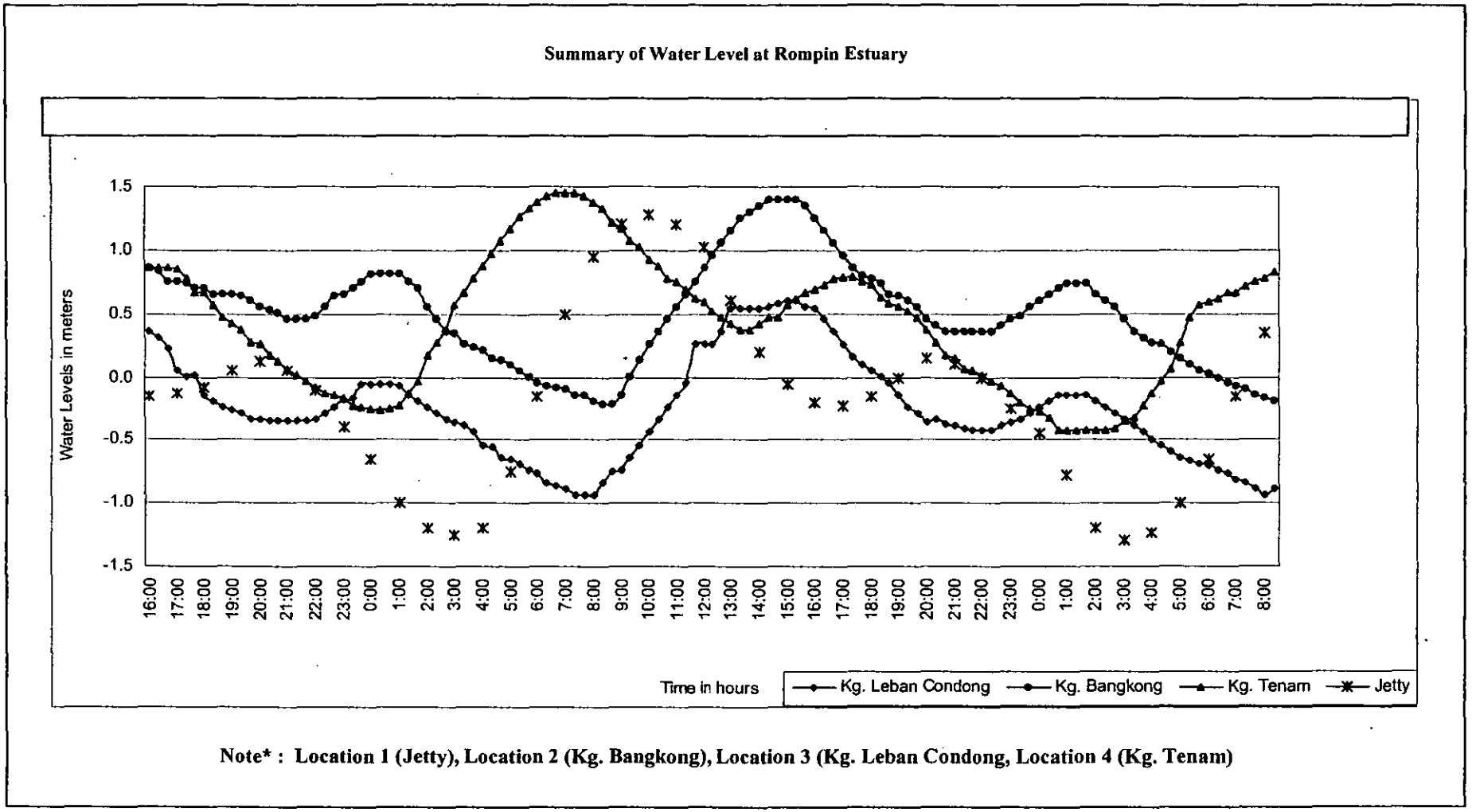

Figure 5.17 – Summary of Water Levels for all Stations along Rompin Estuary from 10.7.98 to 12.7.98

thus the reading showed that there was some salinity residual presences in the river.

5.2.5 Salinity Profiles

Figure 5.15 shows the longitudinal averaged salinity reading along the river reach and the salinity reading at each location at various depths respectively. The salinity readings was taken for a period of the three days as shown in **Table 5.9**. The salinity reading was not detected beyond 35km upstream. **Table 5.8** shows the water level and time where salinity measurement was taken for the Rompin Estuary. There was a reduction of salinity reading after the 8km as shown in **Figure 5.15**. This was due to two main factors that can be observed from the field data. Firstly, the water from the swamp flow into the river and diluted the saline water in the river during flooding. Secondly, the river had a negative gradient of -0.05% from the estuary mouth to a distance of 39 km and a positive gradient of 0.038% from the 39th km onward. This phenomenon was quite similar to the Sedeli Estuary.

5.2.6 River Flow

The freshwater inflow for the Rompin Estuary was obtained from the gauging station owned by the Department of Irrigation and Drainage of Malaysia (DID). No addition measurement was carried out for this river since DID had a 50 years flow records for this estuary. The location of this gauging station was located at about 25.85km downstream of Kg. Tenam *(Location 4)*. **Table 5.11** shows the discharge for the Rompin Estuary from 1.7.98 to 19.7.98. The flow during the three days ranging between 5.89 m^3/s to 9.50 m^3/s.

Table 5.8 – Water Level and Time at location 2 of Rompin Estuary

Time in Hour	Water Level in Meter
0800	Data not available
0900	Data not available
0945	Data not available
1100	Data not available
1200	Data not available
1300	Data not available
1400	Data not available
1500	Data not available
1600	0.8
1700	0.7
1800	0.6
1900	0.6

Water Level at location 2 on 10.7.98

Time	Water Level in Meter
0820	-0.2
0900	-0.3
0933	0.0
1000	0.5
1100	0.6
1200	0.8
1300	1.0
1400	1.3
1500	1.4
1600	1.3
1700	1.0
1800	0.7
1900	0.6

Water Level at location 2 on 11.7.98

Table 5.9 – Salinity Along Rompin Estuary with Respect to Time and Distant (cont)

1. Salinity Along Rompin Estuary on 10.7.98

Time	Distance in Km	Salinity in ppt
10.35	1.67	33.40
10.41	3.27	32.74
10.45	5.01	32.74
10.52	6.45	32.33
10.56	8.25	31.41
11.00	10.24	23.45
11.05	12.56	15.07
11.10	14.86	12.30
11.15	17.47	10.78
11.20	19.94	9.08
11.25	21.78	8.32
11.30	22.22	6.10
11.35	26.13	4.19
11.40	28.66	3.23
11.45	31.30	2.25
11.50	33.38	1.20
11.55	35.63	0.20
12.00	37.04	0.00
12.05	38.73	0.00

2. Salinity Along Rompin Estuary on 11.7.98

Time	Distance in Km	Salinity in ppt
10.45	0.00	33.28
10.50	1.48	33.23
10.54	3.21	33.33
10.56	4.95	33.05
11.00	6.47	32.36
11.04	8.26	27.91
11.08	10.11	17.54
11.13	12.57	13.78
11.18	15.29	10.93
11.23	17.10	9.89
11.28	19.47	7.90
11.30	20.67	7.31
11.34	21.10	6.69
11.40	26.62	5.12
11.45	26.95	3.36
11.50	28.93	2.84
11:55	33.20	1.63
12.00	33.63	0.69
12.05	35.83	0.00
12.10	37.30	0.00

Table 5.9 – Salinity Along Rompin Estuary with respect to Time and Distant

3. Salinity along Rompin Estuary on 12.7.98

Time	Distance in Km	Salinity in ppt
11.27	0.00	33.38
11.35	1.67	33.28
11.41	3.14	33.21
11.45	5.07	32.43
11.50	6.33	32.07
11.54	8.16	27.95
11.57	10.13	19.55
12.02	12.51	13.77
12.07	15.31	10.81
12.11	17.05	9.27
12.15	19.39	6.93
12.20	20.83	6.49
12.22	21.28	6.09
12.25	23.75	4.47
12.32	26.71	2.90
12.36	28.91	2.42
12.43	31.67	1.29
12.47	33.69	0.20
12.53	35.88	0.00
12.58	37.50	0.00

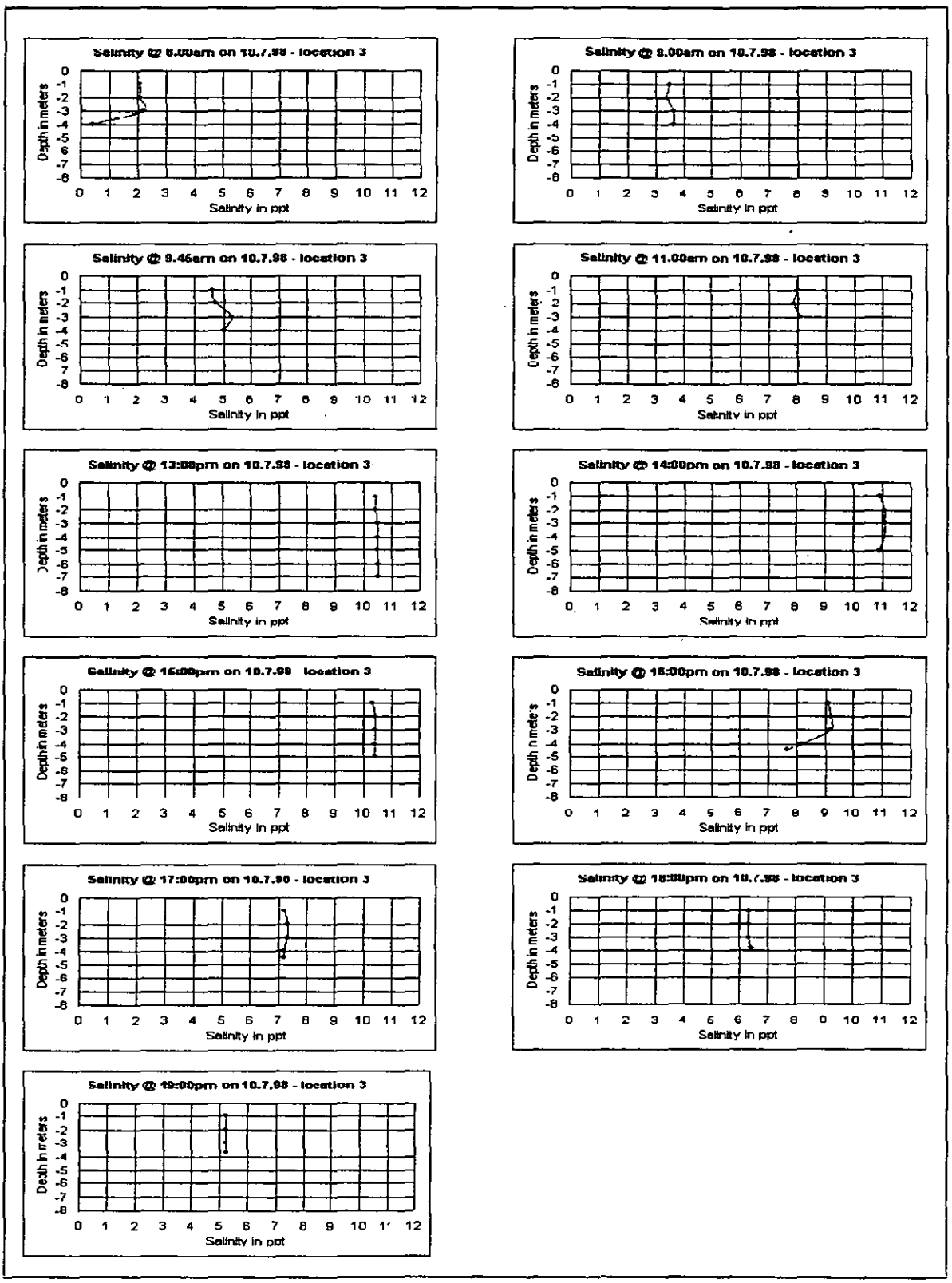

Figure 5.18 - Salinity Distribution at Location 2 Rompin Estuary 10.7.98 (cont)

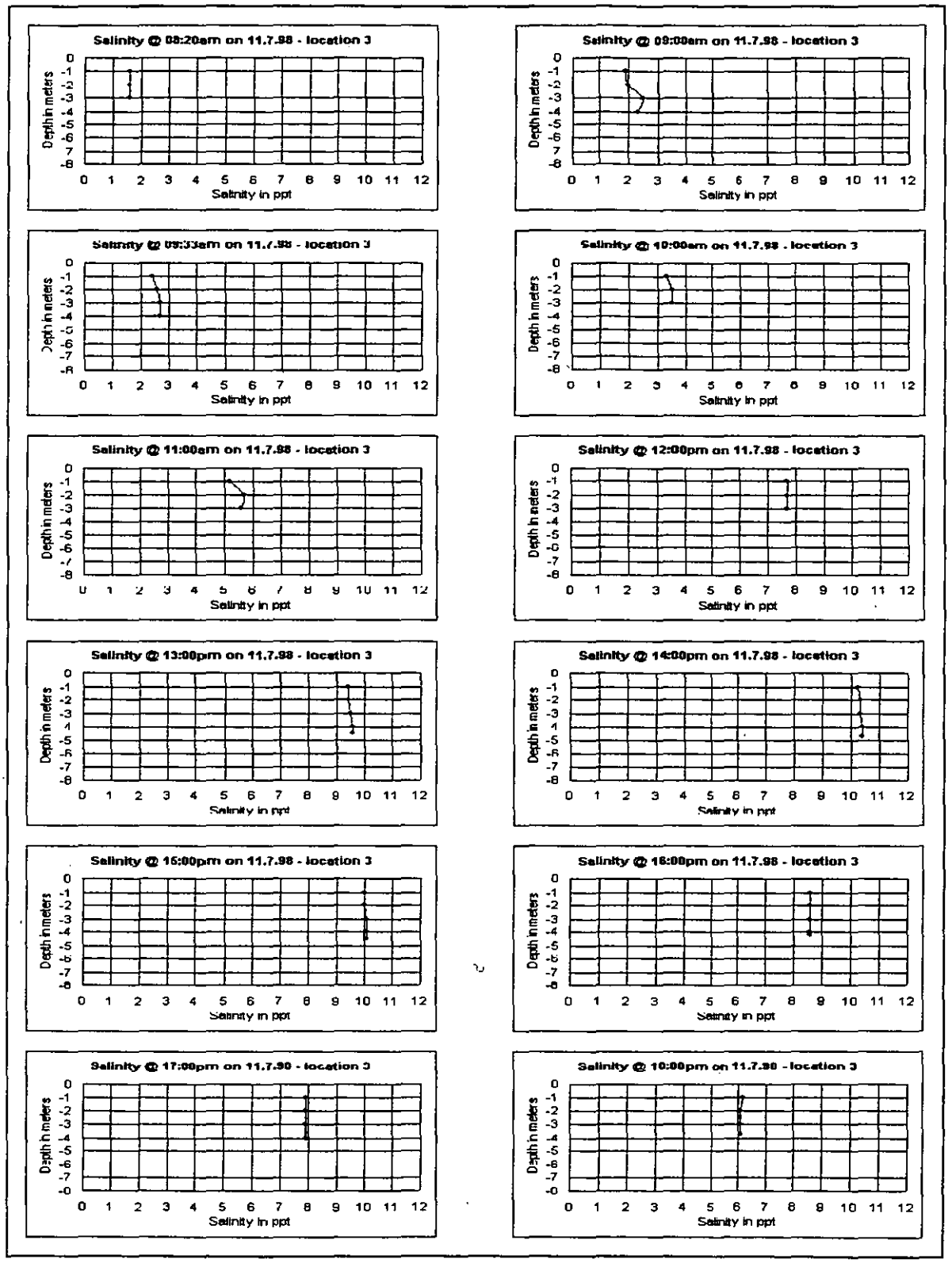

Figure 5.18 - Salinity Distribution at Location 2 of Rompin Estaury 11.7.98

5.2.7 Characteristic of Rompin Estuary

Like Sedeli estuary, the same methodology was used to determine the characteristics of Rompin estuary. **Figure 5.18**, shows the salinity distribution at various depths at *location 2* for the Rompin estuary during spring tide. The salinity stratification was very weak as shown at this location at 0945 hour and 1600 hour on 10.7.98. A similar salinity distribution pattern could be observed at 09:00 hours to 11:00 hours on 11.7.98. For most of the time, there was stratification formed throughout the depth at *location 2* for this estuary. A similar analysis was carried for this estuary using the Simmons (1955) to determine the classification of stratification. **Table 5.10** shows the results of classification for the Rompin Estuary. It can been seen that most of the time the stratification was in a well-mixed category. Therefore, it could be concluded that the Rompin estuary was as a well-mixed estuary similar to the Sedeli estuary as discussed earlier. **Figure 5.19** shows the salinity distribution against water levels at *location 2* from 10.7.98 to 12.7.98. The salinity reading could be detected up to a distance of 39.0km from the estuary mouth as shown in **Figure 5.15.** This distance coincided with the deepest point along the river as shown in **Figure 5.16**. Similar phenomenon like the Sedeli estuary occurred for this estuary. Unlike Sedeli estuary, this estuary was not fully vegetated with mangrove swamps on both floodplains along the river reach.

Table 5.10 – Analysis of Salinity Stratification using Simmons (1955) for Sedeli Estuary

Time	0800	0900	1000	1100	1200	1300	1400	1500	1600	1700	1800	1900
Simmons(1955)	1.16	0.02	0.10	0.0	0.0	0.0	0.0	0.0	0.0	0.0	0.0	0.0
Type of Stratification	H	W	W	W	W	W	I	W	W	W	W	W

Analysis of Salinity Stratification using Simmons (1955) Method for Rompin Estuary at location 2 on 10.7.98

Analysis of Salinity Stratification using Simmons (1955) Method for Rompin Estuary at location 2 on 11.7.98

Time	0820	0900	0933	1000	1100	1200	1300	1400	1500	1600	1700	1800
Simmons (1955)	0.0	0.27	0.08	0.06	0.07	0.0	0.02	0.0	0.0	0.0	0.0	0.0
Type of Stratification	W	P	W	W	W	W	W	W	W	W	W	W

I – Inflow of Water from Floodplain

H – Highly Stratified

P – Partially Stratified

W – Well-Mixed

Table 5.11 – Flow Discharge of Rompin Estuary

HOURLY MEANS FLOWS FOR JULY 1998 AT SG. ROMPIN, KUANTAN/SEGAMAT BRIDGE FLOW IN m^3/s

Hour / Day	1	2	3	4	5	6	7	8	9	10	11	12	13	14	15	16	17	18	19	20	21	22	23	24	Mean
1	0.77	0.75	0.73	0.71	0.69	0.66	0.65	0.64	0.63	0.61	0.59	0.56	0.53	0.50	0.48	0.48	0.47	0.46	0.44	0.44	0.43	0.43	0.42	0.42	0.56
2	0.42	0.42	0.41	0.41	0.41	0.41	0.40	0.40	0.40	0.40	0.40	0.40	0.40	0.40	0.40	0.40	0.40	0.41	0.41	0.42	0.42	0.44	0.45	0.47	0.41
3	0.49	0.50	0.52	0.54	0.57	0.60	0.63	0.65	0.66	0.67	0.67	0.68	0.69	0.70	0.69	0.68	0.68	0.67	0.67	0.67	0.67	0.67	0.68	0.69	0.64
4	0.70	0.73	0.75	0.78	0.83	0.88	0.94	1.00	1.06	1.12	1.16	1.21	1.24	1.28	1.30	1.32	1.33	1.34	1.34	1.33	1.32	1.30	1.27	1.23	1.11
5	1.19	1.17	1.15	1.14	1.13	1.12	1.11	1.10	1.10	1.10	1.10	1.12	1.14	1.15	1.17	1.19	1.22	1.26	1.29	1.33	1.37	1.42	1.46	1.49	1.21
6	1.53	1.55	1.57	1.60	1.67	1.82	2.05	2.34	2.70	3.10	3.57	4.08	4.62	5.20	5.77	6.24	6.67	7.09	7.38	7.77	8.18	8.59	9.06	*	4.74
7	*	*	*	*	*	*	*	*	*	*	*	*	*	*	*	*	*	*	*	*	*	*	*	*	13.38
8	*	*	*	*	*	*	*	*	*	*	*	*	*	*	*	*	*	*	*	*	*	*	*	*	15.00
9	*	*	*	*	*	*	*	*	*	*	*	*	*	*	*	*	*	*	*	*	*	*	*	*	11.71
10	9.50	9.35	9.22	9.09	8.93	8.77	8.63	8.49	8.36	8.23	8.09	7.96	7.84	7.70	7.57	7.49	7.41	7.35	7.31	7.23	7.13	7.04	6.94	6.85	8.02
11	6.75	6.66	6.56	6.47	6.36	6.27	6.19	6.11	6.03	5.97	5.89	5.97	6.04	6.07	6.10	6.14	6.18	6.23	6.27	6.32	6.38	6.45	6.51	6.57	6.27
12	6.64	6.70	6.77	6.83	6.90	6.96	7.03	7.08	7.13	7.17	7.22	7.26	7.29	7.32	7.35	7.39	7.42	7.45	7.48	7.52	7.55	7.58	7.61	7.64	7.22
13	7.68	7.71	7.74	7.77	7.78	7.80	7.82	7.83	7.85	7.87	7.88	7.91	7.93	7.96	7.98	8.01	8.03	8.06	8.08	8.09	8.11	8.11	8.10	8.10	7.92
14	8.08	8.05	8.02	8.00	7.99	7.98	7.98	7.98	7.99	7.99	8.00	8.02	8.04	8.06	8.08	8.11	8.14	8.17	8.20	8.21	8.23	8.24	8.25	8.26	8.09
15	8.26	8.27	8.27	8.26	8.25	8.24	8.23	8.23	8.22	8.21	8.20	8.20	8.21	8.22	8.23	8.25	8.29	8.32	8.36	8.40	8.44	8.49	8.53	8.57	8.30
16	8.60	8.63	8.66	8.68	8.69	8.70	8.71	8.70	8.68	8.66	8.65	8.62	8.59	8.56	8.55	8.54	8.53	8.52	8.52	8.52	8.53	8.54	8.54	8.55	8.60
17	8.56	8.56	8.57	8.58	8.59	8.59	8.60	8.61	8.61	8.61	8.61	8.61	8.61	8.61	8.60	8.60	8.60	8.59	8.59	8.59	8.58	8.58	8.58	8.57	8.59
18	8.56	8.55	8.54	8.53	8.54	8.55	8.56	8.58	8.60	8.64	8.67	8.71	8.75	8.79	8.82	8.84	8.87	8.89	8.92	8.94	8.95	8.96	8.97	8.98	8.74
19	8.99	9.00	9.02	9.03	9.05	9.07	9.09	9.10	9.12	9.15	9.19	9.22	9.32	9.43	9.48	?	?	?	?	?	?	?	?	?	

- *Data not Available
- Data from Department of Irrigation And Drainage, Malaysia (DID)

5.3 Sedeli Estuary versus Rompin Estuary

This section discusses the comparison made between both the estuaries in order to determine their similarities. From the analysis made, both the estuaries could be categorised as a well-mixed type since the salinity reading showed a very weak stratification formed at an irregular interval and for a short time period. For most of the time, the salinity reading showed no stratification formed. From the longitudinal sections, both estuaries have a positive and a negative gradients where the deepest point was several kilometres upstream. This deepest point acted like a trough which stored the freshwater during ebbing. During high water this freshwater would dilute the incoming saline water from the estuary mouth. The saline water from both estuaries does not penetrated beyond the deepest point even though the water levels showed some tidal effects further upstream. Both estuaries have diurnal tides which meant that they have two levels of high and low water reading at the estuary mouth. On the bed formation, both estuaries have similar characteristics in term on how the river beds formation where tidal, freshwater flow and inflow from mangrove swamps became the main mechanism for the bed profiles

formation.

Sedeli estuary had a less river discharge compared to the Rompin estuary and it had a shorter reach and a smaller catchment area. From the vegetation aspect, the Sedeli Estuary had a higher mangrove density compared to the Rompin Estuary. In term of the water level profiles for both the estuaries, it could be seen that the water levels at the Sedeli Estuary resembled to the tidal fluctuations but with some phase difference. The Sedeli Estuary had a gentler bed slope gradients compared to the Rompin Estuary.

5.4 Summary

In this chapter, two estuaries were analysed to determine their characteristics. Comparisons were made based on their stratifications, bed profiles, and salinity readings. The two estuaries were compared for their similarities. From the analysis, both estuaries can be categorised as a well-mixed estuary since the stratification formed was relatively weak. For the Sedeli Estuary, the salinity propagated to a distance of 29 km while for the Rompin Estuary, it propagated up to a distance of 39km. There was an indication that some traces of salinity reading was observed during ebbing. This was contributed by the inflow of saline water from the swamp which covered most of their floodplains. Furthermore, both estuaries showed some similarities on the bed formation which was either due to the influence of floodplains or river flow. In term of the longitudinal section, both estuaries have a negative gradient from the estuary mouth to the deepest location and a positive gradient upstream. At the deepest location, the area was filled with freshwater during ebbing which would dilute the saline water during the high tides. The effect of the mangrove had some influence on the flow structure in the river channel. In the next chapter a CFD code was used to study the effect of vegetated floodplains on the flow structure of the river channel.

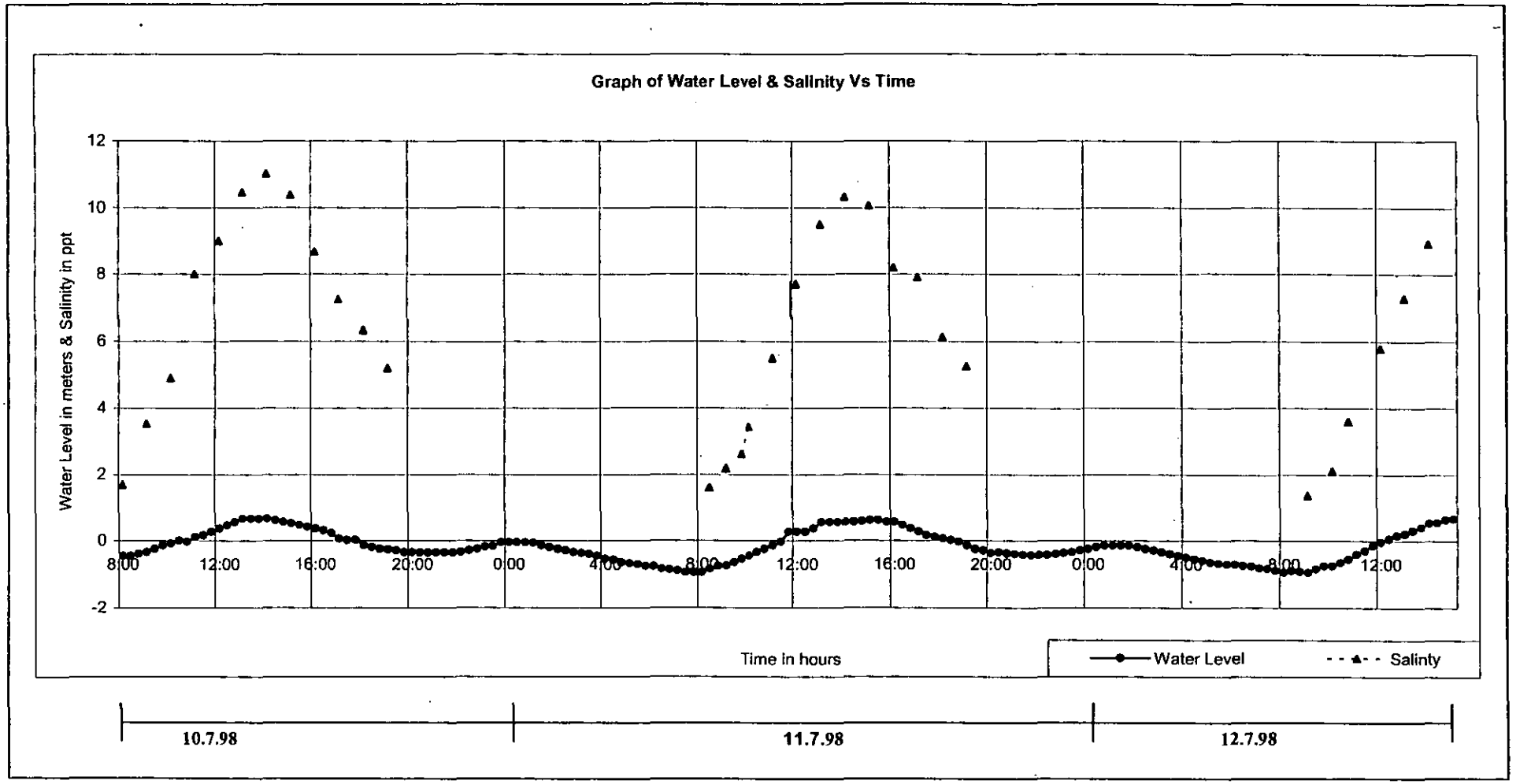

Figure 5.19- Shows The Salinity and Water Level at Kg. Bangkong (Section 2)

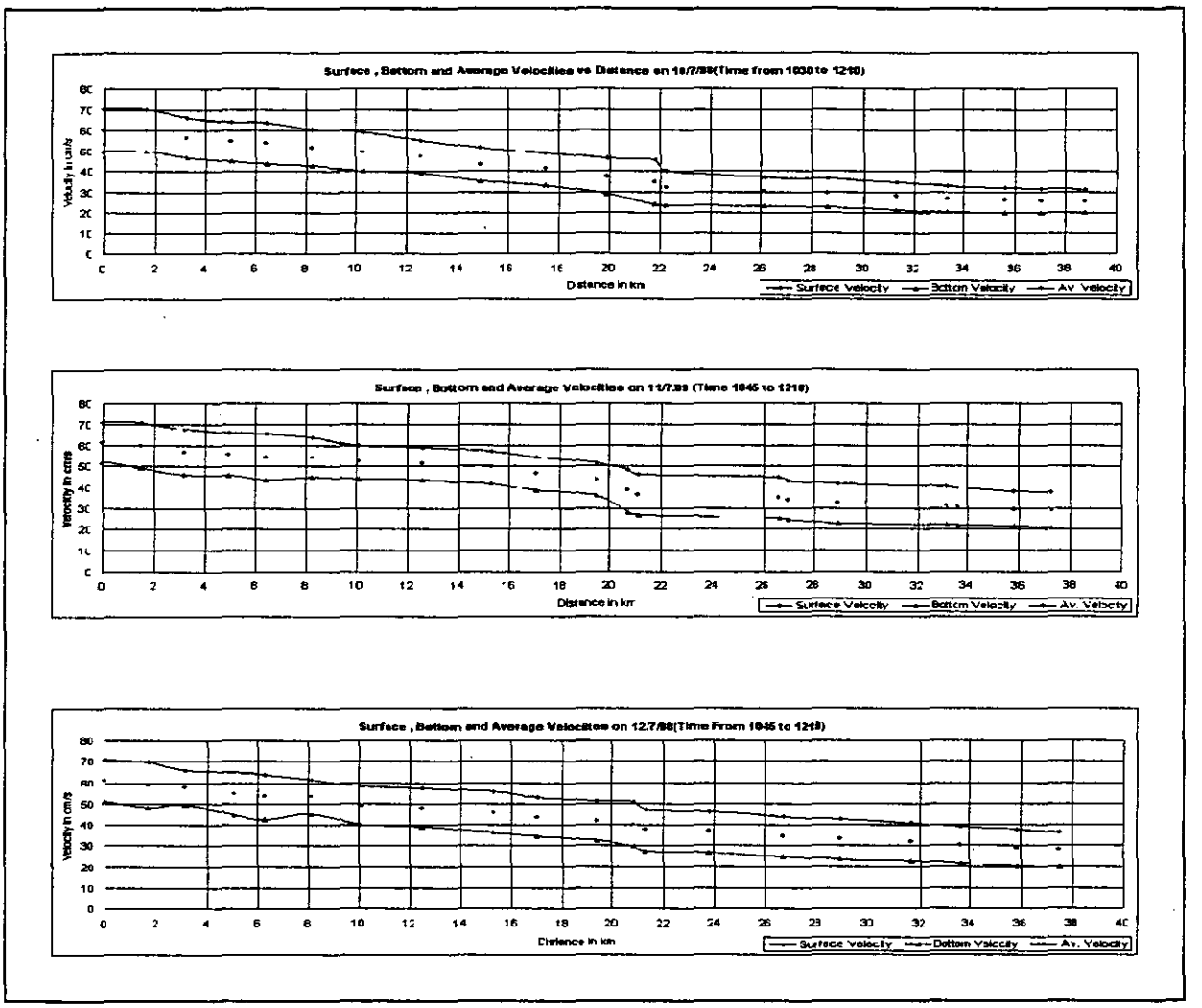

Figure 5.20 – Velocities Profiles against Distance along Rompin Estuary During High Water (Surface, Bottom and Average)

Appendix A

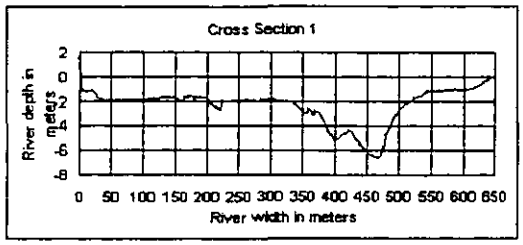

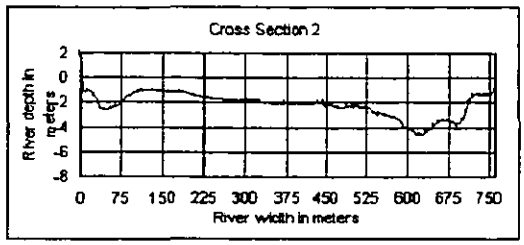

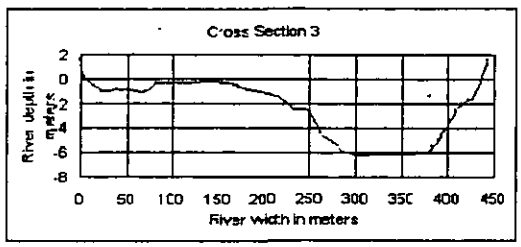

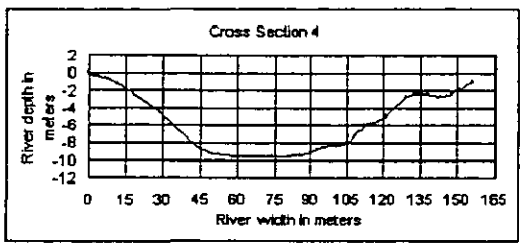

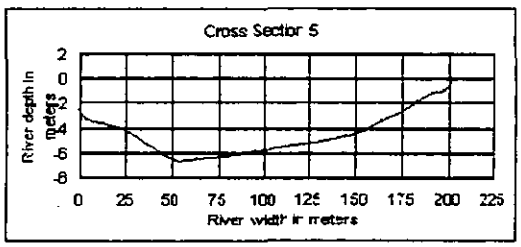

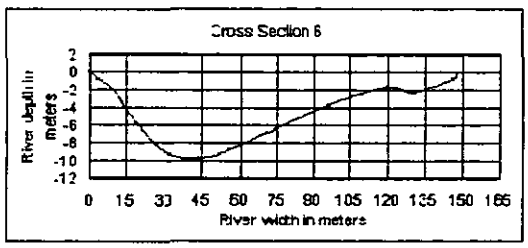

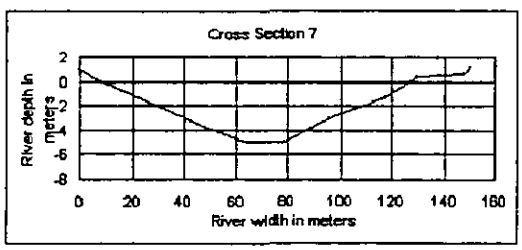

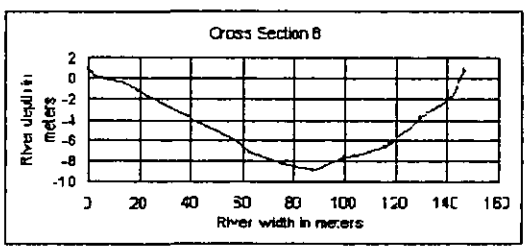

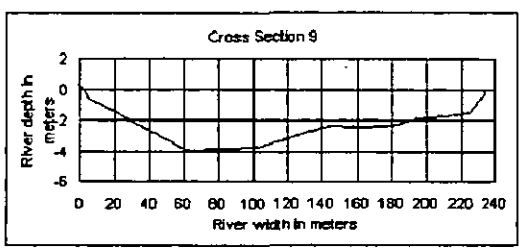

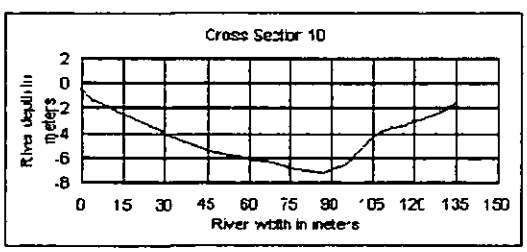

Sedeli River Cross Sections (cont)

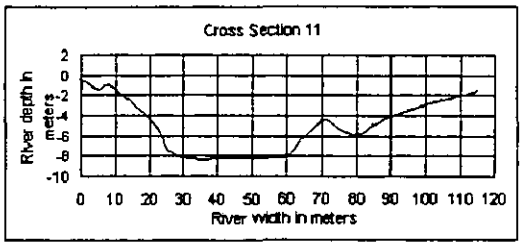

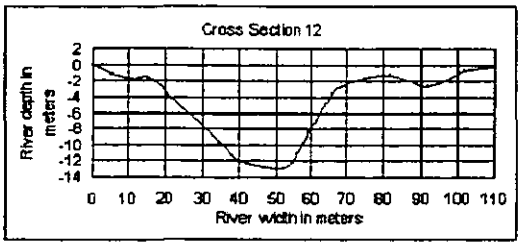

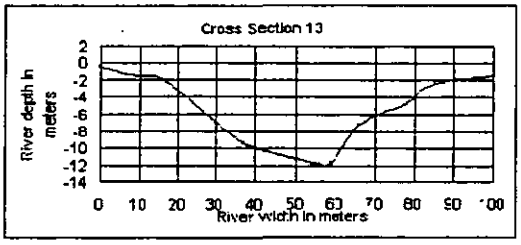

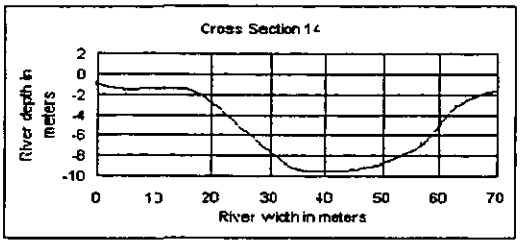

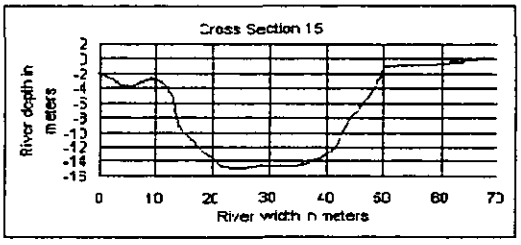

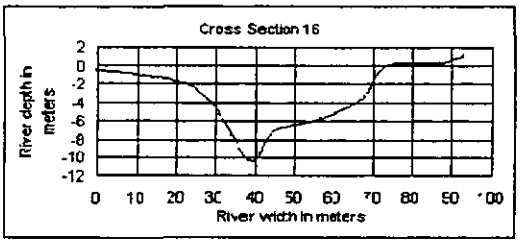

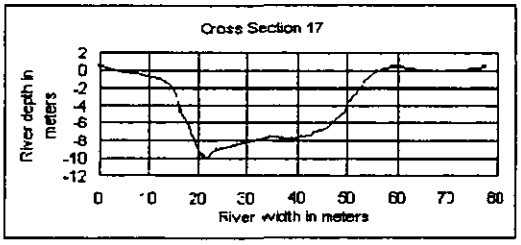

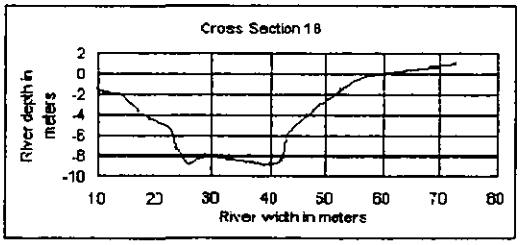

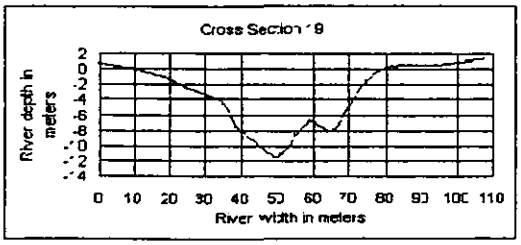

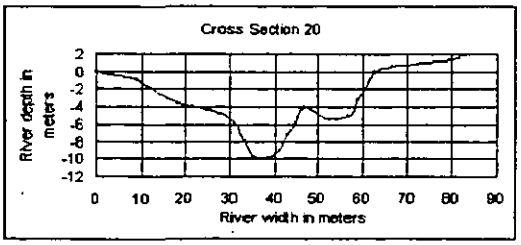

Sedeli River Cross Sections (cont)

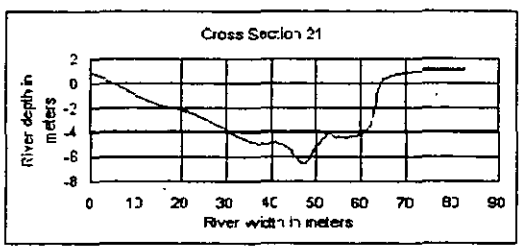

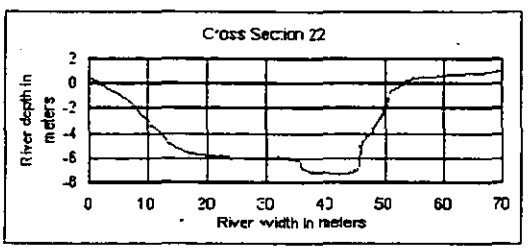

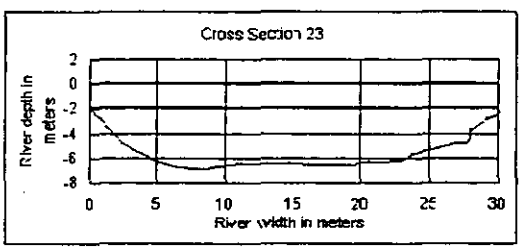

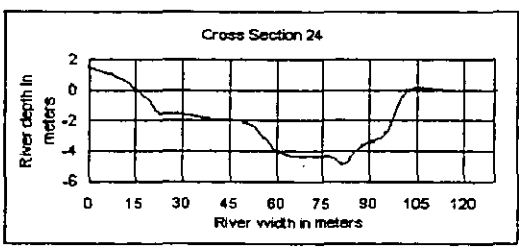

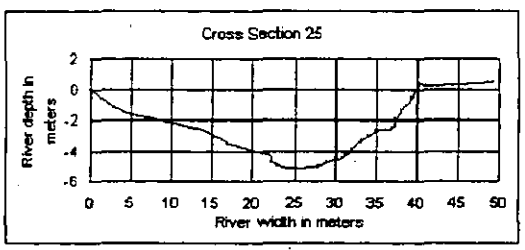

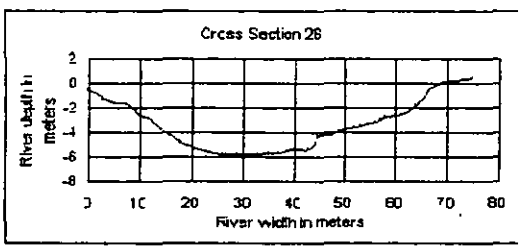

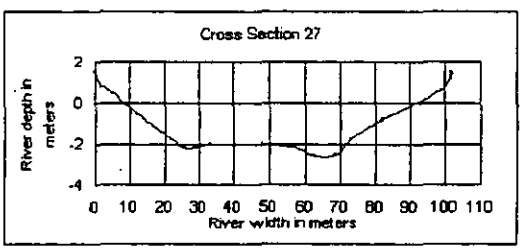

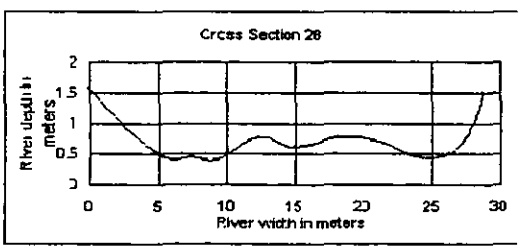

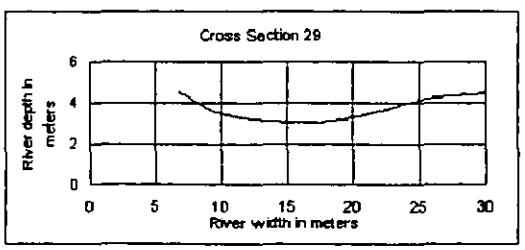

Sedeli River Cross Sections

Appendix B

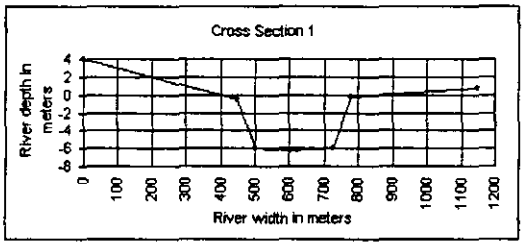

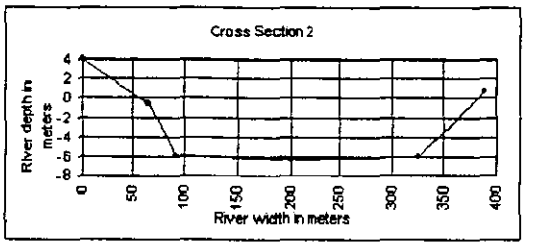

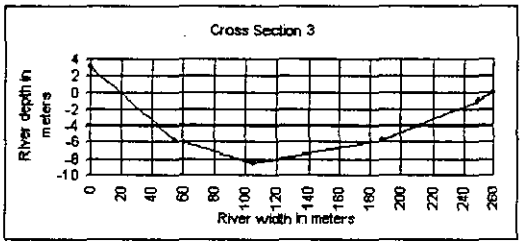

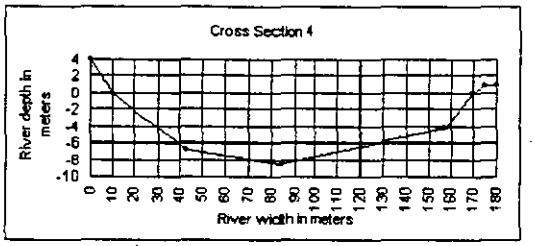

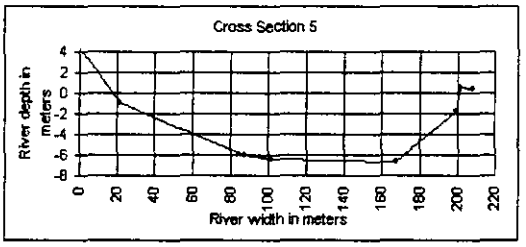

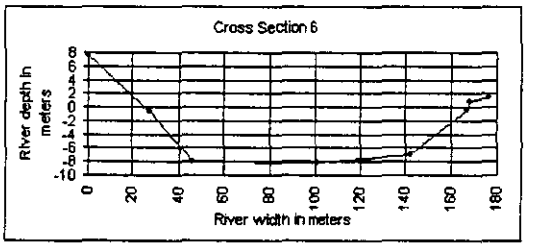

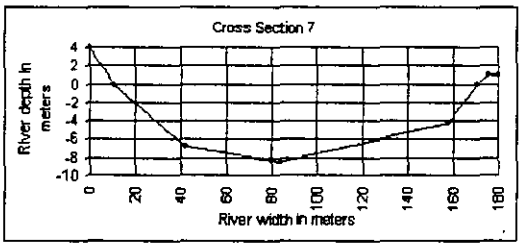

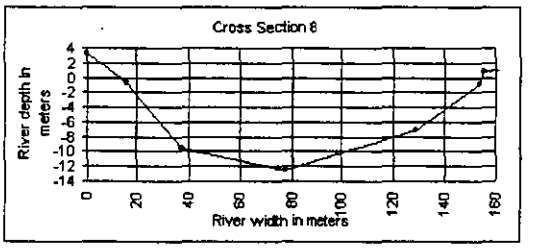

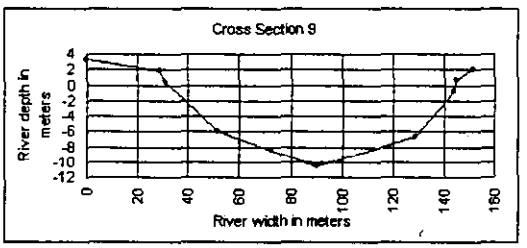

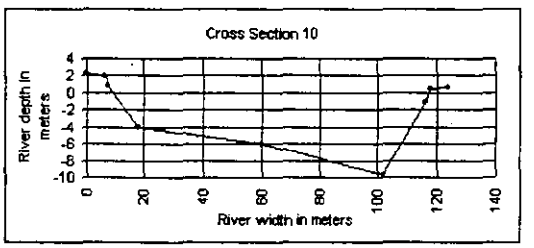

Rompin Estuary Cross-Sections (cont)

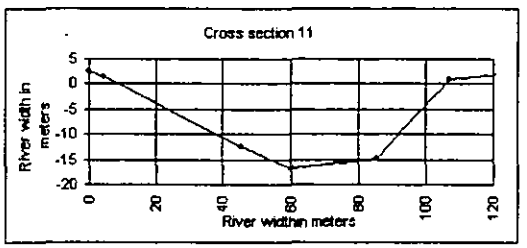

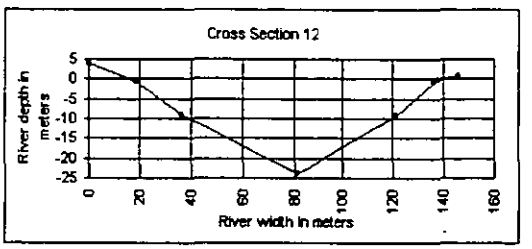

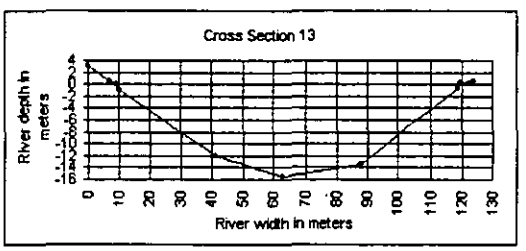

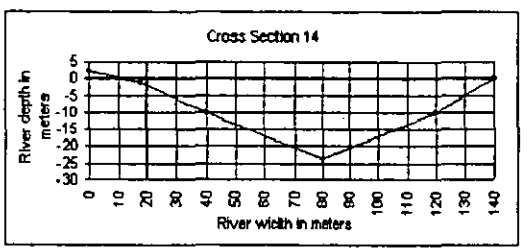

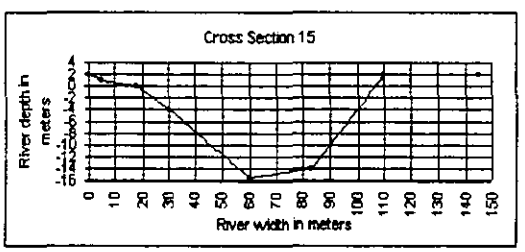

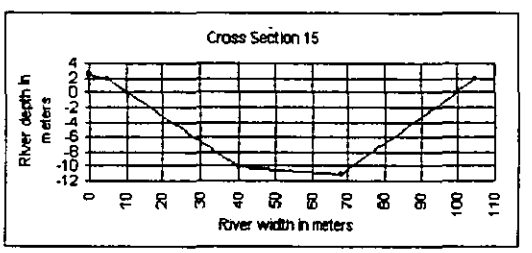

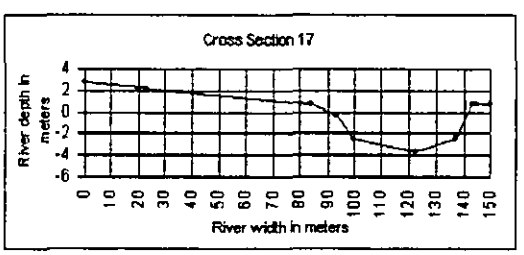

Rompin Estuary Cross-Sections

CHAPTER 6

COMPUTATIONAL RESULTS AND DISCUSSIONS

6.0 Introduction

This section reviews the techniques and application of TELEMAC used to predict flows in Sedeli estuary. In this study, three cases were considered to determine the flows, water levels, velocities and salinity distribution in the Sedeli Estuary. In order to understand the effect of the floodplains on the flow structures, three cases were studied namely an estuary with very wide floodplains, the second an estuary with a narrow floodplain and finally an estuary without floodplain. Further simulations were also done for swamps covered with mangrove. This was to determine the effects of vegetated swamp on the flow structures. Two types of turbulent models (the Constant Eddy Viscosity and the Elder's Turbulent Model) and three advective schemes (the Method of Characteristics, the Streamline Upwind Petrov-Galerkin and the Centred semi-implicit scheme) were therefore used in the simulations.

TELEMAC-2D was used in all the simulations. The reason for choosing TELEMAC-2D instead of TELEMAC-3D was that the estuary was well-mixed and salinity stratification was weak. This stratification only occurred for a short duration of time. Therefore a two-dimensional modelling was adequate. Furthermore a three-dimensional modelling was expensive and time consuming. It took more computational memory and it required a very higher computer configuration to make it more practical.

Two different mesh densities were used to determine the mesh independence for the numerical simulation. Simulations were also carried out on different estuary shapes to determine the extend they affected the computation results. Single and multiple Manning's roughness coefficients were used for simulations with vegetated floodplain.

This chapter elaborates on the following simulations ,

1. Six (6) simulations are carried out using six different types of configuration in order to determine the effect of shape factors on the flow structures with and without floodplains.

2. Ten (10) simulations using Constant Eddy Viscosity turbulent model with different mesh sizes, different Manning's values and different advection schemes with floodplains.

3. Two (2) simulations using Elder's turbulent models with the same and different Manning's values for the main channel and vegetated floodplains.

6.1 Digitising the domain

The Sedeli Estuary was digitized using ERDAS Imaging Version 7.0 software which was available at the Civil Engineering computer laboratory. Contour maps produced by the Malaysian Survey Department were used in the digitizing works. Data for the river bathymetry and cross-sections were obtained from the field works. The cross-sections of the estuary are shown in **Figure 5.2** of Chapter 5. For sea bathymetry, the data were obtained from the Bathymetry Maps produced by the Royal Malaysian Navy. Tide tables were used to check the highest and lowest tides at the estuary (Royal Malaysian Navy 1998).

6.2 The Software

TELEMAC Version P5V4 was used in all the simulations. The personal computer used in this simulation had the following configuration,

1. Hard disk capacity : 40 Gigabyte
2. Pentium 4 processor with CPU 2.66GHz
3. Memory RAM : 1.0 Gigabyte RAM
4. System used : Windows 2000 Service Pack 4

6.3 Computational Criteria

6.3.1 Grid Constructions

The *Matisse* software were used to generate mesh for this study. Six mesh densities were generated for the shape factor analysis as shown in **Table 6.3**. For other simulations, two additional mesh densities were generated for actual bed with floodplains. **Table 6.1** shows the details of the mesh elements and nodes. The meshes were acronym as Mesh A and Mesh B. Mesh A has the most numbers of mesh elements compared to Mesh B. The coarse mesh has a mesh density of 150 metres while the refined mesh has two mesh density sizes which are 45 metres and 55 metres consecutively. Due to the limitation of computer capability, it was not possible to refine the mesh further. During the mesh generation, two files namely the geometric and boundary condition files were generated. These files were required for the simulations work.

Table 6.1 - Summary of Meshes for Actual Bed with Floodplain

Mesh Type	No. of Elements	No. of Nodes	Coarse Mesh Size(m)	Refine Mesh Size(m)	Long Edges	Small Edges	Max. Stretch	Max. Surface Ratio
1. Mesh A	62455	31708	150	45	225.57	19.777	9.332	5.51
2. Mesh B	34567	18081	150	55	224.496	20.806	8.205	5.452

6.3.2 Numerical Discretisation Parameter

TELEMAC offers a variety of advection schemes for the continuity and momentum equations. The various advection schemes include Method of Characteristics (MOC), Centered Semi-Implicit Scheme plus Streamline Upwind Petrov Galerkin (SUPG), PSI and N (for parallelisation) schemes. The Centered Semi-Implicit Scheme with SUPG is normally used to solve the advection equations for velocities, depth and tracers. In the SUPG scheme, Galerkin weighting test functions were modified in the direction of the streamline for the descretisation of transport terms (Brooks and Hughes 1982).

This scheme was to ensure mass conservation and it was less numerically diffusive than other schemes (Malcherek 2000, Rameshwaran and Shiono 2003). For computation of velocities, the decentring equal to unity (decentring uses the classic SUPG method, which is more stable for Courant Number was less than 1) was applied whereas, for depth and tracers, the decentring equal to Courant Number (modified SUPG method, more stable when Courant Number is greater than 1) was used. For estuaries and large water bodies, a Courant Number of 50 was acceptable (Bates *et al.* 1998).

For this simulation the following schemes are used,

1. Velocity in U and V - Method of Characteristics and SUPG
2. Water Depth – Conservation Scheme + SUPG Upwind
3. Tracer (salinity) – Centred semi-implicit scheme + SUPG Upwind

6.3.3 Stability Criteria and Convergence

Numerical schemes are often subjected to stability criteria related to the Courant Number, given in one dimensional for pure advection. TELEMAC employs Fractional Step Method as illustrated in the following equation.

$$C_r = u\frac{\Delta t}{\Delta x}$$

In this equation, C_r is the Courant Number, u is the velocity in x-direction, Δx is the mesh distance and Δt is the time step used. For the calculation of Courant Number, TELEMAC split the equation into advection and propagation components. In this case both components as well as the quantity ($|u|+c$) must be taken into consideration.

The total Courant Number for TELEMAC is given by Courant-Fiedrichs-Lewy which is defined as

$$C_r = (|u|+c)\frac{\Delta t}{\Delta x}$$

where u and c are defined as local velocity and wave celerity respectively.

The value of c is defined as

$$c = \sqrt{gA^*/B^*}$$

where A* and B* are defined as the cross-sectional area (m^2) and the top width (m) respectively.

For this simulation, the Courant Number was set to be less than 1 in the steering file. Another important aspect in the numerical simulation was the convergence during simulation. By adjusting the time step, the convergence for the simulation could be achieved. In this simulation, a time step of 15 seconds was chosen after a series of trial and error was done.

6.3.3 Coriolis Force

The effect of Coriolis force was taken into consideration. TELEMAC has the capability for imposing the effects of Coriolis force in the simulation. The value of Coriolis coefficient used in the simulation was 2.532E-6. This value was calculated based on the equation (2.22) in Chapter 2 of this thesis.

6.3.5 Turbulence Models

Within the numerical framework provided by TELEMAC, four turbulence closure schemes can be used. They are the simple zero equation Constant Eddy Viscosity model, the more complicated Elder's model, the k-ε model and the Smagorinsky model (for large eddy simulations). For this work, two types of turbulence models were used. They were the Constant Eddy-Viscosity and Elder's models. The Constant Eddy-Viscosity model uses a constant value of eddy viscosity for the whole domain. This value has a considerable influence on the shape, the size of re-circulation and also on the model dispersion. Research has shown that the eddy viscosity concept can be applied and is able to give a considerably good prediction even for complex flows (Wormleatin 1998, Shiono and Knight 1989, Shiono and Knight 1990).

6.4 Model Calibration and Sensitivity Analysis

For model calibration, ten simulation runs were carried out. The Sedeli estuary with floodplains on both banks was used for the simulations. **Table 6.2** shows the parameter used for the model calibration and sensitivity analysis. TELEMAC-2D was used in all the simulations using the Constant Eddy Viscosity turbulence model with two different advection schemes. The Manning's coefficient was adjusted by trial and error to obtain the output water levels that would match with the actual data. Several simulations was carried out on trial and error basis to determine the suitable Manning's values that would able to run the simulation. The result showed that the Manning's values ranging from 0.012 to 0.1 would was able to run TELEMAC successfully. These values were able to prevent the results from diverged. TELEMAC version P5V4 do not has a provision for drag force instead, Manning's roughness coefficient was commonly used in the software. The value of Manning's n=0.1 for mangrove swamp was commonly used in most study where the roots shall deem have taken into consideration in the roughness coefficient (Bates *et al.* 2005). Furthermore, it was impossible to determine the density of all roots on very wide floodplains

Two values of Manning's coefficients for 'n' = 0.012 and 'n' = 0.03 were chosen for the calibration and sensitivity analysis. These values were also based on the value that was commonly used for research works. Sensitivity analysis was done to determine the parameters that would influenced the output results. Three types of boundary conditions were used in the simulation. For the open boundary, the tide levels were obtained from the recording station whilst at the inlet, the reading was from the gauging station located at *location 4*. Both boundary conditions were in a dynamic state. For the other boundaries around the domain, a non-slip condition with zero flux was imposed.

Ten different types of simulation were carried out to determine the sensitivity analysis. They are listed below,

1. The Constant Eddy Viscosity turbulent model uses n = 0.012. The velocities (u and v) used the MOC and the depth (h) uses the Conservation Scheme + the Streamline Upwind Petrov-Galerkin Upwind advection

schemes with Mesh A and Mesh B.

2. The Constant Eddy Viscosity turbulent model uses n = 0.03. The velocities (u and v) used the MOC while the depth (h) using the Conservation Scheme + the Streamline Upwind Petrov-Galerkin Upwind advection schemes with Mesh A and Mesh B

3. The Constant Eddy Viscosity turbulent model uses n = 0.012. The velocities (u and v) used the MOC and the depth (h) uses the Centered Semi Implicit Scheme + the Streamline Upwind Petrov-Galerkin advection scheme with Mesh A and Mesh B.

4. The Constant Eddy Viscosity turbulent model uses n = 0.03. The velocities (u and v) used the and the depth (h) uses the Centered Semi Implicit Scheme + the Streamline Upwind Petrov-Galerkin advection scheme with Mesh A and Mesh B.

5. Elder's turbulent model uses n = 0.012. The velocities (u and v) and the depth (h) uses the Centered Semi Implicit Scheme + the Streamline Upwind Petrov-Galerkin advection scheme with Mesh A.

6. Elder's turbulent model uses n = 0.03. The velocities (u and v) and the depth (h) uses the Centered Semi Implicit Scheme + the Streamline Upwind Petrov-Galerkin advection scheme with Mesh A.

6.4.1 Simulated Results Versus Actual Data

In these simulations, Mesh A and Mesh B were used with Manning's roughness coefficients 'n' equal to 0.012 and 0.03. **Figure 6.1** and **Figure 6.2** showed the results of water levels at the four locations for Mesh A and Mesh B. **Figure 6.1** shows the water levels at locations 1, 2, 3 and 4 using Mesh A with Manning's coefficients equal to 0.012 and 0.03. Simulations were carried out for a period of 69 hours so that a good representation of water level could be obtained.

Table 6.2 – Table Shows the Parameter Used in Determining the Calibration and Sensitivity Analysis

Simulation No.	Mesh Type	Manning's Coefficient	Advection Scheme		
			h	u	v
1	Mesh A	0.012	2	1	1
2	Mesh A	0.03	2	1	1
3	Mesh A	0.012	5	1	1
4	Mesh A	0.03	5	1	1
5	Mesh B	0.012	2	1	1
6	Mesh B	0.03	2	1	1
7	Mesh B	0.012	5	1	1
8	Mesh B	0.03	5	1	1
9	Mesh A	0.012	2	2	2
10	Mesh A	0.03	2	2	2

Advection Scheme:
1 = Method of Characteristics (MOC)
2 = Centered Semi Implicit Scheme + Streamline Upwind Petrov-Galerkin
5 = Conservative Scheme + Streamline Upwind Petrov-Galerkin

The following chapter described a comparison made between water level and time when using different '*n*' and meshes density. Subsequently, a comparison between the actual data and the simulated data would be made to determine the mesh density and '*n*' to be used for further analysis. For theses analysis, the first 12 hours was ignored. This was to enable the water level to develop and stablised. At *location 1*, the water levels were almost identical for both 'n' except at time T = 24 hours and T = 15 hours. For $n = 0.03$ the water level at T = 24 hours was higher while at T = 51 hours was lower compared to n=0.012. At *location 2*, the tidal had an influenced on the water levels. The water level was sinusoidal and fluctuated above the mean sea level. The reading at this location ranged between 1.0m to – 1.0m for $n = 0.03$ and it showed a higher reading compared to $n = 0.012$.

At *location 3,* for n = 0.03, the water level showed a higher tidal influenced. The difference of water levels between both 'n' was less than 2.0% during high and lower water at time T = 33 hours and T = 51 hours. At the *fourth location*, the water level was identical for both 'n'. The water level for both Manning's showed a minimum fluctuation. At this location, the fluctuation of water level was purely due to the inflow of fresh water into the domain. The choice of Manning's coefficients had an influenced on the water levels with n=0.03 showed greater influenced compared to n=0.012.

Figure 6.2 shows the simulation using Mesh B for n=0.012 and n=0.03. By applying the same turbulence model and advection scheme, comparisons were made on the water level. At *location 1,* the water level was almost similar for *both 'n'* except at time T=24 hours and T=33 hours. During this duration, the water level for n=0.03 showed a higher reading. Similarly, for the *first location*, the tidal significantly influenced the water level. At *location 2,* the water level profile for both 'n' were found to have a similar pattern with n=0.03 showed a slightly higher fluctuation at time T = 33 hours and T=39 hours. The water level ranged between -0.7 m to 0.8m while for n = 0.012 it was between -0.6 m to 0.8m. At the *third location*, the water level for both 'n' were found to have the same pattern but with a different in amplitude especially at time T=27 hours, T=36 hours, T=67 hours and T=66 hours. The water level reading was between 0.0m to 0.8m for n=0.03 while between 0.3m to 0.8m for n=0.012. At this location, both water levels showed that there was some tidal influenced with n=0.03 had a higher fluctuation. At location 4, n=0.03 showed a greater fluctuation although they have a similar water level pattern. The tidal influenced at this location was minimum compared to the inflow of fresh water as discussed for Mesh A. The water levels for all the cases were taken with respect to the mean sea level and time. During this interval, the tides fluctuated between 1.5m to -1.5 m with respect to the mean sea levels at the estuary mouth. Comparing both results, Mesh B showed a higher diffusion then Mesh A especially at *location 4*. For n=0.03, due to a higher resistance of flow, the inflow of water from the floodplain into the river would caused the water level to be higher compared to n=0.012. This could be observed at *location 3*, where the presence of floodplain affected the water level.

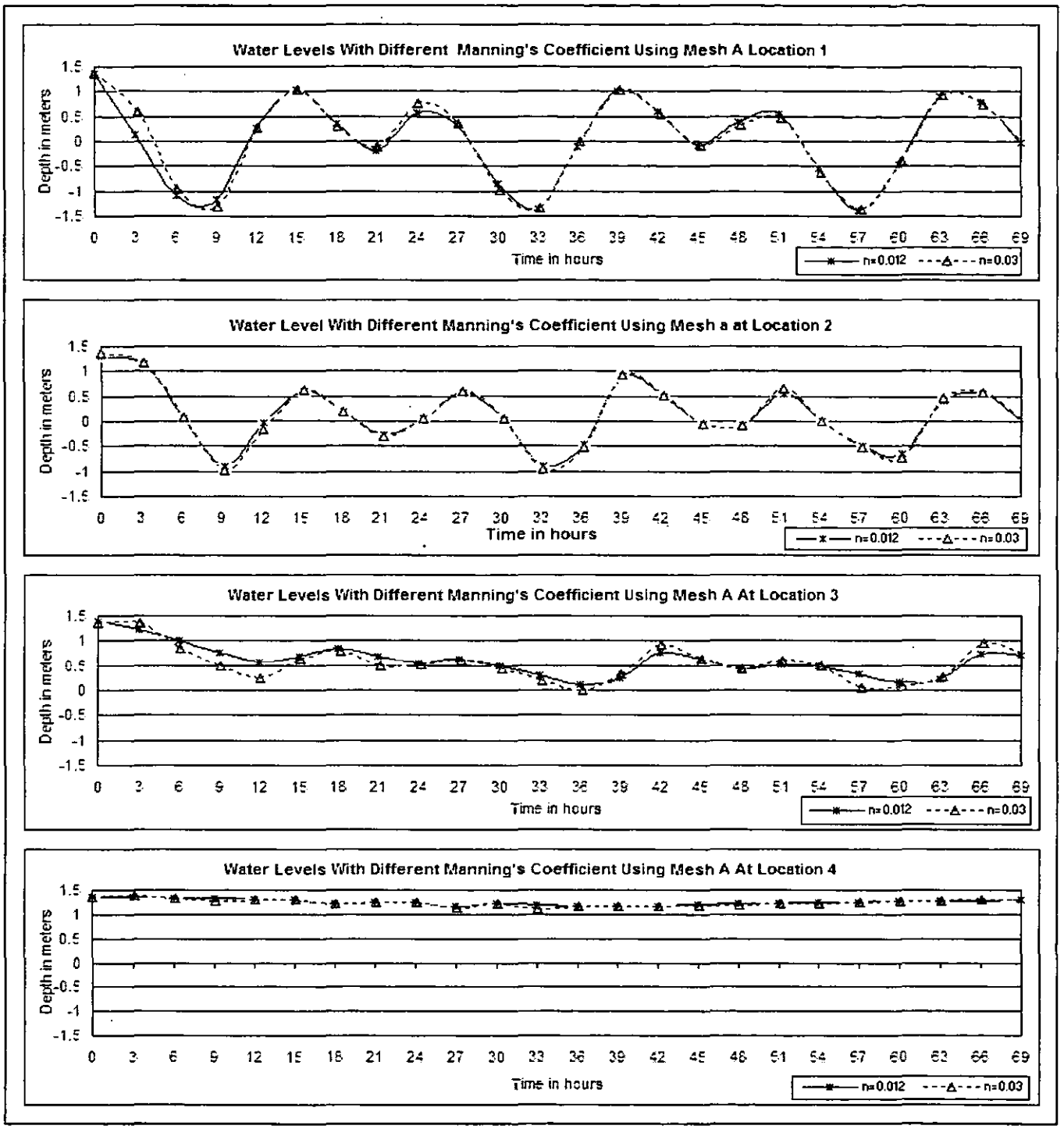

Figure 6.1 – Water Levels with Manning's Coefficient of $n = 0.012$ and $n = 0.03$ with Mesh A (fine mesh density) using Constant Eddy Viscosity with Method of Characteristics and Centered Semi Implicit Scheme+ Streamline Upwind Petrov-Galerkin at Location 1, 2, 3 and 4

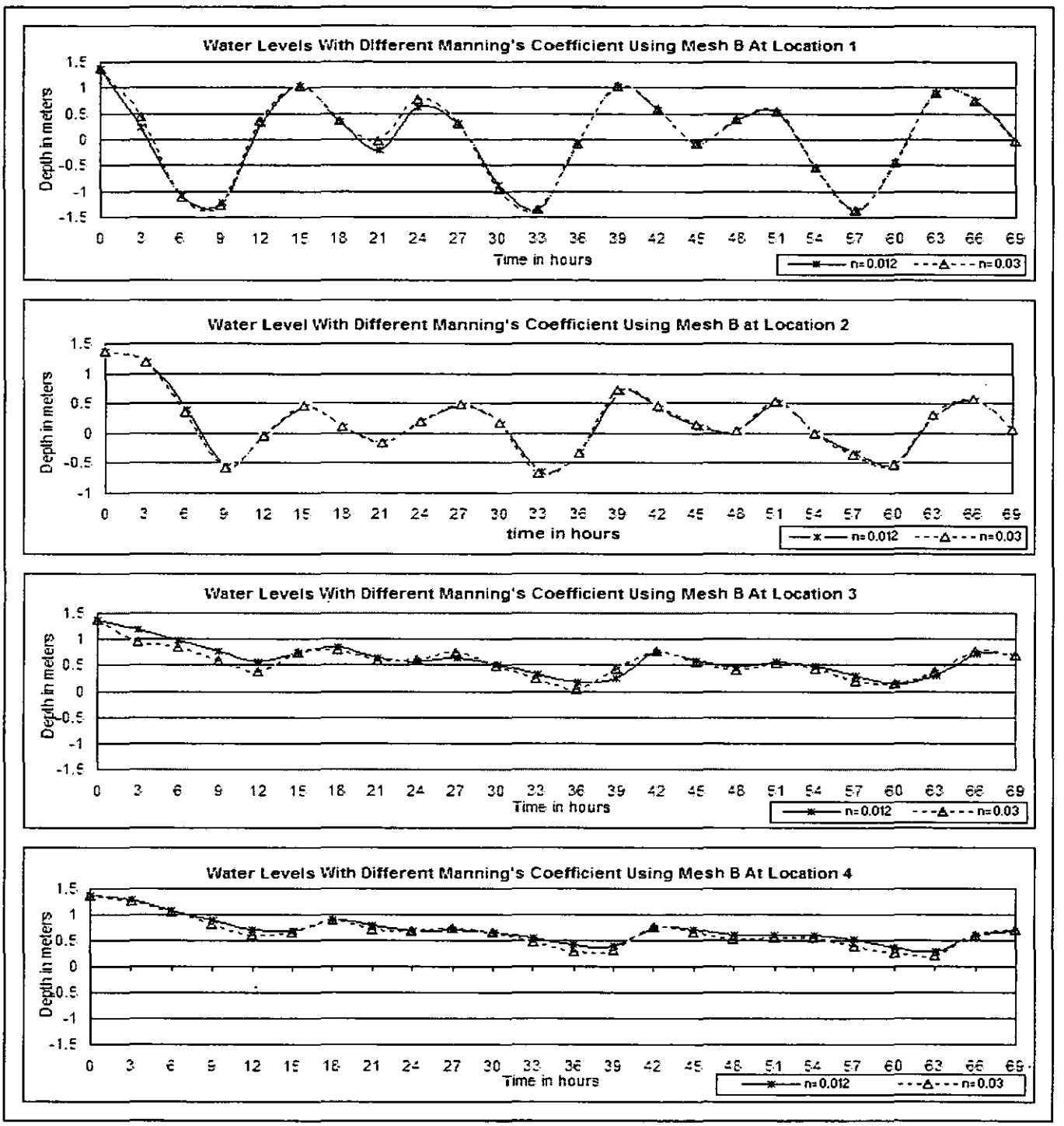

Figure 6.2 – Water Levels with Manning's Coefficient of n = 0.012 and n = 0.03 with Mesh B(coarse mesh density) using Constant Eddy Viscosity with Method of Characteristics and Centered Semi Implicit Scheme+ Streamline Upwind Petrov-Galerkin at Location 1, 2, 3 and 4

Figure 6.3 shows the comparison made between Mesh A and Mesh B for n = 0.012. The water levels at *location 1* for both meshes were almost identical. The diurnal tides for both high and low water tides ranged between –1.5m to 1.0m at the first peak (T=33 hours and T=39 hours) and –0.1m to 0. 5m at the second peak (T= 45 hours and T=51 hours). *Location 1* was located closest to the sea, therefore the tidal had an influenced on the water level. At *location 2*, the water level for Mesh A fluctuated between -1.0m (T= 33 hours) to 1.0 m (T=39 hours) while for Mesh B was between -0.7m (T=33 hours) to 0.7m (T=39 hours) with Mesh A showed a greater fluctuation. At *location 3*, the water level at time T=36 hour was 0.0 m and 0.1m for Mesh A and Mesh B respectively. While at time T=66 hours, the reading was 1.0m for Mesh A and 0.7 m for Mesh B. The water level for both meshes showed there were some tidal effects. At *location 4,* the water level for Mesh A showed no fluctuation while for Mesh B, it fluctuated between 0.3m (T=36 hours) to 0.8m (T=42 hours) as shown in **Figure 6.4**. The water level for all other locations showed a similar pattern to Mesh A for n=0.03 when using the same advection scheme.

Comparison was made to determine the effect of Manning's coefficient and mesh density on the water levels. **Figure 6.5** and **Figure 6.6** showed the water levels for Mesh A and Mesh B for both 'n' with the actual water level. **Figure 6.5** shows the simulated water level with the actual water levels at location 1. Both water levels have a same amplitude but lagged by three hour between them at time T= 24 hours at the second high and low water tides. The water level fluctuated between –1.5m to 1.0m for both cases at time T=39 hours. For the second high water tide, the simulation reading fluctuated between - 0.1m to 0.5m, whereas for the actual data, it fluctuated between -0.5m to 0.8m at time T=45 hours to T = 51 hours. At *the second location*, the water level for Mesh A showed good resemblance to the actual water levels. Although the reading was underestimated between 33.0% to 50.0% for Mesh B. The results from Mesh A showed a reasonable good representative with the actual water levels.

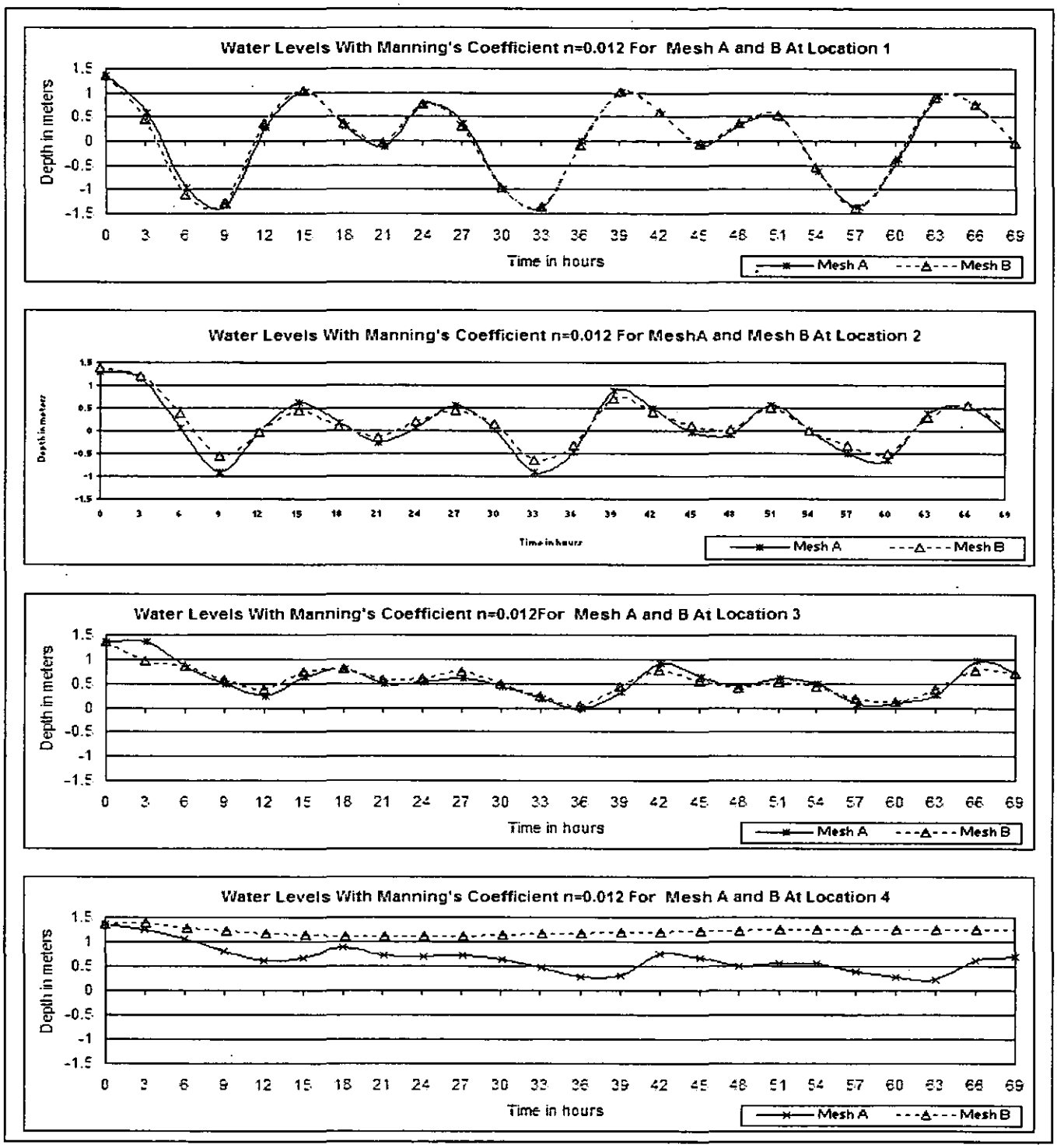

Figure 6.3 - Water Levels for Mesh A (fine mesh density) and B (coarse mesh density) with Manning's Coefficient n = 0.012 using Constant Eddy Viscosity Model and Method of Characteristics and Centred Semi Implicit Scheme+ Streamline Upwind Petrov-Galerkin (Advection Scheme) at Location 1, 2, 3 and 4

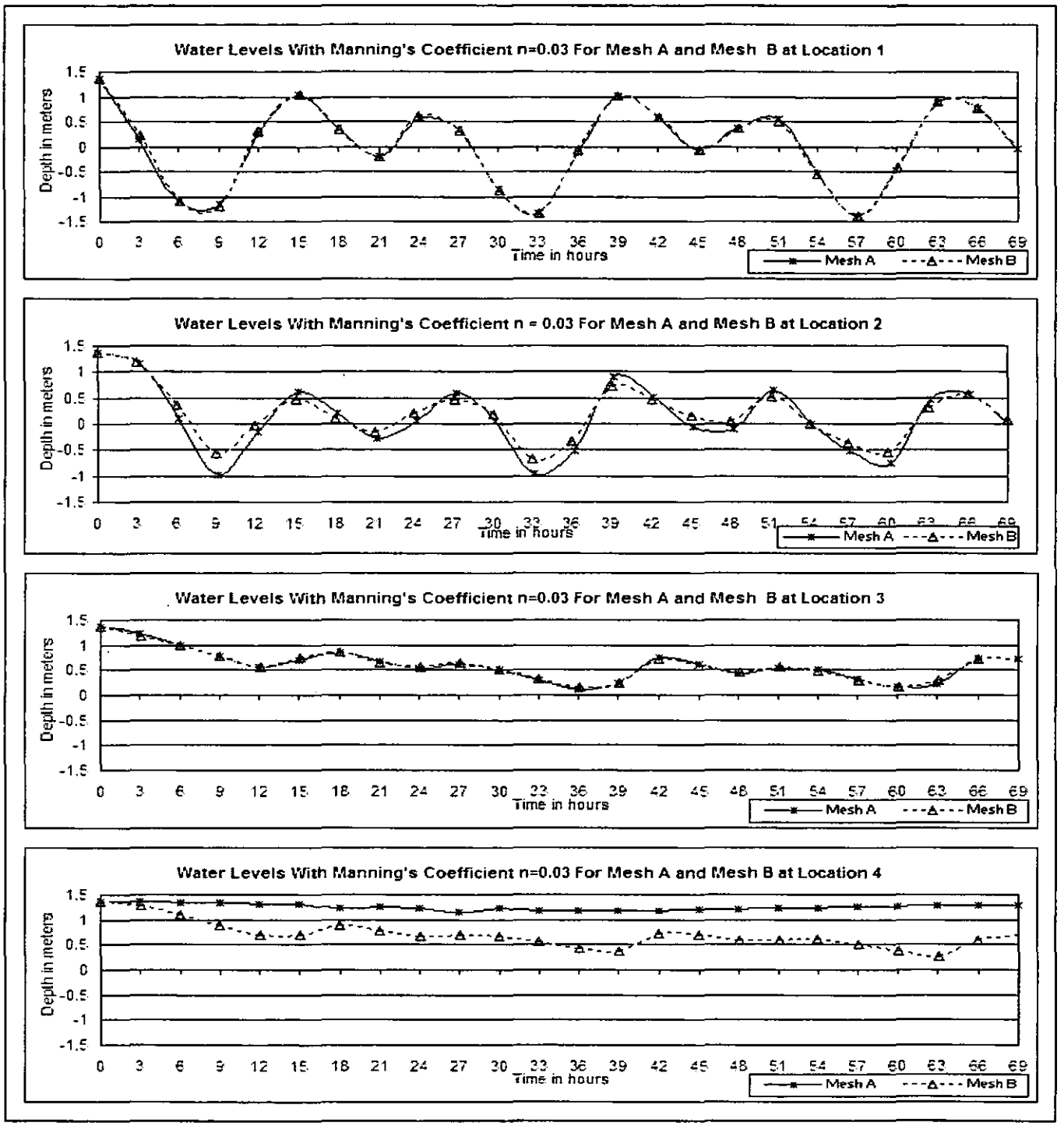

Figure 6.4 - Water Levels for Mesh A (fine mesh density) and B (coarse mesh density) with Manning's Coefficient n = 0.03 using Constant Eddy Viscosity Model and Method of Characteristics and Centered Semi Implicit Scheme+ Streamline Upwind Petrov-Galerkin (Advection Scheme) at Location 1, 2, 3 and 4

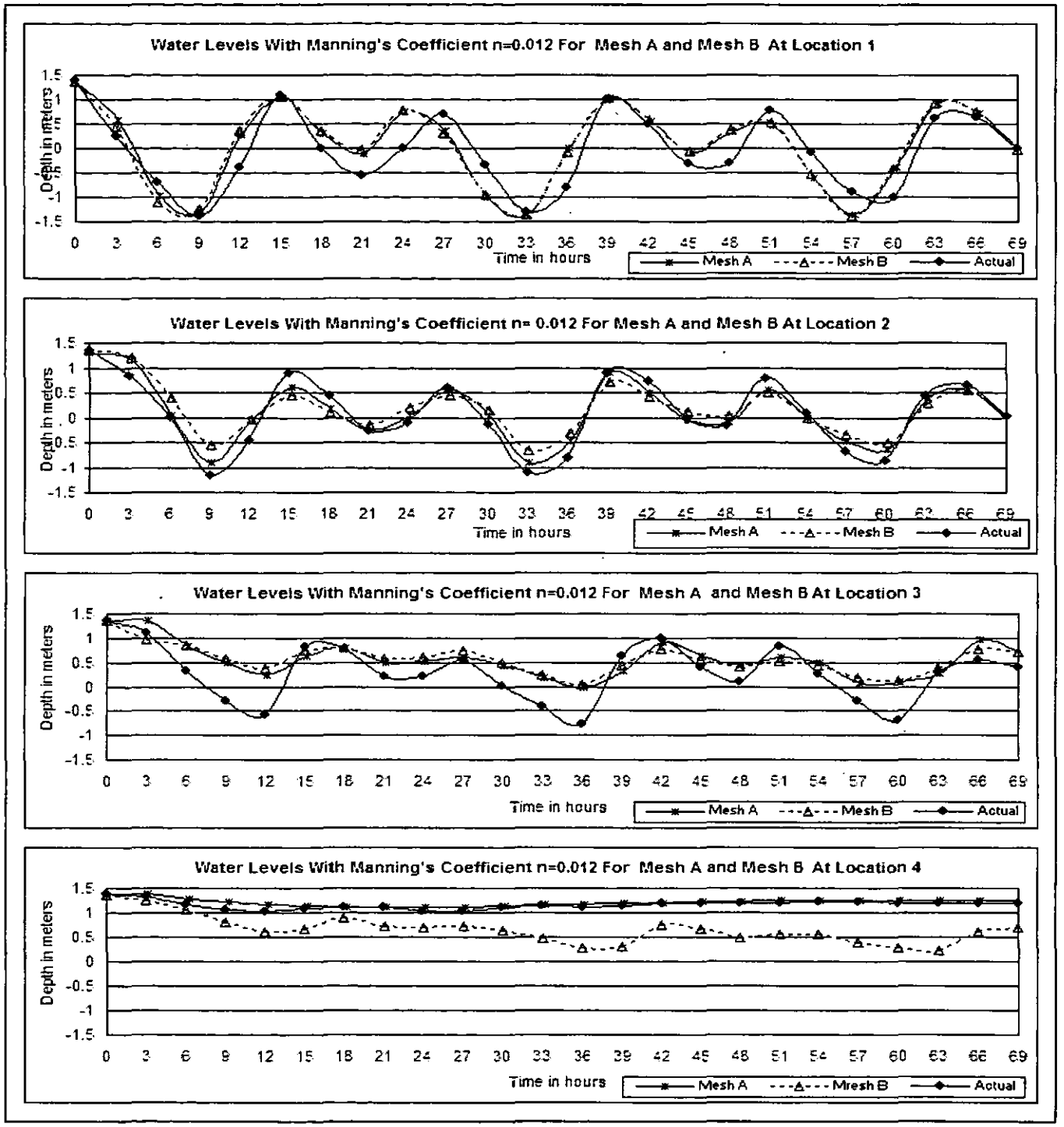

Figure 6.5 - Water Levels for Mesh A (fine mesh density) and Mesh B (coarse mesh density) with Actual with Manning's Coefficient n = 0.012 Using Constant Eddy Viscosity Model and Method of Characteristics and Centered Semi Implicit Scheme + Streamline Upwind Petrov-Galerkin (Advection Scheme) at Location 1, 2, 3 and 4

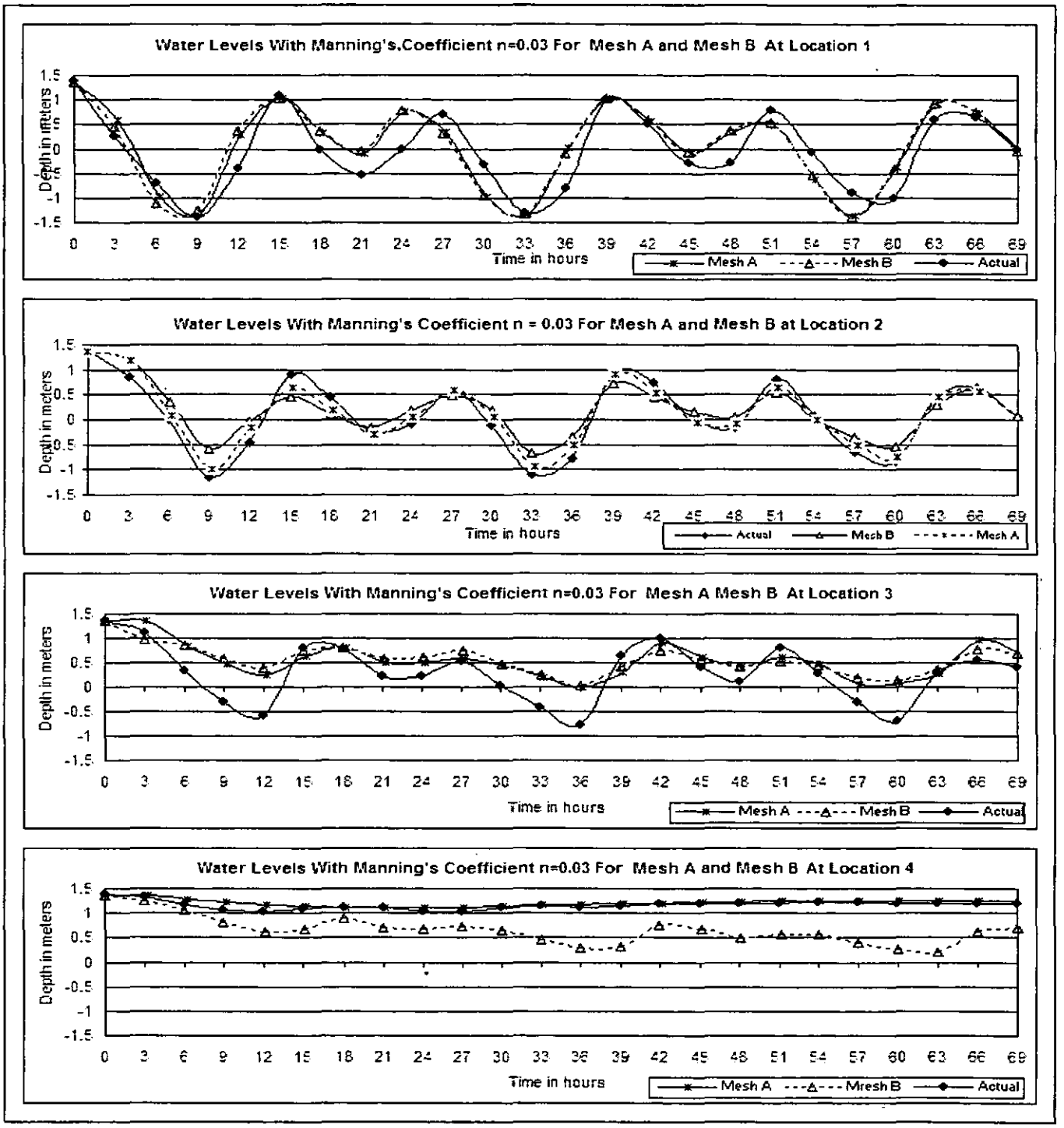

Figure 6.6 - Water Levels for Mesh A (fine mesh density) and Mesh B (coarse mesh density) with Actual Data with Manning's Coefficient n = 0.03 using Constant Eddy Viscosity Model and Method of Characteristics and Conservation Scheme + Streamline Upwind Petrov-Galerkin (Advection Scheme) at Location 1, 2, 3 and 4

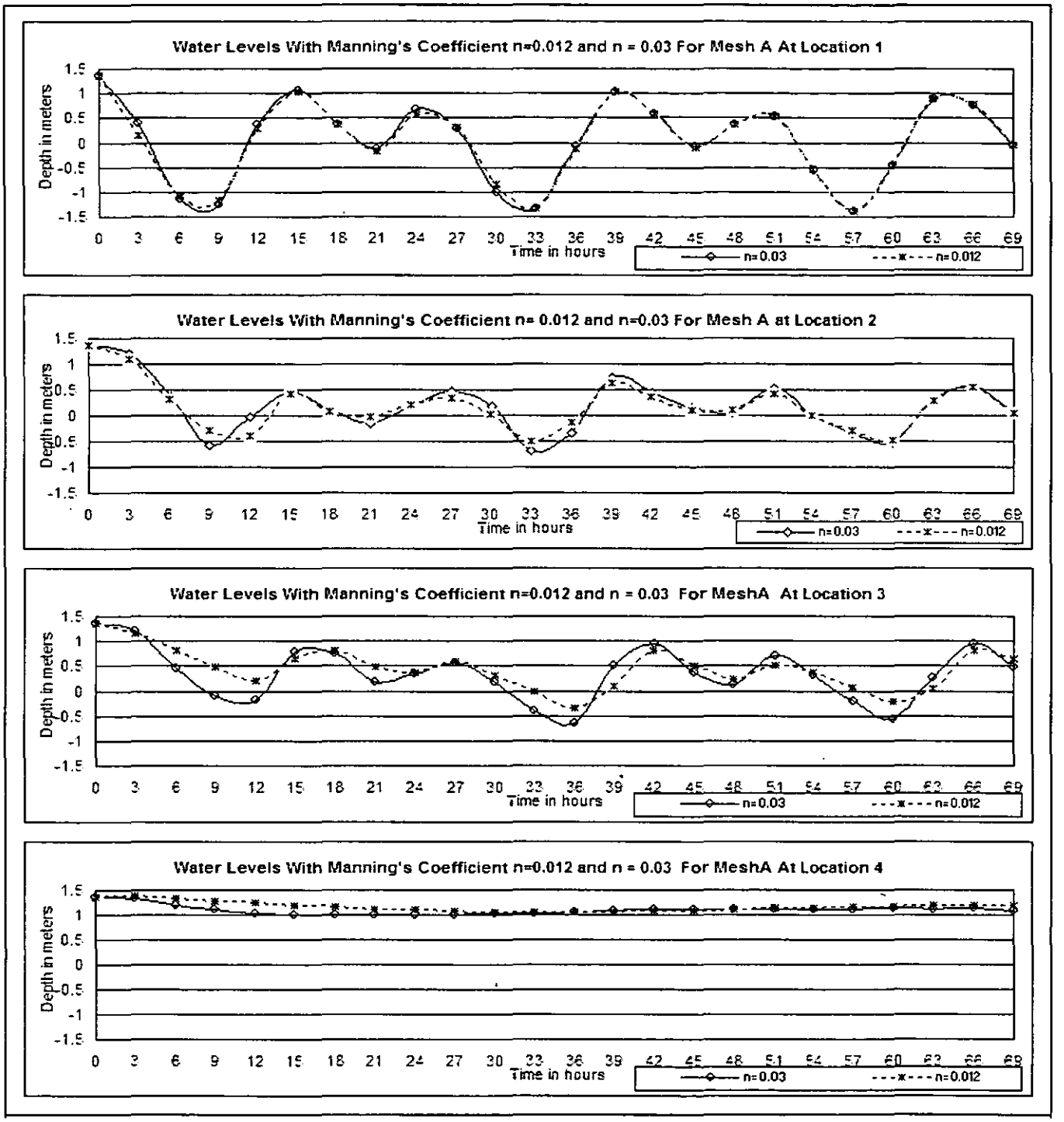

Figure 6.7– Water Levels using Method of Characteristics and Conservative Scheme Streamline Upwind Petrov-Galerkin Scheme with n = 0.012 and n = 0.03 for Mesh A (fine mesh density) at Location 1, 2, 3 and 4

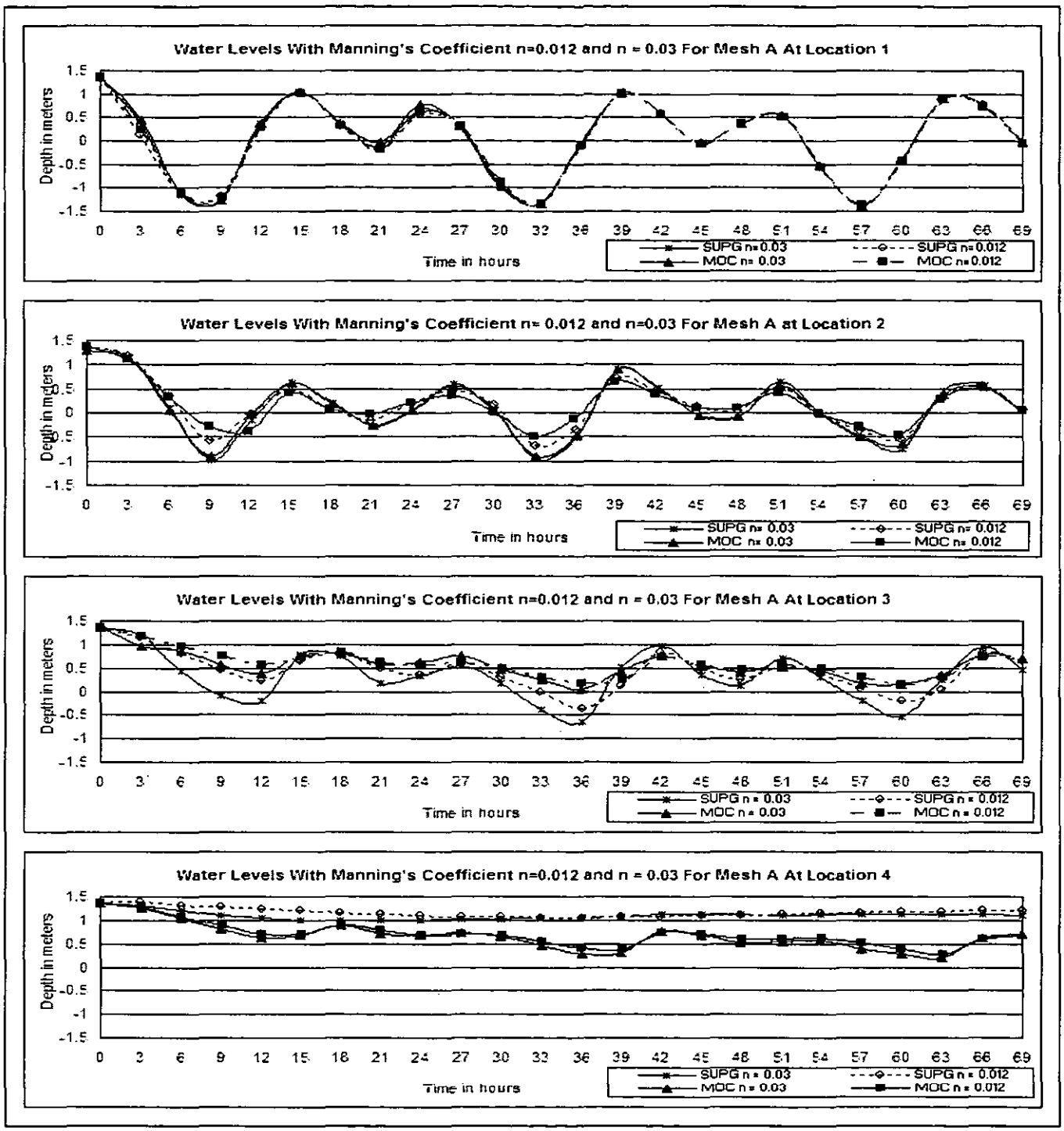

Figure 6.8–Water Levels for Advection Schemes of SUPG* and MOC* for Mesh A (fine mesh density) for Manning's Coefficient n = 0.012 and n = 0.03 at Location 1, 2, 3 and 4

MOC* = Method of Characteristics and Conservative Scheme + Streamline Upwind Petrov-Galerkin
SUPG* = Method of Characteristics and Centered Semi Implicit Scheme + Streamline Upwind Petrov-Galerkin

At *location 3*, the water level for the simulated reading had higher amplitude compared to the actual water level at both high and low water tides. At high water tide, the simulations and the actual water level ranged between 33.0% to 34.0% with a phase difference of 1.5 hours. However, during the second low water tide, there was a significantly difference in water level between 78.0% to 81.0%, with the actual water level showed a higher fluctuation pattern. The actual water level had a similar pattern to the simulated water level using Mesh A. **Figure 6.6** shows the simulated and actual water levels at the four locations. The mesh density influenced the water levels with Mesh A gave a good comparison with the actual data. Mesh B had a higher diffusion due to the coarser mesh density.

Computation was done using different advection schemes for the continuity and momentum equations. Two advection schemes was used in this simulation namely the Method of Characteristics and Centered Semi Implicit Scheme + Streamline Upwind Petrov-Galerkin and the Method of Characteristics and Conservative Scheme + Streamline Upwind Petrov-Galerkin. **Figure 6.7** shows the summary of water levels for both 'n' using Mesh A with the Method of Characteristics (MOC) and the Conservative Scheme Streamline + Upwind Petrov-Galerkin (CS + SUPG) advection scheme was used in this simulation. The MOC and (CS + SUPG) was assigned to water depth (h) and velocity (u and v) respectively. This was to determine the effects of advection schemes on the water levels. The water level at *location 1* showed a higher fluctuation for n=0.03 compared to n=0.012. It fluctuated between -1.4m to 1.0m at time T=33 hours to T= 39 hours and also at time T=57 hours to T=63 hours. Similarly at *locations 2* and *3*, the water levels for n=0.03 dominant over when n=0.012. At *location 4*, the water levels for both *'n'* showed no tidal effect.

Comparisons were made between the Method of Characteristics and Centered Semi Implicit Scheme + Streamline Upwind Petrov-Galerkin with the Method of Characteristics and Conservative Scheme + Streamline Upwind Petrov-Galerkin advection schemes to determine their effects on the water levels. **Figure 6.8** shows the two advection schemes with *'n'* equal to 0.012 and 0.03. At the *first location*, all the four cases

showed a similar pattern of water level without much difference between them. Whereas at *location 2*, the water levels for both the advection schemes for $n = 0.03$ showed a higher fluctuation. The water levels fluctuated between -1.0m to 1.0m at time between T=33 hours to T=39 hours. At *location 3*, all the four cases have the same water level pattern but with different in amplitude among them. The Method of Characteristics and Centered Semi Implicit Scheme + Streamline Upwind Petrov-Galerkin for $n = 0.03$ showed a higher reading compared to the other cases. The water for this particular case, fluctuated between -0.7m to 1.0m at time between T= 36 hours and T=42 hours. At the *fourth location*, both the advection schemes showed a higher fluctuation for n=0.012. The water levels for n=0.03 was constant at the four locations. The Method of Characteristics and Conservative Scheme + Streamline Upwind Petrov-Galerkin had a higher diffusion and less mass conservation compared to the Method of Characteristics and Centered Semi Implicit Scheme + Streamline Upwind Petrov-Galerkin. Therefore, the Method of Characteristics and Centered Semi Implicit Scheme + Streamline Upwind Petrov-Galerkin advection scheme was used in the simulations because it gave a more realistic water level at all the four locations.

Figure 6.9 shows the comparison made between the Method of Characteristics and Centered Semi Implicit Scheme + Streamline Upwind Petrov-Galerkin using Mesh A with the actual water levels. At *location 1*, the deviation of water level was between 13% to 16.1% when using the Method of Characteristics and Centered Semi Implicit Scheme + Streamline Upwind Petrov-Galerkin with $n = 0.03$. The water level for this advection scheme gave a similar pattern to the actual water level but with a lower amplitude (T=51 hours, T=57 hours and T= 63 hours) and a phase lagging difference of 3 hours (T=24 hours, T=48 hours and T=57hours). For other locations, the water levels gave a similar pattern with the actual water levels for n=0.03. At *location 2*, Mesh A with $n = 0.03$ gave a good predicted of water level although there was an underestimated of 25%. At *location 3*, this advection scheme showed a similar pattern with the actual water level with a slight phase difference ranged between 5.0% to 6.0%. For the fourth *location*, the water levels showed there was a significant agreement in water level between them. Therefore Mesh A

with Manning's coefficient equal to $n = 0.03$ was used in the simulations.

Elder's turbulence model was used in this study. **Figure 6.10** shows the water levels using the Elder's, Eddy Viscosity turbulence model and the actual water level. Overall, the water level using the Elder's turbulence model gave the closest agreement to the actual water level compared to the Eddy Viscosity turbulence model although there was some minor differences in the amplitude and phase frequency. The Elder's turbulent model (Cooper 2004) was suitable for salt transport and mass conservation.

6.4.2 Sensitivity Analysis

For Sedeli Estuary, the sensitivity analysis was focused on the selection of Manning's roughness coefficient and type of advection scheme that would be used for the simulation. As discussed in section 6.4.1, the choice of Manning's roughness coefficient had a significant effect on the results especially at *second location*. The water level could deviated up to 25% for both '*n*' using Mesh A while for Mesh B was between 6.5% to 15.9%.

Rameshwaran and Shiono (2003) have bench marking the combination of some of the advection schemes available in TELEMAC. They concluded that Manning's roughness coefficient was vital to obtain good accuracy in predicting the flow in a meandering two-stage compound channel. In their finding, they concluded that the Method of Characteristics and Centered Semi Implicit Scheme + Streamline Upwind Petrov-Galerkin and the Multidimensional Upwind Residual Distribution (MURD) advection scheme had the least numerical diffusion. In this thesis the Method of Characteristics and Centered Semi Implicit Scheme + Streamline Upwind Petrov-Galerkin was used in all the simulations since it had proven to give a reasonably accurate results.

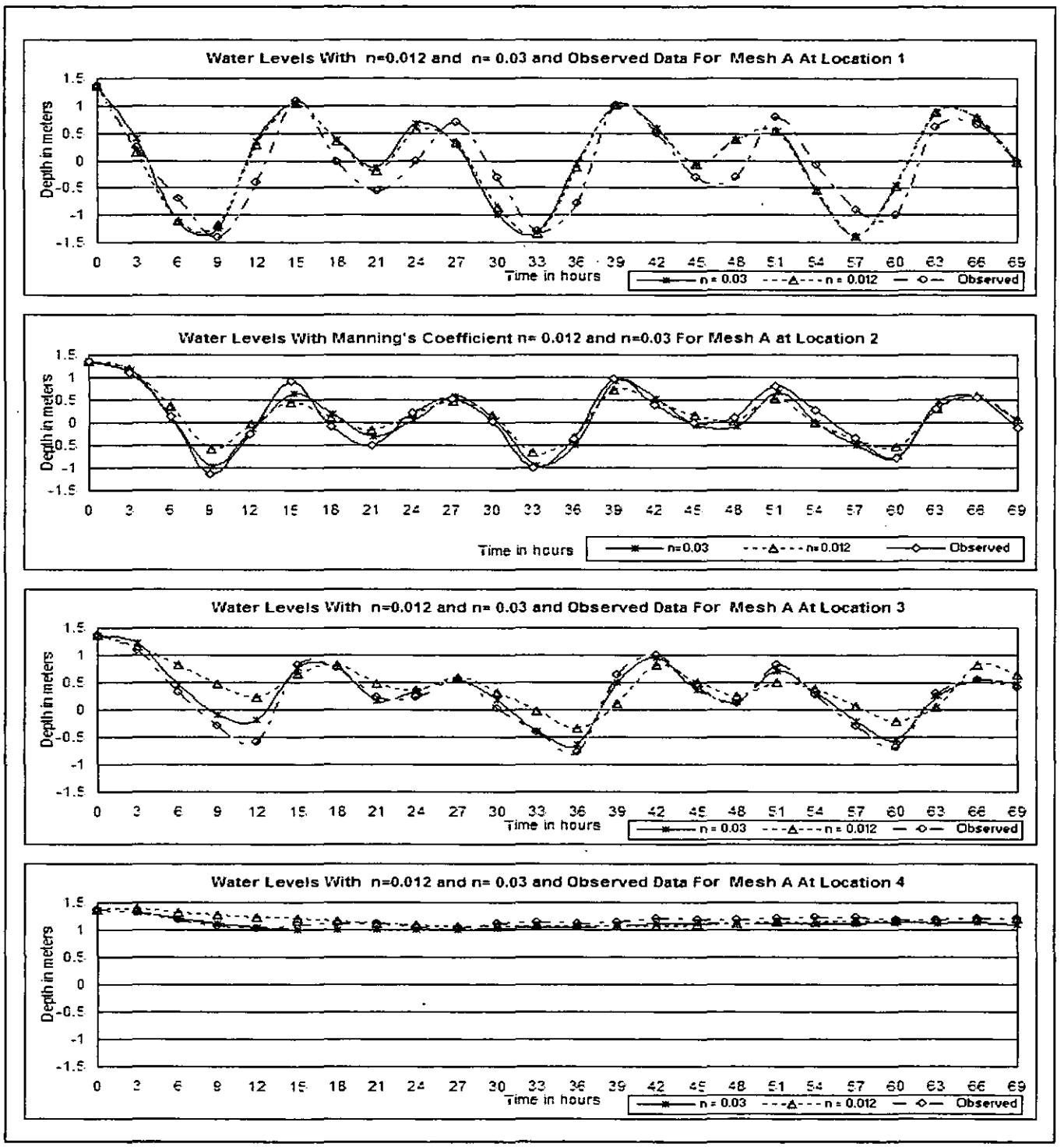

Figure 6.9 – Water Levels for Constant Eddy Viscosity Using Method of Characteristics and Centred Semi Implicit Scheme + Streamline Upwind Petrov-Galerkin Advection Scheme for n = 0.012, n = 0.03 for Mesh A and Actual Water Levels

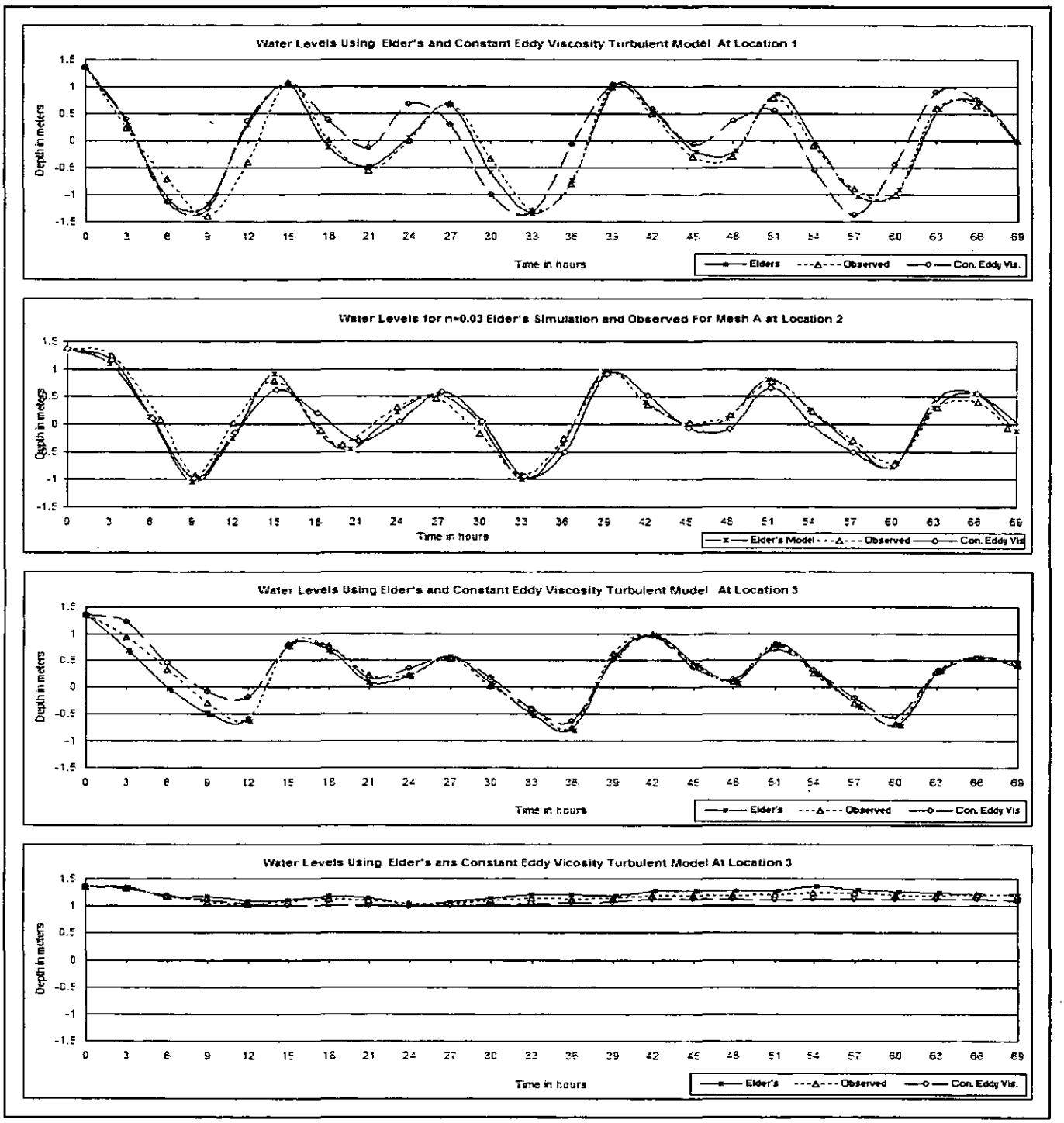

Figure 6.10 – Water Levels Using Elder's and Constant Eddy Viscosity Turbulent Models Method of Characteristics and Centred Semi Implicit Scheme + Streamline Upwind Petrov-Galerkin (Advection Scheme) using with '*n*' = 0.03 for Mesh A and Actual Water Level

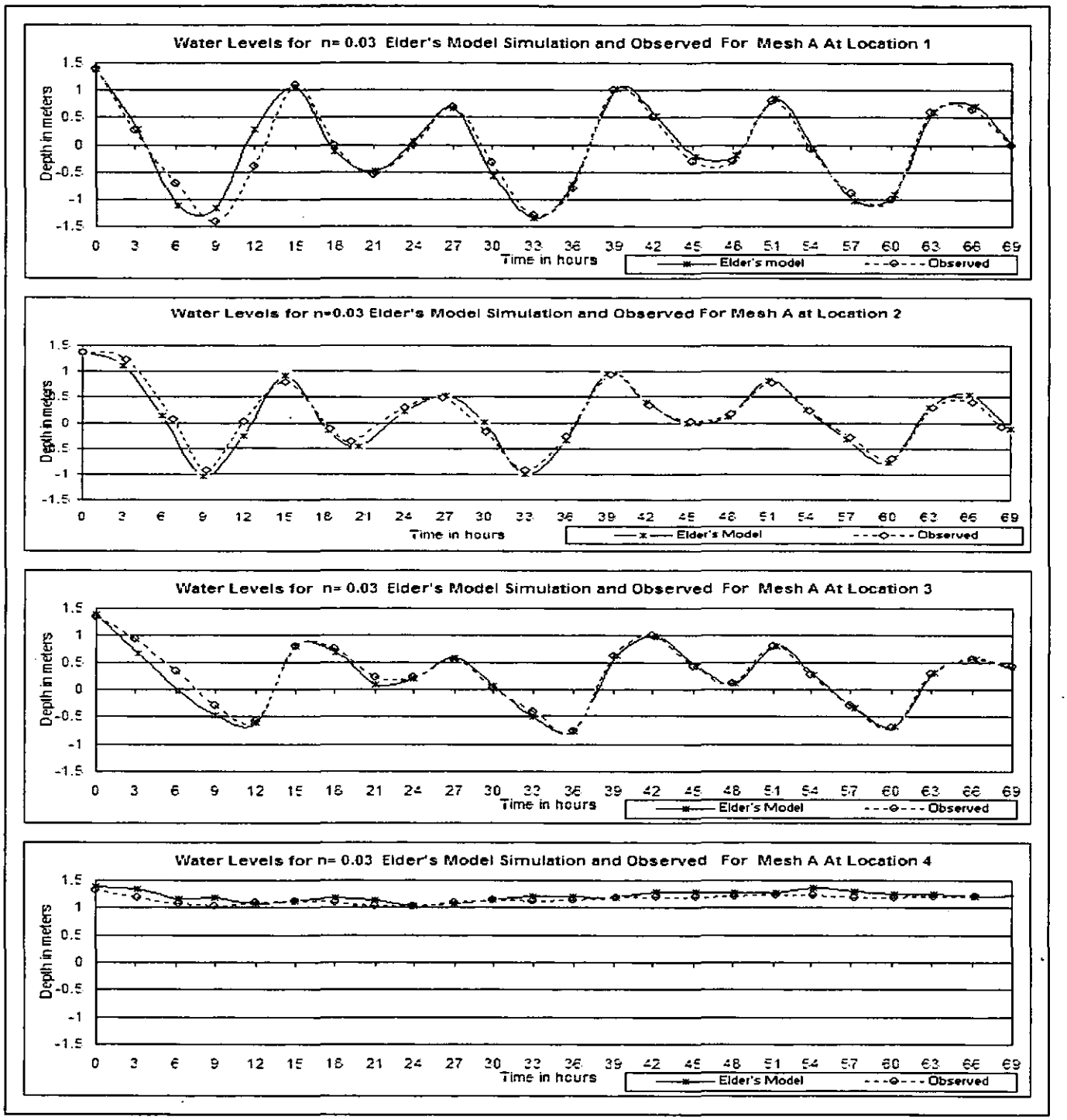

Figure 6.11 – Water Levels for Elder's Turbulent Models Using the Centred Semi Implicit Scheme + Streamline Upwind Petrov-Galerkin (Advection Scheme) and Actual Water Level for n = 0.03 for Mesh A

6.4.3 Model Calibrations

The first step in any model calibration process is to obtain a good agreement between the simulated and the actual water levels. In this thesis, two different turbulent models was used for the model calibration. The Manning's roughness coefficient used was n = 0.03 with the Method of Characteristics and Centered Semi Implicit Scheme + Streamline Upwind Petrov-Galerkin advection scheme. **Figure 6.11** shows the comparison between Elder's turbulent models with the actual water levels. For further simulations, the Elder's turbulent model was used since the results showed that there was a closed agreement with the actual water levels.

6.5 Shape Factors

In this research, shape factors were used to analyse their effect on flow structures. In reality, it was impossible to model a perfect real life conditions due to the complexity of the river configuration and the uncertainties feature of the estuary *(Bates et al. 2005).* Therefore, it is important that the entire salient features required to be incorporated carefully during simulations. The accuracy of the simulation results would determine by the input information. Many research works on shape factors have been carried out experimentally to study their effect on the flow structures among them were Wormleaton and Ewunetu (2006). They simulated a small-scale physical model using the UK-FCF model at HR Wallingford with various floodplain layouts.

In this research, six (6) different simulations were considered for the effect of shape factors on water levels and velocity (v and u) at the three locations along the estuary. A sinusoidal tidal cycle using a sine function ($\sin \omega t$) was introduced in the simulations by modifying the *'sl'* subroutine program in the TELEMAC utility file. For this simulation, a constant value of 70 m^3/s and 2.0 meters was prescribed at the inlet (upstream) and outlet (sea) boundary conditions. A single Manning's coefficient of n = 0.03 was used for the main channel and the floodplain.

The *'sl'* subroutine program in the TELEMAC would generate a semi-diurnal tide. The simulation was carried out for 12 tidal cycles equivalent to 72 hours.

The six cases used for the simulations are,

1. An estuary with the actual bed and floodplains (*Case 1*)
2. An estuary with a flat bed and floodplains (*Case 2*)
3. An estuary with an incline bed and a narrow floodplains (*Case 3*)
4. A straight with a tapered rectangular estuary with a flat bed and a narrow floodplains (*Case 4*)
5. An estuary with the actual bed but without floodplains (*Case 5*)
6. An estuary with a flat bed but without floodplains (*Case 6*)

Table 6.3 shows the summary for all the cases. For *Case 1*, the configuration and layout of the river was digitised from the topographic and the surveyed cross-section maps. The sea bathymetry levels were obtained from Bathymetry Map produced by the Royal Malaysian Navy. While for *Case 2*, the bed was assumed to have a flat bed with a depth of -10.0 m throughout the river reach and having the same layout as *Case 1*. For Case 3, the bed slope was set to a gradient of 0.33% (the actual riverbed slope for positive gradient as discussed in Chapter 5) increasing upstream. For *Case 4*, the river channel was assumed to have a rectangular river cross section with a flat bed. It had a straight layout with a narrow floodplain. The total length of the river reach was 73 km long. The objective of these simulations was to determine the effect of shape factors and floodplains on the water depths and flow velocity in the main channel.

Case 5 had the same layout as *Case 1* but without floodplains. Similarly, for *Case 6* had the same river layout as Case 2 but without floodplains. For *Case 5* and *Case 6*, the riverbank was assumed to have the zero datum at mean sea level. Comparison was made between *Case 1* with *Case 5* and *Case 2* with *Case 6*. This was to study the effect of floodplains on the water levels and the velocity distributions in the main channel. The Manning's coefficient used was n=0.03 for the bed roughness and on the floodplains. The analysis was done at time T = 57 hours and T = 63 hours which coincided with flooding and ebbing condition.

Table 6.3 – Summary of Meshes Influence by Shape Factors

	No. of Elements	No. of Nodes	Long Edge	Smaller Edge	Max. Stretch	Max. Surface Ratio
1. Actual Bed with Floodplain	62,455	31,708	225.573	19.777	9.333	5.567
2. Flat Bed with Floodplain	36,217	18,687	215.292	13.328	99.59	9.504
3. Inclined Bed with Floodplain	65,484	33,445	178.465	12.714	47.105	8.46
4. Flat Rectangular Channel with Narrow Floodplain	51,703	26,744	151.889	9.9	12.593	11.656
5. Actual Bed without Floodplain	14,605	8,464	211.103	16.349	4.279	4.045
6. Flat Bed without Floodplain	15,172	8,752	221.146	18.404	4.372	3.575

6.5.1 Water Levels

The Constant Eddy Viscosity and the Elder's turbulence model was used in this research. **Table 6.3** shows the summary for all the meshes used in the simulations. **Figure 6.12** shows the water levels for *Case 1* at all the three locations. These locations were taken at the same location as the measuring points mentioned in **Chapter 5**. Similarly, **Figure 6.13, 6.14, 6.15, 6.16 and 6.17** showed the water levels for the other five cases. The analysis was done after the seventh tidal cycles. This was to ensure that the water levels have developed adequately in the domain.

- ***Location 1***

Water levels were used to compare for all the cases. This location was situated at the estuary mouth. The water levels at *location 1* for all the cases except for *Case 3* fluctuated sinusoidally between -2.0m to 2.0m, which was similar to the imposed tidal level at the outlet boundary. From the water level profiles, the inflow from floodplain and the effect bed profile had a minimum effect on the water level. The tidal had a stronger effect on the formation of water levels. Whereas for *Case 3,* the water level had a different pattern from the other five cases due to the gradient of the bed elevation. The movement

of water for this case was restricted from propagating inland. The water level for Case 3 fluctuated between -0.2m to 2.0m. The bed elevation had stronger influenced on the water level as shown in **Figure 6.14**.

- ***Location 2***

This location was situated at a distance of 20.12 km upstream of *location 1*. For the *first case* and *second case,* the water level fluctuated between 0.8m to 2.5m and between 0.5m to 1.5m respectively. For the first case, the water level for all the high water tides was above the imposed tidal level at the outlet boundary. The inflow of water from floodplain was a major factor that gave rise to this phenomenon. While for the *second case*, the bed elevation had an influenced on the water level as shown in **Figure 6.13**. The water fluctuated between level 0.2m to 0.6m, which was less than Case 1. *For Case 3*, the water level showed there was a slight fluctuation between 0.8m to 1.2m. As mentioned earlier, the bed elevation played a main role in determining the water level at this location. For the *fourth case*, water level fluctuated sinusoidally between -1.5m to 2.2m. The water level had the same pattern as the imposed tidal level but with a lesser in amplitude. For this case, the tidal level had an influenced on the water. While for *Case 5* and *Case 6,* the water level fluctuated between 1.0m to 1.5m and between 1.0m to 1.8m respectively. *Case 6* showed a higher fluctuation as shown in **Figure 6.16**. At this location, the bed elevation had a minimum effect on the water level.

- ***Location 3***

This location was situated at a distance of about 15.71km upstream of the *second location*. A similar comparison was made based on the water level profiles for all the cases. For *first* and *second case,* the water level fluctuated between 1.8m to 2.2m and between 0.4m to 1.2m respectively. A similar observation was made on factor that influenced the water level at this location as discussed for the *second location.* For *Case 3,* the water level showed a slight fluctuation between 0.8m to 1.2m and while for Case 4, the water level had a highest fluctuation between -1.5m to 2.2m. The water levels at this location were similar to the water level at the second location but with a slight phase

difference between them. For *Case 4*, the water level fluctuated sinusoidally, which was similar to the water level at the *second location* but with a slight phase difference. For *Case 5,* the water level was constant at 1.5m above the mean sea level. The inflow of freshwater at this location became the main factor affected the water level. While for *Case 6,* the water level fluctuated between 1.0m to 1.8m which was similar to the water level at the second location.

From the above analysis, the presence of floodplains, tidal, bed elevation and estuary layouts have affected the water level at the three locations.

6.5.2 Comparison on Floodplains Effects

The objective of this simulation was to analyse the effect of floodplain on the flow structures. In this analysis, a comparison was made between *Case* 1 with *Case 5* and *Case 2* with *Case 6.*

- ***Case 1 vs Case 5***

For *Case 1* and *Case 5* the water level at the *first location* showed a sinusoidal profile which was similar to the outlet boundary condition. The tidal had strongly influenced on the water level compared to the freshwater inflow and the floodplain. For Case 5, the water level was sinusoidal which was similar to *Case 1* as shown in **Figure 6.22**. The water level fluctuated sinusoidally between 2.0m and -2.0m.

At the *second location*, the water level for both cases fluctuated with a smaller amplitude compared to the *first location* as shown in **Figure 6.18**. For *Case 1*, the water level had a higher amplitude ranged between 0.8m to 2.5m whereas for *Case 5* the water level ranged between 1.0m to 1.5m. Due to the strong inflow of water from the floodplains into the river, there was an increase of water level in the main channel. Unlike *Case 5*, the water level at this location was far less than *Case 1*. The water level for *Case 1,* showed that the water level at this location had two high and low water tides. The inflow of freshwater from upstream and tidal effect had influenced the water level. Therefore, the presence of floodplain in *Case 1* had significantly change the water level in the river at

this location.

A similar observation was made at *location 3*, where the water level for *Case 1* was higher than *Case 5* as shown in **Figure 6.20**. For *Case 1* the water level fluctuated between 1.8m to 2.3m while for *Case 5* the water level was almost constant at 1.5m above the mean sea level. Similarly, the inflow of water from the floodplain into the river system had affected the water level in the main channel for the first case.

In conclusion, *Case 1* had a good resemblance to the physical condition. The presence of floodplains had affected the formation of water level at *location 2* and *3*. This could be observed for *Case 1*, where the water levels at both locations fluctuated above the imposed tidal level.

- ***Case 2 vs Case 6***

A similar comparison was made for *Case 2* with *Case 6*. **Figure 6.23** shows the water level for *Case 2* and *Case 6*. At *location 1*, the water levels for both cases were identical. The water levels fluctuated between -2.0m to 2.0m which closely resemblance to the tidal elevation. A similar conclusion could be made that the tidal had a major influenced on the water levels for this particular case.

At the *second location*, the water level fluctuated between 0.2m to 1.3m for *Case 2* and between 0.9m to 1.3m for *Case 6* as shown in **Figure 6.19.** *Case 2* showed a higher fluctuation of water level. The inflow of water from the floodplain had influenced the water level during high and low water tides. The high and low water tides for *Case 2* was one hour earlier than *Case 6*. For *Case 2*, the tidal had no influenced on the water level at the second location.

A similar observation was made at the *third location*, the water level for *Case 6* and *Case 2* fluctuated between 1.0m to 1.8m and between 0.4m to 1.1m as shown in **Figure 6.21**. For Case 6 the fluctuation was higher compared to Case 2. This was due to the bed profile, where the water in the river channel could only flow upward since there

was no floodplain. While for Case 2 due to the presence floodplains, the water would flow onto the floodplain. There was a phase difference for both water levels. The inflow of water from floodplain into the river would affected the water level at this location.

In conclusion, the presence of floodplains have a major influenced on the water levels. At *location 1*, the tidal was dominating over inflow of freshwater upstream and the inflow of water from the floodplains. At *location 2* and *3*, the inflow of water from the floodplain and bed profile had a greater influenced on the water levels. This could be observed at *location 2*, for *Case 1*, *Case2, Case 5* and Case *6* where the water level had a different flow levels. A similar observation was also observed at the *third location.*

6.5.3 Depth Average Velocities

The depth averaged velocity (longitudinal and lateral velocity) for the six cases were analysed at the three locations. Firstly, two sets of time duration was chosen for the analysis. The time chosen was at T=57 hours (flooding) and T=63 hours (ebbing) respectively which coincided with high and low water tides. Secondly, comparison was made for all the cases to determine their velocity profile. Thirdly, analysis was done to determine the effect of floodplain on the velocity flow structures in the main channel. The 'U' and 'V' denoted the lateral and longitudinal velocity respectively.

- ***Location 1***

Comparison was made for the six cases. The objective of this analysis was to analyse the velocity distributions among various river configurations. **Figure 6.24** shows the simulated velocity distributions for all the cases at time T = 57 hours (flooding). The longitudinal velocity for *Case 4* was 1.0 m/s located at the centre of the main channel. This value was the highest compared to the five other cases at this location. The maximum longitudinal velocity for *Case 3* was 0.3 m/s and was located at the centre of the main channel. For *Case 1* and *Case 5*, the longitudinal velocity was higher at the outer section of the apex. By comparing these two cases, the longitudinal velocity for *Case 1* and *Case 5* was 0.5 m/s and 0.25m/s respectively with a difference of 50%. The maximum

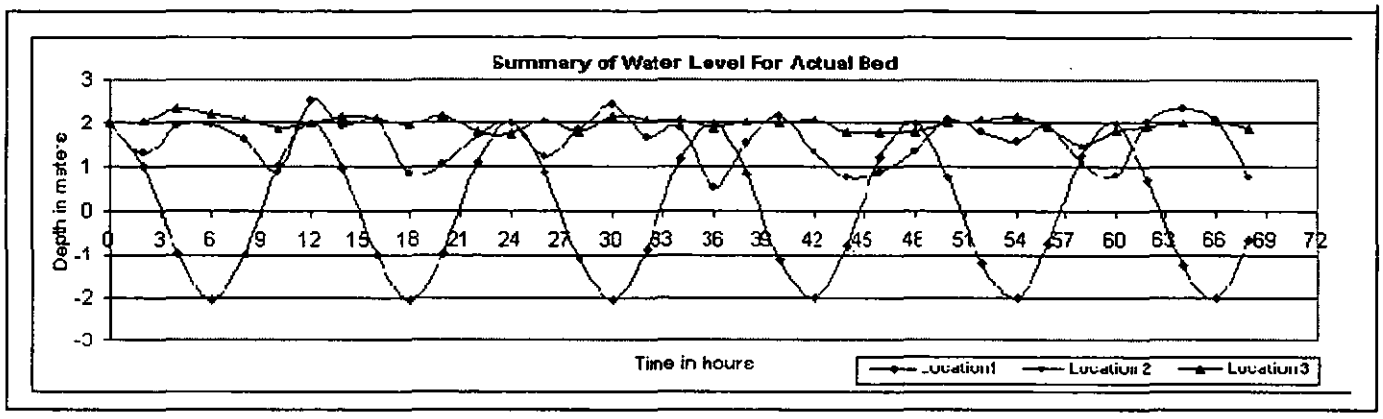

Figure 6.12 –Summary of Water Level for Case 1(Actual Bed with Floodplains)

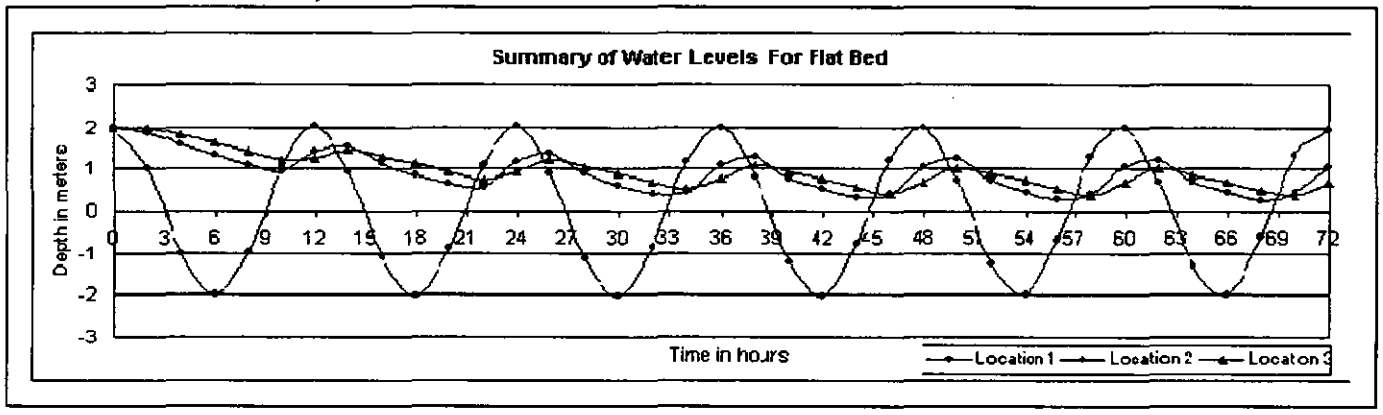

Figure 6.13 – Summary of Water Level for Case 2 (Flat Bed with Floodplains)

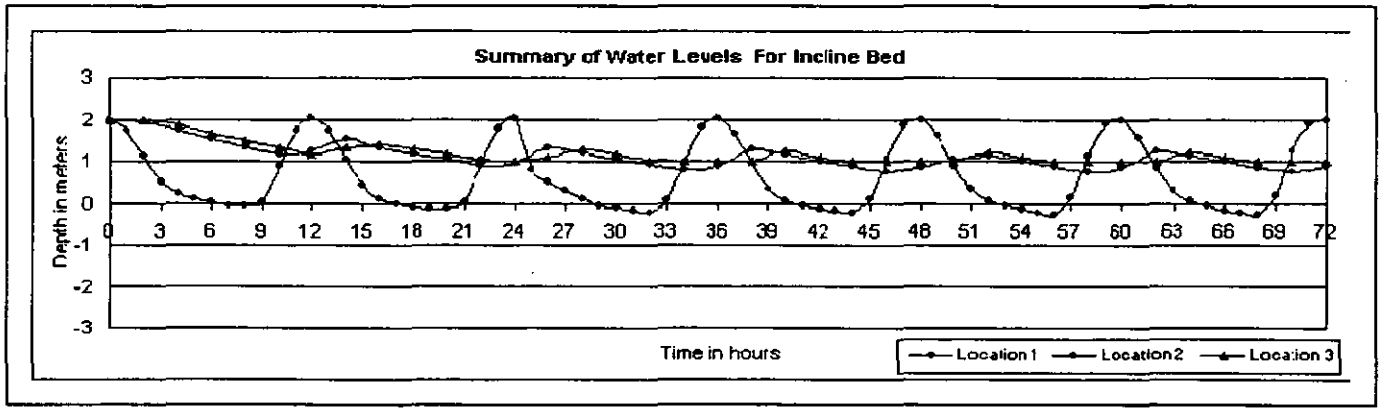

Figure 6.14 – Summary of Water Level for Case 3 (Inclined Bed with Floodplains)

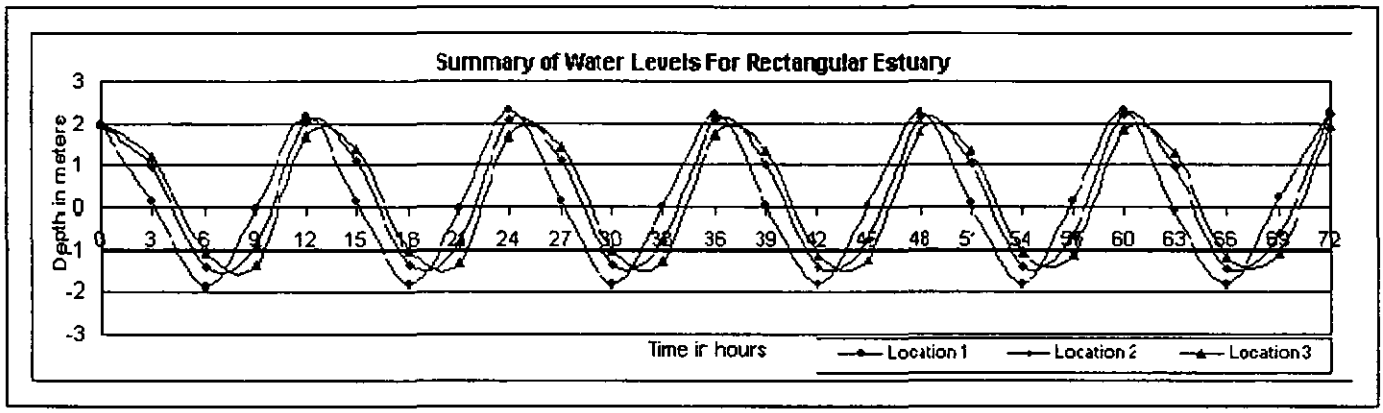

Figure 6.15 – Summary of Water Level for Case 4 (Straight, Tapered and Flat Bed with Narrow Floodplains)

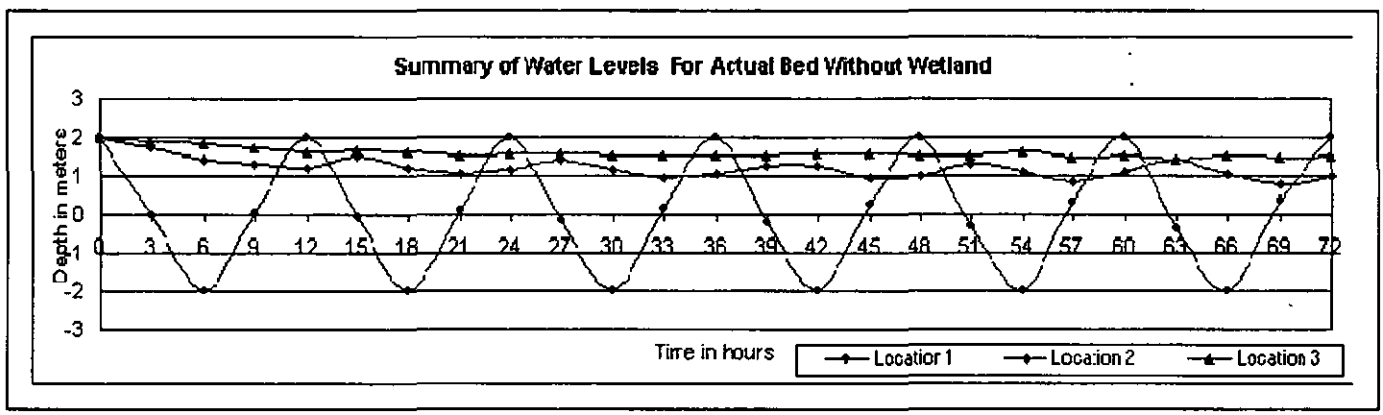

Figure 6.16 – Summary of Water Level for Case 5 (Actual Bed without Floodplain)

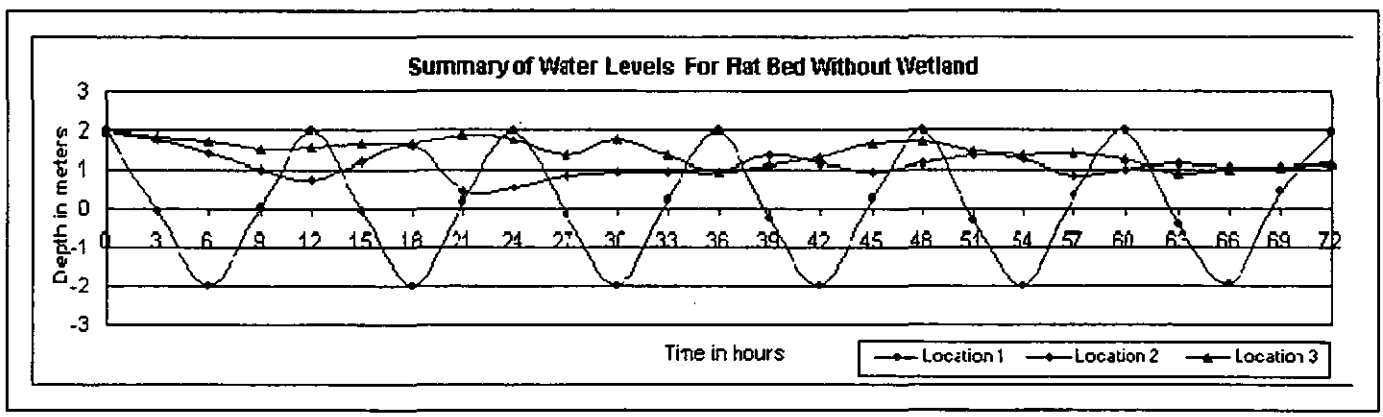

Figure 6.17 –Summary of Water Level for Case 6 (Flat Bed without Floodplain)

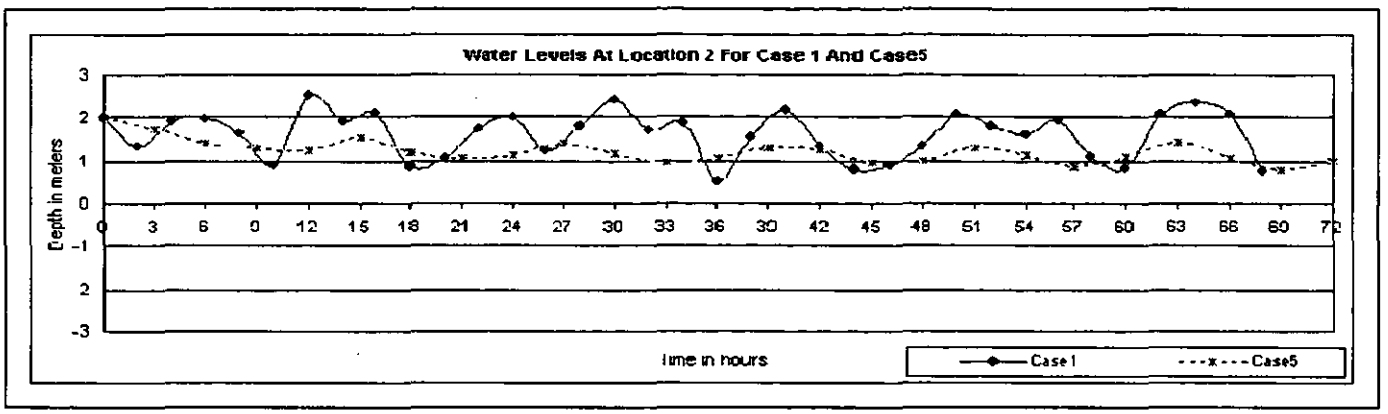

Figure 6.18– Water Levels at Location 2 for Case 1 (Actual Bed with Floodplains) and Case 5 (Actual Bed without Floodplains)

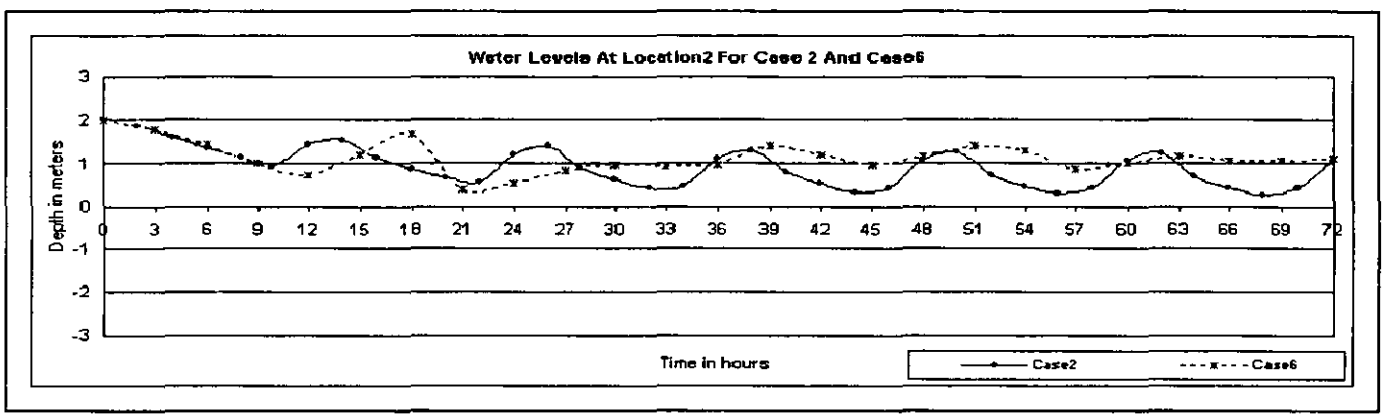

Figure 6.19 – Water Levels at Location 2 for Case 2 (Flat Bed with Floodplains) and Case 6 (Flat Bed without Floodplains)

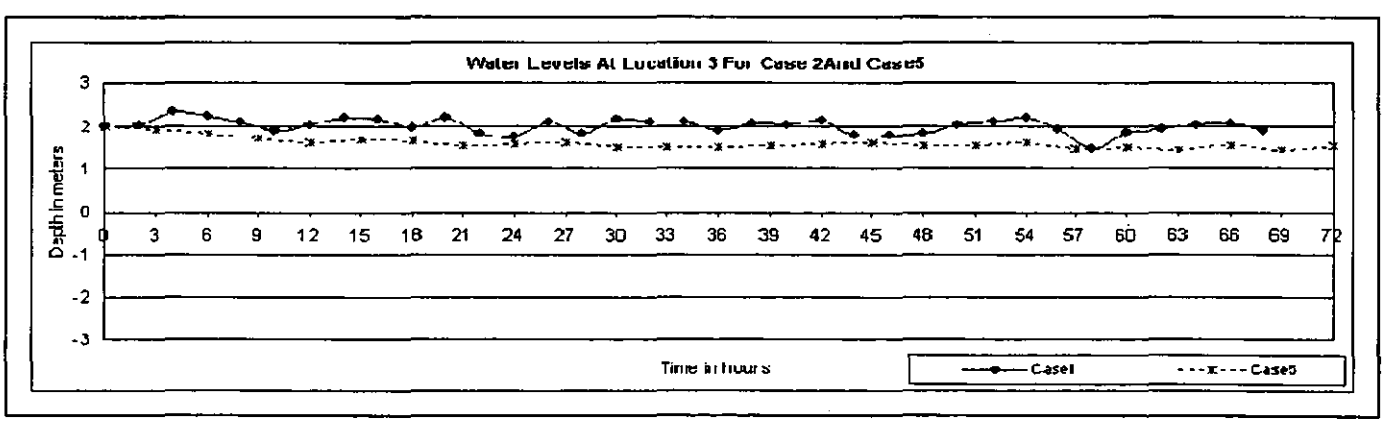

Figure 6.20– Water Levels at Location 3 for Case 1 (Actual Bed with Floodplains) and Case 5 (Actual Bed without Floodplains)

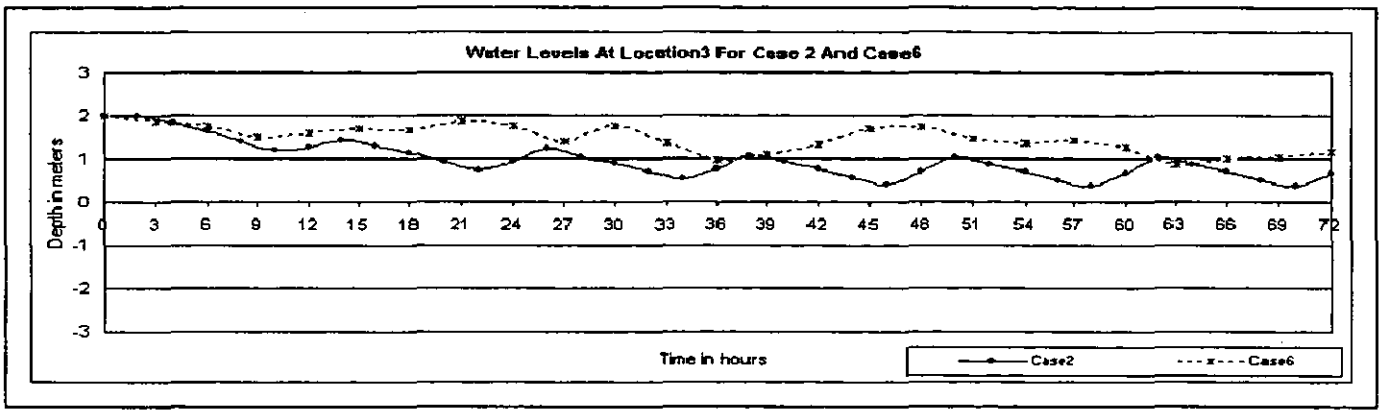

Figure 6.21 – Water Levels at Location 3 for Case 2 (Flat Bed with Floodplains) and Case 6 (Flat Bed without Floodplains)

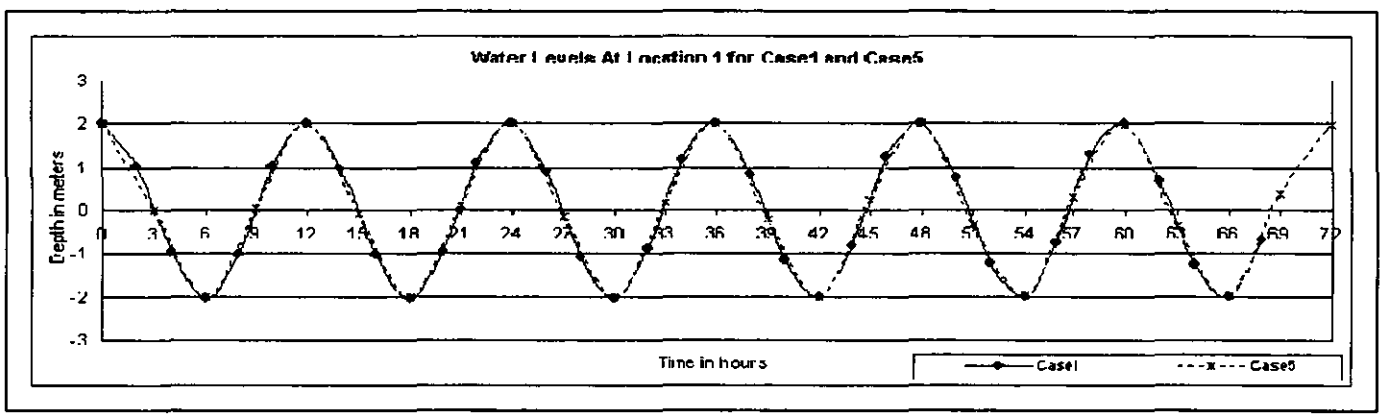

Figure 6.22 – Water Levels at Location 1 for Case 1 (Actual Bed with Floodplains) and Case 5 (Actual Bed without Floodplains)

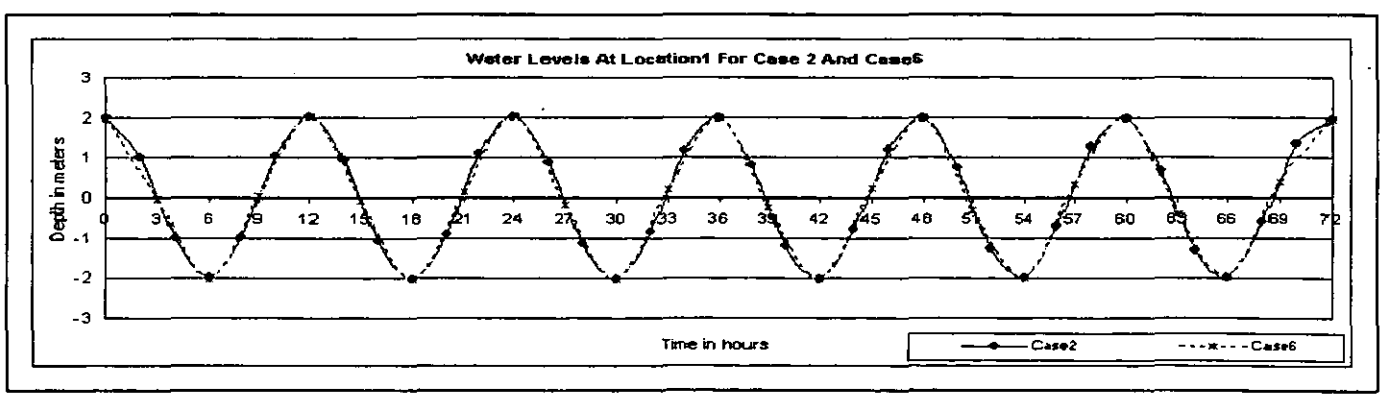

Figure 6.23 – Water Levels at Location 1 for Case 2 (Flat Bed with Floodplains) and Case 6 (Flat Bed without Floodplains)

longitudinal velocity for *Case 2* was 0.2m/s and was located at the centre of the main channel. While for *Case 6*, the maximum longitudinal velocity was 0.3 m/s and was also located at the centre of the main channel.

The lateral velocity for *Case 1*, *Case 4* and *Case 6* was almost negligible as shown in **Figure 6.24**. While for *Case 2 and Case 3*, the maximum lateral velocity was 0.2 m/s and 0.3 m/s respectively both located at the centre of the channel. The velocity for this Case 3 fluctuated throughout the cross-section of the main channel. The lateral velocity for *Case 2* and *Case 3* was higher on the left bank (outer side of the meandering section) compared to the right bank. For *Case 5*, the lateral velocity was higher at the centre of the main channel with a reading of 0.2 m/s.

Figure 6.25 shows the longitudinal and the lateral velocity for the six cases during ebbing at time T = 63 hours. The figure showed generally that there was a reduction of velocity in the main channel. The longitudinal velocity for *Case 1* and *Case 5* was 0.8m/s and 0.6m/s respectively. The velocity for *Case 5* was located at the centre of the main channel. For *Case 2*, the maximum longitudinal velocity was located at the centre of the main channel with a reading of 0.5m/s while for *Case 6* the velocity was 0.2m/s and almost constant through the cross-section. The longitudinal velocity for *Case 3* fluctuated throughout the cross-section of the main channel with a reading of 0.4m/s while for *Case 4* the maximum longitudinal velocity was located at the centre of the main channel with a reading of 1.2m/s. This velocity was the highest among the six cases.

The lateral velocity (u) for the six cases have a minor variation across the river section except for *Case 2* and *Case 3*, where the lateral velocity reading was 0.3m/s and 0.4m/s respectively. The longitudinal velocity was dominant over the lateral velocity for all the six cases. Furthermore, the velocity distributions for the six cases have different readings, which was dependent on the bed formation and the floodplains although the same boundary conditions was imposed during the simulations.

- ***Location 2***

Figure 6.26 shows the longitudinal and lateral velocity distributions for the six cases at time T = 57 hours (flooding). Similar to the *first location*, the highest longitudinal velocity was for *Case 4*, which was 0.8m/s and located at the centre of the main channel. During this period, the water level reading was at -0.5m below the mean sea level and it was flooding with reference to the water level at the first location as shown in **Figure 6.15**. All the water levels in this analysis was referred to the water level at the first location. For *Case 1*, the highest velocity was toward the riverbanks. The longitudinal velocity at this location was 0.18m/s while the reading at the centre of the main channel was zero. The water level was at 0.5m above the mean sea level and it was ebbing. This phenomenon was due to the inflow of water from the floodplains into the river channel. For *Case 5*, the longitudinal velocity was constant with zero reading. During this period the water level was at below 1.0m and was ebbing. For *Case 2*, the highest longitudinal velocity was 0.4 m/s and was located at the deepest location of the main channel. The water level at this location was at 0.3m and the water started to flood as shown in **Figure 6.13**. For *Case 6*, the long longitudinal velocity was 0.2m/s and was located at the middle section of the main channel. The water level was at 1.0m below the mean sea level and it was ebbing. For *Case 3*, the longitudinal velocity was 1.8m/s constant throughout the main channel. The water level profiles were almost identical for *Case 5* and *Case 6* as shown in **Figure 6.16** and **Figure 6.17** respectively.

The lateral velocity for all cases were almost negligible except for *Case 1* and *Case 6* where the lateral velocity was 0.2m/s and 0.8m/s respectively. For *Case 1* the lateral velocity was constant across the main channel while for Case 6 the maximum lateral velocity was at the right bank.

Figure 6.27 shows the longitudinal and lateral velocity profiles for all the cases at time T = 63 hours (ebbing). For *Case 1*, the longitudinal velocity decreased toward the left bank of the main channel and was higher on the right floodplain. The maximum and minimum longitudinal velocity was 0.2 m/s and -0.18m/s respectively. The negative sign indicated that the longitudinal velocity was in the opposite direction of flow. The velocity

was in an opposite direction at both banks. The water level during this duration was at 2.3m as shown in **Figure 6.12**. The water tends to rotate from upstream toward the downstream direction during flooding. This rotational of water would causes some scouring effect at the bottom of the main channel as shown in **Figure 5.3** at section 13 in **Chapter 5**. The highest velocity was on the floodplains. This was due to the inflow of water from the floodplains into the main channel, which causes the longitudinal velocity to be higher on the floodplains. For *Case 5*, the longitudinal velocity was 0.02m/s and was constant except at the centre of the channel. The water level during this interval was at 1.5m above the mean sea level as shown in **Figure 6.16**. For *Case 2*, the highest longitudinal velocity was 0.2m/s and was located at the main channel. The water level was at 1.0m and it was flooding. For *Case 6*, the maximum longitudinal velocity was -0.8m/s and was located at the centre of the main channel. The water level during this interval was at 1.0m and it was ebbing. For *Case 3*, the longitudinal velocity was zero and was relatively constant throughout the cross-section. The water level at this time was 1.2m and it was ebbing. For the *Case 4* (rectangular channel), the longitudinal velocity was 0.8m/s and was located at the centre of the main channel. The water level at this time was 1.0m and it was ebbing.

In **Figure 6.27**, *Case 1* and *Case 6* have the highest lateral velocity compared to the other four cases. The lateral velocity for *Case 4* and *Case 6* was 0.2m/s and 1.0m/s respectively. For Case 1, the lateral velocity on the right floodplain while for Case 6 it was at the centre of the channel. The lateral velocity for this Case 1 fluctuated across the river channel and on the floodplains. While for *Case 2* and *Case3*, the lateral velocity was very small and it distributed across the channel section with a reading of 0.1m/s and 0.2m/s respectively. For *Case 5*, the maximum lateral velocity reading was 0.1m/s and it was located at the centre of the main channel.

The river layouts, the bed gradients and the presence of floodplains significantly influenced the longitudinal and lateral velocity profiles in the main channel. From the analysis, the highest velocity for all the cases was at the middle section of a main channel. Shape factors were also important parameter in obtaining a realistic and accurate results.

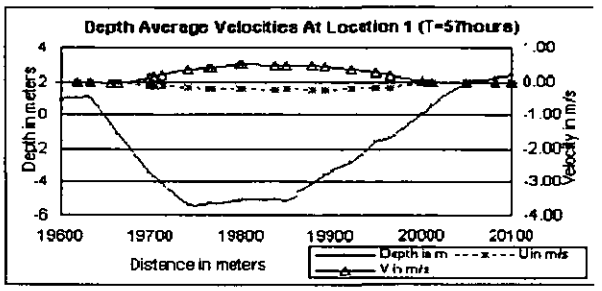

Case 1

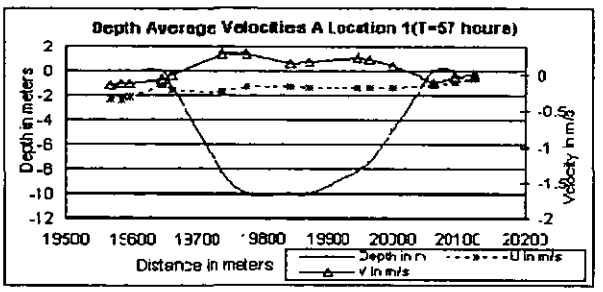

Case 2

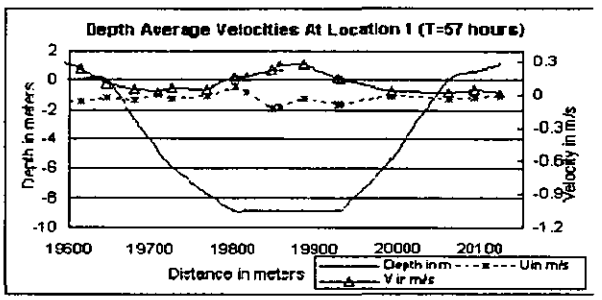

Case 3

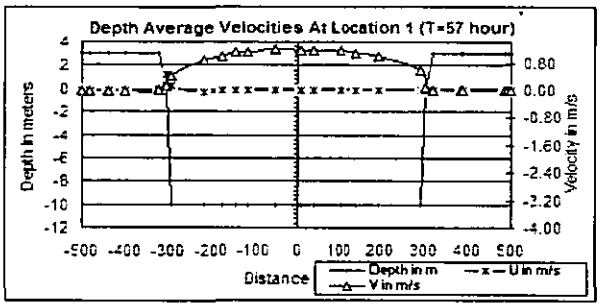

Case 4

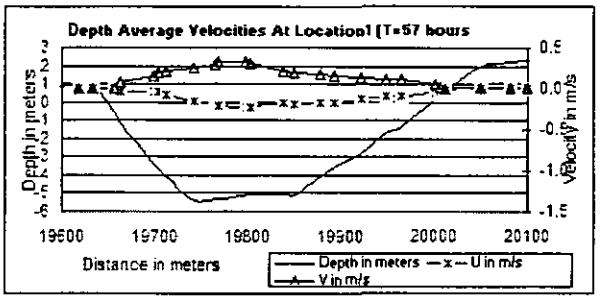

Case 5

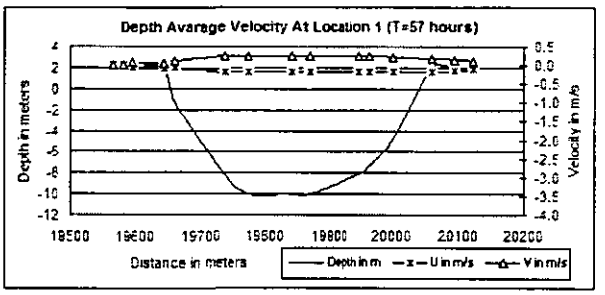

Case 6

Case 1 - An estuary with the actual bed and floodplains

Case 2 - An estuary with a flat bed and floodplains

Case 3 - An estuary with an incline bed and a narrow floodplains

Case 4 - A straight and tapered rectangular estuary with a flat bed and a narrow floodplains

Case 5 - An estuary with the actual bed but without floodplains

Case 6 - An estuary with a flat bed but without floodplains

U - Lateral velocity

V - Longitudinal velocity

Figure 6.24 – Depth Average Velocity at Location 1 During Flooding (T = 57 hours)

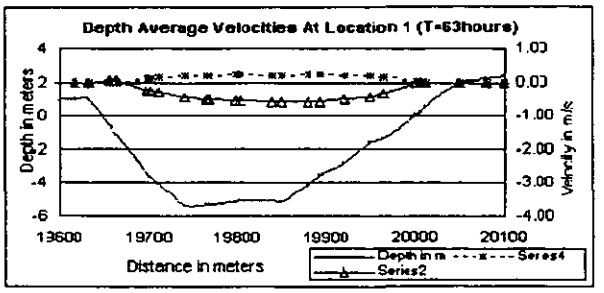

Case 1

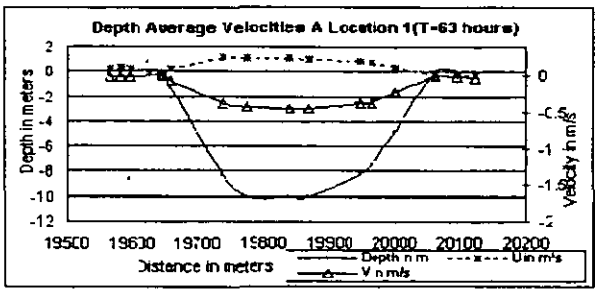

Case 2

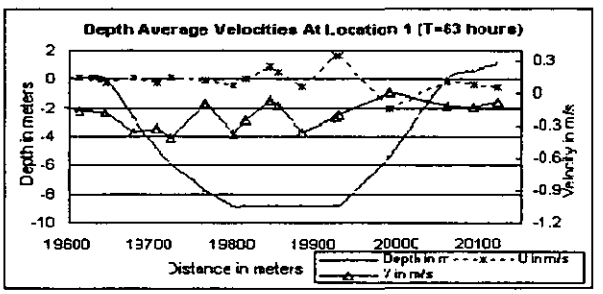

Case 3

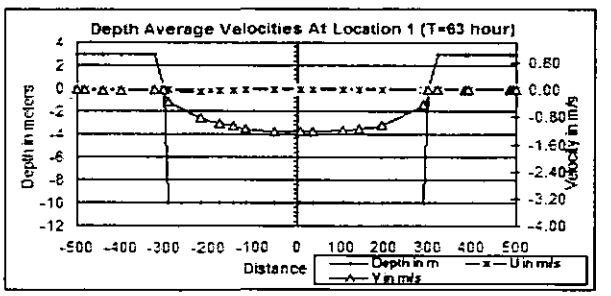

Case 4

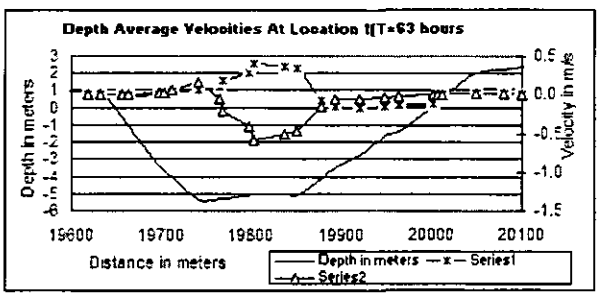

Case 5

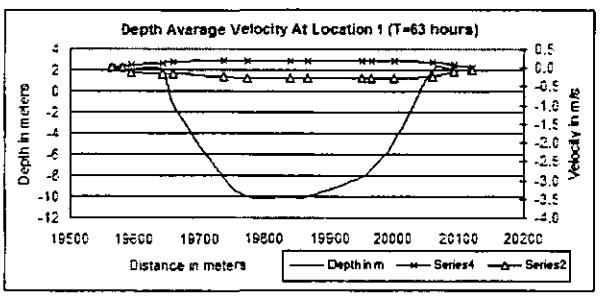

Case 6

Case 1 - An estuary with the actual bed and floodplains

Case 2 - An estuary with a flat bed and floodplains

Case 3 - An estuary with an incline bed and a narrow floodplains

Case 4 - A straight and tapered rectangular estuary with a flat bed and a narrow floodplains

Case 5 - An estuary with the actual bed but without floodplains

Case 6 - An estuary with a flat bed but without floodplains

U - Lateral velocity

V - Longitudinal velocity

Figure 6.25 – Depth Average Velocity at Location 1 During Ebbing (T = 63 hours)

- ***Location 3***

Location 3 was situated at a distance about 35.83km upstream of *location 1*. The salinity does not flow beyond the 28th km from the estuary mouth. **Figure 6.28** shows the longitudinal and the lateral velocity distribution for all the cases at *location 3* at time T = 57 hours (flooding). For *Case 1*, the longitudinal velocity was higher on the left bank with a reading of 0.08m/s. The longitudinal velocity was zero and was located at the centre of the main channel while the reading on the right bank was 0.04m/s. **Figure 6.12** shows the water level at this location was 1.5m and it was ebbing. For *Case 5*, the longitudinal velocity was -0.5m/s and it was located at the left bank of the main channel and it then gradually reduced to zero as it approached the right bank. The water level at this duration was 1.0m (at low water tide). For *Case 2*, the longitudinal velocity was zero and was constant across the main channel. While for *Case 3*, the longitudinal velocity was 0.05m/s and was located at the left bank. The water level for *Case 2* and *Case 3* during this duration was at 0.5m (low water tide) and 0.9m (low water tide) respectively as shown in **Figure 6.13** and **Figure 6.14**. For *Case 4*, the longitudinal velocity was 0.6m/s. The velocity distribution was symmetrical and was located at the centre of the main channel. The water level during this duration was at -0.5m below the mean sea level and it was flooding as shown in **Figure 6.15**. While for *Case 6*, the longitudinal velocity located toward the bank with a reading of -0.2m/s and it gradually reduced to zero toward the banks. The water level was at 0.9m above the mean sea level and it was ebbing as shown in **Figure 6.17**.

The lateral velocity was also analysed for all the case as mentioned above. For *Case 1*, the maximum velocity was at the middle of the main channel with a reading of 0.18m/s. The minimum velocity was -0.1m/s at it occurred at the deepest location of the main channel. For *Case 2*, the maximum velocity was 0.2m/s, which occurred at the centre of the main channel and again it then gradually reduced to zero toward the floodplains. While for *Case 3*, the maximum lateral velocity followed a similar pattern as the longitudinal velocity with the reading of 0.6m/s and it was toward the left bank. The lateral velocity for *Case 4* was zero across the main channel. For *Case 5*, the highest velocity was toward the left bank with a reading of 0.3m/s. The velocity at the left bank

was 0.2m/s and subsequently it then reduced to zero at the right bank. For *Case 6*, the maximum velocity was at the left bank of the main channel with a reading of 0.04m/s.

Figure 6.29 shows the velocity at time T = 63 hours (ebbing). For *Case1*, the maximum velocity was at the centre and at both banks of the main channel. At the centre section, the velocity was 0.1m/s whiles the velocity at the left and the right bank was 0.8m/s and 0.9m/s respectively. Comparison was also made with *Case 5*, which had the same layout but without the floodplain along its banks. The maximum velocity for *Case 5* was at the left bank with a reading of -0.7m/s while the velocity at right bank was zero. The water level at this particular interval was at 1.5m (at high water tide) as shown in **Figure 6.16**. The velocity for *Case 2* was constant throughout the cross-section and the floodplain with a velocity of 0.1m/s while for *Case 6*, the velocity was higher at the left bank compared to the right bank. This velocity was constantly reduced from -0.7m/s at the left bank to zero toward the right bank. For *Case 3*, the longitudinal velocity was higher at the left floodplain compared to the main channel and the right floodplain. The velocity on the left floodplain was 0.06m/s. While for *Case 4*, the maximum velocity was located at the centre of the main channel with a reading of -0.4m/s.The lateral velocity was higher at the banks of the main channel and it was in the opposite direction. The velocity at the left bank was 0.1m/s while on right bank the reading was -0.09m/s. The longitudinal and lateral velocity crosses each other at the centre of the main channel. The water level at this interval was at 2.0m and it was relatively stable without any fluctuation. In *Case 3*, the longitudinal and the lateral velocity were paralleled to each other over the entire cross-section. The longitudinal velocity was dominant over the lateral velocity. For *Case 4*, the highest velocity was found to be at the centre of the main channel with the lateral velocity was dominant over the longitudinal velocity.

- **Velocities for *Case 1* vs *Case 5***

A comparison was also made on the velocity distributions for *Case 1* and *Case 5*. At time T = 57 hours, the water level at *location 1* for both cases were identical. The velocity distribution at this location showed that the longitudinal velocity (v) for *Case 1* was 0.5 m/s while for *Case 5* it was 0.25m/s. **Figure 6.24** shows the location of maximum

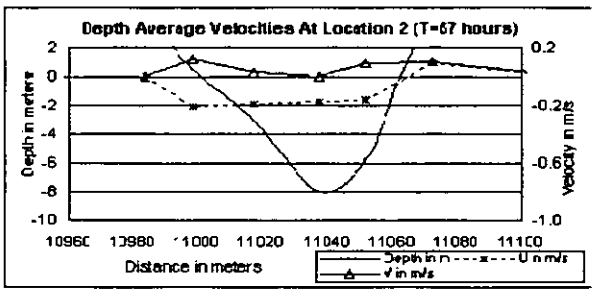

Case 1

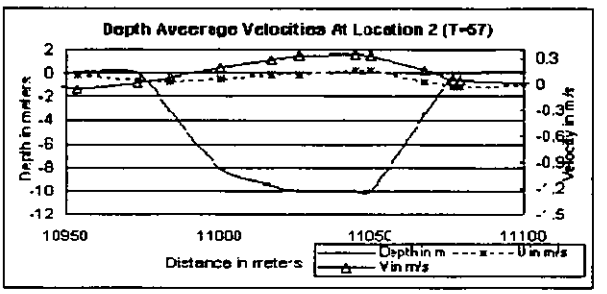

Case 2

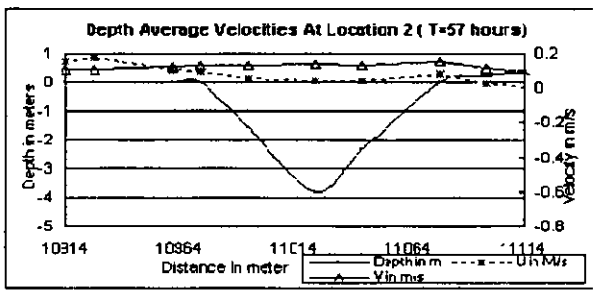

Case 3

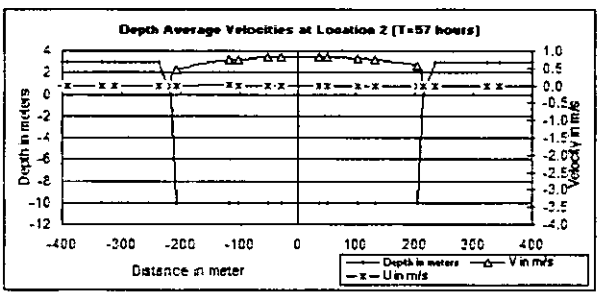

Case 4

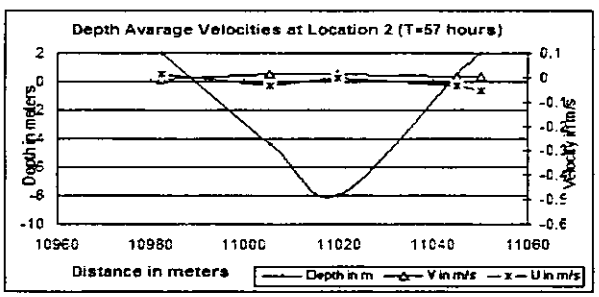

Case 5

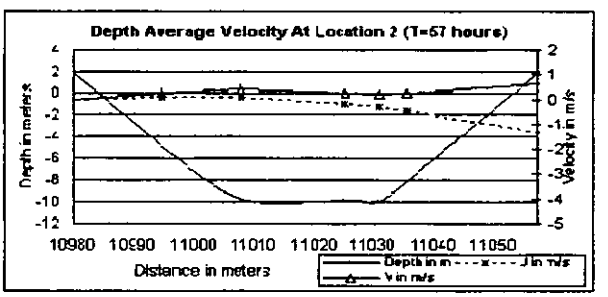

Case 6

Case 1 - An estuary with the actual bed and floodplains

Case 2 - An estuary with a flat bed and floodplains

Case 3 - An estuary with an incline bed and a narrow floodplains

Case 4 - A straight and tapered rectangular estuary with a flat bed and a narrow floodplains

Case 5 - An estuary with the actual bed but without floodplains

Case 6 - An estuary with a flat bed but without floodplains

U - Laterall velocity

V - Longitudinal velocity

Figure 6.26 – Depth Average Velocity at Location 2 During Flooding (T = 57 hours)

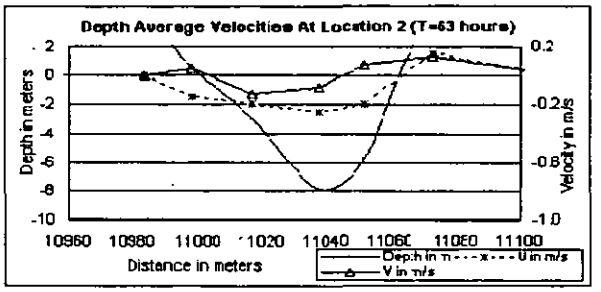

Case 1

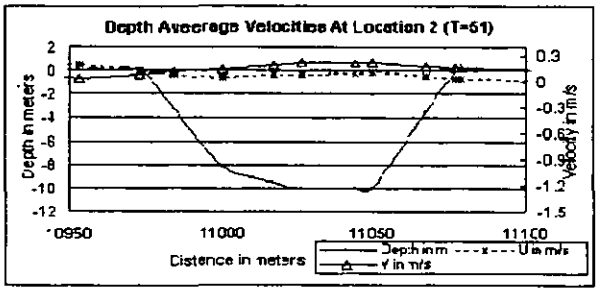

Case 2

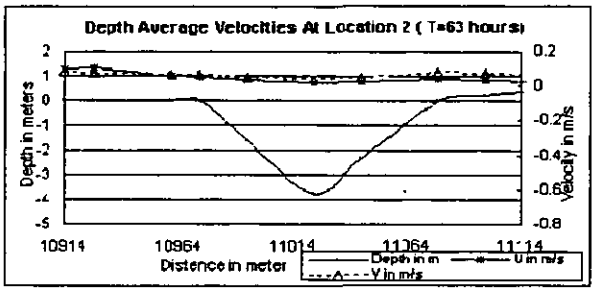

Case 3

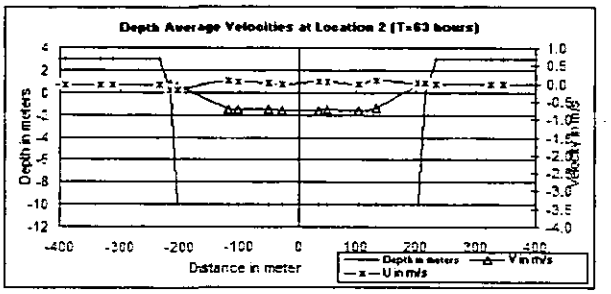

Case 4

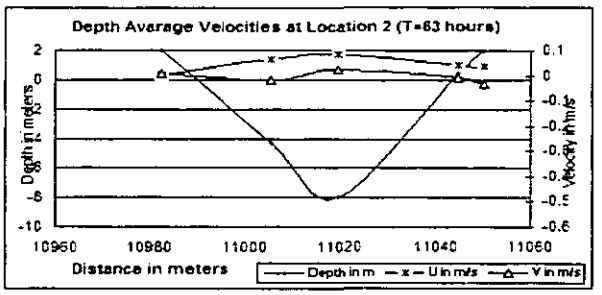

Case 5

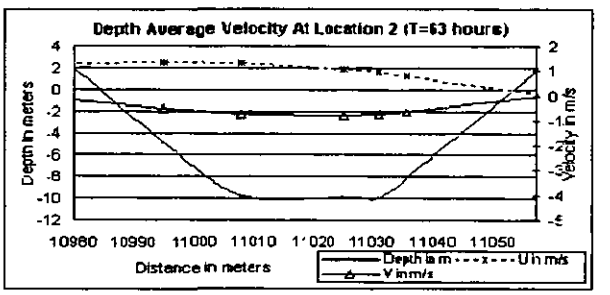

Case 6

Case 1 - An estuary with the actual bed and floodplains

Case 2 - An estuary with a flat bed and floodplains

Case 3 - An estuary with an incline bed and narrow floodplains

Case 4 - A straight and tapered rectangular estuary with a flat bed and a narrow floodplains

Case 5 - An estuary with the actual bed but without floodplains

Case 6 - An estuary with a flat bed but without floodplains

U - Lateral velocity

V - Longitudinal velocity

Figure 6.27 – Depth Average Velocity at Location 2 During Ebbing (T = 63 hours)

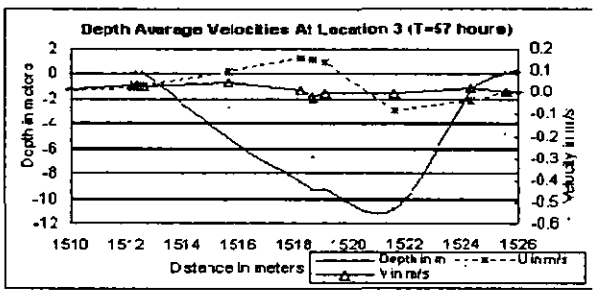

Case 1

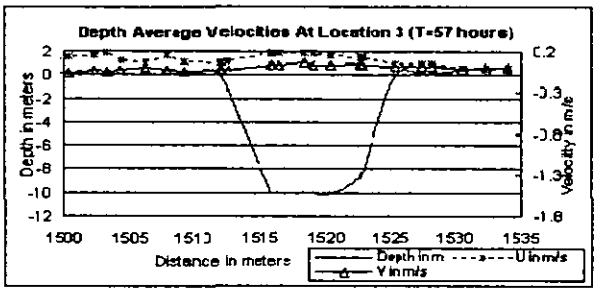

Case 2

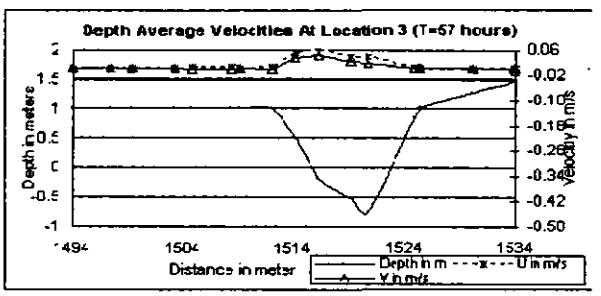

Case 3

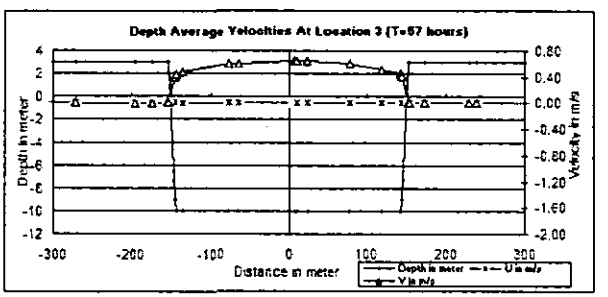

Case 4

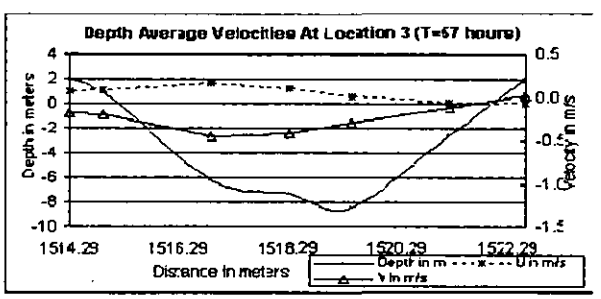

Case 5

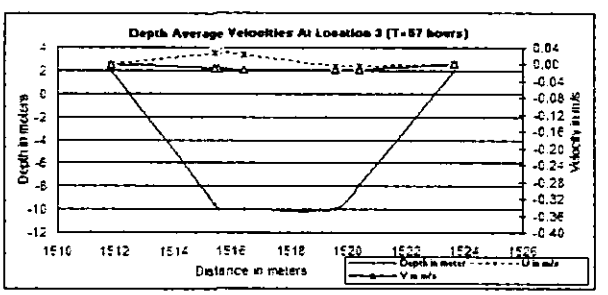

Case 6

Case 1 - An estuary with the actual bed and floodplain

Case 2 - An estuary with a flat bed and floodplains

Case 3 - An estuary with an incline bed and a narrow floodplains

Case 4 - A straight and tapered rectangular estuary with a flat bed and floodplains

Case 5 - An estuary with the actual bed but without floodplains

Case 6 - An estuary with a flat bed but without floodplains

U - Lateral velocity

V - Longitudinal velocity

Figure 6.28 – Depth Average Velocity at Location 3 During Flooding (T= 57 hours)

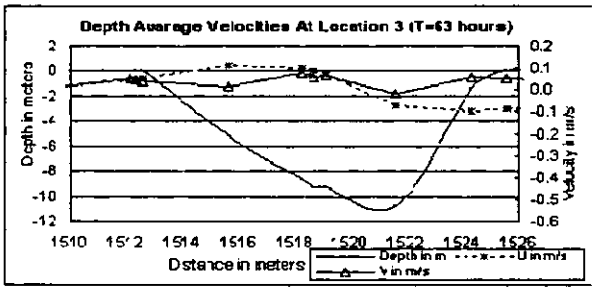

Case 1

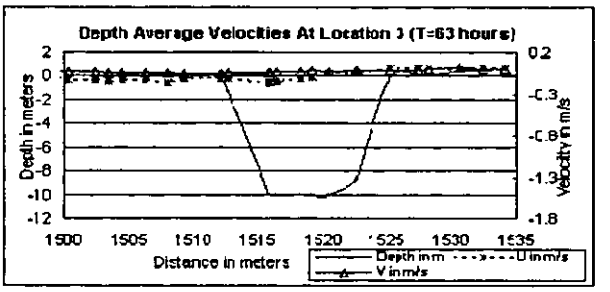

Case 2

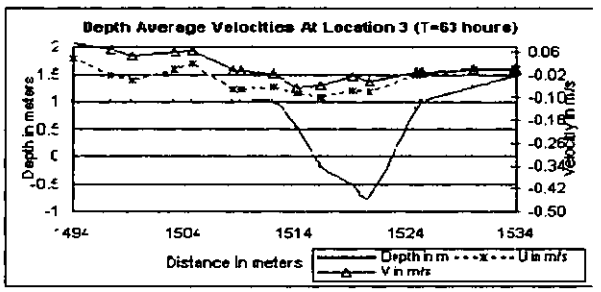

Case 3

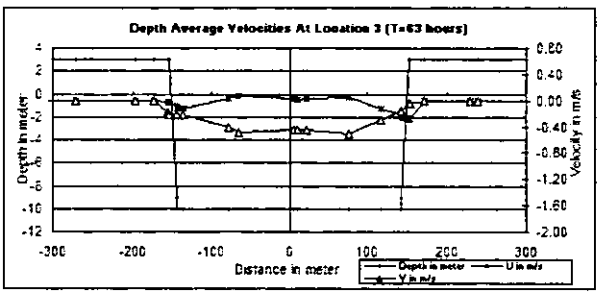

Case 4

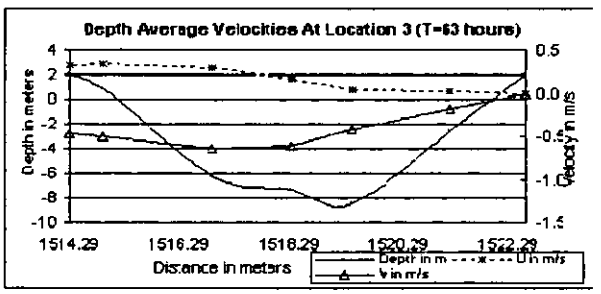

Case 5

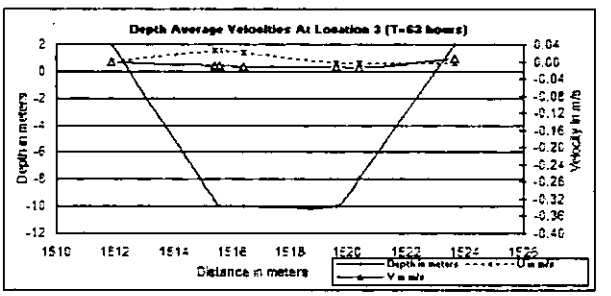

Case 6

Case 1 - An estuary with the actual bed and floodplains

Case 2 - An estuary with a flat bed and floodplains

Case 3 - An estuary with an incline bed and a narrow floodplains

Case 4 - A straight and tapered rectangular estuary with a flat bed and a narrow floodplains

Case 5 - An estuary with an actual bed but without floodplains

Case 6 - An estuary with a flat bed but without floodplains

U - Lateral velocity

V - Longitudinal velocity

Figure 6.29 – Depth Average Velocity at Location 3 (T = 63 hours)

velocity for *Case 1* occurred at the centre of the main channel while for *Case 5* it was at the left bank. The lateral velocity (u) for both cases was almost identical over the entire cross-section. At time T = 63 hours, the lateral velocity for *Case 5* was much higher compared to *Case 1*. For *Case 5* the lateral velocity was 0.4m/s and for *Case 1* it was 0.2m/s. The maximum velocity for both cases was found to be located at the centre of the cross-section as shown in **Figure 6.25**. This was due to the differential of velocity between the floodplains and the main channel. The difference in velocity would lead to the shear force effect at the interface of the flow. Hence, the flow in the main channel would be retarded due to the shear force and thus affected the velocity distribution in the main channel. This was due to the formation of the secondary currents generated at the interface.

At the *second location* when time T = 57 hours, the lateral velocity (u) for *Case 1* was dominant over the longitudinal velocity (v) especially at both the banks as shown in **Figure 6.26**. This was due to the flow of water from the floodplains into the main channel during ebbing which created a higher velocity profile on the floodplains compared to the other locations across the main channel. The water in the main channel at this time was ebbing as shown in **Figure 6.12**. Whilst for *Case 5*, the longitudinal velocity was dominant and had a higher value at the middle section of the main channel. At time T = 63 hours, a similar observation was made for *Case 1*, except that the longitudinal velocity on both banks were in the opposite direction. The longitudinal velocity at this location was 0.0m/s. This location was situated at the deepest section of the river. The lateral velocity at *location 2* was 0.25m/s. For *Case 5*, the longitudinal velocity was dominant and the maximum velocity was found to be at the centre of the main channel. **Figure 6.27** shows the velocity distribution at *location 2* at time T = 63 hours.

Similarly at the *third location* when time T = 57 hours, the lateral velocity for *Case 1* was once again dominant over the longitudinal velocity. One observation made at this location was that the lateral velocity distribution was fluctuated with a positive velocity (highest) when the longitudinal velocity was at its minimum. The highest negative lateral velocity occurred at the deepest location in the main channel as shown in **Figure 6.28**.

During this duration the water level in the main channel was about to flood as shown in **Figure 6.12.** Therefore due to the minimum flow resistance at the centre of the main channel compared to the banks, the velocity was found to be higher at the centre. For *Case 5*, the longitudinal velocity was dominant over the entire section. While for *Case 1* at time T = 63 hours, the velocity distribution was observed to be similar to the velocity distribution at time T = 57 hours. The only obvious difference for *Case 1* was that the velocity crosses each other at the highest positive velocity at time T = 57 hours. For *Case 5* at time T = 57 hours, the velocity distribution was similar to the velocity at time T = 63 hours except that this velocity was much higher as shown in **Figure 6.29.**

The shapes and the cross-sections of the main channel were the main factor that influenced the water levels and the velocity distributions as discussed above. This could be observed from the comparison made between *Case 1* and *Case 5*. Although they have the same main channel configuration but they gave a different velocity profiles.

- **Velocities for *Case 2 vs Case 6***

A similar observation was observed for *Case 2* and *Case* 6, where the velocity distribution followed the same pattern to the previous case as discussed earlier. Tthe shapes and configurations of the estuary were the major factors that would influence the velocity distribution in an estuary.

In conclusion, the estuary shape and the presence of floodplains have some major effects on the flow structure in the main channel. This floodplain acted like storage along the main channel. During flooding, the saline water would flow and stored onto the floodplains. While during ebbing, it would then discharge the saline water into the main channel and thus affected the water depth as well as the velocity distribution in the main channel. A study by Wu *et al.* (2000) had shown that the presence of mangrove swamp had significantly retarded the water flow in the main channel at the Merbok Estuary in Malaysia.

6.6 Results from Salinity Simulation

For the salinity simulations, a 24 tidal cycles were taken into consideration. This was to ensure that the salinity profile had adequately developed in the domain. In this simulation, the water level was initially set at high water tide which was similar to the imposed tidal data at the outlet boundary. The domain was initially assumed to be full with saline water and fresh water was introduced at the inlet. The fresh water would then push the saline water downstream toward the estuary. The salinity reading was initially set to 34 ppt. A single and multiple Manning roughness coefficient was used in the simulation . The salinity was based on the data obtained from the field study while the *'n'* value was based on the commonly value used in river modelling studies. Floodplains effect were taken into consideration in this simulation. The Method of Characteristics and Centered Semi Implicit Scheme + Streamline Upwind Petrov-Galerkin advection scheme was used as an advective scheme. While Elder's turbulence model was used in this simulation.

6.6.1 Predicted Salinity Distributions and Flow Mechanisms

Simulations were done to determine the salinity distribution. The salinity result from the numerical modelling was compared with the measured salinity during spring tides (from 24.6.98 to 26.6.98) along the Sedeli Estuary. **Figure 6.30** shows the simulated and actual salinity profiles for the three days. The actual salinity on the 24.6.98 showed that there was under predicted by about 60% (15 ppt) at the 15th km away from the estuary mouth. A similar pattern of salinity distribution was observed on the 25.6.98. The differences between the simulated and the actual salinity varied by about 40% (10 ppt). On the 26.6.98, the simulation and the actual salinity was under predicted except at the 15th km. After this location, the simulated salinity was under predicted to a distance of about 26th km after which the salinity was significantly diminished.

Figure 6.31 shows the salinity profile at the highest flooding and lowest ebbing along the Sedeli Estuary from 24.6.98 to 26.6.98. The results showed that the saline water (salinity of 0.43 ppt) moved to a distance of 28.13 km upstream of the estuary mouth. During ebbing, the salinity at this location was reduced to 0 ppt. The salinity difference was found to occur between the 4th km up to the 18th km. The maximum salinity

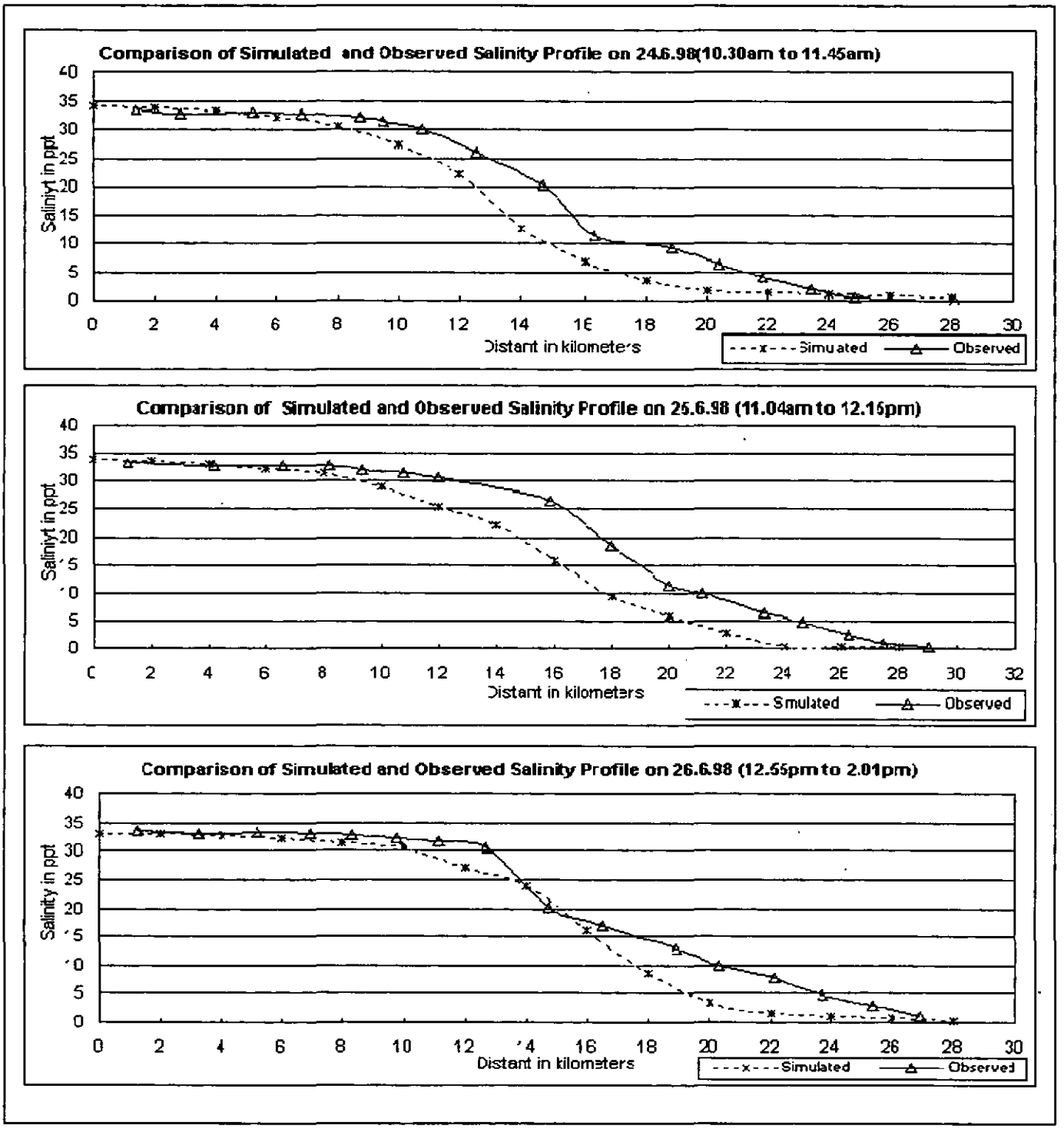

Figure 6.30 - Comparison of Simulated and Actual Salinity Profile at Sedeli Estuary for 24.6.98, 25.6.98 and 26.6.98 During High Water Tide

a difference occurred at the 9thkm with a reading of 9 ppt (36%). The flow of saline water from the floodplains into the main channel was retarded by the presence of vegetation on the floodplains. This would result in higher traces of salinity during ebbing. Several studies have shown that the presence of vegetation on the floodplains have significantly effects the flow structures in the main channel, among them were (Wu, Falconer *et al.* (2001)), (Furukawa, Wolanski *et al.* (1997)), (Nepf, Mugnier *et al.* (1997)) and (Fathi-Maghadam and Kouwen (1997)). They concluded that the presence of different vegetations would affect the flow structures differently. The drag force from these vegetations would retard the flow on the floodplain as well as in the main channel. In this study, a single value of Manning's roughness coefficient of n=0.012 was used for the vegetation on the floodplains. This was to show that the presence of vegetation on the floodplains would affect the velocity distribution in the main channel

6.7 Flows Through Mangrove Swamp

Two additional simulations were carried out to determine the flow structure and the salinity distribution with the presence of mangrove swamp on the floodplains. For the first case, a single Manning's roughness coefficients of $n = 0.012$ was used for main channel and floodplains. While for the second case, the Manning's roughness coefficients used was $n = 0.03$ for main channel and $n = 0.1$ for floodplains. The floodplains was covered with mangrove swamp on both sides of the main channel. Analysis was carried out at two locations along the main channel during flooding (time of simulation at 51th hours) and ebbing (time of simulation at 59th hours) conditions. The first location was taken at the straight section of the main channel, which was about 4.25 km away from the estuary mouth. While the second location taken was at the apex of the meandering section which was about 3.25 km away from estuary mouth as shown in **Figure 5.2** in **Chapter 5.** The second simulation was analysis at a distance of 20.12km from the estuary mouth at the straight section, which was at the measured salinity location. Comparison was made between the simulation result and the actual salinity data. **Figure 6.32 (a)** and **(b)** shows the water level, tidal and the velocity profile for a period of 65 hours of simulation time at the apex section. Single and multiple Manning's coefficients was used to analyse the

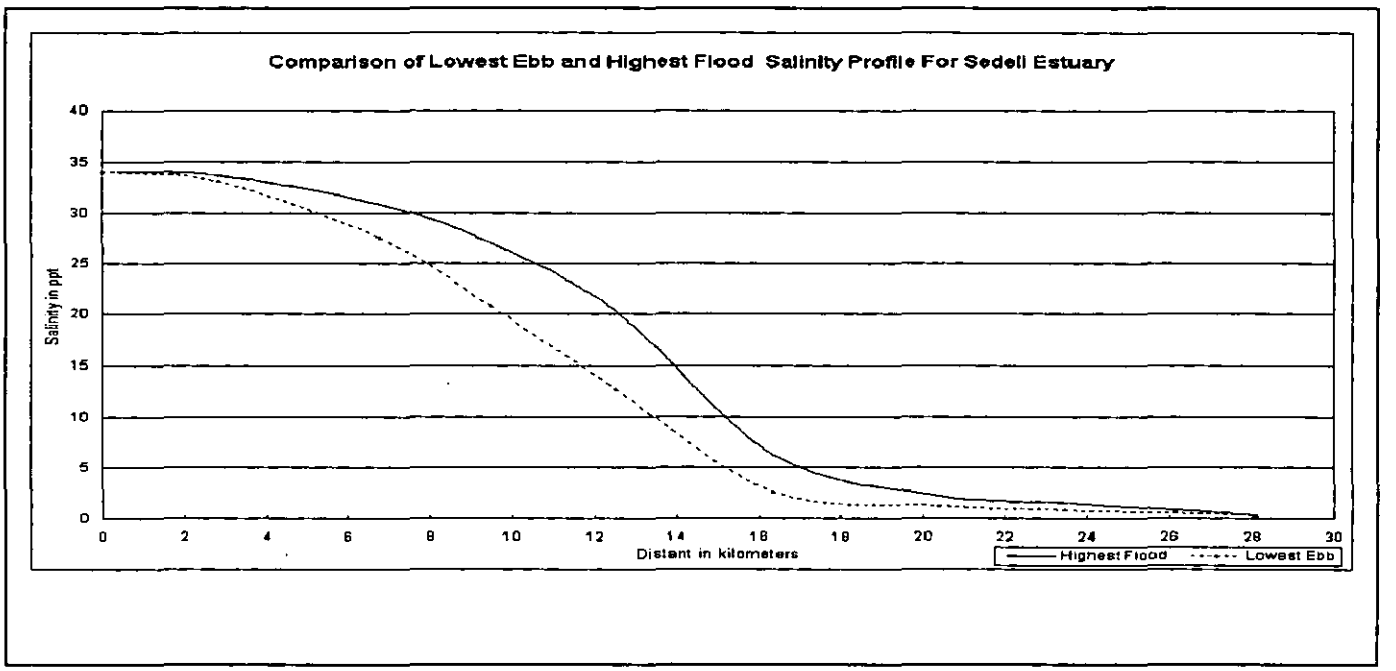

Figure 6.31 - Comparison of Highest Flood and Lowest Ebb Salinity Profile for Sedeli Estuary

velocity distribution and water level in the main channel and on the floodplains.

6.7.1 Flow Velocities at Apex of Two-Stage Meandering Section for Multiple and Single Manning's Values

The velocity in the channel and on the floodplains varied between -0.06m/s to 0.04m/s and between -0.03m/s to 0.02m/s (the negative sign showed that the velocity was flowing in the opposite direction) respectively. Both the velocities appeared to be paralleled to each other and varied according to the tidal and the water level. Similarly **Figure 6.32 (b)** shows the tidal level, the water level and the velocity profile in the main channel and on the floodplain using single Manning's coefficient at the apex. In this case the velocity in the main channel varied between -0.08 m/s to 0.15 m/s while on the floodplain it varied from -0.65 m/s to 0.02 m/s.

- **Main Channel Velocity**

Figure **6.32 (a)** and **(b)** shows the velocity profiles in the main channel. During high water at time T = 51hours, the velocity at the centre of the main channel was 0.02m/s

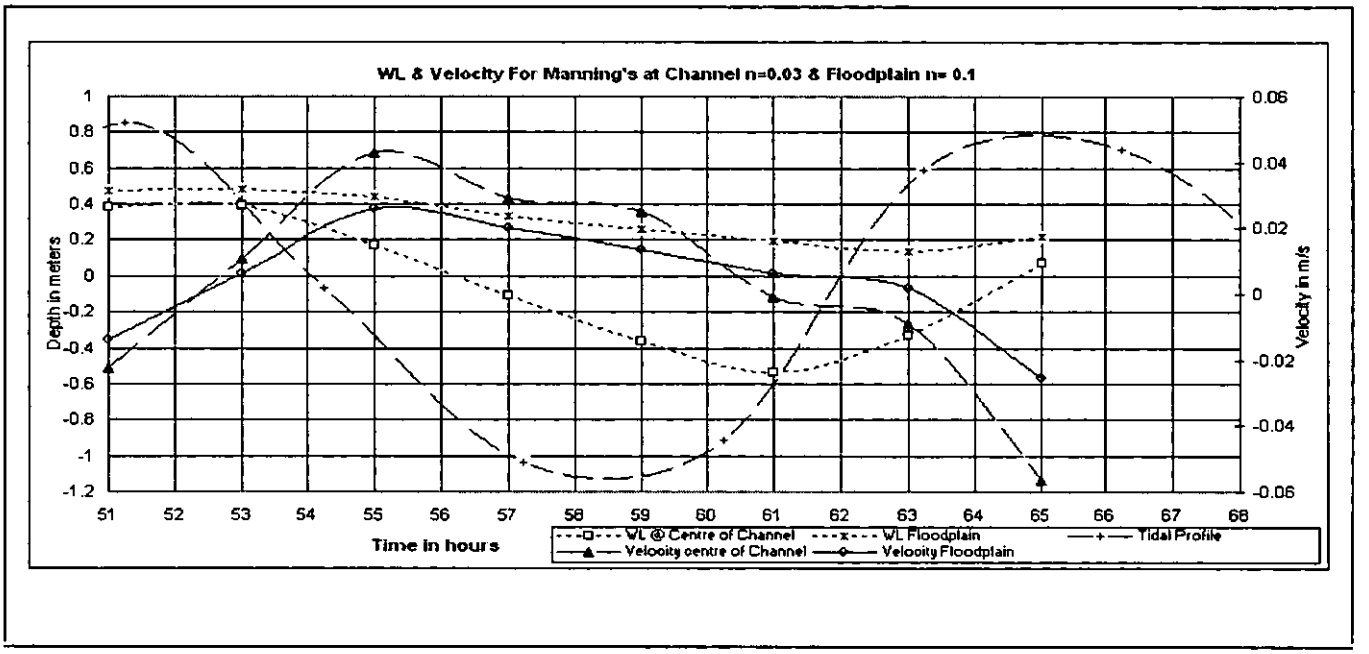

Figure 6.32(a) - Water Level and Velocity Profile Main Channel and Floodplain Having Different Manning's Values at Apex

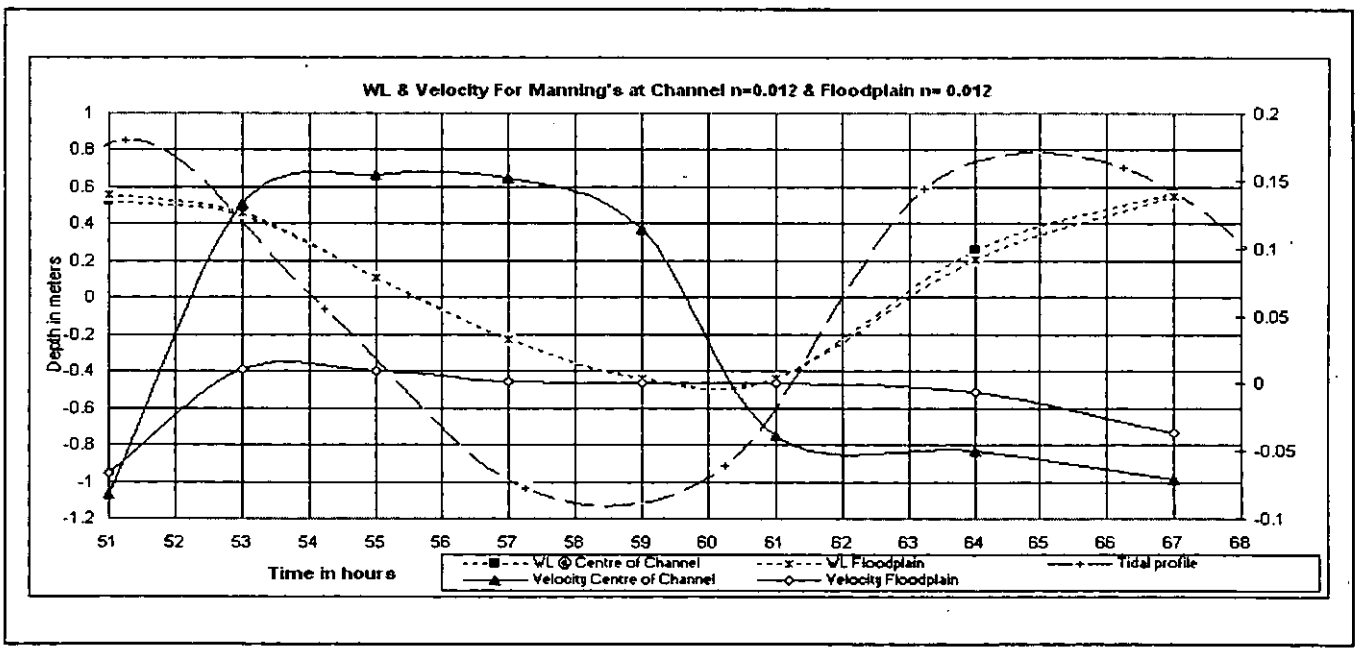

Figure 6.32(b) - Water Level and Velocity Profile Main Channel and Floodplain Having the Same Manning's Values at Apex

as shown in **Figure 6.32 (a)** and -0.08m/s as shown in **Figure 6.32 (b)**. While during low water tide at time T = 59 hours the velocity was 0.03m/s as shown in **Figure 6.32 (a)** and 0.13 m/s as shown in **Figure 6.32 (b)**. The difference in flow velocity at the centre of the main channel for multiple and single Manning's was about 75%, with the later showed a higher reading during the high water tide. Similarly, during low water tide the difference in velocity was 77.0% where single Manning's had a higher velocity due to the minimum drag force occurred between the floodplain and the main channel. The water on the floodplain for single Manning's decreased faster compared to multiple Manning's. In multiple Manning's, due to the greater drag force formed on the floodplain, the flow was slower compared to the flow in the main channel. This would create a higher resistance of flow at the interface between the floodplain and the main channel.

- **Floodplain Velocity**

A similar analysis was investigated to determine the flow characteristics on the floodplains for both single and multiple Manning's. During high water tide at time T = 51 hours, the velocity on the floodplain was -0.4 m/s (**Figure 6.32 (a)**) and -0.7 m/s (**Figure 6.32 (b)**) while during low water tide at time T = 59 hours the velocity was 0.2m/s (**Figure 6.32 (a)**) and -0.4m/s (**Figure 6.32 (b)**). The flow velocity for multiple Manning's was 86.0% lower compared to single Manning's. From the result, for multiple Manning's there was a disparity in the velocity profile on the floodplain and the main channel which was not so significant compared to single Manning's. The velocity on the floodplain for multiple Manning had was higher then single Manning and vice versa for the velocity in the main channel. The floodplains would influence the velocity distribution in the main channel.

6.7.2 Water Levels at Apex of Meandering Section for Multiple and Single Manning's Values

Comparison was also made on the water levels at the apex and straight sections. Multiple and single Manning's values were used in the simulation. This was was to determine the effect of Manning's on the water levels in the main channel and on the floodplains.

- **Water Level in the Main Channel**

During high water tide at time T = 51 hours, the water levels in the main channel for multiple Manning's was 0.4m while for single Manning's the water level was 0.55m as shown in **Figure 6.32(a)** and **(b).** The water level in the main channel for single Manning's was 37.5% higher compared to multiple Manning's. At this time, the flow of water from the river channel onto the floodplain was retarded due to the presence of mangrove swamps and the water on the banks. The formation of high water tide for the multiple Manning's was delay compared to the single Manning's. This was due to the very wide floodplains where it contained water for most of the time. For single Manning's, the water level on the floodplain and in the main channel of the river had the same elevation. The water level for both the floodplain and main channel would rise at the same time during high water tide. There was not resistance to retard the flow between the main channel and the floodplains. While during low water tide at time T = 59 hours, the water level for multiple Manning's was -0.35m and for single Manning's the level was -0.42m. At this instance, the inflow of water from the floodplain into the main channel was delayed due to the higher resistance from the mangrove on the floodplains which would affected the water level for multiple Manning's. While for the single Manning's the decreased of water level was much faster since there was less resistance on the floodplain. It was observed that during low water tide, the water levels for multiple Manning's was 20.0% lower compared to single Manning's

- **Water Level on the Floodplain**

Similar analysis was done on the floodplain to determine the effects of the roughness coefficient on the water levels. During high water tide at time T = 51 hours, the water level for multiple Manning's and single Manning's was 0.5m and 0.58m respectively. There was a difference of water level of about 14.0% between them. The water level for multiple Manning's was delayed due to the higher resistance of flow onto the floodplain as discussed earlier. During low water tide at time T = 59 hours, the water level for multiple Manning's was 0.28m while for the single Manning's the level was -0.42m. There was no water on the floodplain for the single Manning's. The negative sign was to indicate that both the water levels decreased simultaneously for the floodplain and the

main channel for single Manning's.

6.7.3 Comparison of Flow Velocity and Water Level at the Apex and the Straight Sections

Analysis was done to determine the velocity profile and the water level flow characteristic at the same location at the apex and the straight sections of the river. Similar Manning's coefficients was used for this analysis.

- **Flow Velocity**

Figure 6.33(a), (b) and **Figure 6.34 (a), (b)** shows the lateral and longitudinal velocity at the apex and the straight sections during high water tide at time T = 51 hours (flooding) and T = 59 hours (ebbing) respectively. The longitudinal velocity was dominant at time T = 51 hours at the apex. The velocity in the main channel and on the floodplain was -0.03m/s was -0.01m/s respectively. At the straight section, the velocity in the main channel was -0.05m/s while on the floodplain it was zero as shown in **Figure 6.33(b)**. The lateral velocity on the floodplains for both cases was less than the velocity in the main channel. Similarly **Figure 6.34 (a)** and **(b),** shows the velocity for both sections at time T = 59 hours. The longitudinal velocity at the apex was -0.01m/s and on the floodplains, it varied from -0.01m/s to zero as shown in **Figure 6.34(a)**. **Figure 6.34(b)** shows the longitudinal and lateral velocity at the straight section, which was -0.05 m/s and zero respectively. From the figures, the flow velocity in the main channel at the straight section was higher compared to the apex section. At the apex, both velocities have the same velocity profile to the longitudinal velocity. While at the straight section, the lateral velocity was consistently zero throughout the cross-section.

- **Water Level**

Figure 6.35 shows the water level at the apex and the straight section at time T = 51 hours. The water level at the centre of main channel for the apex section was 0.5m lower than the water level on the floodplain. While for the straight section the water level throughout the cross-section was the same for the main channel and the floodplain. **Figure 6.36** shows the comparison made on the water level at time T = 59 hours which was at low

water. A similar pattern of water level was observed at time T=51 hours. There was a greater interaction of the water level between the floodplain and the main channel flow at the apex section.

6.7.4 Salinity Distribution for Multiple and Single Manning's Values on Vegetated Floodplain

Salinity distribution for multiple and single Manning's roughness coefficient was used to simulate the flow on vegetated floodplains at the straight section of the river which was situated at about 20.12km upstream of the estuary mouth. The chosen location was situated at same location where actual measurement was done. This analysis was to determine the effects of roughness coefficient on the salinity distribution in the main channel.

- **Multiple Manning's Roughness Coefficients**

Figure 6.37 shows the result for the salinity distribution for multiple Manning's. During high water tide at time T = 51 hours, the salinity distribution on the floodplain and in the main channel was 4.25 ppt and 4.0 ppt respectively. **Figure 6.37** also shows that the salinity was decreasing as the water level decreased. The salinity on the floodplain decreased slower than in the main channel. During this condition, the salinity concentration on the floodplain was higher than in the main channel. As the water level in the main channel increase, the salinity in the main channel would also increase. The increment was faster compared to the floodplain as shown at time T = 63 hours and T = 65 hours. At time T = 65 hours which was during high water tide, the salinity in the main channel and floodplain was 4.25ppt and 3.0ppt respectively

The choice of Manning's roughness coefficient had a great influenced on the flow velocity, the water level and the salinity distribution in the main channel as well as on the floodplain. During ebbing, the saline water on the floodplain would flow slowly into the main channel. This was due to the higher drag force on the floodplain. As a result, the salinity distribution on the floodplain was higher than in the main channel. **Figure 37** shows that during flooding at time T=51 hour to T= 65 hour, the saline water from the main channel would flow slowly onto the floodplain. The presence of very wide

floodplains also contributed to this phenomenon. The equilibrium condition would reached for the salinity to be balanced between the floodplain and the main channel.

- **Single Manning's Roughness Coefficient**

The result from single Manning's value was shown in **Figure 6.38.** Analysis was done at time T = 51 hours during high water tide. The salinity on the floodplain and in the main channel was 4.5ppt throughout the cross section of the river. As the water level decreased, the salinity on the floodplain and the main channel would also decreased. The salinity decreased faster in the main channel compared to the floodplains. One distinct observation could be observed from this analysis was that the decreased in salinity on the floodplain for single Manning's was faster compared to multiple Manning's as discussed in the earlier. As the water level in the main channel increase, the salinity in the main channel would also increase compared to the floodplain which was emptied at time T=63 hours. The salinity distribution would be the same for both the floodplain and in the main channel during high water tide at time T= 63 hours. At this condition, the salinity during flooding was the same for the floodplain and the main channel. Similar to single Manning's, as the water level decreased, the salinity on the floodplain was higher than in the main channel. The decreased in salinity was faster compared to multiple Manning's. The choice of Manning's coefficient was an importance factor for the main channel and the floodplain.

The result from the simulated salinity was compared with the actual data during high water tide. This salinity data was taken at the same location as the salinity station at the location as mentioned earlier (at section 13 in **Figure 5.2**). A salinity for multiple Manning's at high water tide was 4.0 ppt while the reading obtained from actual data was 4.2 ppt at time T = 51 hours as shown in **Figure 6.37** and on the 25.6.98 at time T = 1300 hours as shown in **Figure 5.10.** This value wouldl gradually reduced to 0.2 ppt at time T= 61 hours while for the actual data the salinity reading at this interval was it was reduced to 0.0 ppt at low water tide. The salinity started to increase as the water level increase. While for the single Manning's, the low water tide occurred at time T= 56 hour. The salinity for single Manning's at this time was 4.0 ppt and for multiple Manning's the

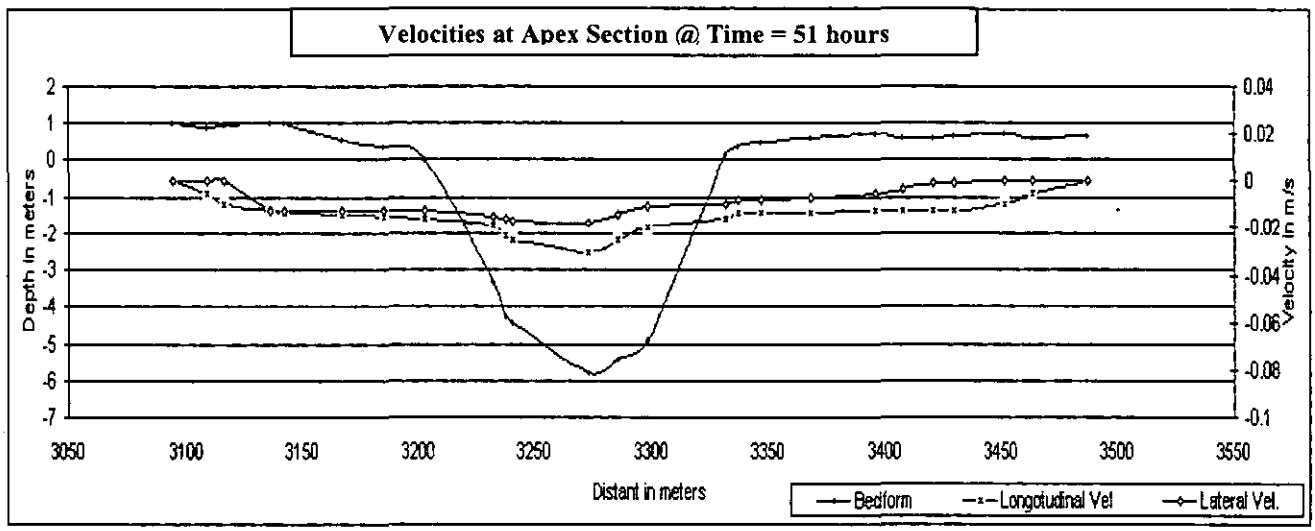

(a) Velocities at Apex Section at Time T= 51hrs

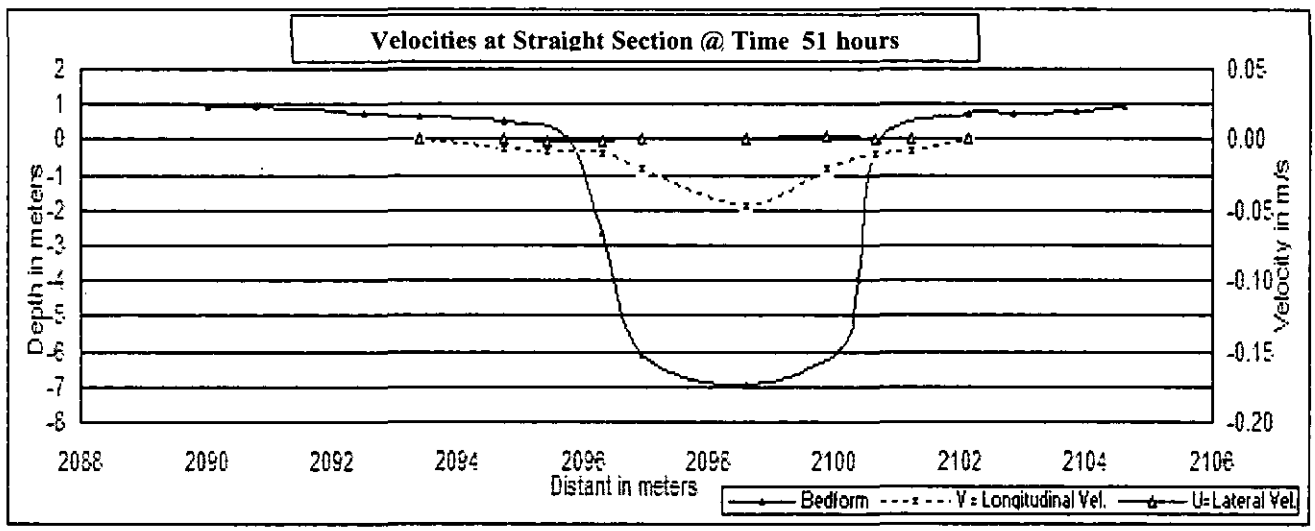

(b)Velocities at Straight Section at Time T= 51hrs

Figure 6.33 – Velocities at Apex and Straight Section for n = 0.03 Channel and n = 0.1 Floodplain at T= 51 Hours (Flooding)

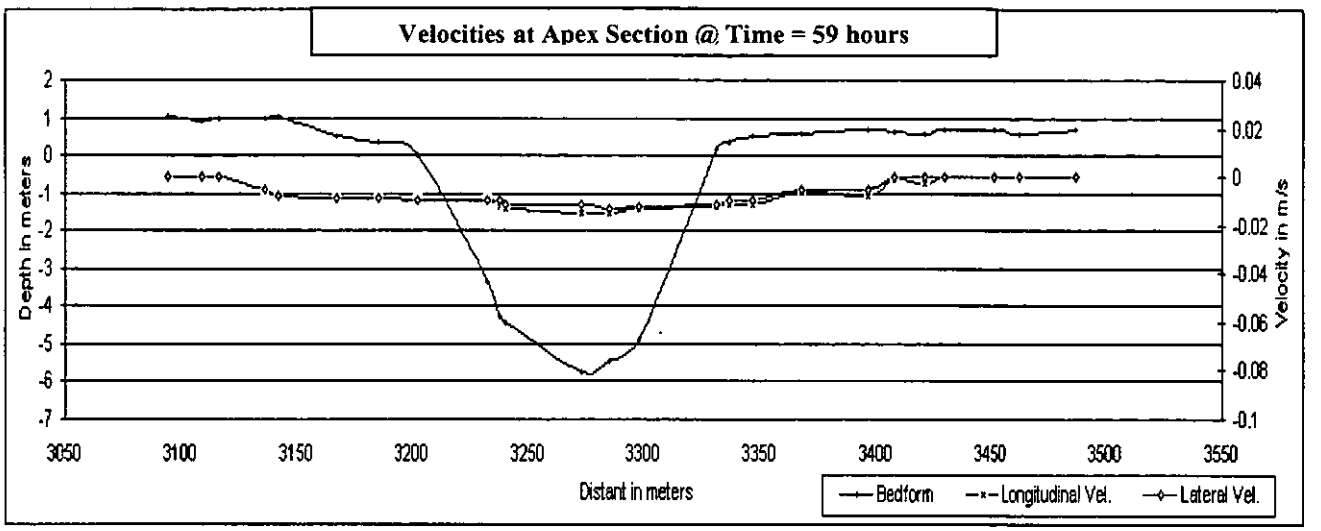

(a) Velocities at Apex Section at Time T=59hrs

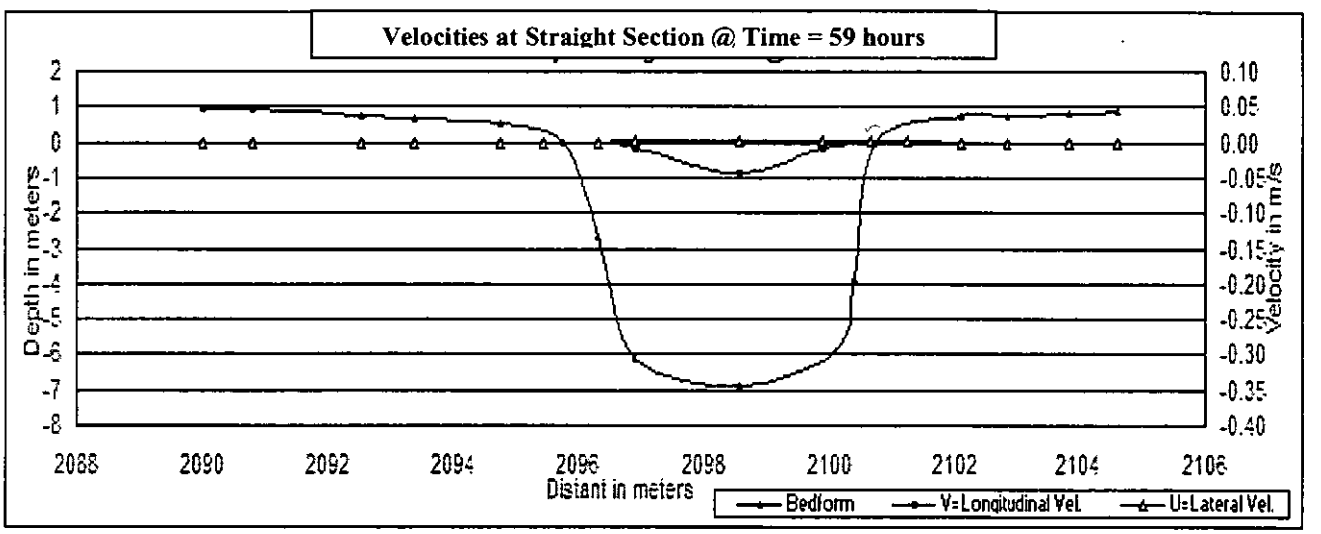

(b) Velocities at Straight Section at Time T=59hrs

Figure 6.34 – Velocities at Apex and Straight Section for n = 0.03 Channel and n = 0.1 Floodplain at T= 59 Hours (Ebbing)

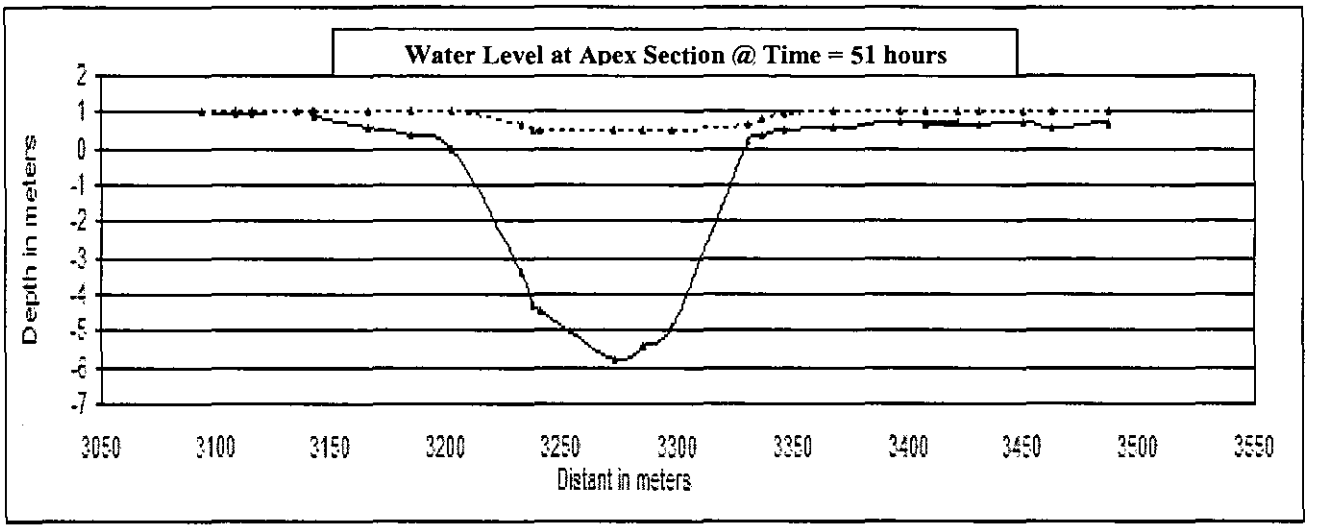

(a) Water Level at Apex Section at Time T = 51Hours

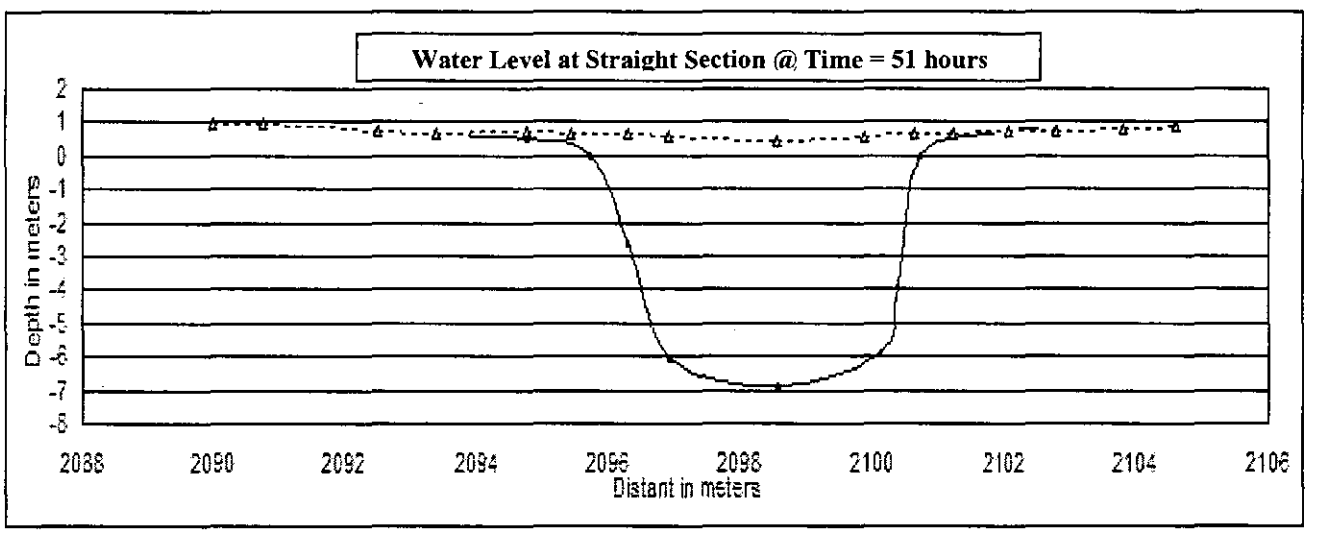

(b) Water Level at Straight Section at Time T= 51Hours

Figure 6.35 – Water Levels at Apex and Straight Section for n = 0.03 Channel and n = 0.1 Floodplain at T = 51 Hours (Flooding)

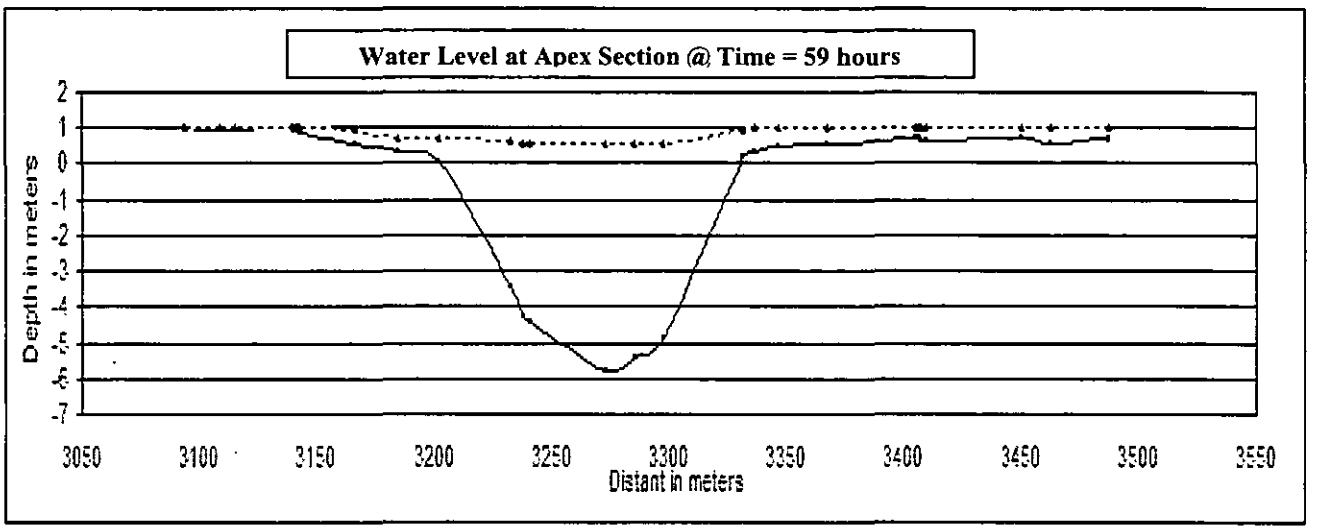

(a) Water Level at Apex Section at Time T= 59hrs

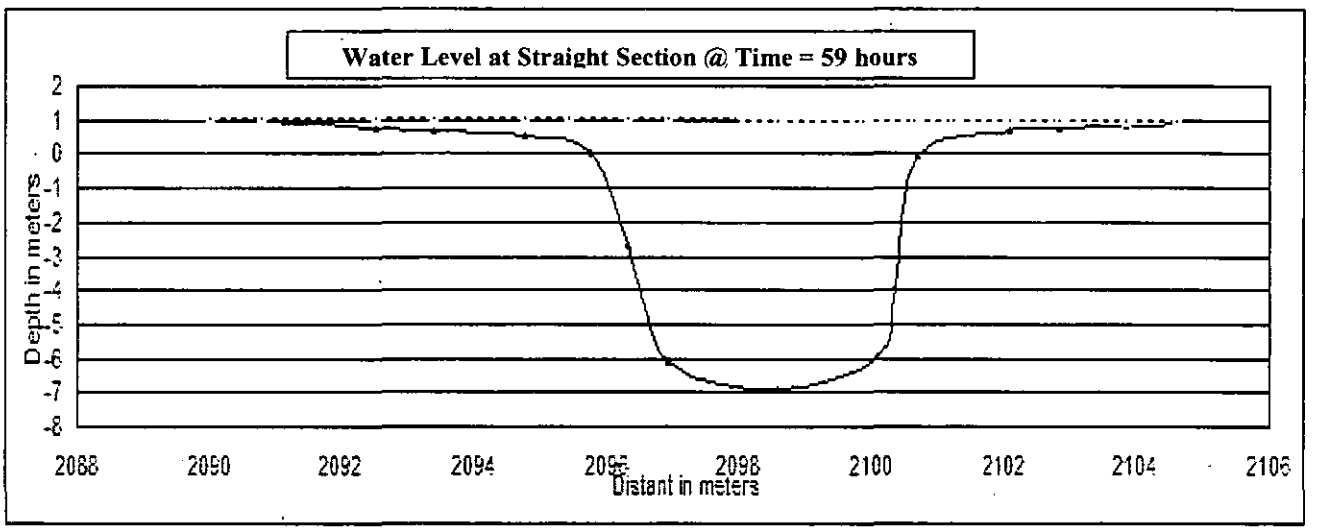

(b) Water Level at Straight Section at Time T= 59hrs

Figure 6.36 – Water Levels at Apex and Straight Section for n = 0.03 Channel and n = 0.1 Floodplain at T = 59 Hours (Ebbing)

reading was 2.0ppt. While for the reading actual data was 1.0ppt. From the results, multiple Manning's had some similarities to the actual data compared to single Manning's.

Figure 6.39 shows the salinity distribution for actual salinity data, multiple and single Manning's taken at the *second location*. During high water tide at time T=51hours, single Manning's had a reading of 4.5ppt whereas for multiple Manning's and actual data had reading of 4.2 ppt and 4.0 ppt respectively. As the tidal decreased at time T=59 hours, single Manning's showed a zero salinity while for multiple Manning's there was traces of salinity reading of 0.4 ppt. This was due to a higher resistance on the floodplain, where the inflow of water from the floodplain into the main channel was delayed and this would result on salinity residue found during low water tide.

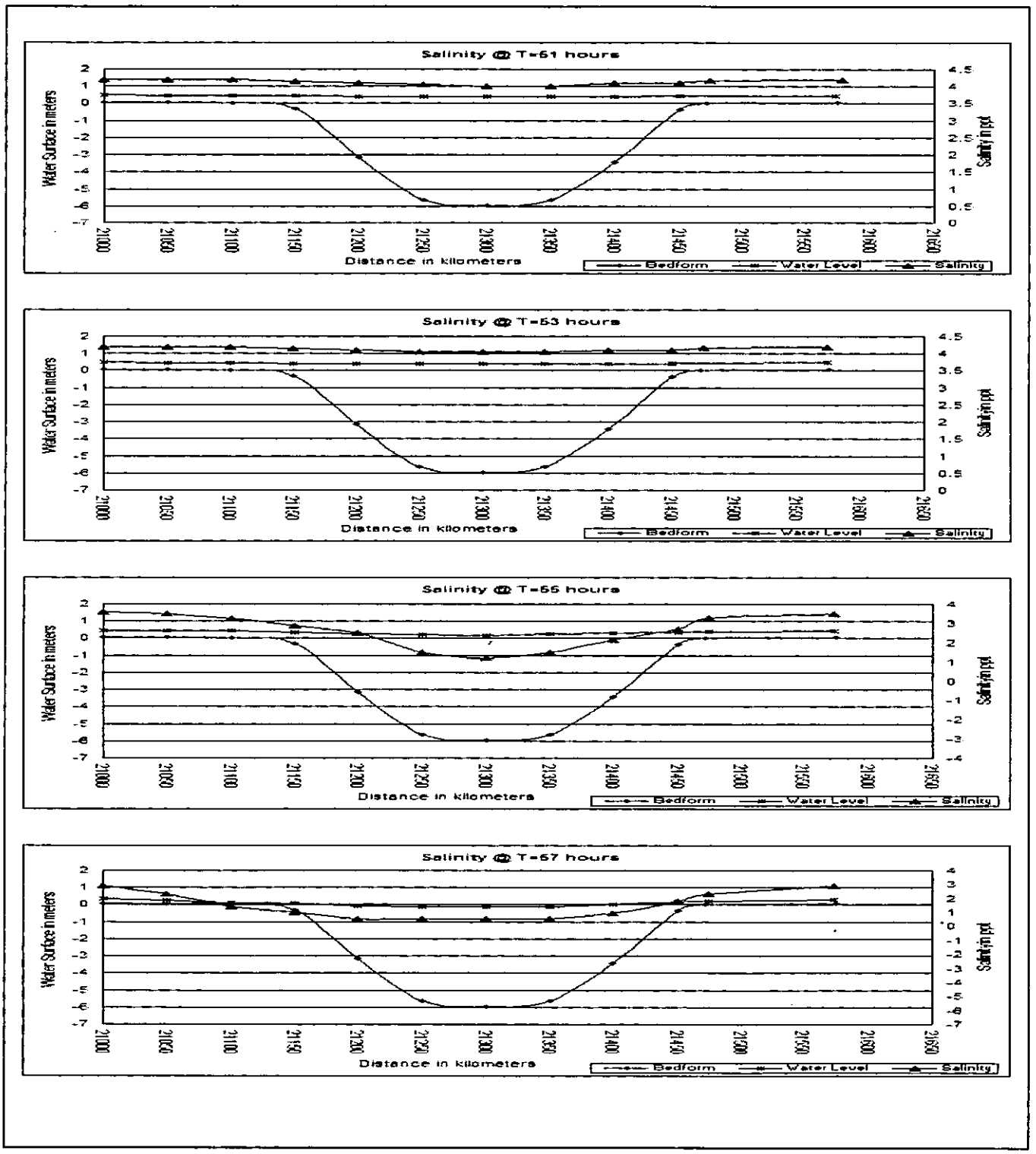

Figure 6.37 – Salinity Distribution at Straight Section for Main Channel (n= 0.03) and Floodplain (n = 0.1) at distant of 20.12km from the estuary mouth during high water tide (cont)

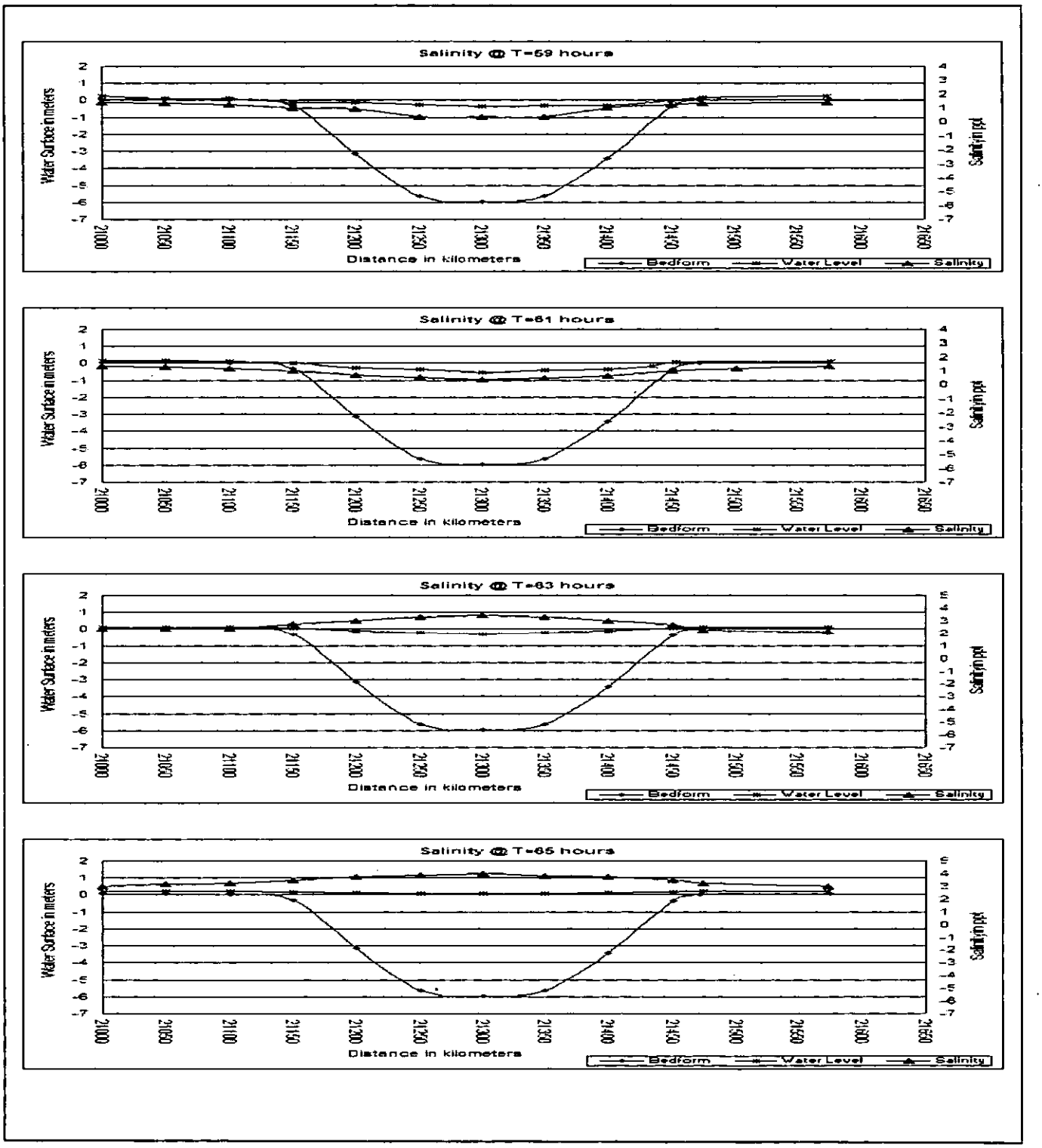

Figure 6.37 – Salinity Distribution at Straight Section for Main Channel (n = 0.03) and Floodplain (n = 0.1) at distant of 20.2km from the estuary mouth during high water tide

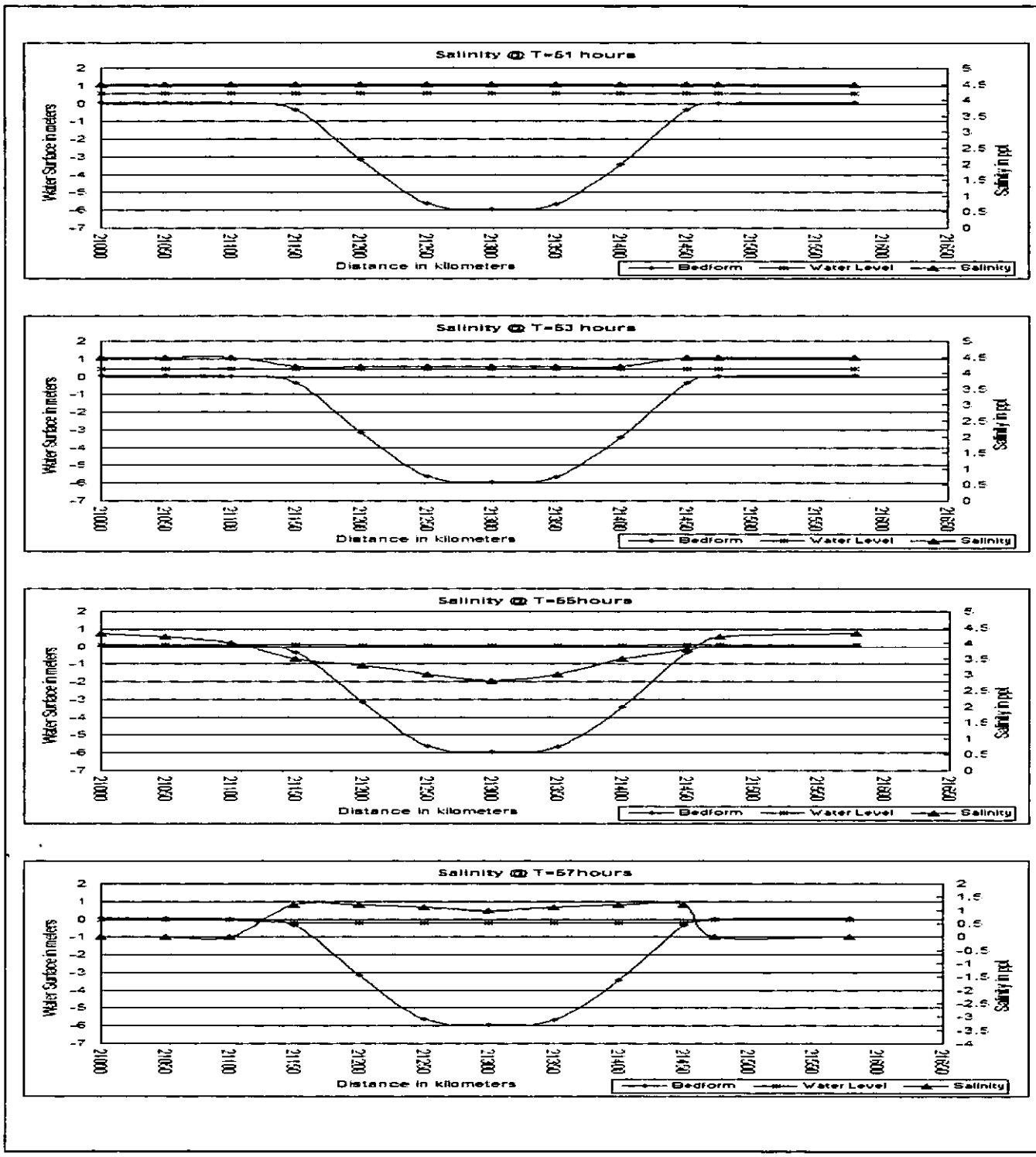

Figure 6.38 – Salinity Distribution at Straight Section for Main Channel (n = 0.012) and Floodplain (n = 0.012) at distant of 20.2km from the estuary mouth during high water tide(cont)

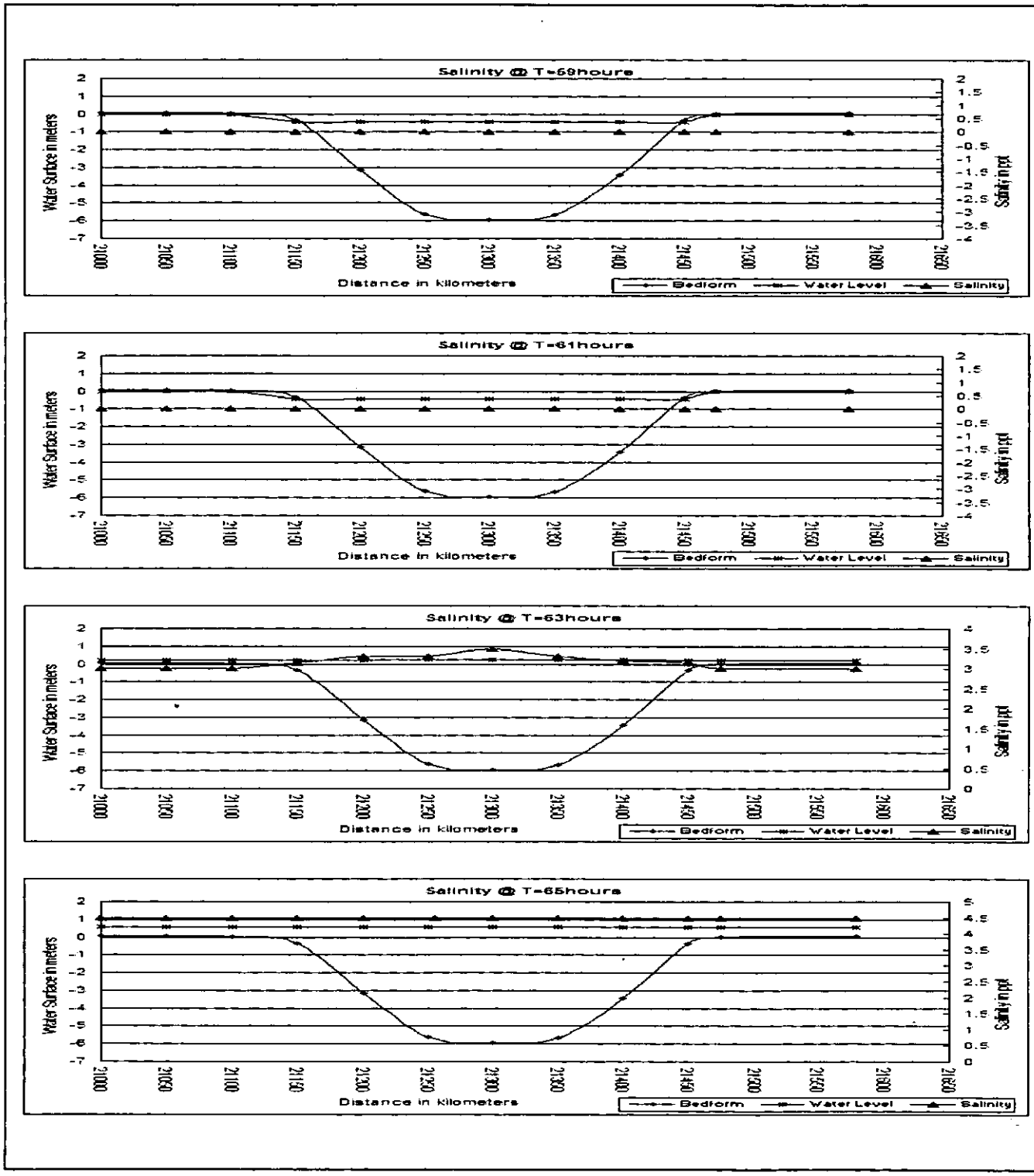

Figure 6.38 – Salinity Distribution at Straight Section for Main Channel (n = 0.012) and Floodplain (n = 0.012) at distant of 20.2km from the estuary mouth during high water tide

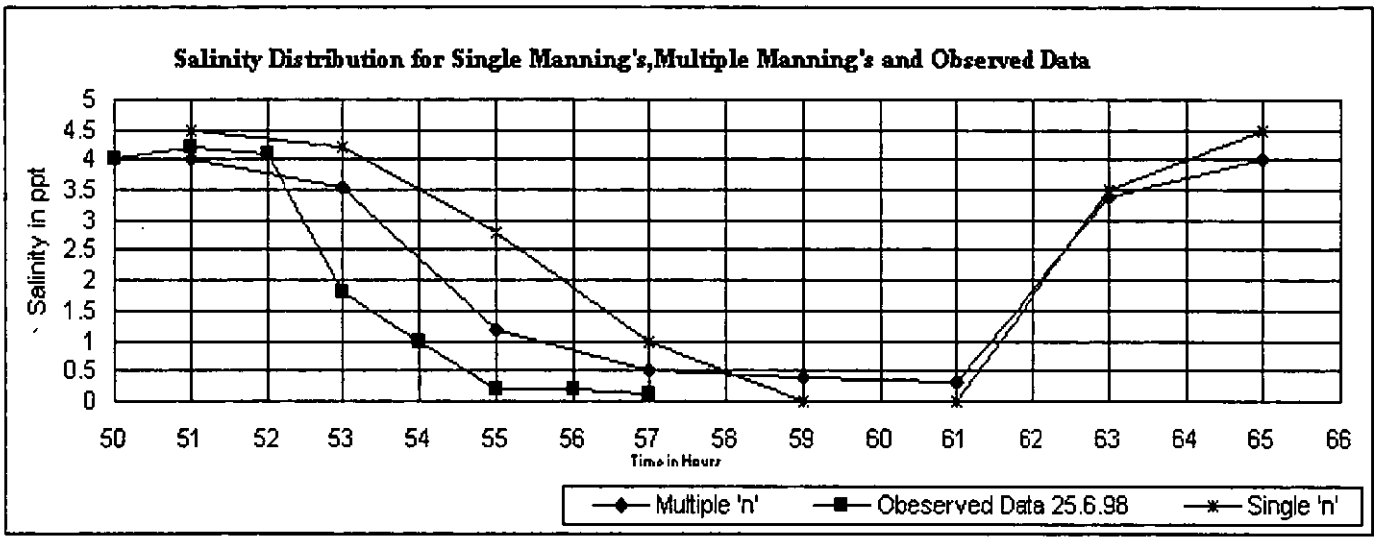

Figure 6.39 – Comparison of Salinity Distribution at location 2 for Single Manning's (n=0.012 For Channel and Floodplain), Multiple Manning's (n=0.03 for channel and n=0.1 for floodplain) and Actual Data on 25.6.98

6.8 Summary

This chapter discussed the application of a commercial Computational Fluid Dynamics (CFD) software TELEMAC–2D which was applied to the complex estuary to simulate the water levels, velocity profiles, flow profiles and salinity intrusions in rivers. Detailed development and application of an unsteady free-surface flow model to simulate estuarine and coastal water has been studied and analysed in this thesis. The model was based on the finite element method, which deployed an unstructured triangular mesh. This model was applied to predict the water levels, velocity and salinity distributions in a real estuary. Simulation was also done to determine the effects of vegetation on the flow structures using a single and a multiple Manning's roughness coefficients. A case study was investigated out for the Sedeli Estuary. The results obtained from the simulations were then compared to the actual data taken from the field site. Actual data for Sedeli estuary was analysed based on the water levels, the velocities, the salinity readings and the stratifications. In this chapter the effects of the following parameters were taken into consideration,

- Mesh density
- Manning's roughness coefficient *'n'*
- Advection schemes
- Turbulence models
- Shape factors effect on flow structures
- Effect of swamp on flow structures
- Flow structures at apex and straight sections

The modelling results showed that the overall accuracy was satisfactory compared to the actual data. Particularly, when considering a very wide domain area with a complex river configuration and bathymetry coupled with dynamics boundary condition prescribed in the simulation works.

- ***Mesh Density***

The mesh density was vitally important in obtaining an accurate solutions in the simulations. Two types of mesh densities were used in the simulation. They were Mesh A which contains 62,455 elements and Mesh B which contains 34,567 elements. In this study, the results showed that the errors in water level can varied from 19.7% to 69.8 % when using different mesh density. **Figure 6.3** shows that Mesh A gave a better results compared to Mesh B when *'n'* = 0.012. This could also be observed at *location 4,* where Mesh A showed it was very sensitive to the tidal effects. Similarly in **Figure 6.4,** when *'n'* = 0.03 the error ranged from 6.1% to 50%. Using Mesh A, the results gave a better resemblance to the actual data at Sedeli estuary as discussed. Therefore, Mesh A was used for all the simulation works.

- ***Manning's Roughness Coefficient 'n'***

As mentioned above the choice of Manning's roughness coefficient *'n'* had some major significant effects in obtaining an accurate solutions. In this study, the two *'n'* values used were 0.012 and 0.03. **Figure 6.1** and **Figure 6.2**, shows the water level when using a different values of *'n'*. The water level fluctuated significantly when $n = 0.03$ compared to $n = 0.012$. There was a significantly difference in water level at *location 3*,

where the reading varied from 5% to 10% when using Mesh A. While when using Mesh B, the different in water level at *location 3* varied from 10% to 30%. At *location 4,* it varied with a similar percentage. For this study, the value of *'n'* equal to 0.03 was used in all the simulation works.

- ***Advection Schemes***

Table 6.2 shows the ten (10) combinations of advection schemes that were used in this study. The main objective for this analysis was to calibrate and to investigate the sensitivity analysis of the model. Different advection schemes were assigned to the lateral velocity (u), the longitudinal velocity (v) and the water depth (h). **Figure 6.8** shows the water level using different advection schemes for Mesh A. There was a significant difference of water level results when using a different advection scheme and *'n'* values. **Figure 6.9** shows the water level using the Method of Characteristics (MOC) and the Centered Semi Implicit Scheme + the Streamline Upwind Petrov-Galerkin advection scheme when using Mesh A with Manning's n = 0.012 and n = 0.03. The Streamline Upwind Petrov-Galerkin was used to ensure that there would be a mass conservation and oscillation-free solution without any excessive mesh refinement or any additional artificial diffusivity. This would enable for complex with long floodplain topographies to be represented in a more efficient manner. **Figure 6.5** and **Figure 6.6** shows the water level when using the Method of Characteristics and the Conservative Scheme + the Streamline Upwind Petrov-Galerkin advection scheme with Mesh A and Mesh B. In this simulation the *'n'* used was equal to 0.012 and 0.03. From the figures, the Method of Characteristics and the Centered Semi Implicit Scheme + the Streamline Upwind Petrov-Galerkin advection scheme would give a better prediction of water levels which was relatively resemblance to the actual water levels.

- ***Turbulence Models***

In this study, two types of turbulence models were used in the simulation works. They were the Constant Eddy Viscosity and the Elder's Turbulence Model. **Figure 6.9** and **Figure 6.11** shows the water levels for the Constant Eddy Viscosity and the Elder's turbulent model together with the Method of Characteristics and the Centered Semi

Implicit Scheme + the Streamline Upwind Petrov-Galerkin advection scheme. While the Manning's value used was n = 0.03. The results were then compared with the actual data. **Figure 6.10** shows the summary of water levels for the Constant Eddy Viscosity, the Elder's model and the actual data. From the figures, the Elder's turbulence model showed a better resemblance to the actual data without any phase lagging. The difference in water levels varied from 5% to 10% from the actual data at time T = 51 hours. While for the Constant Eddy Viscosity, it showed that there was phase lagging and the water level varied from 25% to 50% at time T=51 hours. Therefore, in this study the Elder's Turbulence Models together with the Centered Semi Implicit Scheme + the Streamline Upwind Petrov-Galerkin gave a better prediction of water levels.

- ***Shape Factors***

Six types of shape layouts were used to determine the effect of shape factors on the flow structures as mentioned in **Table 6.3. Figure 6.12** to **Figure 6.17** shows the water level with different estuary configuration. The comparisons were made between the six cases based on the shape configurations and bed level for river with and without the floodplains. The first comparison was made between the actual model configuration with actual bed with swamp and without swamp *(Case1 and Case 5)*. The analysis results showed that the difference in water level varied from 66% to 33% (at time T = 63 hours at *location* 2 and *3* respectively). The water level for *Case* 1 was found to be dominant over *Case 5*. At the estuary mouth, the water levels for both cases were almost identical. The second comparison was between the flat bed with swamp and without swamp *(Case 2 and Case 6)*. Similarly, the difference in water levels varied from 38% to 5% (at time T = 63 hours at *location* 2 and *3* respectively). For this particular case, the result showed that the water level for *Case 2* was dominant over *Case 6*. A similar observation was also made at the *first location* as mentioned previously where the water level fluctuated according to the tidal movement. **Figure 6.14** and **Figure 6.15** shows the water level for the inclined *(Case 3)* and the rectangular shape with flat bed *(Case 4)*. The result showed that the water level for these two cases were found to be totally different from the other four cases mentioned earlier.

Analysis was also made on the velocity distributions for the six cases mentioned above. **Figure 6.24** and **Figure 6.25** shows the velocity distributions for all the cases at time T = 57 hours (flooding) and T = 63 hours (ebbing). The result showed that all the six cases have different velocity distributions. The lateral velocity was dominant over the longitudinal velocity. Therefore, it can be concluded that the shape factors have significantly affected the water levels and the velocity distributions in the main channel as well as on the floodplain.

Analysis was also made for the six cases in order to understand the effect of shape factor on the water levels in the main channel. **From Figure 6.12** to **Figure 6.17**, showed the straight estuary with tapered rectangular cross-section *(Case 4),* it had a minimum effect on the water levels at the three locations. The water level was found to be the same to each other. While for the estuary with the inclined bed and with swamp *(Case 3),* it had a highest effect on the water level as shown at the *first location*. Comparisons were also made for *Case 1* (actual bed with swamp) with *Case 5* (actual bed without swamp) and *Case 2* (flat bed with swamp) with *Case 6* (flat bed without swamp). This was done in order to study the effect of swamp on the water levels. **Figure 6.18** to **Figure 6.23** shows the water level at each location along the river. The results showed that *Case 1* had a water level which resemblance to the water level at the site. The effect of swamp had influenced the water levels especially at the *second* and *third* locations as shown in the figures.

- ***Effect of swamp on flow structures***

The presence of vegetation on the floodplain of a meandering two stage compound channel significantly affected the conveyance capacity during the overbank flows. The effects of these riparian vegetations on the flow structures have been investigated for a straight compound channel but little was known of their effect on a meandering two-stage compound channel. In this study, both floodplains were assumed to be vegetated with mangrove swamps. Two analyses were done by using a single and a multiple *'n'* values. For the first case, the channel and floodplains have the same *'n'* value (0.012) while for the second case the channel was assigned with n = 0.03 and the floodplain with n= 0.1. **Figure 6.32 (a)** and **(b)** shows the simulated results for both the cases. Similarly, the

reading was taken at time T = 51hours and T = 59 hours which happened to be at high and low water tide respectively.

Analysis was also carried out on the velocity and the water level for single and multiple *'n'* values. The velocity at the centre of the main channel for multiple *'n'* was 75% lower compared with the single *'n'* at high water tide. During low water tide, the reading showed that the velocity for the multiple *'n'* was 76.9% lower than the single *'n'* value. While on the floodplain, the velocity for the multiple *'n'* was 87.5% lower than single *'n'* at high water tide. At low water tide, there was no flow on the floodplains for the single *'n'* while some flow could be detected for the multiple 'n'. The reason was that for the multiple *'n'* there was a higher resistance to the flow due to the greater *'n'* value. This will result the flow velocity on the floodplain will be reduced and thus it became slower compared to the single *'n'* which had a less flow resistance.

The analysis on the water level showed that there were some differences between the two cases. The water level at the middle of the main channel for the single *'n'* was 27.3 % higher than the multiple *'n'* at high water tide. The single *'n'* was 23.6% higher than the multiple *'n'* at low water tide as shown in the figures. For the floodplain, the single *'n'* was 14% higher compared to multiple *'n'* at high water tide. Whereas at low water tide the result showed that the reading for single *'n'* was 60% higher than the multiple *'n'*. A similar argument can be concluded for the velocity profile as mentioned earlier for the water level.

A salinity distribution analysis was also done in order to determine their distribution in the main channel and on the floodplains. The location chosen was at the straight section of the river which was situated at a distance of about 21.0km away from the estuary mouth. This was to determine on how the roughness coefficients may affected the salinity distribution. The analysis was done based on the single and the multiple *'n'* values at high and low water tides with different time duration. The time used in this simulation was between 51 hours to 65 hours which formed one tidal cycle. At high water tide the salinity distribution was the same throughout the cross-section for the single *'n'*.

While for the multiple *'n'*, the salinity was found to be lower at the centre of the main channel compared to the floodplain.

- ***Flow structures at the apex and the straight sections***

As mentioned earlier, the overbank flow in a meandering two-stage compound channel with floodplains involved a number of complex hydraulic processes. A turbulent shear-mixing region formed at the main channel and the floodplain interface, resulting in the generation of secondary currents, bed-generated turbulence and free-surface effects. In this study an additional parameters namely the dynamic tidal and the variable river discharged was used which made the simulation to become more complicated. **Figure 6.33** to **Figure 6.36** shows the velocity distribution and water level at the apex and the straight sections using multiple *'n'*. In this simulation, the *'n'* values used were 0.03 for the channel and 0.1 for the vegetated floodplains. The apex and straight sections of the meandering two-stage compound channel which was situated at a distance of about 3.25km and 2.0km away from the estuary mouth respectively.

The velocity distribution at time T = 51 hours during high water tide, the difference in velocity at the apex section was 39%. The longitudinal velocity was dominant over the lateral velocity at the apex section. Both velocities were almost paralleled to each other in the main channel. While for straight section, the velocity difference was 90%. Similarly, the longitudinal velocity was dominant over the lateral velocity with the maximum velocity occurred at the centre of the main channel. The velocity at time T = 59 hours during ebbing, the difference in velocity distribution at the apex was 8% while at the straight section the difference was 50%. It was observed that at this location, the longitudinal velocity was dominant over the lateral velocity. A similar velocity distribution pattern was observed at the apex section during flooding and ebbing.

The difference of water level at the apex and the straight section was 20% at time T = 51 hours. The results showed that the water level at the apex was dominant over the straight section. While at time T=59 hours, the difference in water level between the straight and apex section was 50% where the straight section was dominant over the later. This velocity distribution patterns were almost the same for others flooding and ebbing.

conditions.

6.8.1 Comparison with Other Studies

The result from this study was compared with other researched works done by Rameshwaran (1997), Morvan (2000), Spooner (2003), Shukla (2006), and Ismail (2007). Comparisons were made on the flow in a meandering two-stage compound channel, the shape factors, the flow structures and with vegetated floodplains. Majority of these studies were done based on a laboratory work with steady state flow using either a physical model or computer software. None of the above researchers has carried out any works based on a real meandering two-stage compound channel with a complex bathymetry and vegetated floodplain using a dynamic boundary conditions. Comparisons were made based on the basic flow structures between this study with the above researchers for flow at the straight and the apex sections. Similarly a comparison was also made on the drag force created due to the concrete blocks placed along a meandering two-stage compound channel with various arrangements and block densities.

Rameshwaran (1997) had examined the conveyance behaviour for overall flow in a meandering two-stage compound channel. A laboratory experimental works were done at the Aberdeen University flume to determine the parameter that influenced the flow structures. He analysed ten parameters that would affects the flow structures for the inbank and the overbank flow. The aspect ratio, the cross-sectional shape and the bank side slope of the main channel and the system scale were among the parameters that were considered. In his work, the floodplains were considered smooth. He concluded that the two main factors that highly affected the conveyance flow in any meandering two-stage compound channel were the main channel sinuosity and the system scale.

Morvan (2001) had conducted his researched by applying a CFD code to his experimental data and some actual data from a natural river with floodplain. He used TELEMAC 3D and CFX to model the flow structures of a meandering two-stage compound channel at the Glasgow University flume, the UK-FCF and also some actual data collected from the Severn River and the Ribble River in the United Kingdom. He applied the result from his experimental data to the actual river simulation. The results

showed it was consistent with his experimental works. He acknowledged that, it was almost impossible to get a perfect result due to the complex geometry of the main channel cross-section and the natural bedform. This was due to the uncertainties in the selection of Manning's roughness coefficient *'n'* for the main channel and the floodplain which was significantly influenced the result of the simulations. In his works, the effect of riparian vegetation was not taken consideration due to the difficulties in determining a reasonable *'n'* values for the floodplains.

Spooner (2003) had studied the flow structures in a meandering two-stage compound channel with flat and natural bedform. He used the Loughborough University flume, the data from the UK-FCF and Muto's (1998) experimental data to determine the relationship of bedform with discharge capacity of the main channel. From his experimental works, he concluded that the natural bedform in the main channel had significantly reduced to about 30% of the discharge capacity compared to flat bedform during bankfull flow depth condition. The secondary flow circulations were found in the natural bed case, particularly at higher flow depth. These secondary circulations were caused by centrifugal force, where the flow entered the main channel from the floodplain and reversed the flow as it passes over the ridges in the natural bed.

Shukla (2006) had carried out a computer simulation in order to investigate the flow mechanisms for a three-dimensional flow in a compound meandering channel. He used TELEMAC-3D with a non-hydrostatic version to simulate the UK-CFC results and compared with Muto's (1998) experimental data from the Bradford University flume. In his works, he used a κ-ε turbulence model with several variable parameters such as the sinuosity layouts, the *'n'* parameters, the main channel aspect ratio, the relative depths, the model scales and the floodplain flow depths. The floodplain was considered to be smooth with the main channel side slope of 45°. Analyses were carried out to determine the flow structures at the apex and the cross-over region by predicting the turbulent kinetic energy (*TKE*). He concluded that the shear at the bankfull level was generated by the differential in velocity between the top and bottom layers of the flow. This shearing effect of the main channel flow and the velocity below the bankfull level was higher than the velocity of

flow above the bankfull level.

Ismail (2007) had studied the flow at the Loughborough University flume with a non-vegetated and vegetated floodplains for an overbank flow. The aimed of his study was to investigate on how the density and the arrangements of concrete blocks placed along the floodplain influenced the stage-discharge, the flow resistance, the sediment transport and the flow behaviours. He used concrete blocks with different layout arrangement as a model for rigid, unsubmerged vegetation placed on the floodplain adjacent to the meandering two-stage compound channel. These blocks would acted as vegetations in his experimental works. A steady flow condition was used with a constant inflow rate at the inlet was introduced. A similar Manning's roughness coefficient *'n'* was used for the main channel and the floodplains. The experimental results showed that the presence of energy losses due to the momentum exchange between the main channel and the floodplain as well as the different densities of the blocks on a floodplain. This would induce an additional flow resistance to the main channel flow, particularly for a shallow overbank flow. He also used TELEMAC 3D to verify his experimental results. From the analysis, he concluded that for the non-vegetated floodplains, the shearing flow in the main channel would occur as the water from the floodplain plunged into and over the main channel that will influence the mean and turbulent flow structures, particularly at the cross-over region. While for the vegetated floodplain where blocks were placed along cross-over section, he concluded that the reduction of shearing effect on the main channel flow as the floodplain flow plunged into and over the main channel. This could be observed from the cross-sectional distributions of the streamwise velocity (U), lateral velocity (V), and secondary flow vectors. In addition, the vegetated floodplain along the apex bend region showed a small velocity gradient within region. However, a strong secondary flow at the cross-over section suggested that the flow interaction was quite similar to the non vegetation case at the cross-over section region.

As mentioned earlier, the main aimed of this research was to bridge the gap between the previous works done by other researchers. In this studied, TELEMAC 2D was used to model the flow structures in Sedeli River. The results obtained from this

studied was analysed against the previous work done by others in order to determine their differences.

6.8.2 Constraints and Limitations

The main difficulty in applying the CFD to the estuary lies in the representation of the geometry and topography. There was antinomy between the requirements of the TELEMAC code for a well-behaved geometry that can be determined mathematically and the nature of the estuary and river which was highly irregular. Additionally the quality of the topographical may affects the accuracy of the computations. Furthermore, the scale factors, shapes and roughness coefficients chosen may influenced the quality of results obtained from the simulations. Calibrations and roughness coefficients were the major constraints in the implementation of CFD for estuaries and rivers engineering. Roughness coefficient in particular was an uncertainty factors that would required indepth investigation, as the linked between the numerical calibration values and the knowledge gained from experimental work sometime remain poorly understood.

Regarding the accuracy of the models, calibration seem to be hindrance factor in the sense that different set of parameters might gave a similar flow features when comparing with sparse or limited actual data especially for free surface code such as TELEMAC. Indeed as models became more complex, then more parameters were needed to incorporate into them. Therefore it was difficult to perform a perfect calibration on the models, especially when dealing with high level of uncertainties associated with the lacked of data from the field study. This can be seen from the results in Chapter 5 where shape factors have a major influenced on the results obtained. Reasonably detailed information on the geometry and bathymetry of the river and estuary need to be obtained for model to gives a good and accurate result.

In general, CFD works reasonably well in estuary modelling eventhough there was some limitations in the calibration of the model. Furthermore, the evidence presented in this chapter showed that a reasonably good numerical prediction could be made and used for the salinity intrusion modelling in estuaries for civil and coastal engineering design.

Water levels and river discharge can be regulated upstream to control the effect of salinity intrusion in an estuary. In conclusion the model displayed a reasonably good results that was very similar to the observation data in Chapter 5.

Finally, one of the main difficulties for the application of CFD to estuary lies in the construction and discretisation of the domain. This implied that the technique was relatively expensive to be used. An accurate and lot of information were critically needed for modelling purposes in order to obtain good results. Sensitivity analysis and model parameters were also an important issue in any modelling works that need to be addressed before it can be used to solve problems on full scale basis. With free-surface models, sensitivity to these conditions may lead to multiple solutions.

CHAPTER 7

CONCLUSIONS AND RECOMMENDATIONS

7.0 Conclusions

This thesis has presented an investigation of a well-mixed estuarine dynamics associated with the Sedeli river flow using a commercial CFD code TELEMAC-2D. A total number of eighteen simulations were carried out. Six simulations were used to determine the shape factors using different shapes domain, meshes, and roughness coefficients. Ten simulations were used for the sensitivity analysis and model calibrations and one simulation was for salinity intrusion. Two additional simulations were also carried out with different roughness coefficient for the floodplain and the main channel and analysis was done at the apex and straight section of the river reach. As mentioned in Chapter 6, TELEMAC-2D was chosen due to the nature of the estuary and stratifications along the river was weak. A comparison between the salinity stratification of Sedeli with Rompin estuaries was also made to determine the similarities and the characteristics of both estuaries. This was due to the lack of measured data at Sedeli Estuary. **Figure 5.9** and **Figure 5.26** shows the salinity profiles at four locations at both Sedeli and Rompin estuaries respectively. For Sedeli Estuary, the observed data were obtained from 24.6.98 to 26.6.98 shows a very weak salinity stratification. **Figure 5.11** shows the measurements made from 24.6.98 to 26.6.98 along the Sedeli Estuary. The salinity stratification was found to be weak and it was justified to use TELEMAC-2D instead of TELEMAC-3D for this thesis. A detailed summary of the chapters was elaborated at the end of each chapter. The results from this simulations were also compared with previous works done by other researchers of a similar nature.

7.1 Model Constructions

Among the challenging problems with the numerical modelling for flow in estuary and river was the complexity of the geometry and its disruptive effects on the numerical

solution. TELEMAC code used unstructured grid offered a more flexibility and appeared to be more appropriate to model estuary and river flow. It also had the capability to refine resolution at the interface between dry and wet cells, which was an advantageous to allow for a better representation of the free surface.

Finite element techniques were mass conservative, and therefore grid resolution had impacts not only on the continuity equations but also on the spatial distribution of mass within the domain. In this thesis the used of fine grids would ensure mass conservation and mass-independent solution as shown in **Chapter 6**. Roughness coefficient did play an important role in obtaining accurate results. In this work the Manning's roughness coefficient '*n*' was determined by running a couple of simulations with different values and these results were compared with the observed data. The value of '*n*' was refined so that the water levels form the simulation matched the observed data. For this work, the '*n*' value used was 0.012 and 0.03 for all the simulations.

The choice of turbulent models was important to predict the results satisfactorily. In this thesis Elder's turbulent model is used together with the Streamline Upwind Petrov-Galerkin (SUPG) for depth (h) and velocities (u and v). From results obtained, the water levels and the salinity profiles gave a good agreement with the observation.

7.2 Scalability and Topography

Scalability and accuracy of topography also affect the quality of the simulation results. With limited field data such as the cross sections, flow measurements, and detailed survey of estuary and riverbeds bathymetry, interpolation had to be done between the known values of bed bathymetry. This may not reflect the real condition of the bed and domain layout. The simulation results might showed the real physical flows in the river and estuary. In **Chapter 6**, these problems were highlighted by simulating six different types of bed profiles together with and without the floodplains. The results showed that there were differences of water levels and velocities between them. A conclusion can be drawn from these simulation was that shape factors, quality and adequate field data was vital in obtaining

good results. Nevertheless with all the limitations, the numerical modelling still became the cheapest and the important tools in understanding the complex flow in rivers and estuaries.

7.3 Contribution of the Thesis

The application of CFD in the real world becomes a new challenge to researchers when dealing with rivers and floodplains that have complex structure and geometry, bed structures, type vegetations and boundary conditions. The questions of sensitivity parameters, grid scales, roughness of vegetations on the floodplains and many other uncertainties become issues that still debatable that needs to be addressed.

This thesis had established that TELEMAC-2D was used successfully to model estuary and river, which flows through vegetated floodplains, complex terrains and bed structures. The contributions of this thesis are as follow,

1) Bench Marking the use of CFD in an Environmental Applications

Many research previously was done experimentally in the laboratory with steady state flows using artificial vegetations on the floodplains. In this research, CFD code was apply to natural river conditions with dynamics boundary condition and complex configuration. There was not many studies carried out using the CFD or in laboratory under the above constraints. Due to this limitation, a very spare information was available for bench marking the flow structures under this condition. As quoted in many literatures, the flows in compound channel was fully turbulence over a wide range of space scales and unsteady in time. Simulations of such complexity were very complicated in nature. Therefore one contribution of this thesis is for bench marking the use of CFD in an environmental application under such a conditions so that future research could be based and compared with these results when using other CFD codes.

2) Roughness Coefficients for Flows Through Vegetation

Many rivers are influenced by instream and bank-side vegetation. Despite volume of research into bed roughness issues in rivers, it is surprising that that vegetation has been

given little attention. In this research, the mangrove swamps was the main vegetation on the floodplains. Manning's roughness coefficient of n=0.1 was used as a substitute of drag force. The choice of Manning's over the drag force was consistence with Bates *et al.* (2005). Where he suggested that hydraulic resistance could be lump together taken into consideration of the skin friction, form drag and the impact of acceleration and deceleration of flow. This was due to the complexity and uncertainties of vegetation on the floodplains. Furthermore, there were a limited number of researches done associated with the presence of mangrove swamp on the floodplains. The results from simulation of this research shows that the comparison of water levels matched the actual data was within the accuracy of 0.3% to 4.7% when using Manning's coefficient. This accuracy was within tolerable limit for practical purposes taken into consideration the scale of the domain and the complexity of the geometry. In this thesis is was determined that the used of Manning's roughness coefficient for mangrove swamps was able to produce a excellent results taken into consideration on the complexity of the domain and boundary conditions. This research had showed that the usage of Manning's roughness coefficient have made the simulation much easier without compromising the results

3) Flows Velocity and Between Floodplain and Main Channel

The flood inundation process for floodplains with vegetations involves the complex lateral transfer of mass and momentum from the river channel to the floodplains. There flows are strongly three-dimensional in nature. Away from the channel, shallow water flows become dominant that is strongly two-dimensional. These flows will move rapidly across the floodplains interacting strongly with the floodplain topography and vegetation. This can result in computational difficulties due to the large number of elements that play no part in the solution for much of the time until they were inundated. In this research, the river bed and the floodplains have variable contours that made the simulation more complex. From the analysis done at the apex and straight section of the river using different Manning's, the result showed there was a contrast different of velocity profile at both locations. This velocity between the main channel and the floodplains could deviated from 55% to 60% for multiple '*n*' values during high and low water. While for single '*n*' the difference was 25% during

high water at the apex section.

4) Advective Scheme and Turbulence Model

Advective scheme and turbulent model and were the two fundamental criteria to ensure the conservative of mass and momentum. The Method of Characteristics (MOC) and the Centered Semi Implicit Scheme + the Streamline Upwind Petrov-Galerkin scheme used in this research gave a good agreement with the measured data. The choice of this scheme was also consistence with the finding made by Rameshwaran and Shiono (2003). In this research, the Elder's turbulence model was used for the salt transport. No research in CFD had ever made using this turbulence model before as far as the author is aware. From the analysis, the Elder's turbulence gave excellent agreement with the measured data compared to the Eddy Viscosity turbulence model especially for problems related to salt transport.

5) Shape Factors

Most of the study on shape factors was done in the laboratory using simple channel configuration with steady state flows to determine their effect on the flow structures. However, in this research shape factors was done on the natural estuary with various configurations, dynamic boundary conditions, different advection schemes and turbulence models. This was to give some insight knowledge on how the shape factors will affect the water level profiles and the velocity distributions in the main channel. The results from this research shows that the shape factors have significant influenced on the flows structure for various configuration. Therefore, one of the contributions of this thesis is on the shape factors which need further research to understand the mechanic of flow for various configuration and complex boundary conditions.

6) Other Finding

It was discovered in this study that there was a interesting phenomenon for river which has a negative and positive gradient. At this location, there was an interaction of flow between saline propagating from the sea, incoming freshwater and the freshwater that was trapped at the lowest region of the river. The velocity at this region was found to be rotating at the mid section of the river. They were high turbulence and vigorous circulations at this

region due to the differential of density and shear force at the interface between the saline and freshwater. This finding need to be explored in the laboratory using physical models before it be used to model real world problem. Matters pertaining mechanism of flows and interaction of forces between different water densities should be understood before any conclusion could be drawn from this phenomenon.

7.4 Recommendations for Further Research

Before CFD to be widely used in rivers and estuaries engineering, several unresolved issue needs to be addressed. Among them are,

1. Further validation work to suit the application for practical uses was needed in other rivers and estuaries, to ensure that some of the conclusions drawn by the author from scare data were fully valid. It would benefit and advantage to have a research group to work together on river and estuary by measuring them thoroughly instead of collecting a few secondary data due to limited manpower and resources. However, the author was well aware that research needed to fit within a tight period normally 3-4 years with constraint budget and facilities. Nevertheless, data collection for small and large scales remains an essential step in the development of numerical code in river and estuary modelling.

2. Further investigation need to be carried out to determine the different types of vegetation in the wetland. This was necessary in getting the effective roughness coefficient, which influence the flow and salinity profiles in the river and estuary.

3. To simulate multi-dimensional flow of large domains with sophisticated turbulence closure. This apply to flow in natural channel with relatively small grid size to study on how flow-vegetation interactions and flows in the near wall region.

4. Bench marking the velocity distributions, water levels and salinity intrusion using other turbulent models with various advection schemes were also needed so that comparison

could be made to obtain results that were more realistic. This will help to understand the effects of turbulent models on the flows in river and estuary. A more comprehensive data such as longer tidal records, velocity and salinity measurement data would needed to be obtained so that the simulation reflected the actual condition in the environment.

5. Although there exist an excellent guides regarding verification and validation in CFD (AIAA 1998), the author thinks that it would be essential for civil and hydraulic engineering community to developed their own guideline and code of practice which would be suitable to be applied in practices. The AIAA was initiated for the aeronautical and mechanical community, which was more meaningful and suited for their application. The applications of CFD to the environmental issues have some fundamentally different characteristics from other applications of this technology, and as a consequence such applications may have very different research priorities. For the civil engineers, environmental scientists and geographers community they should have their own guide criteria. Where they are normally involved large and complex scale problems with high uncertainty. It would also contribute to address the end-users needs in a more practical way. This included the acceptable tolerance limit of accuracy using the CFD compared to the field reconnaissance study.

REFERENCES

Abbott, M.B. (1997). "Range of Tidal Flow Model' *Journal of Hydraulic Division ASCE*, Vol.123, No.4.

AIAA (1998). "Guide for the Verification and Validation of Computational Fluid Dynamics Simulations." *AIAA G-077-1998*, AIAA.

Akanbi, A.A., & Katopodes, N.D., (1988)." Model in Flood Propagation on Initially Dry Land." *Journal of Hydraulic Engineering, ASCE*, Vol. 114, No. 7, pp. 689-707.

Antze, T.F., Stösser, T., Bates, P., & Olsen, N. R. B. (2001). "3D Numerical Modelling of Open-Channel Flow with Submerged Vegetation", *IAHR Journal of Hydraulic Research*, No. 3.

Ammer, M., & Valentin, F.(1993). "A Hierarchical Finite Element for Three-Dimensional Free Surface Flow." *Proceeding 5th International Symposium on Refined Flow Modeling and Turbulence Measurements,* Paris, France, pp.711 - 718.

Bates, P. D., & Anderson, M.G. (1993). " A Two Dimensional Finite Element Model for River Flow Inundated.", *Proceeding Royal Society London*, Vol. 440, pp. 481-491.

Bates, P.D., Anderson, M.G., Price, D.A., Hardy, R.J., & Smith, C.N. (1996). "Analysis and Development of Hydraulic Models for Floodplain Flows." *Floodplain Processes*, Edited by Anderson, M.G., Walling, D.E. and Bates, P. D. Chichester, England.

Bates, P.D., Stewart, M.D., Siggers, G.B., Smith, C.N., Hervouet, J-M., & Sellin, R.H.J. (1998). "Internal and External Validation of 2 Dimensional Finite Element Code for River Flood Simulation." *Proceeding Institution of Civil Engineers Water, Maritime and Energy* (Issue:130): pp. 127- 140.

Bates, P.D., Wilson, C.A.M.E., Hervouet, J-M., & Stewart, M.D. (1999). "Two Dimensional Finite Element Modelling in Floodplain Flow." *La Houlille Blanche* Vol. 3/4, pp. 61-67

Bates, P. D., & Hervouet, J. M. (2000). "The TELEMAC Modelling System Special Issue." *Hydrological Processes* Vol. 14(No.13).

Benqué, J-P., Haughel, A., & Viollet, P-L. (1983). "Numerical Models in Environmental Fluids Mechanics." *Engineering Application of Computational Hydraulics*, Alexandre Preissmann, Vol. 2 Abbott and Cunge, Pitman.

Blumberg, A. F., & Mellor, G.L. (1983). "Diagnostic and Prognostic Numerical Circulation Studies of the South Atlantic Bight." *Journal of Geophysical Research,* Vol.88, No.C8, pp. 4579-4592.

Blumberg, A.F., Signell, R.P., & Jenter, H.L.,(1993). "Modelling Transport Processes in the Coastal Ocean." *Journal of Marine Environmental Engineering*, Vol.1, pp. 31-52.

Bowden, K. F. (1963). "The Mixing Processes in a Tidal Estuary." *International Journal of Air, Water and Pollution,* Vol.7.

Bredberg, J. (2001). "On Two-Equation Eddy-Viscosity Models." 01/8, *Chalmers University of Technology*, Dept. of Thermo and Fluids Dynamics, Goteberg.

Brebbia, C.A., Gray, W.G., & Pinder, G.F. (1978). "Finite Elements in Water Resources." *Proceedings of the 2nd International Conference on Finite Elements in Water Resources*, London.

Brooks, A. N., & Hughes, T. J. R. (1982). "Streamline Upwind/Petrov-Galerkin Formulations for Convection Dominated Flows with Particular Emphasis on the Incompressible Navier-Stokes Equations." *Computer Methods in Applied Mechanics and Engineering,* Vol.32.

Bruce, R. M., Donald, F. Y., & Theodore, H. O. (1994). "Fundamentals of Fluid Mechanics." *John Wiley and Son*, Inc, New York.

Cameron, W. M., & Pritchard, D. W. (1963). "Estuaries" - ed. Hill, M.N., - *The Seas* ; Vol.2. New York, John Wileys & Sons.

Carollo, F.G., Ferro, V., & Permini, D. (2005). " Flow Resistance Law in Channels with Flexible Submergerd Vegetation." *Journal of Hydraulic Engineering, ASCE*, Vol.131, No.7, pp.554-564

Cerco, C. F. (2003). "Scientific versus Engineering Modelling." *Journal of Environmental Engineering Division ASCE,* Vol. 129, Issue 8, pp. 681-682

Chen, M., Chan, E.S., & Khoo, B.C. (1997). "Three Dimensional Circulation Singapore Coastal Water." *Conference Proceedings of Oceanology International 97, Pacific Rim* Vol. 1.

Cheng, R.T., (1982). "Modeling of Tidal and Residual Circulation in San Francisco Bay, California." *Proceedings, Seminar on 2-D Flows, HEC Report,* U.S. Army Corps of Engineers, Davis, Calif., July 1981, pp. 172-185.

Choi, S.U., & Kang, H. (2004)" Reynolds Stress Modelling of Vegetated Open-Channel Flow." *Journal of Hydraulic Research*, Vol.42 No.1, pp. 3-11.

Chow, V. T. (1959). "Open Channel Hydraulics." *McGraw-Hill Book Co.*, New York.

COEI (2002). "Hydraulic Study for the Feasibility of the Proposed Penang Second Crossing, Penang, Malaysia." *Malaysia University of Technology.*

Cooper, A.J. (2004). "Personal Conversation." *HR Wallingford, UK.*

Cruise, J. F., Singh, V. P., & Sherif, M. (2003). "Elementary Hydraulics."

Csanady, G. T. (1973). "Wind Induced Barotropic Motions in Long Lakes." *Journal of Physical Oceanography* Vol.3.

Cunge, J.A., Holly, F. M., & Vewey, A. (1980). "Practical Aspects Computational River Hydraulics". *Pitman, Boston.*

Darbyshire, E. J., & West, J. R. (1992). "Turbulence and Shear Induced Mixing Processes in Estuaries." ed. Prandle, D. - Dynamics and Exchanges in Estuaries and Coastal Zone, Coastal and Estuarine Studies No.4. *American Geophysical Union*, Washington DC.

DeCastro, M., Gómez-Gesteira, M., Prego, R., Taboada, J. J., Montero, P., Herbello, P., & Pérez-Villar, V. (2000). "Wind and tidal Influence of water Circulation in a Galician Ria - North West of Spain." *Estuarine, Coastal and Shelf Science* Vol.51, Issue No. 2.

Demirdzic, A.D. Gosman, R.I. Issa, & Peric, M. (1987). "A Calculation Procedure for Turbulent Flow in Complex Geometries." *Computational Fluids*, Vol.15. pp:251-273.

Dyer, K. R. (1972). 'Estuaries: A Physical Introduction", *John Wiley &Sons.*

Elder, J.W. (1959). "The dispersion of marked fluid in turbulent shear flow." *J. Fluid Mech.* Vol. 5, pp. 544-560.

Ervine, D. A., & Ellis, J. (1987). "Experimental and Computational Aspects of Overbank Floodplain Flow." *Transaction of the Royal Society of Edinburgh: Earth Sciences*, Vol. 78, pp. 315-325.

Ervine, D. A., & Jasem, H. K. (1989). "Flood Mechanism in Meandering Channels with Floodplain Flow." *Proceedings of the XXIII IAHR Congress*, Ottawa, Canada, 21-25 August 1989, pp.B449-B456.

Ervine, D. A., Willetts, B.B., Sellin, R. H. J., & Lorena, M. (1993). "Factors Affecting Conveyance in Meandering Compound Flows." *Journal of Hydraulic Engineering*, Vol. 119, No.12, pp. 1383-1399.

Elliot, A.H., (2001) "Settling of Sediment in a Channel with Emergent Vegetation", *Journal of Hydraulic Division ASCE*, Vol.126, No.8

Falconer, R. A. (1980), 'Numerical Modeling of Tidal Circulation in Harbors', *Journal of Hydraulic Engineering,* ASCE, Vol. 106, No.1, pp. 31-48.

Falconer, R.A.(1984). 'Temperature Distribution in Tidal Flow Field.' *Journal of Environmental Engineering, ASCE*, Vol. 110, No.6, pp. 1099-1116

Falconer, R.A.(1980). 'Numerical Modeling of Tidal Circulation in Harbour.' Journal of the Waterway, Port and Coastal Division, Vol106, pp32-33.

Falconer, R. A., & Lin, B., (1997). "Three-dimensional Modelling of Water Quality in the Humber Estuary." *Water Research*, IAWQ 31(5).

Falconer, R.A. & Lin, B. (2003). " Hydro-Environmental Modeling of Riverine Basins Using Dynamic Rate and Partitioning Coefficients." IAHR, *Intl. J. River Basin Management* Vol. 1, No. 1, pp. 81–89

Fathi-Mghadam, M., & Kouwen, N. (1997). "Non-rigid, Non-submerged Vegetation Roughness on Floodplains." *Journal of Hydraulic Engineering*, Vol. 123, No. 1, pp. 51-57.

Ferziger, J.H., & Peric, M. (1996). "Computational Methods for Fluids Dynamics." *Springer*

Festa, J. F., & Hansen, D. V. (1976). "A Two Dimensional Numerical Model of Estuarine Circulation: The Effects of Altering Depth and River Discharge." *Estuarine, Coastal and Shelf Science* Vol.4.

Fischer, H. B. (1972). "Mass Transport Mechanism in Partially Stratified Estuaries." *Journal of Fluid Mechanics*, Vol.53.

Fischer, H. B. (1976). "Mixing and Dispersion in Estuaries." pp.107-133.

Fischer, H. B., List, E. J., Koh, R. C. Y., Imberger, J., & Brooks, N. H. (1979). "Mixing in Land and Coastal Waters." *Academic Press*, Inc,

Fukuoka, S., & Watanabe, A. (2000). " Numerical Analysis on Three Dimensional Flow and Bed Topography in a Compound Meandering Channel." *Proceeding of 4th International Conference of Hydroinformatics, Iowa City, USA.*

Furukawa, K., Wolanski, E., & Mueller, H. (1997). "Currents and Sediment Transport in Mangrove Forests." *Estuarine, Coastal & Shelf Science* 44, pp.51-57

Giraud, F., Faure, J. B., Zimmer, D., Lefeuvre, J. C., & Skaggs, R. W. (1997). "Hydrologic Modelling of a Complex Wetland." *Journal of Irrigation and Drainage Engineering , ASCE,* Vol.123(No.5).

Fukuoka, S., & Fujita, K. (1989). "Prediction of Flow Resistance in Compound Channels and Its Application to Design of River Courses." *Proc. JSCE*, Vol. 411, pp. 63-72 (in Japanese).

Gerhart, P. M., & Gross, R. J. (1985). "Fundamentals of Fluid Mechanics." *Addison Wesley Publishing Co.*, Don Mills, Ontario.

Greenhill, R. K., & Sellin R. H. J., (1993). "Development of a Simple Method to Predict Discharge in Compound Meandering Channels." *Proc. of Instn. of Civ. Engrs. Wat., Marit. & Energy*, Vol. 101, pp 37-44.

Gross, E.S., & Koseff, J.R. (1999). "Three Dimensional Salinity Simulations of South San Francisco Bay." *Journal of Hydraulic Engineering, ASCE,* Vol. 125, No.11, pp. 1199-1209.

Hall, M., Shiono, K., & Falconer, R.A., (1992). "Three Dimensional Layer Averaged Model for Tidal Flows." *Proceeding 2nd International Conference Hydraulic Modelling and Environmental Modelling*, Bradford, UK.

Hansen, D. V., & Rattray, M. J. (1966). "New Dimension in Estuary Classification." *Limnology and Oceanography* Vol.11(3).

Hankin, B.G., Hardy, R.J., Kettle, H. & Beven, K.J. (2001). " Using CFD in a GLUE Framework to Model the Flow Dispersion." *Earth Surface Process and Landforms.* Vol.26, pp.667-687.

Hardy, R. J., Bates, P.D., Anderson, M.G., Moulin, C., & Hervouet, J-M. (2000). "Development of a Reach Scale Two Dimensional Finite Element Model for Floodplain Sediment Transport." *Proceeding Institution of Civil Engineers Water, Maritime Engineering* Vol.142, pp.141-156.

Hardy, R. J., Bates, P. D., & Anderson, M.G. (1999). "The Importance of Spatial Resolution in Hydraulic Models for Floodplain Environments." *Journal of Hydrology*, Vol.216 ,pp.124-136

Henderson, F. M. (1966). "Open Channel Flow." *Macmillan Co. Ltd.*

Hervouet, J. M. (1991). "Characteristics and Mass Conservation-New Developments in TELEMAC-2D." *EDR-DER. LNH Chatou, France, Groupe Hydraulique Fluviale, Report HE-43/92-41.*

Hervouet, J. M. (2000). "TELEMAC Modelling System: An Overview." *Hydrological Processes* Vol.14(No.13).

Hervouet, J. M., & Rouge, D., (1996). "Numerical Simulation of a Malpasset Dam Break Flood Wave." *EDF-DER, LNH Chatou, France, Groupe Hydraulique Fluviale, Report HE-43/96/040/A*

Hervouet, J. M., & Janin, J. M. (1994). "Finite Element Algorithms for Modelling Flood Propagation - Modelling Flood Propagation over Initially Dry Areas." *ASCE*, USA.

Hervouet, J. M., & van Haren, L. (1995). "TELEMAC 2D Version 3.0 - Principle Note", *Report HE-43/94/052*, EDF-DER,LNH Chatou, France.

Horritt, M. S. (2000). "Calibration of Two Dimensional Finite Element Flood Flow Model Using satelite Radar Imagery." *Water Resource Research* Vol.36(No.11).

Howarth. & Pugh (1993). "Physical Oceanography of Coastal and Shelf Seas." - (ed) Johns, B. New York, *Elsevier Science Publishers.*

Idelsohn, S. R., & Onate, E. (1994). "Finite Volumes and Finite Elements: Two Good Friends." *International Journal For Numerical Methods in Engineering* Vol.37.

Ippen, A. T. & Harleman, D. R. F. (1961). "One Dimensional Analysis of Salinity Intrusion in Estuaries." *Tech. Bull. 5*, Comm. Tidal Hydraulics, Corps. of Engineers. U.S. Army.

Ismail, Z (2007). "A Study of Overbank Flows in Non-Vegetated and Vegetated Floodplains in Compound Meandering Channels." *Ph.D Thesis,* Dept. of Building and Civil Engineering ,Loughborough University, U.K.

Issacson, E., Stoker, J.J., & Troesh, B.A.. (1980) "Numerical Solution of Flood Prediction and River Regulation Problems (Ohio-Mississippi Floods)." *in Cunge, J.A., Holly, F.M., & Verwey, A.*

James, C.S., Birkhead., A.L., Jordanova., A.A., & O'Sullivan., J.J., (2004), "Flow Resistance of Emergent Vegetation. "*Journal of Hydraulic Research*, Vol.42 No.4, pp 390-398.

James, C. S., & Wark, J. B. (1992). "Conveyance Estimation for Meandering Channels." *Report SR 329*, HR Wallingford Ltd, UK.

Jarvela, J. (2002). "Determination of Flow Resistance of Vegetated Channel Banks and Floodplains." *River Flow 2002,* Bousmar & Zsch (eds), pp. 311-318.

Kadlec, R.H. (1990), " Overland Flow in Wetlands: Vegetation Resistance." *Journal of Hydraulic Engineering*, ASCE, Vol 116, No.5.

Karki, K.C. & Patankar, S.V. (1998)."*Numerical Heat Transfer.*" Vol.14, pp.295-307 (1988).

Kiely, G. (1990). "Overbank Flow in Meandering Compound Channels – The Important Mechanism." *International Conference on River Flood Hydraulics*. W. R. White. Chichester, England, John Wiley & Sons, pp.207-217.

Knight, D. W., & Shiono, K. (1996). "River Channel and Floodplain Hydraulics." *Floodplain Processes,* Anderson, M.G., Walling, D.E., & Bates, P.D. -eds., John Wiley and Sons, pp. 139-181.

King, I.P., & Roig, L.C., (1978). "Recent Application of RMA's Finite Element Models for Two Dimensional Hydrodynamics and Water Quality." *In Brebbia, Gray and Pinder (1978).*

King, I.P., & Roig, L.C., (1991). "Finite Element Modeling of Flow in Wetland." *Proceeding National Conference of Hydraulic Engineering, ASCE*, pp.286-291.

Kobashi, D., & Mazda, Y., (2005). "Tidal Flow in Riverine -Type mangrove." *Wetland Ecology Management.*, (In press)

Koutitas, C., & Oconnor, B., (1980), "Modeling Three-Dimensional Wind Induced Flow." *Journalof the Hydraulic Division, ASCE*, Vol. 106,No. 11, pp.1843-1871.

Kouwen, N., & Fathi-Moghadam, M. (1997). "Non Rigid, Non-submerged, Vegetative Roughness on Floodplains." *Journal of Hydraulic Division ASCE*, Vol.123, No.1

Kouwen, N., & Fathi-Moghadam, M. (2000). "Friction Factors for Coniferous Trees Along Rivers." *Journal of Hydraulic Division ASCE*, Vol.126, No.10.

Kuipers, J., & Vreugdenhil, C. B. (1973). "Calculation of Two-Dimensional Horizontal Flow." *Report S163, Part I, Delft Hydraulic Laboratory, Delft*, The Netherlands.

Lavedrine, I. (1996). "Evaluation of Three Dimensional Models to River Flood Problems." *Report TR6*, HR Wallingford, UK.

Lavedrine, I. (1997). "Evaluation of Three Dimensional Models to River Flood Problems." *Report TR26*, HR Wallingford, UK.

Leendertsee, J. J. (1967). "Aspects of a Computational Model for Long Water Wave Propagation." *Rand Corporation, Memorandum RH-5299-RR.* Santa Monica.

Leendertsee, J. J., Alexander, R.C., & Liu, S.K., (1973). "A Three Dimensional Model for Estuaries and Coastal Seas: Principal of Computation." *RAND Corporation Report, Santa Monica, California, USA Report RM 5294-PR*

Leendertsee, J.J. & Liu, S.K. (1978). "A Three-Dimensional Turbulent Energy Model for Non-Homogeneous Estuaries and Coastal Sea Systems." *Intl. Jou. Comp. J. Nihoul (ed.), Hydrodynamics of Estuaries and Fjords*: pp.387-405. Amsterdam: Elsevier.

Leopold, L.B., & Wolman, M.G. (1957). "River Channel Patterns : Braided, Meandering and Straight." *U.S. Geological Survey Professional Paper,* 282-B, pp.39-85

Li, R. M. & Shen, H. W. (1973). "Effect of Tall Vegetations on Flow and Sediment." Journal of Hydraulic Division, Vol. 99, No. 5, pp. 793-814.

Lin, J. D., Liao, W. G., Qiu, K-J, & Lefor, M. W. (2002). "A Two-dimensional Hydrodynamic Model for Coastal River-Marsh Systems: User's Manual, Version 1.0." *Report No. JHR 02-275, June, 2002.*

Liu, W., & James, C. S. (1997). "Effects of Floodplain Geometry on Conveyance of Meandering Compound Channels." *HR Wallingford Limited*, pp. 81-90.

Liriano, S. L., Marriott, M. J., & Day, R. A. (2001). "Experimental Observations of Obstruction on Floodplains." *Proc. Of the XXIX IAHR Congress*, Vol.1, pp.332-337.

Lyness, J. F., Myers, W. R. C., & O'Sullivan, J. J. (1998). "Hydraulics Characteristics of Meandering Mobile Bed Compound Channels." *Proc. of Instn. of Civ. Engrs. Wat., Marit. & Energy*, Vol.130, pp.179-188.

Lynch, D.R. & Gray, W.G. (1990). "Finite Element Simulation of Flow in Deformation Regions." *Journal of Computational of Physics*, Vol.36, pp.135-153

Magi, M., (2000). "The Study on the Physical Processes and Hydrodynamics in Mangrove Area." *Doctoral Thesis,* Tokai University, Japan

Malcherek, A. (2000). "Application of TELEMAC 2D in a Narrow Estuarine Tributary." *Hydrological Processes* Vol.14(No.13).

Mazda, Y., Wolanski E., King B., Sase A., Ohtsuka D., & Magi, M., 1997a – "Drag Force Due to Vegetation in Mangrove Swamps." – *Mangroves & Salt Marshes*, 1(3):pp. 193-199

Mazda, Y., Kobashi, D., & Okada, S. (2005). "Tidal Scale Hydrodynamics within Mangrove Swamps." *Wetlands Ecology and Management*, 13:pp.647-655

McGuirc, J. J., & Rodi, W. (1978). "A Depth-Averaged Mathematical Model for the Near Field of Side Discharges into Open-Channel Flow." *J. Fluid Mech.* 86(4), pp. 761-781.

McKeogh, E. J., & Kiely, G. K. (1989). "Experimental Study of the Mechanics of Flood Flow in Meandering Channels." *Proc. 23rd IAHR Congress,* pp. B491-B498.

Mellor, G. L., & Blumberg, A. F. (1980). "A Coastal Ocean Numerical Model." *Proc., Int. Symp. on Math. Modelling of Estuarine Phys.* Sundermann, J., & Holz, K.P. eds., Springer, Berlin, pp.202–219.

Molinaro, P., & Natale, L. "Modelling Flood Propagation Over Initially Dry Area." *Journal of Hydraulic Engineering, ASCE.*

Morvan, H. P. (2001). "Three Dimensional Simulation of River Flood Flows." - Dept. of Civil Engineering, Glasgow, *Ph.D Thesis*, The University of Glasgow.

Muto, Y (1997). "Turbulent Flow in Two-Stage Meandering Channels." *PhD Thesis*, Bradford University, UK.

Muto, Y., & Shiono, K. (1998). "Three Dimensional Flow Structure for Overbank Flow in Meandering Channels." *Journal Hydroscience & Hydraulics Engineering*, Vol. 16, No. 1, pp.97-108.

Myers, W.R.C. (1978). "Momentum Transfer in a Compound Channel." *Journal of Hydraulic Research,* Vol. 28,No.2 pp.144-151.

Myers, W.R.C. (1987). "Velocity and Discharge in Compound Channel." *Journal of Hydraulic Division ASCE*, Vol.113, No.6 , pp.753-766.

Nepf, H.M., Mugnier, C.G., & Zavistoski (1997). "The Effects of Vegetation on Longitudinal Dispersion." *Journal of Estuarine, Coastal and Shelf Science.*

Nepf, H. M. (1999). "Drag, Turbulence and Diffusion in Flow Through Emergent Vegetation." *Journal of Water Resource Research*, Vol. 5, pp.271-279.

Nezu, I., & Rodi, W. (1985). "Open-Channel Flow Measurements with a Laser Doppler Anemometer." *Journal of Hydraulic Engineering,* Vol. 112, No. 5, pp.335-355.

Nicholas, A.P., & Mclleland, S.J. (2004). "Computational Fluid Dynamics Modelling of Three-Dimensional Processes on Natural River Floodplain", *Journal of Hydraulic Research*, Vol.42 No.2, pp.131-143

Wilson, C. A. M. E., Stoesser, T., Olsen, N. R. B. & Bates P. D. (2003). "Application and Validation of Numerical Codes in the Prediction of Compound Channel Flows." *Proceedings of the Institution of Civil Engineers, UK, Water and Maritime Engineering,* No. 153, pp.117-128.

Wilson, C. A. M. E., Boxall, J. B., Guymer, I. & Olsen N. R. B. (2003) "Validation of a 3D Numerical Code in the Simulation of Pseudo-Natural Meandering Flows." ASCE Journal of Hydraulic Engineering, Vol. 129, No. 10, October.

Wilson, C.A.M.E., Olsen, N. R. B., Boxall, J. B. & Guymer, I. (2003) "Three-Dimensional Numerical Simulation of Solute Transport in a Meandering Channel." *XXX IAHR Congress,* Thessaloniki, Greece

Olsen, N. R. B. (2003) "3D CFD Modeling of a Self-Forming Meandering Channel." *Journal of Hydraulic Engineering, ASCE,* No. 5, May 2003.

Paquier, A., & Farissier, P. (1997). "Assessment of Risks of Flooding by Use of a Two Dimensional Model." *IAHS Publication*, No.239, pp. 137-143

Patankar, S. V. & Spalding, D. B. (1972). "A Calculation Procedure for Heat, Mass and Momentum Transfer in Three-dimensional Parabolic Flows." *International Journal for Heat and Mass Transfer*, **15**, pp.1787-1806.

Patra, K. C., & Kar, S. K. (2001). "Flow Interaction of Meandering Channel River with Floodplains." *Journal of Hydraulic Engineering*, Vol. 126, No. 8, pp.593-604.

Patra, K. C., Kar, S. K., & Bhattacharya, A. K. (2004). "Flow and Velocity Distribution in Meandering Compound Channels." *Journal of Hydraulic Engineering,* Vol. 130, No. 5, pp.398–411.

Peltier., Le Normant, C., Teisson, C., Malcherek, A., Markofsky, M., Zielke, W., Cornlisse, J., Molinaro, P., Corti, S. & Greco, G., (1996). "Three Dimensional Numerical Modeling of Cohesive Sediment Transport Processes in Estuaries Environment." *Final Report to EC Contract MAS2-CT92-0013, EDF-DER, LNH Chatou, France, Report HE-423/96/047/A.*

Petryk, S., & Bosmajian, G. I. (1975). "Analysis of Flow through Vegetation." *Journal of Hydraulic Division,* Vol. 101, No. 7, pp.871-884.

Platmann, G.W. (1958). "A Numerical Computation for of the Surge of 26 June 1954 on Lake Michigan." *Geophysical* Vol.6, pp.407-438

Pritchard, D. W. (1955) "Estuarine Circulation Patterns." *Proceedings of the American Society of Civil Engineers* 81, No 717, pp.1-11.

Pritchard, D. W. (1971). "Hydrodynamic Models - In Estuarine Modelling: An Assessment." *Environmental Protection Agency Rep.* 16070DVZ 02/71.

Rameshwaran, P., & Shiono, K. (2003). "Computer Modelling of Two Stage Meandering Channel Flows." *Proceeding Institution of Civil Engineers Water, Maritime Engineeringy* Vol.156, No. 4.

Rameshwaran, P., & Shiono, K. (2002). "Predictions of Velocity and Boundary Shear Stress in Compound Meandering Channel." *River Flow 2002.*

Rameshwaran, P (1997). "Conveyance Prediction for Meandering Two-Stage Channel Flows". - Dept. of Civil Engineering, *Ph.D Thesis*, University of Aberdeen

Rajaratnam, N. & Ahmadi, R.M. (1979). "Interaction Between Main Channel and Flood-plain Flows." *Journal of Hydraulic Engineering, ASCE,* Vol. 105, pp. 573-588.

Rastogi, A. K., & Rodi, W. (1978). "Prediction of Heat and Mass Transfer in Open Channels." *Journal of Hydraulic Division ASCE*, Vol.104(HY3), pp.397 420.

Rodi, W. (1993). "Turbulence Models and their Applications in Hydraulics — A State of the Art Review." *IAHR Monograph*, 3rd edition, Balkema, Rotterdam.

Royal Malaysian Navy -1988. "Malaysian Tide Tables 1998."

Sleight, P.A., Gaskell, P.H., Berzins, M., & Wright, N.G. (1998). "An Unstructured Finite-Volume Algorithm for Predicting Flow in Rivers and Estuaries." *Computational and Fluids,* Vol. 27, No.4, pp. 479-508.

Sellin R. H. J. (1964). "A Laboratory Investigation into the Interaction between the Flow in the Channel of a River and That over Its Floodplain." *La Houille Blanche*, Vol. 7, pp.793-802.

Sellin, R.H.J., (1991). "Towards the Identification of Flow Mechanisms in Channels of Complex Geometry." Proceeding 24yh IAHR, Congress, Madrid, Spain pp.A523-A530

Sellin, R. H. J., Ervine, D. A., & Willetts, B. B. (1993). "Behaviour of Meandering Two-Stage Channels." *Proc. Instn. Civ. Engrs Wat., Marit. & Energy*, Vol. 101, pp.99-111.

Sellin, R. H. J., & Willets, B. B. (1996). "Three-Dimensional Structures, Memory and Energy Dissipation in Meandering Compound Channel Flow." *Floodplain Processes,* Edited by Anderson, M.G., Walling, D.E., & Bates, P.D. - John Wiley & Sons, pp.255-297.

Sheng, P., (1999). "Validation and Intercomparison of Three Dimensional Numerical Models of Estuarine and Lake Hydrodynamic."*Hydrodynamics Model Validation*

Shukla, D. R. (2006). "Three-dimensional Computational Investigations of Flow Mechanisms in Compound Meandering Channels." *Ph.D Thesis*, Dept. of Building and Civil Engineering, Loughborough University, U.K.

Shukry, A. (1949). "Flow Around Bends in an Open Flume." *Transactions, American Society of Civil Engineers,* Vol.115, pp 751-788.

Shiono, K., Al-Romaih, J. S., & Knight, D. W. (1999). "Stage-Discharge Assessment in Compound Meandering Channel." *Journal of Hydraulic Engineering*, Vol. 125, No. 1, pp. 66-77.

Shiono, K., & Knight D. W. (1991). "Turbulent Open-Channel Flows with Variable Depth across the Channel." *Journal of Fluid Mechanics*, Vol. 222, pp.617-646.

Shiono, K., and Knight, D. W. (1990) "Mathematical Models of Flow in a Two or Multistage Straight Channels." *Proceedings of International Conference on River Flows Hydraulics.* pp.229-238

Shiono, K., and Knight, D. W., (1989), "Transverse and Vertical Reynolds Stress Measurements in a Shear Layer Region of a Compound Channel." *Proceedings of The Seventh Symposium on Turbulent Shear Flows*, Stanford University, USA.

Shiono, K., & Muto, Y. (1998). "Complex Flow Mechanisms in Compound Meandering Channels with Overbank Flow." *Journal of Fluid Mechanics*, Vol. 376, pp. 221-261.

Shiono, K., Muto, Y., Imamoto, H., & Ishigaki, T. (1993). "Flow Discharge Characteristics for Overbank Flow in Meander Channels." *Proc. of the 1st Int. Conf. on Hydro-Science and Engineering*, Washington D. C., pp. 1309-1316.

Shiono, K., Muto, Y., Imamoto, H., & Ishigaki, T. (1993). "Flow Discharge Characteristics for Overbank Flow in Meander Channels." *Proc. of the 1st Int. Conf. on Hydro-Science and Engineering*, Washington D. C., pp. 1309-1316.

Shimizu, Y., Yamaguchi, H. & Itakura, T. (1990). " Three Dimensional Computation of Flow and Bed Deformation." *Journal of Hydraulic Engineering*, Vol. 116, No. 9, pp. 1090-1108.

Simmons, H. B. (1955). "Some Effects of Upland Discharge on Estuarine Hydraulics." *Proceeding American Society of Civil Engineers* Vol.81(No.792).

Simpson, J.H., Brown, J., Matthews, J., & Allen, G. (1990). "Tidal Straining, Density Currents, and Stirring in the Control of Estuarine Stratification." *Estuaries* Vol.13, No.2.

Spooner, J (2003). " Flow Structures in a Compound Meandering Channel with Flat and Natural Bedforms", *Ph.D Thesis*, Dept. of Building and Civil Engineering, Loughborough University, U.K.

Sturve, J., Falconer, R.F., & Wu, Y. (2003), "Influence of Model Mangrove Trees on the Hydrodynamics in a Flume." *Journal of Estuarine, Coastal and Shelf Science.* Vol.58., pp.163-171.

Tamai, N., Asaeda, T. & Ikeda, H. (1986). "Generation Mechanism and Periodicity of Large Surfave-Eddies in a Compound Channel Flow." *Proceeding of 5th Congress APD-IAHR Seoul, Repub. Of Korea,* pp. 61-74

Tchamen, G. W., & Kahawita, R.A. (1994). "The Numerical Simulation of Wetting and Drying Areas Using Riemann Solvers." *Proceeding Modelling of flood propagation over initially dry areas, held in Milan, Italy.* pp. 127-136.

Tchamen, G.W., & Kahawita, R.A. (1998). "Modelling Wetting and Drying Effects Over Complex Topography." *Hydrological Processes,* 12(8), pp.1151-1182.

Teigland, R., & Eliassen, I. K. (2001). "A Multiblock/Multilevel Mesh Refinement Procedure for CFD Computations." *International Journal for Numerical Methods in Fluids Vol.36,* Issue 5, pp.519–538.

Toebes, G. H., & Sooky, A. A. (1967). "Hydraulics of Meandering Rivers with Floodplains." *Journal of Hydraulic Waterways and Harbours Division,* Vol. 93, No. 2, pp. 1053-1066.

Tominaga A., Nezu I., & Ezaki K. (1989) "Experimental Study on Secondary Currents in Compound Open-Channel Flow." *Proc. of the 23rd IAHR Congress*, Ottawa, Canada, pp.A15-A22.

Tominaga, N., & Nezu, I. (1991). "Turbulent Structure in Compound Open-Channel Flows." *Journal of Hydraulic Engineering,* Vol. 117, No. 1, pp.21-41.

Taylor, G.I. (1953). "The Dispersion of Solute Matter in a Solvent flowing Slowly Through a Tube." *Proceeding Royal Society, London Series A (219),* 186-203

Townsend, D.R. (1986). "An Investigation of Turbulence Characteristics in a River model of Complex Cross Section." *Proceeding the Institution of Civil Engineers*, 40, pp 155-175.

Uncles, R.J., Ong, J.E., & Gong, W.K. (1990). "Observation and Analysis of a Stratification-Destratification Event in a Tropical Estuary." *Estuarine, Coastal and Shelf Science* Vol.31, Issue 5, pp. 651-665.

U.S Army Corps .of Engineers (1956). " Hydraulic Capacity of Meandering Channels in Straight Floodways." Waterways Experiment Station, Vicksberg, Mississippi, *Technical Memorundum* No.2-429.

Vreugdenhil, C.B., & Wijbenga, J.H.A (1982). "Computation of Flow Patterns in Rivers." *Journal of Hydraulics Division, ASCE*, Vol.108 HY11, Nov.

Van der Kreek, J. (1986). "Lecture Notes on Coastal and Estuarine Studies: Physics of Shallow Estuaries and Bays." *New York, Springer-Verlag.*

Versteeg, H. K., & Malalasekera, W. (1995). "An Introduction to Computational Fluid Dynamics - Finite Volume Method." *Longman* Vol.44., pp. 675-684.

Voillet, P.L., (1977). "Etude de Jets des Courants Traversiiers et dan des Milieux Stratifies." *Thesis, University of Paris*

Wang, Z.J., (2000). "A Fast Nested Multi-Grid Viscous Flow Solver for Adaptive Cartesian/Quad Grids." *International Journal for Numerical Methods in Fluids*, vol. 33, No. 5, pp. 657-680,

Wang, H. F., & Anderson, M. P. (1985). "Introduction to Groundwater Modelling Finite Difference and Finite Element Methods." *Academic Press,* New York,

Wijbenga, J.H.R. (1985). "Determination of Flow Patterns in Rivers with Curvilinear Coordinates." *Proceeding 21st. IAHR Congress, Melbourne, Australia*, pp.131

Willetts, B. B., & Hardwick, R. (1993). "Stage Dependency for Overbank Flow in Meandering Channels." *Proc. Instn. Civ. Engrs Wat., Marit. & Energy*, Vol. 101, pp. 45-54.

Willetts, B. B., & Rameshwaran, P. (1996). "Meandering Overbank Flow Structures." *Coherent Flow Structures in Open Channels,* John Wiley & Sons Ltd, Chapter 29, pp. 609-629.

Wilson, C. A. M. E., Boxall, J. B., Guymer, I., & Olsen, N. R. B. (2003b). "Validation of a Three-dimensional Numerical Code in the Simulation of Pseudo-Natural Meandering Flows." *Journal of Hydraulic Engineering,* Vol. 129, No. 10, pp. 758-768.

Wilson, C. A. M. E., Stoesser, T., Olsen, N. R. B., & Bates, P. D. (2003a). "Application and Validation of Numerical Codes in the Prediction of Compound Channel Flows." *Proc. Instn. Civ. Engrs Wat., Marit. & Energy*, Vol. 156, pp. 117-128.

Wormleaton, P.R. "Determination of Discharge in Compound Channel Using the Dynamic Equation for Lateral Velocity Distribution." *Proceeding of International Conference On Fluvial Hydraulics*, IAHR, Budapest, Hungary.

Wormleaton, P.R., & Ewunetu.M. (2006). "Three Dimensional *K-E* Numerical Modelling of Overbank Flow in a Mobile Bed Meandering Channel with Floodplain of Different Depth, Roughness and Platform." *Journal of Hydraulic Research*, Vol.44 No.1, pp 18-32

Wu, Y, Falconer, R.A., & Struve, J. (2001). "Mathematical Modelling of Tidal Currents in Mangrove Forest." *Environmental Modelling and Software.*, Vol.16, pp 19-29.

Wu, W., Rodi, W., & Wenka, T. (2000). "3D Numerical Modelling of Flow and Sediment Transport in Open Channels." *Journal of Hydraulic Engineering*, Vol. 126, pp. 4-15.

Wu, F. C., Shen, H. W., & Chou, Y. J. (1999). "Variation of Roughness Coefficients for Unsubmergeed and Submerged Vegetation." *Journal of Hydraulic Engineering*, Vol. 125, No. 9, pp. 934-942.

Yen, B. C., & Yen, C. L. (1983). "Flood Flow over Meandering Channels." *River Meandering* (ed. C.M. Elliott), pp. 554-561.

Zheleznyakov, G.V. (1971). " Interaction of Channel and Flood Plain Flows." *Proceeding of 14th International Congress of IAHR*, Paris, pp.144-148.

Zheleznyakov, G.V. (1965). "Relative Deficit of Mean Velocity of Unstable River Flow, Kinematic Effect in River Beds with Floodplain." *Proceeding of 11th International Congress of IAHR*, Leningrad, USSR

Zoppou, C., & Robert, S. (1999). "Catastrophic Collapse of Water Supply Reservoirs in Urban Areas." *Journal of Hydraulic Engineering*, ASCE, Vol. 125, No. 7, pp. 686-695.